2008-01-01

Effect Of Redox-Cycling Agents On Nitric Oxide Synthase Activity In Vitro And Modulation Of Protein Expression In Vivo: No Nitric Oxide Synthase In Mitochondria

Priya Venkatakrishnan
University of Texas at El Paso, priya603@gmail.com

EFFECT OF REDOX-CYCLING AGENTS ON NITRIC OXIDE SYNTHASE ACTIVITY *IN VITRO* AND MODULATION OF PROTEIN EXPRESSION *IN VIVO*: NO NITRIC OXIDE SYNTHASE IN MITOCHONDRIA

PRIYA VENKATAKRISHNAN

Department of Biological Sciences

APPROVED:

R.T. Miller, Ph.D., Chair

Igor C. Almeida, Ph.D.

Kristin Gosselink, Ph.D.

David Borrok, Ph.D.

Patricia D. Witherspoon, Ph.D.

Dean of the Graduate School

Dedication

To my dearest grandfather Mr. S. Krishna Iyengar, my first guru, a radiantly noble soul and a library of practical wisdom, who continues to teach me the art of living.

EFFECT OF REDOX-CYCLING AGENTS ON NITRIC OXIDE SYNTHASE ACTIVITY *IN VITRO* AND MODULATION OF PROTEIN EXPRESSION *IN VIVO*: NO NITRIC OXIDE SYNTHASE IN MITOCHONDRIA

by

PRIYA VENKATAKRISHNAN, B. Pharm (Hons.), M.S.

DISSERTATION

Presented to the Faculty of the Graduate School of

The University of Texas at El Paso

in Partial Fulfillment

of the requirements

for the Degree of

DOCTOR OF PHILOSOPHY

Department of Biological Sciences

THE UNIVERSITY OF TEXAS AT EL PASO

December 2008

Acknowledgements

First of all, I convey my sincere thanks and gratitude to my mom, Mrs. Renganayaki Venkatakrishnan, who has been with me in all my decisions, sacrificing her interests, supporting morally and financially, whenever needed. I am deeply indebted to my dad, Mr. A. P. Venkatakrishnan for showering me with unconditional love and affection and always believing in my abilities and supporting me in whatever I undertake. I thank my mentor, Dr. R.T. Miller for accepting me as a student at the University of Kentucky as well as at The University of Texas at El Paso, and allowing me to experiment a variety of things by adopting an open-lab system. I am deeply indebted to Dr. Miller for trusting my abilities and results, allowing me to pursue my interests in the laboratory, teaching me how to analyze data and communicate with researchers in a scientific manner. Above all, I owe all my scientific writing abilities to Dr. Miller as he has been patiently helping and correcting me all throughout my doctoral degree. I thank my Ph.D advisory committee members, Dr. Igor C. Almeida, Dr. Kristin Gosselink, Dr. David Borrok for their valuable suggestions and guidance throughout my Ph.D. Special thanks to Dr. Almeida for all the valuable inputs that he gave during the proteomic analyses. Also, I thank Dr. Gary Gairola and my friend, Ernesto S. Nakayasu for their valuable advice and suggestions, but for which I would not have been able to complete my projects. I thank my ex-labmates, Josh for teaching me how to do the biochemical experiments and, Javier for helping me get acclimated in the laboratory, and my current lab-mates, Dr. Joshi and Berenise for being very supportive and taking care of the lab management thereby, allowing me to finish Ph.D at ease. Also, I would like to thank all my friends for being extremely supportive, listening and helping me to stay focused. Special thanks to Harish, Maria, Kalyan and Sujan for their guidance and the last-

minute support while writing the dissertation. I also would like to thank Dr. Miller for providing my stipend from his grant # ES 011982 from the National Institute of Environmental Health Sciences (NIEHS)/NIH. Also, this project was also supported in part by grant (# 5G12RR008124) to the Border Biomedical Research Center (BBRC)/University of Texas at El Paso from the National Center for Research Resources (NCRR)/NIH and by grant (# 03-RDE-005) from the Kentucky Science and Education Foundation (KSEF).

Abstract

This dissertation describes studies conducted in three areas dealing with the interaction of redox-active compounds with the flavin- and heme- containing enzyme, neuronal nitric oxide synthase (NOS). They are as follows:

I. Studies were initiated using extracts from several varieties of tobacco to identify constituent(s) that could interact with nNOS. Results from [^{14}C]-*L*-arginine to [^{14}C]-*L*-citrulline conversion assays to which tobacco extracts were individually added, indicate that there are nNOS inhibitors present in tobacco and they are non-polar, lipophilic and non-volatile in nature. In addition, results from assays in which the tobacco-derived redox-active compound, 2,3,6-trimethyl-1,4-naphthoquinone or 2-methyl-1,4-naphthoquinone were individually incorporated into the nNOS activity assays indicate that single compounds can produce either stimulation or inhibition of *L*-citrulline production depending on the concentration of the quinone to which nNOS is exposed as well as the compound's electrochemical characteristics.

II. Data, both for and against the presence of a mitochondrial NOS isoform (mtNOS) is in the refereed literature. However, irrefutable evidence, either for or against the existence of a mtNOS isoform has not been forthcoming. Therefore, studies were initiated at our laboratory to investigate whether any NOS isoform resides in ultra pure rat liver mitochondria, utilizing 3 independent techniques. Results from activity assays, mass spectrometry (MS) analyses and immunochemical detection for NOS, independently, as well as collectively, refute the claim that a NOS isoform exists within rat liver mitochondria, at least down to the limit of detection.

III. Mitochondria are thought to be involved in modulating the toxicity of redox-active compounds. In order to understand the effect of 1, 1-dimethyl-4,4-bipyridinium ion (paraquat), a redox-active compound, on levels of protein expression in whole liver homogenate as well as rat liver mitochondria during the early stage of paraquat exposure (40 mg/kg, i.p), proteomic analyses were performed 3 hrs after paraquat administration. Mass spectrometric analyses of paraquat-treated rats identified 37 proteins in rat liver mitochondria as well as in whole rat liver homogenate that were either down- and/or up-regulated, at least 2 folds above control levels. GO ontology and Interpro scan analyses identified that the modulated proteins in rat liver mitochondria were oxidoreductases and transferases. In whole rat liver homogenate, the modulated proteins were mainly oxidoreductases, transferases as well as proteins involved in protein binding functions. Additionally, rat liver proteins involved in ubiquitination and the proteolytic pathway were modulated.

In addition to these studies, a cost-effective method was designed and validated for obtaining and purifying the chicken antibodies against the stable, reactive nitrogen species biomarker, 3-nitrotyrosine.

Table of Contents

List of Tables

List of Figures

List of Illustrations

Introduction

Nitric Oxide Synthase

The nitric oxide synthases (NOS) are a family of flavoenzymes that catalyze the stoichiometric conversion of *L*-arginine to equimolar amounts of *L*-citrulline plus nitric oxide (NO•) (Bredt and Snyder, 1990; Furchgott and Vanhoutte, 1989; Ignarro *et al.*, 1987a; Palmer *et al.*, 1987; Pollock *et al.*, 1991; Stuehr *et al.*, 1991b) *via* two sequential mono-oxygenation reactions. NOS depends on (6*R)*-5, 6, 7, 8-tetrahydro-*L*-biopterin (BH_4) (Mayer *et al.*, 1990) and molecular oxygen (O_2) (Griffith and Stuehr, 1995; Kwon *et al.*, 1990) for this reaction and utilizes reduced nicotinamide adenine dinucleotide phosphate (NADPH) as a co-substrate (Scheme 1).

Isoforms of NOS

Physiologically, NO• is produced by three main isoforms of NOS: neuronal (nNOS), endothelial (eNOS) and inducible (iNOS) (Bredt and Snyder, 1990; Forstermann *et al.*, 1991b; Hibbs, 1991; Ignarro *et al.*, 1987a; Stuehr and Nathan, 1989). The isoforms, eNOS and nNOS, are constitutively-expressed and depend on intracellular fluxes of calcium (Ca^{2+}) for the binding of the 18 kDa protein, calmodulin (CaM), which activates NOS (Forstermann *et al.*, 1991a) (Bredt and Snyder, 1990) (Mayer *et al.*, 1990). In contrast, iNOS is non-constitutive in nature, calcium-insensitive, has tightly bound CaM and is expressed only after immune challenge by stimulated macrophages (Hibbs, 1991).

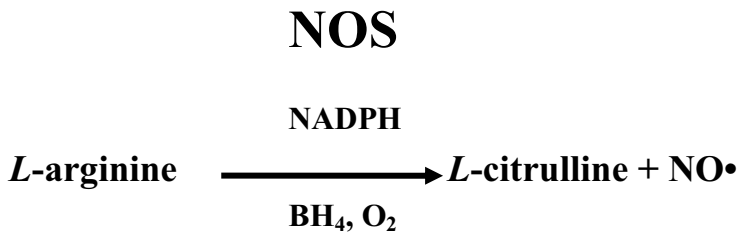

Scheme 1: NOS-catalyzed conversion of *L*-arginine to *L*-citrulline plus NO•

Structure of NOS

NOS is a dimeric protein and each monomer consists of an N-terminal heme-containing oxygenase domain (McMillan *et al.*, 1992; Stuehr and Ikeda-Saito, 1992; White and Marletta, 1992) and a C-terminal flavin-containing reductase domain (Bredt *et al.*, 1991) linked together by a CaM-binding sequence. The oxygenase domain contains heme, BH_4-binding site and the *L*-arginine-binding site (Klatt *et al.*, 1992; McMillan *et al.*, 1992; Stuehr and Ikeda-Saito, 1992; White and Marletta, 1992) and, the reductase domain contains flavin adenine dinucleotide (FAD), flavin mono nucleotide (FMN) and the NADPH-binding site (Hevel *et al.*, 1991; Mayer *et al.*, 1991; Schmidt *et al.*, 1992; Stuehr *et al.*, 1991a) (Scheme 2). The presence of zinc in the tetrathiolate center of heme was initially identified by Raman *et al.* (1998) (Raman *et al.*, 1998) which was confirmed later by Fischmann *et al.* (1999) (Fischmann *et al.*, 1999).

All three NOS isoforms share 50-60% overall sequence similarity but each of the NOS isoforms is intrinsically different from the other in terms of rates of NO• production, cytochrome-*c* reduction and overall rates of electron transfer. Chimeric enzymes in which the heme domain of one isoform is connected to the flavin domain of another (Nishida and Ortiz de Montellano, 1998) indicated that the identity of the flavin domain rather than that of the heme domain determined the rates of NO synthesis and cytochrome-*c* reduction. Porter and Kasper (Porter and Kasper, 1985, 1986) proposed that NADPH-cytochrome p450 reductase (CYPOR) was evolved from the genes coding for bacterial flavodoxins (FMN) and ferrodoxin $NADP^+$ reductase (FAD) based on sequence similarity, which was further solidified by Kim and Masters (Wang *et al.*, 1997). Recently, it is found that NOS reductase also appears to have evolved from these proteins (Jachymova *et al.*, 2005).

Initially, a partial structure consisting only of the FAD-NADPH domain of the nNOS reductase was solved (Zhang *et al.*, 2001) and recently, complete structure is available for the reductase domain of nNOS isoforms (Garcin *et al.*, 2004). The crystal structure of the reductase domain by Garcin *et al.*, 2004 may help us understand the molecular mechanism of interactions that enable the newly identified autoinhibitory helix motif, co-substrate NADPH, the C-terminal tail and its phosphorylation site (putative for iNOS and nNOS) to regulate NOS activity.

Structural Differences and Localization of NOS Isoforms

nNOS (NOS 1) is found in both the central (CNS) as well as the peripheral (PNS) nervous system. In the CNS, nNOS is mainly localized within the cerebellum (Bredt and Snyder, 1990). nNOS is the largest isoform as it contains an additional 90-residue protein recognition molecule at the N-terminus. This region is called PDZ domain which is a 300 amino acid stretch (Scheme 3) that is responsible for association with other proteins such as dystrophin at the sarcolemmal membrane (Brenman *et al.*, 1995), or PSD-95, a channel-associated protein in the brain which helps in sub-cellular localization of nNOS (Brenman *et al.*, 1996).

eNOS (NOS 3) is found mainly in endothelial cells (Forstermann *et al.*, 1991a; Ignarro *et al.*, 1987a) and cardiomyocytes (Balligand *et al.*, 1993). The specialized property of eNOS that enable it to perform its functions includes Ca^{2+} sensitivity and post-translational modifications such as myristoylation (Liu and Sessa, 1994) and palmitoylation (Liu *et al.*, 1995), which mediate its sub-cellular localization (Scheme 3).

iNOS (NOS 2) is calcium insensitive and it can be induced by inflammatory mediators such as cytokines or lipopolysaccharides in activated macrophages as well as in other vascular

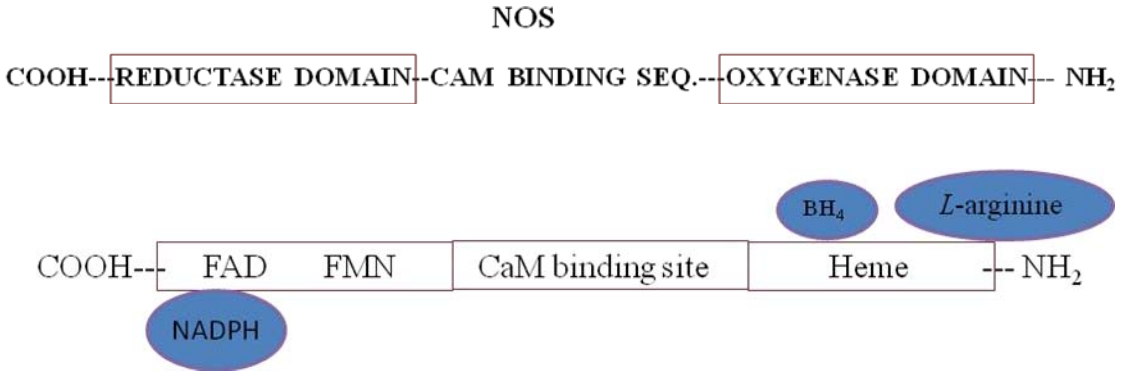

Scheme 2: Domain structure of NOS

cells (Hibbs, 1991; Stuehr and Nathan, 1989). Unlike eNOS and nNOS, there is no sub-cellular targeting sequence in iNOS (Scheme 3). In iNOS, the CaM binding site is always occupied by CaM under physiological conditions whereas nNOS and eNOS require an increase in intracellular calcium for CaM binding.

Electron transfer through NOS

Flow-through of electron in NOS begins with donation of a hydride from NADPH to FAD. One-electron-transfers, then, occur at the reductase domain from FAD to FMN and from FMN to the final acceptor, *i.e.* the heme at the oxygenase domain (Sagami *et al.*, 2001; Siddhanta *et al.*, 1998; Siddhanta *et al.*, 1996) or exogenously added electron acceptor, cytochrome-*c* (Scheme 4). Between the flavins, there is comproportionation of the electrons and then, only one electron enters into the heme at a time. The electrons then catalyze a two-step mono-oxygenation of *L*-arginine that is bound in the active site, through the cysteine thiolate-liganded heme (Klatt *et al.*, 1992; McMillan *et al.*, 1992; Stuehr and Ikeda-Saito, 1992; White and Marletta, 1992). The binding of CaM is required for the NOS isoforms to transfer electrons from the reductase domain (FAD and FMN) to the heme. The electron transfer process between the reductase and the oxygenase domains of NOS resembles the mechanism of CYPOR-P_{450} interaction in terms of hydride transfer (Miller *et al.*, 1999a). The rate-limiting step in electron transfer seemed to be the transfer of electrons from the flavoproteins to the oxygenase domain facilitated by the binding of CaM at increased intracellular Ca^{2+} concentrations. Using stopped-flow kinetics, it is found that modulation of electron transfer rates appears to be regulated at the level of the flavoprotein domains of the NOS isoforms (Miller *et al.*, 1999a).

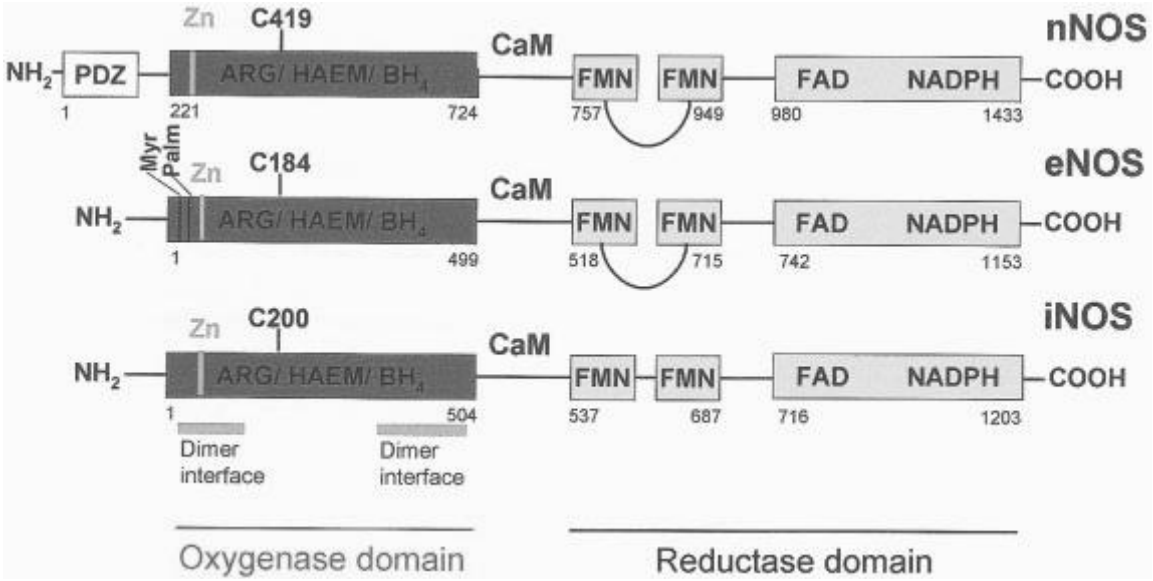

Adopted from Alderton et al., 2001

Scheme 3: Structure of NOS Isoforms

Regulatory Factors Governing NOS Activity

CaM Binding: All NOS isoforms require the binding of CaM for NO• synthesis. In the reductase domain, when calmodulin is absent, the flavin reduction is much slower (Abu-Soud *et al.*, 1994; Matsuda and Iyanagi, 1999; Miller *et al.*, 1999a; Roman *et al.*, 2000a), no reduction of heme and thus no NO• is generated from *L*-arginine (Bredt and Snyder, 1990; Miller *et al.*, 1997; Roman *et al.*, 2000a).

Matsuda and Iyanagi (Matsuda and Iyanagi, 1999) investigated the transfer of electrons to and between the flavins using nNOS reductase domains with or without an intact CaM binding site to determine the effects of CaM. They demonstrated that the air-stable semiquinone form of nNOS is 1 equiv more reduced than the fully oxidized form. Also, by monitoring the rates of flavin reduction, in the presence and absence of CaM using stopped-flow and rapid scan spectrophotometry, they determined that intramolecular transfer of electrons between the flavins of NOS is activated by CaM. CaM stimulates both phases of nNOS biphasic flavin reduction, i.e., the initial flavin reduction and comproportionation or transfer of electrons between the two flavins, by 6-and 2-fold, respectively (Matsuda and Iyanagi, 1999). In addition, they propose that, in the absence of CaM, intramolecular electron transfer is rate-limiting; when CaM is added, the rate of this process increases such that transfer of electrons from NADPH to the FAD becomes rate-limiting, as like in cytochrome P_{450} oxido-reductase (CYPOR). On the other hand, using stopped-flow kinetic studies, Miller *et al.* (1999) (Miller *et al.*, 1999a) proposed that the rate-limiting step in electron transfer is due to the transfer of

Scheme 4: Electron Transfer through NOS

electrons from the flavoprotein to the oxygenase domain facilitated by the binding of CaM at increased intracellular Ca^{2+} concentrations.

Regarding cytochrome-*c* reduction, in the absence of CaM, cytochrome-*c* reduction occurs at a rate about $1/10^{th}$-$1/30^{th}$ of that in the presence of CaM (Gachhui *et al.*, 1996; Matsuda and Iyanagi, 1999; Roman *et al.*, 2000a). The independently expressed NOS reductase domains reduce cytochrome-*c* in the absence of CaM at rates very similar to those of the CaM-free holoenzymes (McMillan and Masters, 1995). In addition, the NOS reductase domain and the holoenzyme are stimulated by CaM to similar extents, indicating that the increased cytochrome *c* reduction in response to CaM binding is at least partially mediated by the reductase domain.

Furthermore, studies using the nNOS holoenzyme that was devoid of heme and BH_4 demonstrated that the CaM effect, in the case of cytochrome-*c* reduction but not NO synthesis, is mediated by the NOS reductase domain (Abu-Soud *et al.*, 1994). Chimeras of NOS in which the reductase domains of the eNOS and iNOS proteins were replaced by that of nNOS catalyze cytochrome-*c* reduction with rates similar to those of the parent reductase domain (i.e., nNOS), supporting the idea that the heme domain does not exert significant control over cytochrome-*c* reductase activity, first shown by Mc Millan and Masters (McMillan and Masters, 1995) and later by Nishida using chimeric constructs (Nishida and Ortiz de Montellano, 1998).

Auto regulatory loop. A 45-amino acid auto-regulatory insert was identified within the FMN binding region of nNOS and eNOS, but not in the inducible isoform, iNOS (Salerno *et al.*, 1995). One role of this autoregulatory insert is the obstruction of electron transfer from the reductase domain into the heme domain in the absence of CaM. In the presence of CaM, this

block is partially relieved, and electron flux from the reductase to the heme can occur. If the autoregulatory insert is completely removed, the rate of electron flow is further increased relative to CaM bound NOS holoenzyme, indicating that this regulatory element regulates electron flow to the heme (Chen and Wu, 2000; Daff *et al.*, 1999).

C- Terminal Tail. Another regulatory element exists at the C-terminus of all known NOS isoforms. An extension of between 21–42 amino acids, beyond the residues found in NADPH-CYPOR called the tail region, appears to be a regulatory mechanism that impedes electron flow through the flavin domain in the absence of CaM (Roman *et al.*, 2000a; Roman *et al.*, 2000b). In the presence of CaM, this blockade is partially removed, presumably by repositioning of the tail, facilitating electron flux between the flavins (Roman *et al.*, 2000a; Roman *et al.*, 2000b). The tail regions of the constitutive NOS isoforms contain a serine residue that is phosphorylated as a result of physiological stimuli, resulting in higher rates of both NO production and cytochrome-*c* reduction (Butt *et al.*, 2000; Chen *et al.*, 1999; Dimmeler *et al.*, 1999; Fulton *et al.*, 1999). Mutation of this residue in either eNOS or nNOS from serine to aspartate mimicked the negative charge of phosphorylation and resulted in an enzyme with increased NO synthesis and cytochrome-*c* reduction rates (Adak *et al.*, 2001; McCabe *et al.*, 2000; Roman *et al.*, 2000a). Partial removal of the tail region of eNOS, starting from $serine_{1179}$ to the end of the molecule, resulted in an enzyme with increased NO synthesis and cytochrome *c* reduction (Lane and Gross, 2002; Roman *et al.*, 2000a).

NOS reductase & CYPOR - Structural Similarity

The flavin-containing reductase domains of NOS possess close sequence homology to CYPOR (Bredt *et al.*, 1991), and also function similarly in the reduction of artificial electron acceptors such as cytochrome-*c* (Bredt *et al.*, 1991; Roman *et al.*, 2003). The crystal structures of CYPOR (Miller *et al.*, 1999a; Wang *et al.*, 1997) and the FAD-NADPH binding sub-domain of nNOS are almost identical (Zhang *et al.*, 2001). Chimeric enzymes that were created in which the FMN and/or FAD binding sub-domains of CYPOR were swapped with analogous domains from nNOS, showed that the FMN binding and FAD-NADPH-binding subdomains of nNOS and CYPOR are discrete and are similar enough in structure to reconstitute electron flow (Roman *et al.*, 2003). Although the amino acid sequence of the nNOS reductase domain is 58% similar to that of CYPOR (Bredt *et al.*, 1991), CYPOR completely lacks both the autoregulatory insert as well as the C-terminal tail.

The geometry of hydride transfer from NADPH to the FAD of nNOS reductase is the same that of CYPOR (Sem and Kasper, 1992). The isolated nNOS reductase as well as CaM-free NOS holoenzyme can stabilize a one-electron-reduced form of flavin, the neutral blue flavin semiquinone [FAD/ $FMNH^{\cdot}$] in a manner similar to CYPOR (Miller *et al.*, 1997; Vermilion and Coon, 1978). As like CYPOR, the one-electron reduced form of nNOS reductase is unable to efficiently transfer its electron to the heme of the oxygenase domain, the endogenous electron acceptor, or to cytochrome-*c*, an exogenous electron acceptor.

Many reactions such as the reduction of quinones, nitroarenes, cytochrome c, 2, 6-dichlorophenolindophenol (DCIP) and ferricyanide, catalyzed by CYPOR are also catalyzed by

nNOS *via* its flavin containing reductase domain (Abu-Soud *et al.*, 1994; Klatt *et al.*, 1992; Sheta *et al.*, 1994; Workman, 1992).

Function of NO•

Although all three NOS isoforms metabolize *L*-arginine to yield the same products, the function of the NO• that is produced varies widely depending on the tissue type and sub-cellular localization of the NOS isoform (Ignarro, 1990b). NO• produced by eNOS acts as vasodilator and modulates vascular dynamics (blood pressure and blood flow) *via* relaxation of smooth muscle cells of the vascular endothelium (Furchgott and Vanhoutte, 1989; Ignarro *et al.*, 1988; Pollock *et al.*, 1991). NO• produced by nNOS acts as a neurotransmitter and modulates chemical messaging within the central nervous system and at the neuromuscular junctions (Knowles *et al.*, 1989). NO• by iNOS in activated macrophages is produced only under inflammatory conditions and is an integral part of the immune response, being used for cellular defense (Hibbs *et al.*, 1988).

Disregulation of NOS

During normal catalysis, nNOS is end-product inhibited. Putatively up to 80% of the enzyme is inactive during steady state catalysis, due to the ability of the NO• to re-bind the heme iron from which it was originated (Abu-Soud *et al.*, 1996; Abu-Soud *et al.*, 1995; Ignarro, 1990a; Scheele *et al.*, 1999). When there is an excess availability of $O_2^{\bullet-}$, such as in the proximity of mitochondria, the $O_2^{\bullet-}$ acts as a trap for the enzymatically-generated NO• to produce $ONOO^-$ at an almost diffusion-limited reaction rate ($6.7 \times 10^9\ M^{-1}\ s^{-1}$; (Huie and Padmaja, 1993)). Thus $ONOO^-$ production lowers the available free NO• concentration, causing a decrease in the extent of NO•-mediated auto-inhibition of nNOS ((Griscavage *et al.*, 1995) and many others). This

decreased level of nNOS auto-inhibition is then responsible for the corresponding increase in production of NO• and *L*-citrulline in the presence of $O_2^{\bullet-}$. Thus, when NOS becomes dysregulated, the result is the overproduction of not only NO• but also reactive oxygen species (ROS) and reactive nitrogen species (ROS).

Redox-Cyclers and Formation of RNS

In addition to donating electrons to the oxygenase domain of NOS, the NOS reductase can catalyze the reduction of certain exogenous electron acceptors including quinones, nitroarenes, cytochrome-*c*, 2, 6-dichlorophenol-indophenol (DCIP), and ferricyanide (Abu-Soud *et al.*, 1994; Klatt *et al.*, 1992; Kumagai *et al.*, 1998; Sheta *et al.*, 1994; Workman, 1992). Since NO• plays key roles in regulating blood pressure and neurotransmission *in vivo* and modulates immune response, electron diversion by nitroarenes and quinones can have detrimental effects on an organism (Bredt and Snyder, 1990; Ignarro, 1989; Moncada *et al.*, 1989). nNOS reductase mediates the production of one electron-reduced quinone and nitroarene intermediates (Kumagai *et al.*, 1998; Miller *et al.*, 1997; Vasquez-Vivar *et al.*, 1997b). The reduced quinone or nitroarene autoxidizes and regenerates the starting quinone or nitroarene. The donation of an electron to O_2 during the process of autoxidation produces the superoxide anion radical ($O_2^{\bullet-}$). This reduction-oxidation cycle is termed redox-cycling

While some quinones are known to inhibit nNOS activity, continued production of NO• along with $O_2^{\bullet-}$ production is possible with some quinones and nitroarenes wherein the electron flux through NOS is sufficient to accommodate electron transfer to some exogenous electron acceptors, yet, maintain sufficient electron flux to the heme in the oxygenase domain to maintain *L*-citrulline and NO• production (Miller *et al.*, 1999b; Miller *et al.*, 1997). With some

nitroarenes and quinones, there is increased *L*-citrulline production by NOS due to the release of the end-product inhibition that NO• normally exerts on nNOS (Abu-Soud *et al.*, 1996; Abu-Soud *et al.*, 1995). Thus, some redox nitroarenes and quinones can change the products of the nNOS reaction from NO• and *L*-citrulline to $ONOO^-$ and *L*-citrulline (Miller, 2002). As a result, generation of RNS and the release of end-production inhibition by redox-cyclers such as quinones and nitroarenes can potentially result in cellular toxicity and cell death (Miller, 2002).

Oxidative and Nitrative Effects of RNS

$ONOO^-$ can directly oxidize carbohydrates, sulfhydryls, lipids and DNA bases as well as mediate endothelial cell toxicity (Ischiropoulos *et al.*, 1992; Radi *et al.*, 1991b). On the other hand, $ONOO^-$ are found to nitrate only few proteins in a given cell type indicating that there is some target specificity in nitration of proteins (Ye *et al.*, 1996). Specifically, $ONOO^-$ thus formed is known to target tyrosine residues on proteins causing tyrosine nitration (Ischiropoulos *et al.*, 1992). The protein tyrosine nitration product, 3-nitrotyrosine, was found to be increased in many disease states including atherosclerosis (Beckmann *et al.*, 1994), acute lung injury (Haddad *et al.*, 1994), adult respiratory distress syndrome(Kooy *et al.*, 1995), biliary cirrhosis (Ottesen *et al.*, 2001), myocardial inflammation (Kooy *et al.*, 1997), Alzheimer's disease (Good *et al.*, 1996) and amyotropic lateral sclerosis (Crow *et al.*, 1997). Both nitration and oxidation reactions may inactivate enzymes causing damage and dysfunction of sub-cellular organelles like mitochondria (Bolanos *et al.*, 1995). RNS can also cause nitrosylation of proteins (heme or thiols) and in fact, increased levels of nitrosylated proteins (even when the cellular redox status is unaltered) can lead to apoptosis and cell death (Eu *et al.*, 2000). The production of ROS and RNS may lead to oxidative stress and/or nitrosative stress within cells resulting in apoptosis or necrosis during the

course of many degenerative disease states including multiple sclerosis, spinal injury and stroke (Beckman, 1994; Dawson and Dawson, 1996; Kamii *et al.*, 1996; Sherman *et al.*, 1992). Accumulation of the ROS- and RNS-mediated damage over the lifetime of an organism may well be responsible for causing many (neuro) degenerative diseases.

References

Abu-Soud, H. M., Rousseau, D. L., Stuehr, D. J., 1996. Nitric oxide binding to the heme of neuronal nitric-oxide synthase links its activity to changes in oxygen tension. J Biol Chem 271, 32515-32518.

Abu-Soud, H. M., Wang, J., Rousseau, D. L., Fukuto, J. M., Ignarro, L. J., Stuehr, D. J., 1995. Neuronal nitric oxide synthase self-inactivates by forming a ferrous-nitrosyl complex during aerobic catalysis. J Biol Chem 270, 22997-23006.

Abu-Soud, H. M., Yoho, L. L., Stuehr, D. J., 1994. Calmodulin controls neuronal nitric-oxide synthase by a dual mechanism. Activation of intra- and interdomain electron transfer. J Biol Chem 269, 32047-32050.

Adak, S., Aulak, K. S., Stuehr, D. J., 2001. Chimeras of nitric-oxide synthase types I and III establish fundamental correlates between heme reduction, heme-NO complex formation, and catalytic activity. J Biol Chem 276, 23246-23252.

Balligand, J. L., Ungureanu, D., Kelly, R. A., Kobzik, L., Pimental, D., Michel, T., Smith, T. W., 1993. Abnormal contractile function due to induction of nitric oxide synthesis in rat cardiac myocytes follows exposure to activated macrophage-conditioned medium. J Clin Invest 91, 2314-2319.

Beckman, J. S., 1994. Peroxynitrite versus hydroxyl radical: the role of nitric oxide in superoxide-dependent cerebral injury. Annals of the New York Academy of Sciences 738, 69-75.

Beckmann, J. S., Ye, Y. Z., Anderson, P. G., Chen, J., Accavitti, M. A., Tarpey, M. M., White, C. R., 1994. Extensive nitration of protein tyrosines in human atherosclerosis detected by immunohistochemistry. Biological chemistry Hoppe-Seyler 375, 81-88.

Bolanos, J. P., Heales, S. J., Land, J. M., Clark, J. B., 1995. Effect of peroxynitrite on the mitochondrial respiratory chain: differential susceptibility of neurones and astrocytes in primary culture. J Neurochem 64, 1965-1972.

Bredt, D. S., Hwang, P. M., Glatt, C. E., Lowenstein, C., Reed, R. R., Snyder, S. H., 1991. Cloned and expressed nitric oxide synthase structurally resembles cytochrome P-450 reductase. Nature 351, 714-718.

Bredt, D. S., Snyder, S. H., 1990. Isolation of nitric oxide synthetase, a calmodulin-requiring enzyme. Proc Natl Acad Sci U S A 87, 682-685.

Brenman, J. E., Chao, D. S., Gee, S. H., McGee, A. W., Craven, S. E., Santillano, D. R., Wu, Z., Huang, F., Xia, H., Peters, M. F., Froehner, S. C., Bredt, D. S., 1996. Interaction of nitric oxide synthase with the postsynaptic density protein PSD-95 and alpha1-syntrophin mediated by PDZ domains. Cell 84, 757-767.

Brenman, J. E., Chao, D. S., Xia, H., Aldape, K., Bredt, D. S., 1995. Nitric oxide synthase complexed with dystrophin and absent from skeletal muscle sarcolemma in Duchenne muscular dystrophy. Cell 82, 743-752.

Butt, E., Bernhardt, M., Smolenski, A., Kotsonis, P., Frohlich, L. G., Sickmann, A., Meyer, H. E., Lohmann, S. M., Schmidt, H. H., 2000. Endothelial nitric-oxide synthase (type III) is

activated and becomes calcium independent upon phosphorylation by cyclic nucleotide-dependent protein kinases. J Biol Chem 275, 5179-5187.

Chen, C. C., Chiu, K. T., Sun, Y. T., Chen, W. C., 1999. Role of the cyclic AMP-protein kinase A pathway in lipopolysaccharide-induced nitric oxide synthase expression in RAW 264.7 macrophages. Involvement of cyclooxygenase-2. J Biol Chem 274, 31559-31564.

Chen, P. F., Wu, K. K., 2000. Characterization of the roles of the 594-645 region in human endothelial nitric-oxide synthase in regulating calmodulin binding and electron transfer. J Biol Chem 275, 13155-13163.

Crow, J. P., Sampson, J. B., Zhuang, Y., Thompson, J. A., Beckman, J. S., 1997. Decreased zinc affinity of amyotrophic lateral sclerosis-associated superoxide dismutase mutants leads to enhanced catalysis of tyrosine nitration by peroxynitrite. J Neurochem 69, 1936-1944.

Daff, S., Sagami, I., Shimizu, T., 1999. The 42-amino acid insert in the FMN domain of neuronal nitric-oxide synthase exerts control over Ca(2+)/calmodulin-dependent electron transfer. J Biol Chem 274, 30589-30595.

Dawson, V. L., Dawson, T. M., 1996. Free radicals and neuronal cell death. Cell death and differentiation 3, 71-78.

Dimmeler, S., Fleming, I., Fisslthaler, B., Hermann, C., Busse, R., Zeiher, A. M., 1999. Activation of nitric oxide synthase in endothelial cells by Akt-dependent phosphorylation. Nature 399, 601-605.

Eu, J. P., Liu, L., Zeng, M., Stamler, J. S., 2000. An apoptotic model for nitrosative stress. Biochemistry 39, 1040-1047.

Fischmann, T. O., Hruza, A., Niu, X. D., Fossetta, J. D., Lunn, C. A., Dolphin, E., Prongay, A. J., Reichert, P., Lundell, D. J., Narula, S. K., Weber, P. C., 1999. Structural characterization of nitric oxide synthase isoforms reveals striking active-site conservation. Nat Struct Biol 6, 233-242.

Forstermann, U., Pollock, J. S., Schmidt, H. H., Heller, M., Murad, F., 1991a. Calmodulin-dependent endothelium-derived relaxing factor/nitric oxide synthase activity is present in the particulate and cytosolic fractions of bovine aortic endothelial cells. Proc Natl Acad Sci U S A 88, 1788-1792.

Forstermann, U., Schmidt, H. H., Pollock, J. S., Sheng, H., Mitchell, J. A., Warner, T. D., Nakane, M., Murad, F., 1991b. Isoforms of nitric oxide synthase. Characterization and purification from different cell types. Biochem Pharmacol 42, 1849-1857.

Fulton, D., Gratton, J. P., McCabe, T. J., Fontana, J., Fujio, Y., Walsh, K., Franke, T. F., Papapetropoulos, A., Sessa, W. C., 1999. Regulation of endothelium-derived nitric oxide production by the protein kinase Akt. Nature 399, 597-601.

Furchgott, R. F., Vanhoutte, P. M., 1989. Endothelium-derived relaxing and contracting factors. FASEB J 3, 2007-2018.

Gachhui, R., Presta, A., Bentley, D. F., Abu-Soud, H. M., McArthur, R., Brudvig, G., Ghosh, D. K., Stuehr, D. J., 1996. Characterization of the reductase domain of rat neuronal nitric oxide

synthase generated in the methylotrophic yeast Pichia pastoris. Calmodulin response is complete within the reductase domain itself. J Biol Chem 271, 20594-20602.

Garcin, E. D., Bruns, C. M., Lloyd, S. J., Hosfield, D. J., Tiso, M., Gachhui, R., Stuehr, D. J., Tainer, J. A., Getzoff, E. D., 2004. Structural basis for isozyme-specific regulation of electron transfer in nitric-oxide synthase. J Biol Chem 279, 37918-37927.

Good, P. F., Werner, P., Hsu, A., Olanow, C. W., Perl, D. P., 1996. Evidence of neuronal oxidative damage in Alzheimer's disease. The American journal of pathology 149, 21-28.

Griffith, O. W., Stuehr, D. J., 1995. Nitric oxide synthases: properties and catalytic mechanism. Annu Rev Physiol 57, 707-736.

Griscavage, J. M., Hobbs, A. J., Ignarro, L. J., 1995. Negative modulation of nitric oxide synthase by nitric oxide and nitroso compounds. Adv Pharmacol 34, 215-234.

Haddad, I. Y., Pataki, G., Hu, P., Galliani, C., Beckman, J. S., Matalon, S., 1994. Quantitation of nitrotyrosine levels in lung sections of patients and animals with acute lung injury. J Clin Invest 94, 2407-2413.

Hevel, J. M., White, K. A., Marletta, M. A., 1991. Purification of the inducible murine macrophage nitric oxide synthase. Identification as a flavoprotein. J Biol Chem 266, 22789-22791.

Hibbs, J. B., Jr., 1991. Synthesis of nitric oxide from L-arginine: a recently discovered pathway induced by cytokines with antitumour and antimicrobial activity. Res Immunol 142, 565-569; discussion 596-568.

Hibbs, J. B., Jr., Taintor, R. R., Vavrin, Z., Rachlin, E. M., 1988. Nitric oxide: a cytotoxic activated macrophage effector molecule. Biochem Biophys Res Commun 157, 87-94.

Huie, R. E., Padmaja, S., 1993. The reaction of no with superoxide. Free Radic Res Commun 18, 195-199.

Ignarro, L. J., 1989. Endothelium-derived nitric oxide: actions and properties. FASEB J 3, 31-36.

Ignarro, L. J., 1990a. Haem-dependent activation of guanylate cyclase and cyclic GMP formation by endogenous nitric oxide: a unique transduction mechanism for transcellular signaling. Pharmacology & toxicology 67, 1-7.

Ignarro, L. J., 1990b. Nitric oxide. A novel signal transduction mechanism for transcellular communication. Hypertension 16, 477-483.

Ignarro, L. J., Buga, G. M., Byrns, R. E., Wood, K. S., Chaudhuri, G., 1988. Endothelium-derived relaxing factor and nitric oxide possess identical pharmacologic properties as relaxants of bovine arterial and venous smooth muscle. J Pharmacol Exp Ther 246, 218-226.

Ignarro, L. J., Buga, G. M., Wood, K. S., Byrns, R. E., Chaudhuri, G., 1987. Endothelium-derived relaxing factor produced and released from artery and vein is nitric oxide. Proc Natl Acad Sci U S A 84, 9265-9269.

Ischiropoulos, H., Zhu, L., Chen, J., Tsai, M., Martin, J. C., Smith, C. D., Beckman, J. S., 1992. Peroxynitrite-mediated tyrosine nitration catalyzed by superoxide dismutase. Archives of biochemistry and biophysics 298, 431-437.

Jachymova, M., Martasek, P., Panda, S., Roman, L. J., Panda, M., Shea, T. M., Ishimura, Y., Kim, J. J., Masters, B. S., 2005. Recruitment of governing elements for electron transfer in the nitric oxide synthase family. Proc Natl Acad Sci U S A 102, 15833-15838.

Kamii, H., Mikawa, S., Murakami, K., Kinouchi, H., Yoshimoto, T., Reola, L., Carlson, E., Epstein, C. J., Chan, P. H., 1996. Effects of nitric oxide synthase inhibition on brain infarction in SOD-1-transgenic mice following transient focal cerebral ischemia. J Cereb Blood Flow Metab 16, 1153-1157.

Klatt, P., Heinzel, B., Mayer, B., Ambach, E., Werner-Felmayer, G., Wachter, H., Werner, E. R., 1992. Stimulation of human nitric oxide synthase by tetrahydrobiopterin and selective binding of the cofactor. FEBS Lett 305, 160-162.

Knowles, R. G., Palacios, M., Palmer, R. M., Moncada, S., 1989. Formation of nitric oxide from L-arginine in the central nervous system: a transduction mechanism for stimulation of the soluble guanylate cyclase. Proc Natl Acad Sci U S A 86, 5159-5162.

Kooy, N. W., Lewis, S. J., Royall, J. A., Ye, Y. Z., Kelly, D. R., Beckman, J. S., 1997. Extensive tyrosine nitration in human myocardial inflammation: evidence for the presence of peroxynitrite. Critical care medicine 25, 812-819.

Kooy, N. W., Royall, J. A., Ye, Y. Z., Kelly, D. R., Beckman, J. S., 1995. Evidence for in vivo peroxynitrite production in human acute lung injury. American journal of respiratory and critical care medicine 151, 1250-1254.

Kumagai, Y., Nakajima, H., Midorikawa, K., Homma-Takeda, S., Shimojo, N., 1998. Inhibition of nitric oxide formation by neuronal nitric oxide synthase by quinones: nitric oxide synthase as a quinone reductase. Chem Res Toxicol 11, 608-613.

Kwon, N. S., Nathan, C. F., Gilker, C., Griffith, O. W., Matthews, D. E., Stuehr, D. J., 1990. L-citrulline production from L-arginine by macrophage nitric oxide synthase. The ureido oxygen derives from dioxygen. J Biol Chem 265, 13442-13445.

Lane, P., Gross, S. S., 2002. Disabling a C-terminal autoinhibitory control element in endothelial nitric-oxide synthase by phosphorylation provides a molecular explanation for activation of vascular NO synthesis by diverse physiological stimuli. J Biol Chem 277, 19087-19094.

Liu, J., Garcia-Cardena, G., Sessa, W. C., 1995. Biosynthesis and palmitoylation of endothelial nitric oxide synthase: mutagenesis of palmitoylation sites, cysteines-15 and/or -26, argues against depalmitoylation-induced translocation of the enzyme. Biochemistry 34, 12333-12340.

Liu, J., Sessa, W. C., 1994. Identification of covalently bound amino-terminal myristic acid in endothelial nitric oxide synthase. J Biol Chem 269, 11691-11694.

Matsuda, H., Iyanagi, T., 1999. Calmodulin activates intramolecular electron transfer between the two flavins of neuronal nitric oxide synthase flavin domain. Biochim Biophys Acta 1473, 345-355.

Mayer, B., John, M., Bohme, E., 1990. Purification of a Ca2+/calmodulin-dependent nitric oxide synthase from porcine cerebellum. Cofactor-role of tetrahydrobiopterin. FEBS Lett 277, 215-219.

Mayer, B., John, M., Heinzel, B., Werner, E. R., Wachter, H., Schultz, G., Bohme, E., 1991. Brain nitric oxide synthase is a biopterin- and flavin-containing multi-functional oxido-reductase. FEBS Lett 288, 187-191.

McCabe, T. J., Fulton, D., Roman, L. J., Sessa, W. C., 2000. Enhanced electron flux and reduced calmodulin dissociation may explain "calcium-independent" eNOS activation by phosphorylation. J Biol Chem 275, 6123-6128.

McMillan, K., Bredt, D. S., Hirsch, D. J., Snyder, S. H., Clark, J. E., Masters, B. S., 1992. Cloned, expressed rat cerebellar nitric oxide synthase contains stoichiometric amounts of heme, which binds carbon monoxide. Proc Natl Acad Sci U S A 89, 11141-11145.

McMillan, K., Masters, B. S., 1995. Prokaryotic expression of the heme- and flavin-binding domains of rat neuronal nitric oxide synthase as distinct polypeptides: identification of the heme-binding proximal thiolate ligand as cysteine-415. Biochemistry 34, 3686-3693.

Miller, R. T., 2002. Dinitrobenzene-mediated production of peroxynitrite by neuronal nitric oxide synthase. Chem Res Toxicol 15, 927-934.

Miller, R. T., Martasek, P., Omura, T., Siler Masters, B. S., 1999a. Rapid kinetic studies of electron transfer in the three isoforms of nitric oxide synthase. Biochem Biophys Res Commun 265, 184-188.

Miller, R. T., Martasek, P., Raman, C. S., Masters, B. S., 1999b. Zinc content of Escherichia coli-expressed constitutive isoforms of nitric-oxide synthase. Enzymatic activity and effect of pterin. J Biol Chem 274, 14537-14540.

Miller, R. T., Martasek, P., Roman, L. J., Nishimura, J. S., Masters, B. S., 1997. Involvement of the reductase domain of neuronal nitric oxide synthase in superoxide anion production. Biochemistry 36, 15277-15284.

Moncada, S., Palmer, R. M., Higgs, E. A., 1989. The biological significance of nitric oxide formation from L-arginine. Biochem Soc Trans 17, 642-644.

Nishida, C. R., Ortiz de Montellano, P. R., 1998. Electron transfer and catalytic activity of nitric oxide synthases. Chimeric constructs of the neuronal, inducible, and endothelial isoforms. J Biol Chem 273, 5566-5571.

Ottesen, L. H., Harry, D., Frost, M., Davies, S., Khan, K., Halliwell, B., Moore, K., 2001. Increased formation of S-nitrothiols and nitrotyrosine in cirrhotic rats during endotoxemia. Free Radic Biol Med 31, 790-798.

Palmer, R. M., Ferrige, A. G., Moncada, S., 1987. Nitric oxide release accounts for the biological activity of endothelium-derived relaxing factor. Nature 327, 524-526.

Pollock, J. S., Forstermann, U., Mitchell, J. A., Warner, T. D., Schmidt, H. H., Nakane, M., Murad, F., 1991. Purification and characterization of particulate endothelium-derived relaxing factor synthase from cultured and native bovine aortic endothelial cells. Proc Natl Acad Sci U S A 88, 10480-10484.

Porter, T. D., Kasper, C. B., 1985. Coding nucleotide sequence of rat NADPH-cytochrome P-450 oxidoreductase cDNA and identification of flavin-binding domains. Proc Natl Acad Sci U S A 82, 973-977.

Porter, T. D., Kasper, C. B., 1986. NADPH-cytochrome P-450 oxidoreductase: flavin mononucleotide and flavin adenine dinucleotide domains evolved from different flavoproteins. Biochemistry 25, 1682-1687.

Radi, R., Beckman, J. S., Bush, K. M., Freeman, B. A., 1991. Peroxynitrite oxidation of sulfhydryls. The cytotoxic potential of superoxide and nitric oxide. J Biol Chem 266, 4244-4250.

Raman, C. S., Li, H., Martasek, P., Kral, V., Masters, B. S., Poulos, T. L., 1998. Crystal structure of constitutive endothelial nitric oxide synthase: a paradigm for pterin function involving a novel metal center. Cell 95, 939-950.

Roman, L. J., Martasek, P., Miller, R. T., Harris, D. E., de La Garza, M. A., Shea, T. M., Kim, J. J., Masters, B. S., 2000a. The C termini of constitutive nitric-oxide synthases control electron flow through the flavin and heme domains and affect modulation by calmodulin. J Biol Chem 275, 29225-29232.

Roman, L. J., McLain, J., Masters, B. S., 2003. Chimeric enzymes of cytochrome P450 oxidoreductase and neuronal nitric-oxide synthase reductase domain reveal structural and functional differences. J Biol Chem 278, 25700-25707.

Roman, V., Zhao, H., Fourneau, J. M., Marconi, A., Dugas, N., Dugas, B., Sigaux, F., Kolb, J. P., 2000b. Expression of a functional inducible nitric oxide synthase in hairy cell leukaemia and ESKOL cell line. Leukemia 14, 696-705.

Sagami, I., Daff, S., Shimizu, T., 2001. Intra-subunit and inter-subunit electron transfer in neuronal nitric-oxide synthase: effect of calmodulin on heterodimer catalysis. J Biol Chem 276, 30036-30042.

Salerno, J. C., Frey, C., McMillan, K., Williams, R. F., Masters, B. S., Griffith, O. W., 1995. Characterization by electron paramagnetic resonance of the interactions of L-arginine and L-thiocitrulline with the heme cofactor region of nitric oxide synthase. J Biol Chem 270, 27423-27428.

Scheele, J. S., Bruner, E., Kharitonov, V. G., Martasek, P., Roman, L. J., Masters, B. S., Sharma, V. S., Magde, D., 1999. Kinetics of NO ligation with nitric-oxide synthase by flash photolysis and stopped-flow spectrophotometry. J Biol Chem 274, 13105-13110.

Schmidt, H. H., Smith, R. M., Nakane, M., Murad, F., 1992. Ca2+/calmodulin-dependent NO synthase type I: a biopteroflavoprotein with Ca^{2+}/calmodulin-independent diaphorase and reductase activities. Biochemistry 31, 3243-3249.

Sem, D. S., Kasper, C. B., 1992. Geometric relationship between the nicotinamide and isoalloxazine rings in NADPH-cytochrome P-450 oxidoreductase: implications for the classification of evolutionarily and functionally related flavoproteins. Biochemistry 31, 3391-3398.

Sherman, M. P., Griscavage, J. M., Ignarro, L. J., 1992. Nitric oxide-mediated neuronal injury in multiple sclerosis. Medical hypotheses 39, 143-146.

Sheta, E. A., McMillan, K., Masters, B. S., 1994. Evidence for a bidomain structure of constitutive cerebellar nitric oxide synthase. J Biol Chem 269, 15147-15153.

Siddhanta, U., Presta, A., Fan, B., Wolan, D., Rousseau, D. L., Stuehr, D. J., 1998. Domain swapping in inducible nitric-oxide synthase. Electron transfer occurs between flavin and heme groups located on adjacent subunits in the dimer. J Biol Chem 273, 18950-18958.

Siddhanta, U., Wu, C., Abu-Soud, H. M., Zhang, J., Ghosh, D. K., Stuehr, D. J., 1996. Heme iron reduction and catalysis by a nitric oxide synthase heterodimer containing one reductase and two oxygenase domains. J Biol Chem 271, 7309-7312.

Stuehr, D. J., Cho, H. J., Kwon, N. S., Weise, M. F., Nathan, C. F., 1991a. Purification and characterization of the cytokine-induced macrophage nitric oxide synthase: an FAD- and FMN-containing flavoprotein. Proc Natl Acad Sci U S A 88, 7773-7777.

Stuehr, D. J., Ikeda-Saito, M., 1992. Spectral characterization of brain and macrophage nitric oxide synthases. Cytochrome P-450-like hemeproteins that contain a flavin semiquinone radical. J Biol Chem 267, 20547-20550.

Stuehr, D. J., Kwon, N. S., Nathan, C. F., Griffith, O. W., Feldman, P. L., Wiseman, J., 1991b. N omega-hydroxy-L-arginine is an intermediate in the biosynthesis of nitric oxide from L-arginine. J Biol Chem 266, 6259-6263.

Stuehr, D. J., Nathan, C. F., 1989. Nitric oxide. A macrophage product responsible for cytostasis and respiratory inhibition in tumor target cells. J Exp Med 169, 1543-1555.

Vasquez-Vivar, J., Martasek, P., Hogg, N., Masters, B. S., Pritchard, K. A., Jr., Kalyanaraman, B., 1997. Endothelial nitric oxide synthase-dependent superoxide generation from adriamycin. Biochemistry 36, 11293-11297.

Vermilion, J. L., Coon, M. J., 1978. Purified liver microsomal NADPH-cytochrome P-450 reductase. Spectral characterization of oxidation-reduction states. J Biol Chem 253, 2694-2704.

Wang, M., Roberts, D. L., Paschke, R., Shea, T. M., Masters, B. S., Kim, J. J., 1997. Three-dimensional structure of NADPH-cytochrome P450 reductase: prototype for FMN- and FAD-containing enzymes. Proc Natl Acad Sci U S A 94, 8411-8416.

White, K. A., Marletta, M. A., 1992. Nitric oxide synthase is a cytochrome P-450 type hemoprotein. Biochemistry 31, 6627-6631.

Workman, P., 1992. Bioreductive mechanisms. International journal of radiation oncology, biology, physics 22, 631-637.

Ye, Y. Z., Strong, M., Huang, Z. Q., Beckman, J. S., 1996. Antibodies that recognize nitrotyrosine. Methods Enzymol 269, 201-209.

Zhang, J., Martasek, P., Paschke, R., Shea, T., Siler Masters, B. S., Kim, J. J., 2001. Crystal structure of the FAD/NADPH-binding domain of rat neuronal nitric-oxide synthase. Comparisons with NADPH-cytochrome P450 oxidoreductase. J Biol Chem 276, 37506-37513.

Chapter 1: Naphthoquinones and Bioactive Compounds from Tobacco as Modulators of Neuronal Nitric Oxide Synthase Activity

1.1 Introduction

There are three main isoforms of nitric oxide synthase (NOS), neuronal (nNOS), endothelial (eNOS) and inducible (iNOS) (Bredt and Snyder, 1990; Forstermann *et al.*, 1991a; Hibbs, 1991; Ignarro *et al.*, 1987a; Stuehr and Nathan, 1989). Each NOS isoform is BH_4- and O_2-dependent (Mayer *et al.*, 1990) and, utilizing NADPH as a co-substrate, NOS catalyzes the conversion of *L*-arginine to *L*-citrulline plus NO• (Kwon *et al.*, 1990).

Although all three NOS isoforms metabolize *L*-arginine to yield the same products, *L*-citrulline and NO•, the function of the NO• that is produced varies widely depending on the tissue type and location (Ignarro, 1990b). For example, NO• produced by eNOS modulates vascular dynamics (blood pressure and blood flow) *via* interactions with smooth muscle cells of the vascular endothelium (Furchgott and Vanhoutte, 1989; Ignarro *et al.*, 1988; Pollock *et al.*, 1991). NO• produced by nNOS modulates chemical messaging within the central nervous system (Knowles *et al.*, 1989) while NO• produced in activated macrophages by iNOS is used for cellular defense (Hibbs *et al.*, 1988). The beneficial effects of NO• occur, for the most part, at low NO• concentrations (high nM to low μM) and/ or in controlled cellular microenvironments. However, when excessive NO• is produced, tissue damage may occur. It has been suggested that both iNOS and nNOS may produce copious amounts of NO• during the course of many neurodegenerative disease states, spinal injury, as well as during and after stroke.

During stroke, the highly regulated production of NO• by nNOS (early phase) and iNOS (late phase) becomes dysregulated, leading to elevated local concentrations of not only NO•, but

also NO•-derived reactive oxygen species (ROS) and reactive nitrogen species (RNS) (Ischiropoulos *et al.*, 1995; Thom *et al.*, 1997). The elevated levels of ROS and RNS under stroke may increase the extent of damage resulting from the brain infarct (Huang *et al.*, 1994; Nagafuji *et al.*, 1992). Studies with rodent models of stroke suggest that prevention of NO• overproduction during and immediately after stroke using nNOS inhibitors, help avoid the accumulation of NO• to toxic levels and thus decreases brain infarct size (Ashwal *et al.*, 1994; Chabrier *et al.*, 1999; Goyagi *et al.*, 2001; Spinnewyn *et al.*, 1999; Zhang *et al.*, 1996; Zhao *et al.*, 2000). On the other hand, gene knockout studies in mice have suggested that production of NO• by eNOS, immediately after stroke, can be beneficial in limiting ischemic damage by helping to maintain tissue perfusion, and thus oxygenation within the area affected by the stroke (Huang *et al.*, 1996). Collectively, these observations suggest that targeted drug development, aimed at identifying selective inhibitors of nNOS and iNOS could lead to promising treatments for patients experiencing ischemic stroke (Dalkara and Moskowitz, 1994; Willmot *et al.*, 2005). It is clear that treatments for stroke, targeted at modulating the NO• pathway, will depend on the identification of NOS inhibitors which possess absolute specificity for the desired NOS isoform.

In addition to its role in modulating tissue damage in many neurodegenerative diseases and stroke, the NO• pathway is also actively involved in modulating neurotoxicity originating from environmental exposure to various chemicals including those present in both tobacco leaf as well as tobacco smoke. Tobacco smoke is composed of pyrolysis or pyrosynthesis products of leaf tobacco and possesses thousands of bioactive compounds (Green, 1996; Stedman, 1968). More recently, studies have focused on identifying nNOS inhibitors present in aqueous extracts of cigarette tobacco (Demady *et al.*, 2003) as well as in tobacco leaves (Lowe *et al.*, 2005).

Earlier studies reported that the aqueous extracts of cigarette tar contained a quinone-semiquinone-hydroquinone cycling system. The auto-oxidizable compounds present in this redox-cycling system of cigarette tar (Schmeltz *et al.*, 1977) was suggested to act as a source for the production of ROS, such as superoxide ($O_2^{\bullet-}$), *via* NAD(P)H-dependent mechanisms (Winston *et al.*, 1993). Since many redox-active compounds, such as quinones, possess the ability to interact with NAD(P)H-dependent, flavin-containing enzyme systems, we have focused on identifying compounds derived from tobacco leaves of various varieties that interact with nNOS to regulate its activity.

Studies utilizing tobacco leaves as a targeted library for identifying possible treatments for Parkinson's disease have uncovered an inhibitor of (another flavoenzyme like NOS) monoamine oxidase–A (MAO-A), 2,3,6-trimethyl-1,4-naphthoquinone (TMN) (Khalil *et al.*, 2000). TMN which was isolated from burley tobacco leaves or smoke and characterized by the Castagnoli group, produced inhibition of both human MAO-A and MAO-B (Khalil *et al.*, 2006; Khalil *et al.*, 2000). Also, *in vivo* studies with mice demonstrated that TMN was neuroprotective in the MPTP model of neurodegeneration (Castagnoli *et al.*, 2003). In order to understand if TMN, a tobacco-derived quinone compound can potentially modulate nNOS activity, we performed nNOS activity assays, using menadione as a positive control.

The following studies describe: 1) the properties of potentially novel nNOS inhibitor(s) derived from hexane tobacco extracts of the TI-1565 tobacco variety, and 2) the concentration-dependent, modulatory effects of the tobacco-derived quinone compound, TMN on nNOS activity. These studies provide insight into the mechanistic events leading up to, and during, modulation of nNOS activity. Furthermore, these studies provide a foundation for planning and

conducting future investigations into the interactions of bioactive compounds derived from tobacco with various enzyme systems.

1.2 Experimental Procedures

Chemicals: 4-(2-hydroxyethyl)-1-piperazineethanesulfonic acid (HEPES), *L*-arginine·HCl, $CaCl_2 \cdot 4H_2O$, bovine brain calmodulin (CaM), (6*R)*-5,6,7,8-tetrahydro-*L*-biopterin (BH_4), reduced nicotinamide adenine dinucleotide phosphate (NADPH), *L*-citrulline, ethylenediaminetetraacetic acid (EDTA), 2-methyl-1,4-naphthoquinone (menadione) and dimethyl sulfoxide (DMSO) were purchased from Sigma (St. Louis, MO). Dowex 50WX8 was purchased from Supelco (Bellefonte, PA). [^{14}C]-*L*-arginine (313 mCi/mmol) was obtained from American Radiolabel Chemicals (St. Louis, MO). Hexane, formic acid, acetonitrile and Scinti-Safe Plus 50%^{TM} scintillation cocktail were purchased from Fisher Scientific. All other chemicals were from common suppliers and were of the highest grade commercially available.

Enzymes: Recombinant nNOS was over-expressed in *E. coli* and purified according to established methodology (Roman *et al.*, 1995).

Tobacco: Several varieties of tobacco seeds, *Nicotiana tabacum* (TI-464, TI-1565), *Nicotiana sandarae* (TW-152), *Nicotiana raimondii* (TW-109), *Nicotiana noctiflora* (TW-88) and *Nicotiana nesophila* (TW-87), were generously provided by Verne A. Sisson, Oxford Tobacco Research Station, North Carolina State University. These varieties of tobacco were grown under identical conditions in a greenhouse. Leaves were collected at maturity (~ 85 days), washed with de-ionized, distilled water and dried at 30°C in a dehydrator under a stream of filtered ambient air. The different dried tobacco leaves were then milled to generate fine powders which were stored at room temperature in air-tight tubes for later extractions. Tobacco powders were sequentially extracted in a three-step process utilizing different solvents, hexane (non-polar;

lipophilic), methanol (polar; amphiphilic) and water (polar). For routine extractions, 2.5 g of the desired tobacco powder was placed in a beaker containing 100 ml of hexane and mechanically stirred overnight. The resulting suspension was vacuum-filtered using a buchner funnel and Whatman # 1 paper. The hexane extract was stored and the resulting solids were transferred to a beaker containing 100 ml of methanol. Again, the solids were rapidly stirred overnight, vacuum-filtered with Whatman # 1 paper, and the resulting solids extracted with deionized, distilled water utilizing the same overnight procedure. Each individual liquid extract was stripped of organic solvent (hexane, methanol) by rotary evaporation and lyophilized. The aqueous extracts were frozen over dry ice/acetone and lyophilized. The weight of each individual extract (powder or oil) was recorded along with starting tobacco powder weight. Extracts were then stored in a dessicator at -20°C until use.

Isolation and Purification of TMN: Burley tobacco were obtained from Murty Pharmaceuticals Inc. (Lexington KY) and, TMN was isolated and purified by the laboratory of Dr. Neal Castagnoli, as described previously (Khalil *et al.*, 2000).

[^{14}C]-L-arginine to [^{14}C]-L-citrulline conversion assay: The conversion of [^{14}C]-*L*-arginine to [^{14}C]-*L*-citrulline was used to estimate NOS activity. Dose-response relationships were established by titrating aliquots of the reconstituted tobacco extracts into the assay incubations. nNOS activity was determined in 250 µl reactions essentially as described previously (Nishimura *et al.*, 1999). nNOS reactions consisted of (final assay concentrations), *L*-arginine·HCl (20 µM) containing [^{14}C]-*L*- arginine (0.14 µCi), $CaCl_2 \cdot 2H_2O$ (200 µM), CaM (200 nM), BH_4 (5 µM), NADPH (100 µM) and nNOS (30nM) in 50 mM HEPES/KOH, pH 7.5. Lyophilized tobacco

extracts were dissolved in water (aqueous extract), 10% DMSO in 50 mM HEPES (methanol extract) or DMSO (hexane extract). TMN or menadione were dissolved in 100 % DMSO. Depending on the experiment, either the tobacco extracts, or TMN or menadione were added to the assay. Reactions were initiated by the addition of nNOS. Incubations were run for 5 mins at 23°C. Reactions were then quenched with an ice-cold stop solution consisting of 1 mM *L*-citrulline and 10 mM EDTA in 100 mM HEPES, pH 5.5. Dowex columns were prepared by converting the resin to the Na^+ form by exposure to 5M NaOH for 20 mins followed by a water wash which was repeated 3-4 times or until the pH approached neutrality (~ pH 7.2). Two ml of resin was then used to prepare each column. Quenched reaction mixtures were placed on previously prepared Dowex columns and then washed twice with 1mL portions of deionized water to effect elution of [^{14}C]-*L*-citrulline. The amount of ^{14}C present as *L*-citrulline in the eluate was determined by liquid scintillation spectroscopy over a 2 min period. Control values from incubations containing all ingredients except enzyme and vehicle, were subtracted from all data points. Values from incubations containing all required cofactors and substrates, but excluding tobacco extract were considered as the basal control activity. Data are expressed as the mean ± s.d. of the mean from duplicate determinations from three independent experiments and were analyzed using Sigma Plot 9.0 (Systat Software, Inc.).

***NADPH Oxidation*:** The assay for nNOS-mediated NADPH oxidation consisted of 50 mM HEPES (pH 7.5), 100 μM *L*-arginine, 200 μM $CaCl_2$, 100 μM NADPH, 110 pmol CaM and +/- TMN or menadione (0-500μM). Reactions were started by adding 30 pmoles of nNOS to the appropriate 1 ml incubations. Reactions were monitored spectrophotometrically and the decrease in absorbance at 340 nm was monitored for 60 seconds at 23°C. Control incubations

contained all ingredients except nNOS. The initial linear rate of NADPH oxidation was read against a "no nNOS" control. The rate of conversion of NADPH to $NADP^+$ was calculated using €= 6.22 $mM^{-1}cm^{-1}$ (Horecker and Kornberg, 1948).

***High Performance Liquid Chromatography (HPLC) Analysis of Tobacco Extracts*:** Chromatograms of the different tobacco extracts were obtained with a Shimadzu SCL-10AVP HPLC system equipped with a semi-preparative column (Beckman Coulter ™ ODS 10 mm x 250 mm) at a flow rate of 2 ml/min. The eluate was monitored at 276 nm. Binary gradient elution was used to effect separation of the constituents present in the extracts from the different varieties of tobacco. The mobile phase solvents were acetonitrile (ACN) and 0.1% formic acid. The specific gradients used for separations were method A, ACN, 50%-100%, 30 min linear gradient for initial fractionation and method B, ACN, 50%-75%, 20 min linear gradient, followed by ACN, 75%-100%, 10 min linear gradient for sub-fractionation of TI-1565.

***Mass Spectrometric Analyses*:** Mass analyses were conducted using mass spectrometry (MS) with electro-spray ionization (ESI) to probe HPLC peak fractions of the various tobacco extracts for predominant ions. Metal content was determined using ICP-OES. ICP-OES was used to analyze fractions of HPLC eluate from hexane extracts of TI-1565 for the presence of metal(s). MS and ICP-OES analyses were conducted in the Dept. of Chemistry at the University of Kentucky, Lexington, KY.

1.3 Results and Discussion

Inhibition of L-citrulline Production by Tobacco Extracts: [^{14}C]-*L*-arginine to [^{14}C]-*L*-citrulline conversion assays were performed (see ***Experimental Procedures***) in the presence of different tobacco varieties that were extracted in hexane, methanol and water. Incubation containing all ingredients including nNOS except tobacco extract was considered as the basal control activity level. The vehicles of tobacco extracts were tested alone and had no significant effect on nNOS activity in the amounts used for experimentation. Results, showing the amount of inhibition of *L*-citrulline production by tobacco varieties, are grouped according to the particular solvent used for tobacco extraction:

Hexane: Hexane extracts of the five tobacco varieties designated TI-1565, TI-464, TW-109, TW-88 and TW-152 were potent nNOS inhibitors (60 - 86% inhibition of *L*-citrulline production) (Fig. 1.1). Inhibition of *L*-citrulline production was observed even at the lowest concentration (125 μg/ml) tested. With the exception of TW-109, the hexane extracts of these tobacco varieties were by far more inhibitory of nNOS-catalyzed *L*-citrulline production than the corresponding methanol or aqueous extracts.

Methanol: Methanol extracts of TW-88 and TI-1565 showed a moderate inhibition (40 - 68% inhibition) of *L*-citrulline production (Fig. 1.2). Furthermore, this inhibition occurred only at their higher concentrations indicating that these methanol extracts were less potent inhibitors of nNOS relative to the corresponding hexane extracts. Other tobacco varieties (TW-87, TW-109, TI-464, and TW-152) could not be tested due to their poor solubility in the vehicle which resulted in very low concentration of the stock solutions. No attempts were made to increase solubility of these extracts.

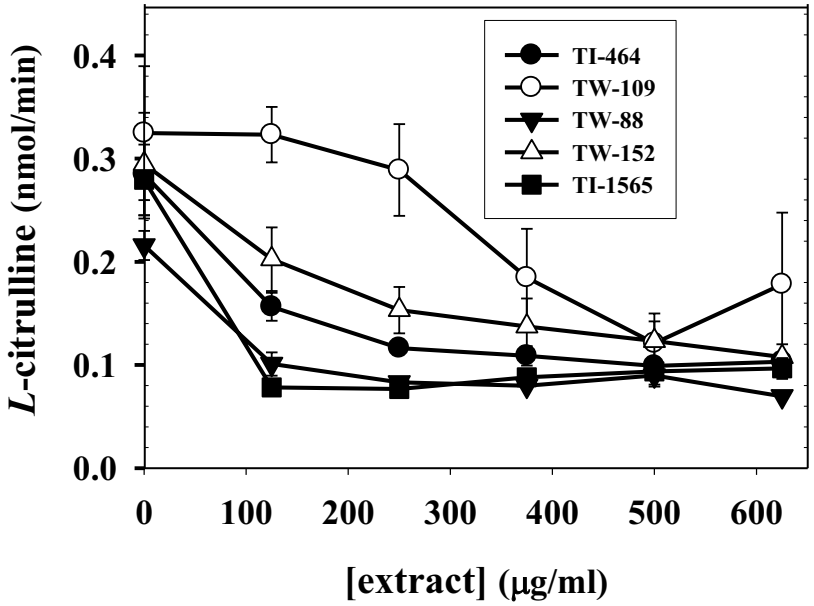

Fig. 1.1. Concentration-dependent inhibition of *L*-citrulline production by hexane extracts of TI-464, TW-109, TW-88, TW-152 and TI-1565. Data are expressed as the mean ± s.d. of duplicate samples from three independent experiments. The vehicle used was DMSO. Control values from incubations containing all ingredients except enzyme and vehicle, were subtracted from all data points.

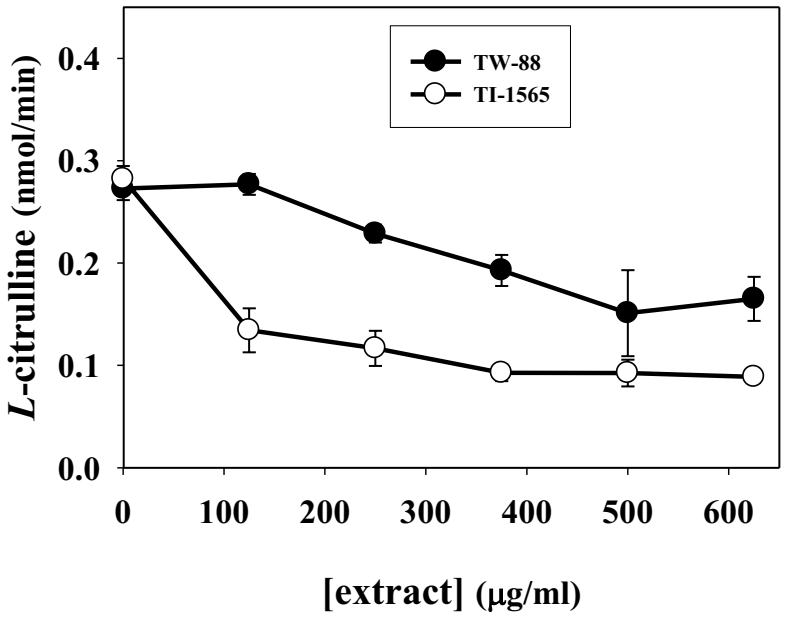

Fig. 1.2. Concentration-dependent inhibition of *L*-citrulline production by methanol extracts of TW-88 and TI-1565. Data are expressed as the mean ± s.d. of duplicate samples from three independent experiments. The vehicle was 10 % DMSO in 50 mM HEPES. Control values from incubations containing all ingredients except enzyme and vehicle, were subtracted from all data points.

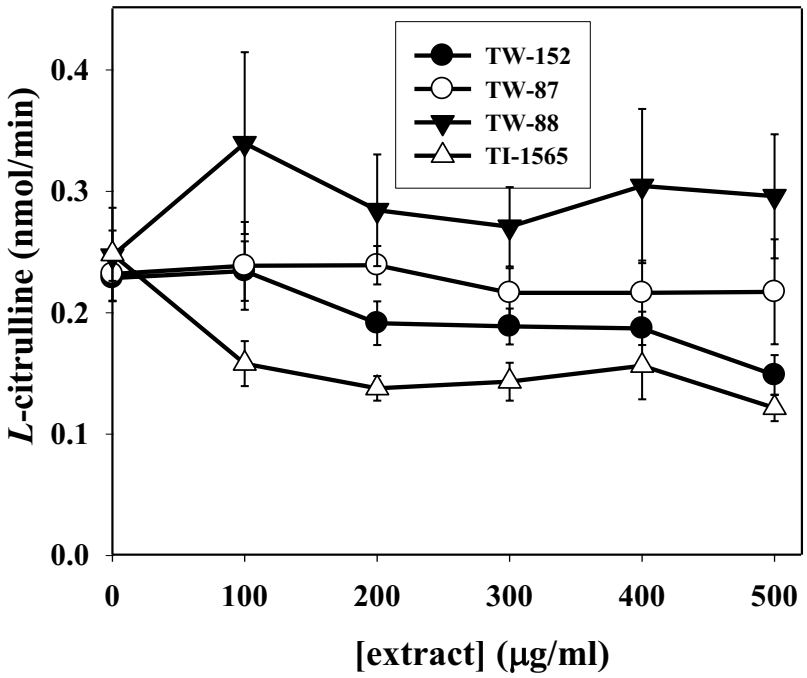

Fig. 1.3. Concentration-dependent inhibition of *L*-citrulline production by aqueous extracts of TW-152, TW-87, TW-88 and TI-1565. Data are expressed as the mean ± s.d. of duplicate samples from three independent experiments. The vehicle used was dH_2O. Control values from incubations containing all ingredients except enzyme and vehicle, were subtracted from all data points.

Water: Minimal inhibition of *L*-citrulline production (< 35% inhibition) was observed when nNOS was exposed to aqueous extracts of TI-1565, TW-88, TW-87 and TI-152 (Fig. 1.3). Other tobacco varieties (TW-109 and TI-464) could not be tested due to their poor solubility in the vehicle. With the exception of the aqueous extract from TI-1565 (~50% inhibition of *L*-citrulline production), results indicated that, when compared to hexane or methanol extracts, the aqueous extracts were essentially not active as potent nNOS inhibitors in this system.

Collectively, these results suggest that inhibition of *L*-citrulline production by nNOS was dependent on the tobacco variety as well as the amount and apparent physico-chemical properties of the compounds contained in the various tobacco extracts. The rank-order potency of the tobacco extracts, in general, as inhibitors of *L*-citrulline production, based on the solvent of extraction, hexane > methanol > water. From these observations, the most potent inhibitor(s) of *L*-citrulline production by nNOS are most likely non-polar and lipophilic in nature due to their extraction into hexane. Based on the higher nNOS inhibitory potency of hexane extracts relative to the corresponding methanol and aqueous extracts (Figs. 1.1, 1.2 and 1.3), all subsequent efforts to isolate inhibitors of nNOS involved fractionation of the hexane extracts of the various tobacco varieties.

Qualitative HPLC Analyses of Hexane Extracts: Three different hexane extracts, TI-1565, TW-109 and TI-464 displaying high, moderate, or low nNOS inhibition, respectively, by [^{14}C]-*L*-arginine to [^{14}C]-*L*-citrulline conversion assay (Figs. 1.1, 1.2 and 1.3). Qualitative comparisons of the chromatograms were made by using reverse phase-HPLC. Individual lyophilized aliquots of each of these hexane extracts were separately dissolved at a concentration of 100 mg/ml in

hexane. One hundred µl of each solution was then analyzed by semi-preparative, reverse-phase HPLC with UV/Vis detection.

In comparing chromatograms from the three different varieties of tobacco, it was clear that each hexane extract possessed a unique and distinct chromatographic profile (Fig. 1.4). Obviously, differences in the amounts of the specific constituents and/or types of compounds present in the three different varieties of tobacco are responsible for the unique chromatographic profiles of the three various hexane extracts. It is tempting to speculate that differences in the detected (major) constituents, contained in each different variety of tobacco, are responsible for the differential nNOS inhibitory potencies of the extracts. However, differences in the potent inhibitor(s) present in small amounts in the three tobaccos should receive equal consideration.

Sub-Fractionation of the Hexane Extract of TI-1565: To investigate the nature of the compound(s) responsible for the nNOS inhibition, the hexane extract of the potent, inhibitory TI-1565 was sub-fractionated. HPLC eluates of TI-1565 were collected at intervals of 5 min following injection onto a reversed-phase column as described in *'**Experimental Procedures**'* (method A). The acetonitrile (ACN) was stripped from each pooled fraction by rotary evaporation and the aqueous volume further reduced (to 25 µl) by vacuum centrifugation (Jouan, Inc., VA) at 45°C. Five µl of the resulting concentrated sample from each consecutive 5 min interval was incorporated into the [^{14}C]-*L*-arginine to [^{14}C]-*L*-citrulline conversion assay and screened for inhibitory activity towards nNOS.

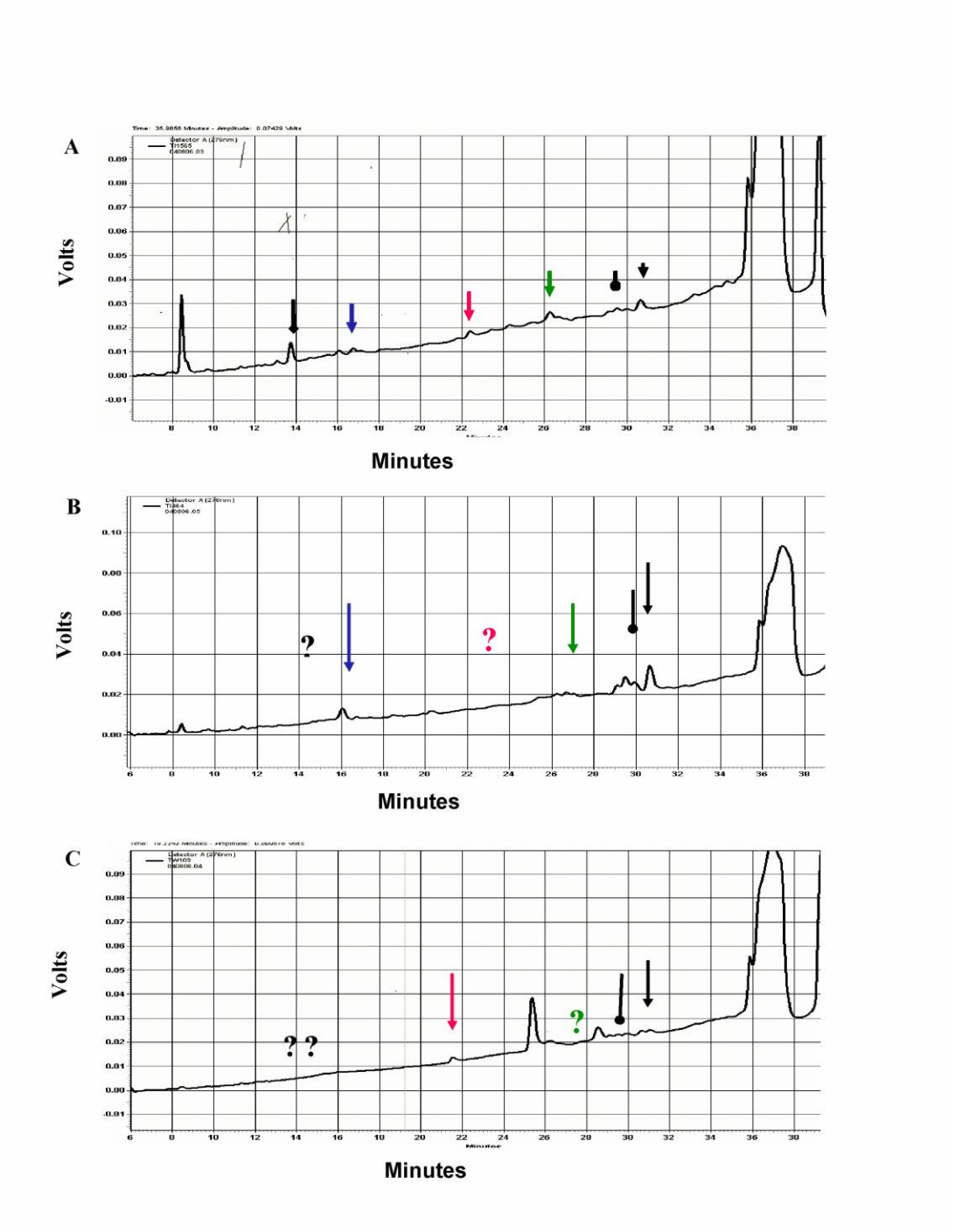

Fig. 1.4. Chromatograms of the hexane tobacco extracts of: A) TI-1565, B) TI-464 and C) TW-109. The chromatograms from the different varieties of tobacco showed unique and distinct chromatographic profiles**.**

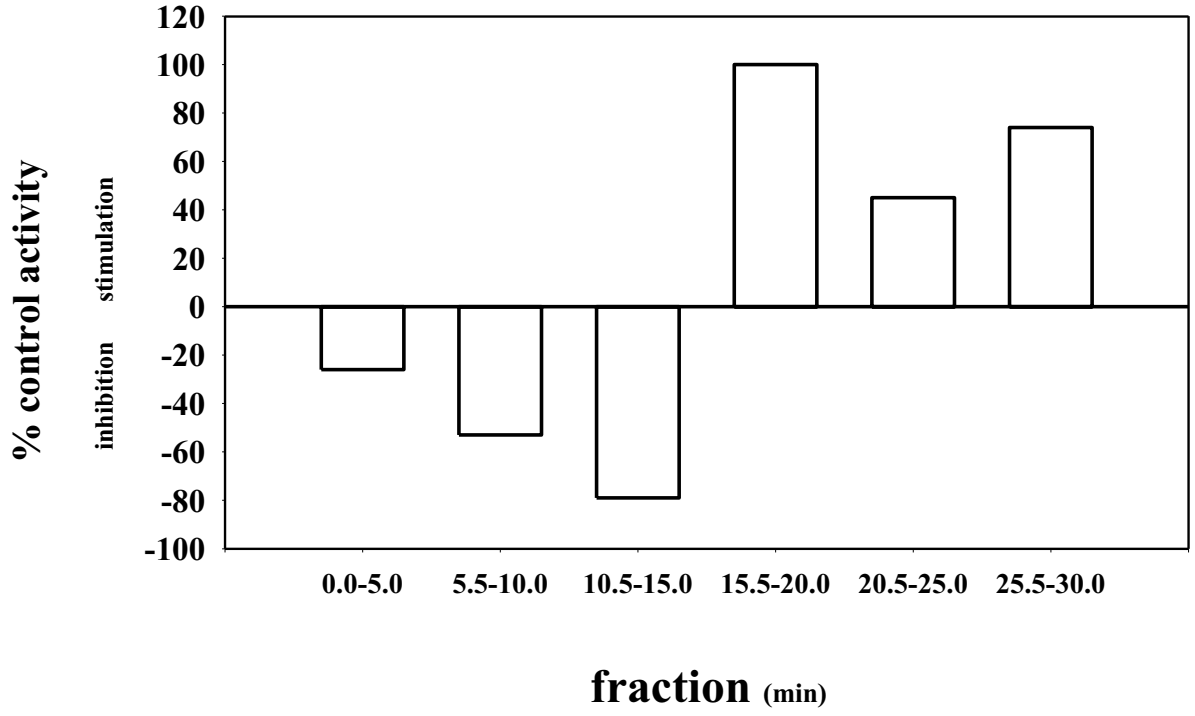

Fig. 1.5. nNOS-catalyzed *L*-citrulline production by successive 5 min-HPLC fractions of TI-1565.

Results indicated that, with each successive 5 min sub-fraction that eluted between 0-15 min, there was an increase in percentage of inhibition of *L*-citrulline production catalyzed by nNOS (Fig. 1.5). Although these studies were initially focused on identifying inhibitors of nNOS activity, quite unexpectedly, each fraction eluting between 15-30 min produced an increase in nNOS-catalyzed *L*-citrulline production indicating that there are both nNOS stimulating as well as inhibiting compound(s) in tobacco. Also, these results imply that a lipophilicity limit exists for compounds to illicit potent inhibition of nNOS.

During normal steady-state catalysis, nNOS is end-product inhibited, putatively up to 80%, due to the ability of the enzymatically-produced NO• to re-bind the heme iron from which it was originated (Abu-Soud *et al.*, 1996; Abu-Soud *et al.*, 1995; Ignarro, 1990b; Scheele *et al.*, 1999). Of those compounds that were identified as constituents of tobacco extract and/ or tobacco smoke, both quinones and nitroarenes can interact with the nNOS flavins and lead to increased production of $O_2^{\bullet-}$ (Kumagai *et al.*, 1998; Miller *et al.*, 1997; Vasquez-Vivar *et al.*, 1997a). $O_2^{\bullet-}$ acts as a trap for the enzymatically-generated NO• resulting in formation of potent oxidant, peroxynitrite ($ONOO^-$) at an almost diffusion-limited reaction rate (Huie and Padmaja, 1993) ($6.7 \times 10^9\ M^{-1}\ s^{-1}$; Scheme 1.1). This reaction lowers the free NO• concentration and causes a decrease in the extent of NO•-mediated auto-inhibition of nNOS (Griscavage *et al.*, 1995). This decreased level of nNOS auto-inhibition by NO• is then responsible for the concomitant corresponding increase in the rate of production of NO• and *L*- citrulline. Compounds that increase product formation by NOS are, for the most part, redox-active (quinones / nitroarenes) or contain a redox-active metal. A mechanism such as this may very

well account for the activation of nNOS that was observed in the present system following exposure of nNOS to various complex tobacco extracts.

In order to narrow the overall number of compounds in TI-1565 which could mediate nNOS inhibition, further sub-fractionation of the above-mentioned 5 min HPLC eluates displaying nNOS inhibition was performed. Separate 0.5 min HPLC eluate fractions of TI-1565 were collected and the fractions were concentrated and the aqueous volume was further reduced (to 30 µl) as mentioned earlier. 5 µl of the resulting concentrated sample of every 0.5 min interval fraction was incorporated into the [^{14}C]-*L*-arginine to [^{14}C]-*L*-citrulline conversion assays and screened for nNOS activity. Results showed that, the fraction eluting between 12.0-12.5 min produced the greatest degree of inhibition of *L*-citrulline production (~30 %, data not shown). Not surprisingly, no one single 0.5 min fraction (except 12.0-12.5 min fraction) produced the degree of nNOS inhibition that was observed with the initial 5 min fractions. We had expected to lose inhibitory activity at some point due to the ever-smaller fraction sizes of HPLC eluate which contained lower amounts of potential nNOS-inhibitory compounds. However, we did also observe many 0.5 min fractions of HPLC eluate which possessed the ability to stimulate nNOS activity.

***Mass Spectrometric Analyses and Sub-Fractionation of TI-1565*:** During HPLC analyses of hexane extracts of TI-1565, six predominant peaks were observed and the corresponding HPLC eluates were collected for further study by ElectroSpray Ionization-coupled Mass Spectrometry (ESI-MS). Results from the mass spectrometric analyses indicated that the fraction eluting between 12.0 and 12.5 min (corresponded to peak 5; data not shown) which produced maximal inhibition of *L*-citrulline production by nNOS, generated a predominant ion at an m/z value of

359. Eluate containing this ion was subjected to further fragmentation by tandem MS (MS/MS). However, interpretation of the resulting daughter ion profile was inconclusive.

Considering that a predominant mass ion peak was observed during MS analysis of the 12.0 - 12.5 min HPLC fraction (method A), and that the maximal nNOS inhibitory activity was contained within the 10-15 min fraction by HPLC eluate (method A), the time interval of 9-13 min was chosen for further sub-fractionation of HPLC. As a next step to further decrease the complexity of the fraction responsible for nNOS inhibition yet maintain an adequate concentration of putative inhibitor(s), fractions of HPLC eluate collected between 9-13 min from several runs were pooled and concentrated. Since the resulting 9-13 min pooled fraction of HPLC eluate still contained many compounds, the HPLC method was changed to method B as described in ***'Experimental Procedures'*** in an effort to further resolve peaks and thus increase purity upon isolation of potential nNOS inhibitory compounds. When method B was employed, the original 9-13 min fraction (method A) eluted between 21-29 min. Using method B, the 0.5 min fractions of HPLC eluate between 21-29 min were collected and pooled from 8 individual HPLC runs. The fractions were concentrated and the volume was reduced to 20 µl as mentioned earlier. Five µl of the resulting concentrated samples were incorporated into the [^{14}C]-*L*-arginine to [^{14}C]-*L*-citrulline conversion assays. Results showed significant nNOS inhibition (~60%) with 0.5 min fractions eluting between the 28-29 min which corresponded to the ~ 12-13 min eluate fraction from HPLC method A. Due to the nature of the isolation and concentration steps, recovery of this inhibitory constituent indicated that the nNOS inhibitor in this fraction from TI-1565 was non-volatile in nature. However, except for the fractions between 28-29 min, there was no significant inhibition of nNOS activity (less than 20%) produced by any of the other 0.5

min fractions (eluting between 21-29 mins). Despite our best efforts to increase or maintain the concentration of putative nNOS inhibitor(s), the lack of inhibition was again most likely due to sample dilution and thus reduction in the concentrations of constituents present in each subsequent sub-fractionation. We speculate that the concentration of putative inhibitor(s) left in these sub-fractions was too low to produce significant inhibition of nNOS.

Interestingly, the major inhibitory fraction eluted between 28 - 29 min (corresponding to 12- 13 min eluate of method A), on pooling over several runs and concentrating to a final volume of 20µl, appeared blue in color. Using Inductively Coupled Plasma-Optical Emission Spectrometry (ICP-OES), we probed the sample for metal content using copper, cobalt, nickel, chromium and vanadium. Results indicated the presence of trace amounts of copper in the concentrated sample. Copper levels were however, far from being stoichiometric amounts. When the [^{14}C]-*L*-arginine to [^{14}C]-*L*-citrulline conversion assay was performed in the presence of authentic copper sulfate or copper chloride (up to 10 mM each), there was no loss of *L*-citrulline production (data not shown) indicating that copper, by itself, or in these salt forms does not cause nNOS inhibition. However, if not a metal, the distinct color of the sample tempts us to further speculate that the nNOS inhibitory compound could be organic in nature and possess conjugated double bonds resulting in the blue color. Quinones, for example, exhibit various colors depending on number of double bonds and/or oxidation state. Studies are needed to further characterize the physical and chemical properties of the nNOS inhibitory compound(s) in tobacco.

***Differential Regulation of nNOS Activity by Naphthoquinones*:** In parallel with the investigations to identify nNOS inhibitors from tobacco extracts, studies were initiated using

2,3,6-trimethyl-1,4-naphthoquinone (TMN), a tobacco-derived flavoprotein inhibitor, and the structurally related 2-methyl-1,4-naphthoquinone (menadione) to evaluate their inhibitory effects on nNOS activity. TMN was isolated from burley tobacco leaves as described (Khalil *et al.*, 2000) Concentration-response curves were generated for the TMN- and menadione- mediated regulation of *L*-citrulline production by nNOS, using the [^{14}C]-*L*-arginine to [^{14}C]-*L*-citrulline conversion assay. The use of menadione as a standard or positive control, for redox-cycling allowed us to compare the concentration-dependent effects of TMN on nNOS activity. Assays without menadione or TMN were used as control to estimate the stimulation or loss of stimulation of *L*-citrulline production by nNOS. Control values from incubations containing all ingredients except enzyme and/or vehicle, were subtracted from all data points.

Menadione: When lower concentrations of menadione (0 - 31μM) were titrated into the [^{14}C]-*L*-arginine to [^{14}C]-*L*-citrulline conversion assay, the rate of *L*-citrulline production by nNOS was progressively stimulated (Fig. 1.6A) and it reached a maximum stimulation at 6.25 μM (67 ± 0.01 % increase above 'no menadione' control) concentration of menadione and plateaued. On the other hand, when higher concentrations of menadione (62.5 - 500 μM) were titrated against nNOS, stimulation of the *L*- citrulline production rate was lost in a concentration-dependent manner (Fig. 1.6A). This loss of stimulation continued well below the'no menadione' control activity (78± 0.01% decrease below 'no menadione' control) at 500 μM, which was the limit of solubility of menadione in our system.

TMN: When low concentrations of TMN (0 - 31 μM) were titrated into the [^{14}C]-*L*-arginine to [^{14}C]-*L*-citrulline conversion assay, an increase in *L*-citrulline production (~40% above 'no TMN' control) was observed from 0.39 μM to 31 μM (Fig. 1.6C). In contrast, when

higher TMN concentrations (62.5 - 500 μM) were incorporated into the assay, stimulation of the rate of *L*- citrulline production was gradually lost in a concentration-dependent manner (27 ± 0.04% decrease from the maximum *L*-citrulline production rate at 62.5μM), up to 500 μM which was also the limit of solubility of TMN in our system (Fig. 1.6D). Here, the loss of stimulation of *L*-citrulline production did not go below the 'no TMN'control activity.

Both menadione and TMN, at lower concentrations stimulated *L*- citrulline production by nNOS in a concentration-dependent manner (Fig. 1.6A & Fig. 1.6C). Redox cycling agents and/or electrophiles can alter nNOS activity by different mechanisms. Quinones, in general, can influence nNOS activity in two ways, 1) by acting as single-electron acceptors which then autoxidizes to create a redox cycle and/or 2) by binding to protein thiol or lysine groups resulting in covalent modification of the nNOS protein. Quinones can act as single-electron acceptors from flavoprotein reductases (Iyanagi, 1990; Iyanagi and Mason, 1973; Matsuda *et al.*, 2000) such as the nNOS reductases and NADPH-cytochrome P450 oxidoreductase to yield a semiquinone radical. The semiquinone radical then transfers its one electron to O_2 *via* auto-oxidation to yield $O_2^{\bullet-}$ (Kappus and Sies, 1981; Kumagai *et al.*, 1998). The resulting redox-cycle then results in unchecked reduction of O_2 concentration and concomitant production of $O_2^{\bullet-}$ at the expense of reduced pyridine nucleotide (NADPH) oxidation. The increase in nNOS activity observed at various concentrations of TMN and menadione is most likely due to increased $O_2^{\bullet-}$ production from this futile redox cycle which traps the NO• produced by nNOS and prevents, at least part, of the NO• -mediated end-product inhibition (Scheme 1). When higher concentrations of TMN and menadione (62.5 -500 μM) were incorporated into assays, both compounds

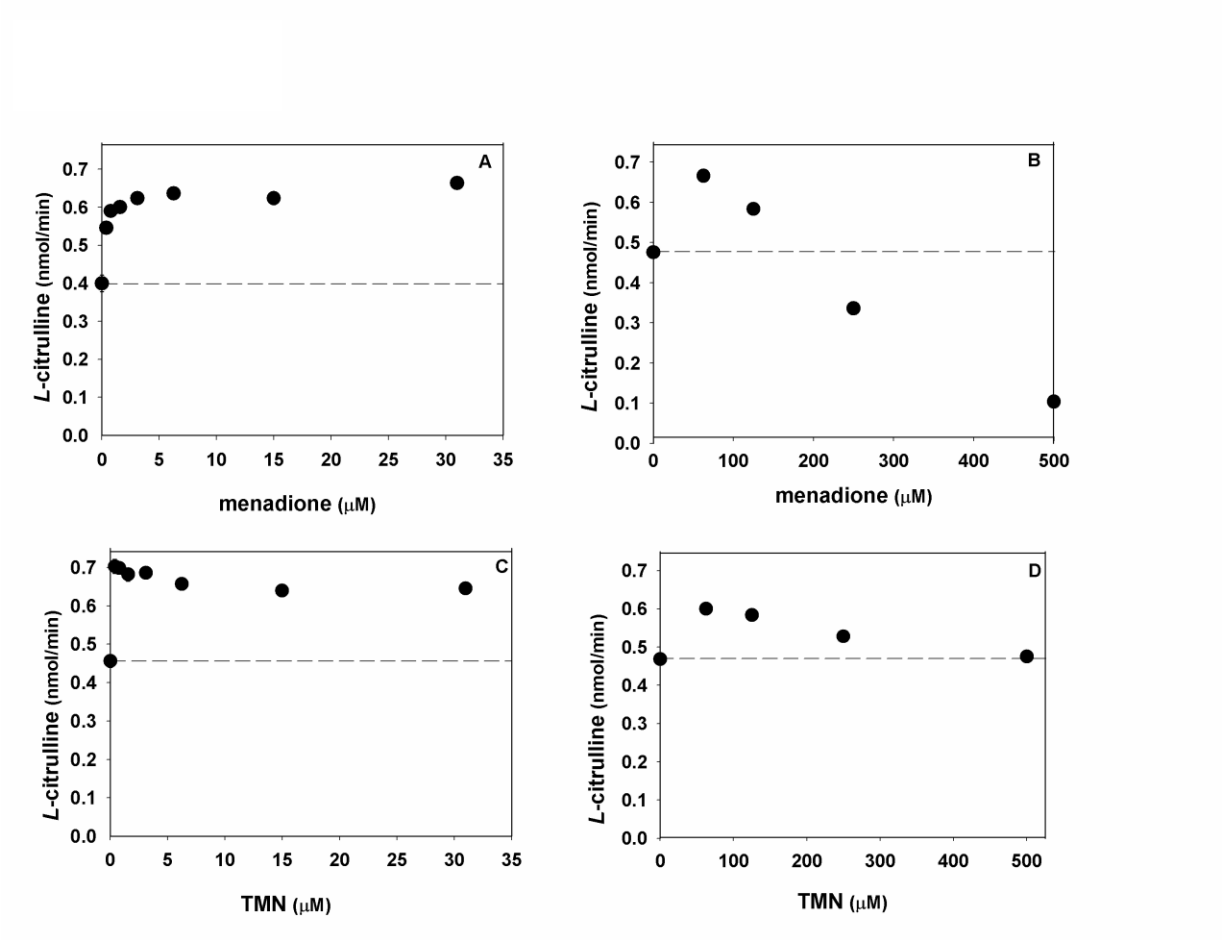

Fig. 1.6. Regulation of nNOS-catalyzed *L*-citrulline production by menadione or TMN. [^{14}C]-*L*-arginine to [^{14}C]-*L*-citrulline conversion assays were performed wherein A) a lower concentration range of menadione (0 - 31 μM), B) a higher concentration range of menadione (62.5 - 500 μM), C) a lower concentration range of TMN (0 - 31 μM), D) a higher concentration range of TMN (62.5 - 500 μM) were used. Data are expressed as the mean ± s.d. of triplicate samples from three independent experiments. The vehicle used was DMSO. Control incubations contained all ingredients except enzyme. Control values from incubation containing all ingredients including nNOS except menadione or TMN are represented using dashed line.

produced loss of stimulation of *L*- citrulline production in a concentration-dependent manner (Fig. 1.6B & Fig. 1.6D). These results suggest that, at higher concentrations of TMN and menadione, insufficient electron flux may be remaining in/through nNOS to support normal levels of NO• and *L*-citrulline production.

The concentration-dependent decrease in *L*- citrulline production by nNOS is in stark contrast to the concomitant increase in NADPH oxidation observed in the presence of both TMN and menadione (Fig. 1.7). At this concentrations of these compounds (≥125 μM), the limit for electron transfer is reached, although different maximal rates occur for TMN and menadione (Fig. 1.7). Similar results were obtained when an NADPH-regenerating system was used to sustain levels of NADPH in the assay (data not shown). One study showed that inhibitory potencies of quinones towards nNOS activity increased with increasing one-electron reduction potentials (-240 mV to -100 mV) of a series of quinones (Kumagai *et al.*, 1998).

The likelihood that quinones and semiquinones of TMN and menadione covalently bind and/or oxidize thiol groups in the nNOS protein seems unlikely because, TMN and menadione were present in great excess (up to 500 μM each), but only catalytic amounts of nNOS (7.5 pmoles) were added. Furthermore, the observed loss of stimulation of *L*-citrulline production in the presence of TMN and menadione is concentration-dependent and the covalent modification on nNOS due to quinones and semiquinones, would most likely not follow in a concentration-dependent manner. The differences in the pattern of modulation of nNOS activity by TMN and menadione at higher concentrations (Fig. 1.6B and Fig. 1.6D), is most likely due to inherent redox-differences between TMN and menadione and/or due to structural differences which increase or decrease quinone-enzyme interactions. Menadione acts as a true inhibitor of nNOS

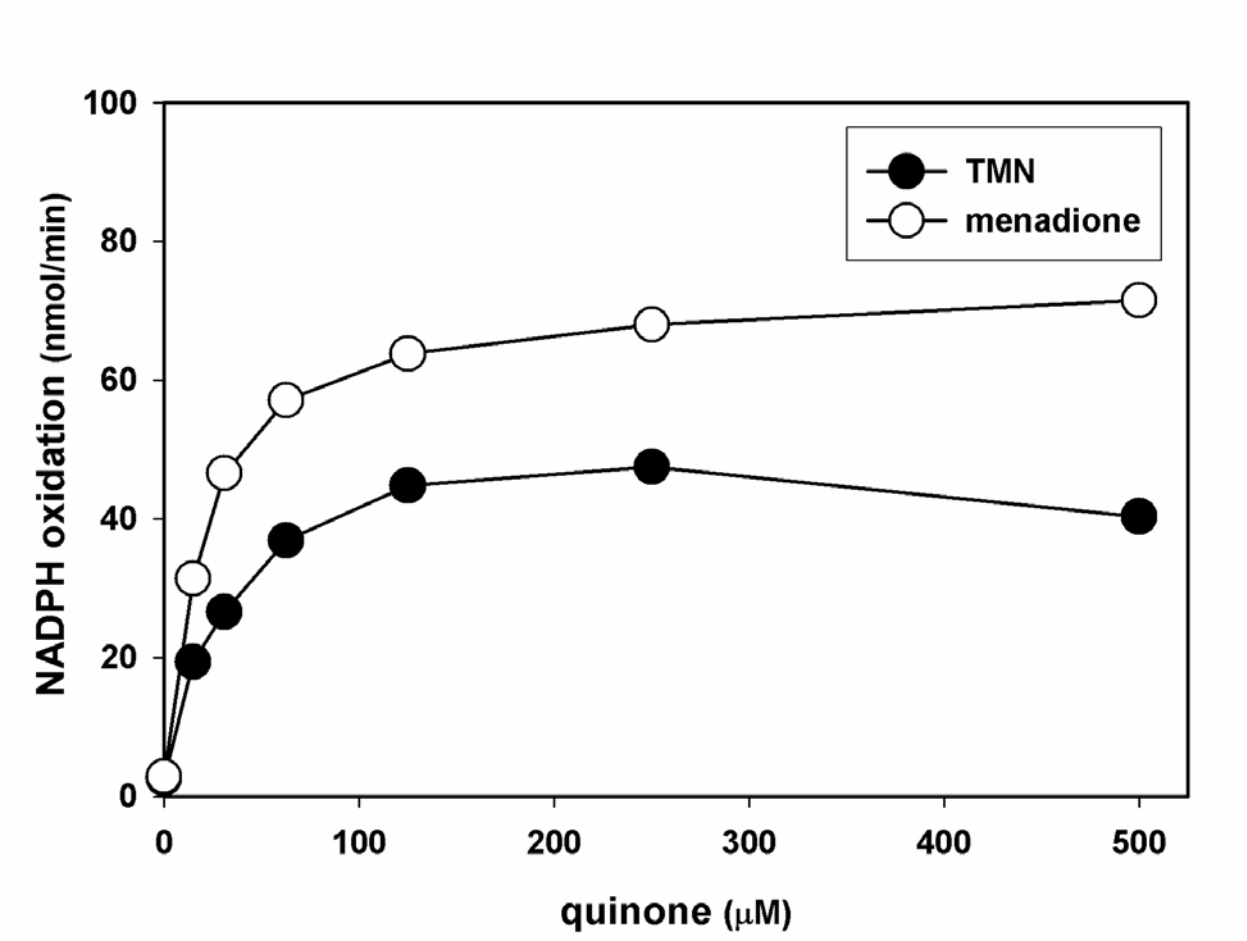

Fig. 1.7. Effect of increasing TMN and menadione concentrations on NADPH oxidation by nNOS. nNOS (30 pmoles) and all other substrates and cofactors were exposed to increasing concentrations of TMN and menadione (0 - 500 μM) in the presence of 100 μM NADPH. Data are expressed as the mean of duplicate samples from two independent experiments.

activity (Fig. 1.6B) whereas the addition of methyl groups in 3 and 6 positions of TMN (when compared to menadione) abolishes nNOS inhibitory activity (Fig. 1.6D). Thus, TMN at higher concentrations (62.5 - 500 μM), causes only the loss of *L*-citrulline production rate and does not act as a true nNOS inhibitor at the concentrations tested (Fig. 1.6D). Collectively, these results indicate that TMN and menadione act as concentration-dependent modulators of nNOS.

Cigarette smoking has been shown to reduce exhaled NO• in humans suggesting that exposure to tobacco smoke alters the synthesis or disposition of NO• (Kharitonov *et al.*, 1995). While raw tobacco contains constituents such as nicotine and tobacco specific nitrosamines that are transferred to tobacco smoke (Andres, 2003), the pyrolysis or pyrosynthesis of the tobacco components produces its own myriad of unique constituents which resides in tobacco smoke (Green, 1996; Torikai *et al.*, 2005). The pyrolysis products present in cigarette smoke have been implicated in causing a decrease in nNOS protein levels and thus overall nNOS activity in penile tissue (Xie *et al.*, 1997). Also, prenatal exposure of rats to cigarette smoke was shown to decrease nNOS protein levels in neonatal brainstem (Hasan *et al.*, 2001).

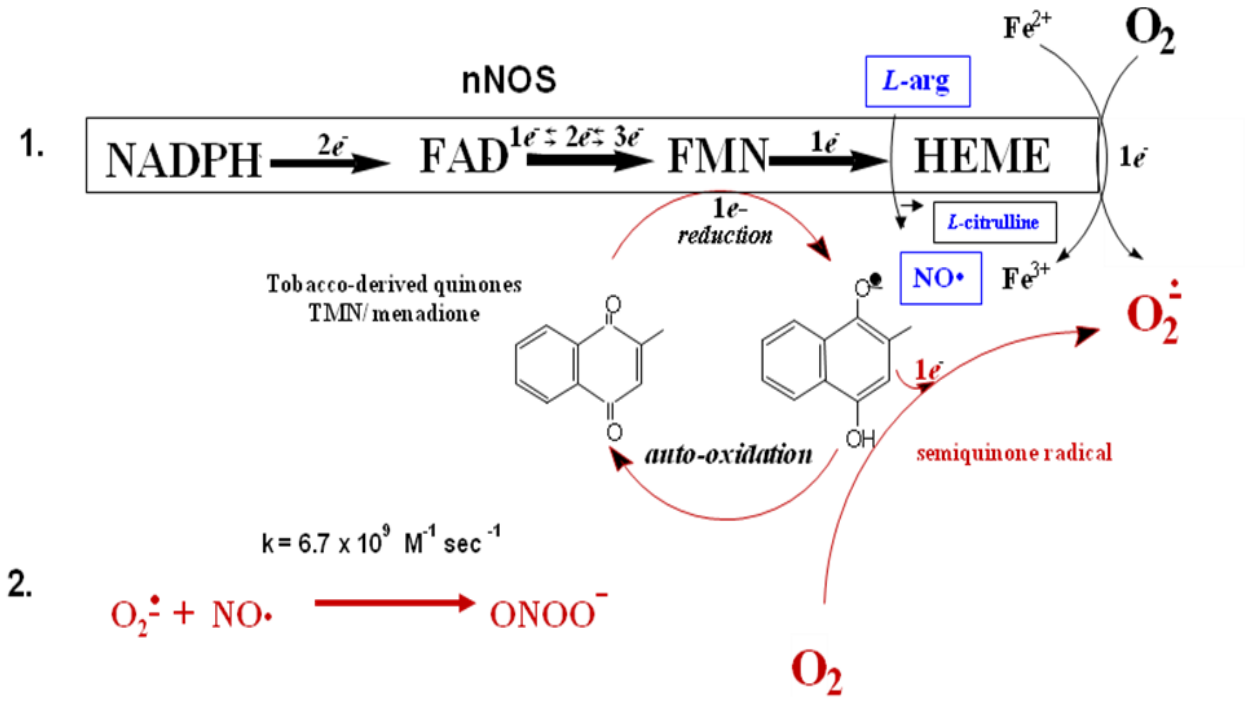

Scheme 1.1. Pathways of electron transfer in nNOS supporting redox-cycling of tobacco-derived quinones. NADPH-derived electrons are passed one at a time through nNOS flavin(s) to various electron acceptors. Quinones present in tobacco extracts may accept an electron from nNOS converting the quinone to a semiquinone radical that upon losing the electron to molecular oxygen (re-oxidation) results in $O_2^{\bullet-}$ production. $O_2^{\bullet-}$ may act on its own to produce toxic peroxy and hydroxyl radicals or may combine with enzymatically generated NO• to form $ONOO^-$ in a reaction rate that approaches the limit of diffusion. *L*-citrulline production is simultaneously increased due to the ability of $O_2^{\bullet-}$ to scavenge NO•, thus preventing the normal physiological auto-inhibition of nNOS. At elevated quinone concentrations, an overall decrease in *L*-citrulline production occurs due to the resulting electron flux, which is insufficient to support NO• production. Thus, quinone compounds via redox cycling processes, may stimulate or inhibit nNOS activity (*L*-citrulline production) depending on concentration, redox properties and physico-chemical properties of the particular quinone.

1.4 Conclusion

Experiments were performed in an attempt to identify properties of various constituent(s) in tobacco extracts that produce nNOS inhibition. The exact number and nature of tobacco constituent(s) responsible for inactivating nNOS remain unknown. Results from [^{14}C]-*L*-arginine to [^{14}C]-*L*-citrulline conversion assays that incorporated extracts from different varieties of tobacco indicate that the nNOS inactivator(s) is non-polar, lipophilic and non-volatile in nature. Variation in content of the major tobacco constituents was evident from comparing HPLC profiles of the various inhibitory hexane extracts. We have shown that there are both activators as well as inactivators of nNOS present in non-burned tobacco. We speculate that there are countless other compounds possessing activity towards nNOS which remain to be identified. Results from experiments with pooled hexane sub-fractions of TI-1565 tobacco extracts provide support for the contention that more than one bioactive compound was present in certain extracts, as nNOS inhibition was produced by multiple fractions of HPLC eluate which spanned a time period of several mins (Fig. 1.3A). Studies in which tobacco-derived redox-active compounds such as TMN or menadione were individually incorporated into the [^{14}C]-*L*-arginine to [^{14}C]-*L*-citrulline conversion assay indicate that single compounds can produce either stimulation or inhibition of *L*-citrulline production by nNOS with effect being dependent on the concentration of the compound used as well as the compound's electrochemical characteristics. Future studies will attempt to identify the exact chemical nature of the compound(s) contained within the hexane extracts of TI-1565 responsible for producing nNOS inhibition. Furthermore, studies into the mechanism of action of these tobacco constituents will be required in order to ascertain the isoform-selectivity of nNOS inhibition.

1.5 Acknowledgements

I thank Ms Bridgette Thacker for performing some of the initial assays for inhibition of nNOS activity. Special thanks to Dr. Gairola for providing leaves of various tobacco varieties and Dr. Castagnoli for providing the tobacco-derived TMN. Support for initial pilot studies was provided by the Kentucky Science and Engineering Foundation (grant # KSEF- 03-RDE-005). This report was made possible by grant # ES 011982 to R.T. Miller from the National Institute of Environmental Health Sciences (NIEHS)/NIH. This project was also supported in part by grant # 5G12RR008124 to the Border Biomedical Research Center (BBRC)/University of Texas at El Paso from the National Center for Research Resources (NCRR)/NIH.

1.6 References

Abu-Soud, H. M., Rousseau, D. L., Stuehr, D. J., 1996. Nitric oxide binding to the heme of neuronal nitric-oxide synthase links its activity to changes in oxygen tension. The Journal of biological chemistry 271, 32515-32518.

Abu-Soud, H. M., Wang, J., Rousseau, D. L., Fukuto, J. M., Ignarro, L. J., Stuehr, D. J., 1995. Neuronal nitric oxide synthase self-inactivates by forming a ferrous-nitrosyl complex during aerobic catalysis. The Journal of biological chemistry 270, 22997-23006.

Andres, S., Boudoux, R., Renaud, J.M., Zuber, J., 2003. TSNA levels in the mainstream smoke of simplified blend prototype. Beitrage zur Tabakforschung 20, 331-340.

Ashwal, S., Cole, D. J., Osborne, T. N., Pearce, W. J., 1994. Dual effects of L-NAME during transient focal cerebral ischemia in spontaneously hypertensive rats. The American journal of physiology 267, H276-284.

Bredt, D. S., Snyder, S. H., 1990. Isolation of nitric oxide synthetase, a calmodulin-requiring enzyme. Proceedings of the National Academy of Sciences of the United States of America 87, 682-685.

Castagnoli, K., Petzer, J. B., Steyn, S. J., van der Schyf, C. J., Castagnoli, N., Jr., 2003. Inhibition of human MAO-A and MAO-B by a compound isolated from flue-cured tobacco leaves and its neuroprotective properties in the MPTP mouse model of neurodegeneration. Inflammopharmacology 11, 183-188.

Chabrier, P. E., Auguet, M., Spinnewyn, B., Auvin, S., Cornet, S., Demerle-Pallardy, C., Guilmard-Favre, C., Marin, J. G., Pignol, B., Gillard-Roubert, V., Roussillot-Charnet, C., Schulz, J., Viossat, I., Bigg, D., Moncada, S., 1999. BN 80933, a dual inhibitor of neuronal nitric oxide

synthase and lipid peroxidation: a promising neuroprotective strategy. Proceedings of the National Academy of Sciences of the United States of America 96, 10824-10829.

Dalkara, T., Moskowitz, M. A., 1994. The complex role of nitric oxide in the pathophysiology of focal cerebral ischemia. Brain pathology (Zurich, Switzerland) 4, 49-57.

Demady, D. R., Lowe, E. R., Everett, A. C., Billecke, S. S., Kamada, Y., Dunbar, A. Y., Osawa, Y., 2003. Metabolism-based inactivation of neuronal nitric-oxide synthase by components of cigarette and cigarette smoke. Drug metabolism and disposition: the biological fate of chemicals 31, 932-937.

Forstermann, U., Pollock, J. S., Schmidt, H. H., Heller, M., Murad, F., 1991. Calmodulin-dependent endothelium-derived relaxing factor/nitric oxide synthase activity is present in the particulate and cytosolic fractions of bovine aortic endothelial cells. Proceedings of the National Academy of Sciences of the United States of America 88, 1788-1792.

Furchgott, R. F., Vanhoutte, P. M., 1989. Endothelium-derived relaxing and contracting factors. Faseb J 3, 2007-2018.

Goyagi, T., Goto, S., Bhardwaj, A., Dawson, V. L., Hurn, P. D., Kirsch, J. R., 2001. Neuroprotective effect of sigma(1)-receptor ligand 4-phenyl-1-(4-phenylbutyl) piperidine (PPBP) is linked to reduced neuronal nitric oxide production. Stroke; a journal of cerebral circulation 32, 1613-1620.

Green, C. R. a. R., A. , 1996. The Tobacco Chemists' Research Conference; A half-century of advances in analytical methodology of tobacco and its products. Recent Advances in Tobacco Science 22, 131-304.

Griscavage, J. M., Hobbs, A. J., Ignarro, L. J., 1995. Negative modulation of nitric oxide synthase by nitric oxide and nitroso compounds. Advances in pharmacology (San Diego, Calif 34, 215-234.

Hasan, S. U., Simakajornboon, N., MacKinnon, Y., Gozal, D., 2001. Prenatal cigarette smoke exposure selectively alters protein kinase C and nitric oxide synthase expression within the neonatal rat brainstem. Neuroscience letters 301, 135-138.

Hibbs, J. B., Jr., 1991. Synthesis of nitric oxide from *L*-arginine: a recently discovered pathway induced by cytokines with antitumour and antimicrobial activity. Research in immunology 142, 565-569; discussion 596-568.

Hibbs, J. B., Jr., Taintor, R. R., Vavrin, Z., Rachlin, E. M., 1988. Nitric oxide: a cytotoxic activated macrophage effector molecule. Biochemical and biophysical research communications 157, 87-94.

Horecker, B. L., Kornberg, A., 1948. The extinction coefficients of the reduced band of pyridine nucleotides. The Journal of biological chemistry 175, 385-390.

Huang, Z., Huang, P. L., Ma, J., Meng, W., Ayata, C., Fishman, M. C., Moskowitz, M. A., 1996. Enlarged infarcts in endothelial nitric oxide synthase knockout mice are attenuated by nitro-*L*-arginine. J Cereb Blood Flow Metab 16, 981-987.

Huang, Z., Huang, P. L., Panahian, N., Dalkara, T., Fishman, M. C., Moskowitz, M. A., 1994. Effects of cerebral ischemia in mice deficient in neuronal nitric oxide synthase. Science (New York, N.Y 265, 1883-1885.

Huie, R. E., Padmaja, S., 1993. The reaction of no with superoxide. Free radical research communications 18, 195-199.

Ignarro, L. J., 1990. Nitric oxide. A novel signal transduction mechanism for transcellular communication. Hypertension 16, 477-483.

Ignarro, L. J., Buga, G. M., Byrns, R. E., Wood, K. S., Chaudhuri, G., 1988. Endothelium-derived relaxing factor and nitric oxide possess identical pharmacologic properties as relaxants of bovine arterial and venous smooth muscle. The Journal of pharmacology and experimental therapeutics 246, 218-226.

Ignarro, L. J., Buga, G. M., Wood, K. S., Byrns, R. E., Chaudhuri, G., 1987. Endothelium-derived relaxing factor produced and released from artery and vein is nitric oxide. Proceedings of the National Academy of Sciences of the United States of America 84, 9265-9269.

Ischiropoulos, H., al-Mehdi, A. B., Fisher, A. B., 1995. Reactive species in ischemic rat lung injury: contribution of peroxynitrite. The American journal of physiology 269, L158-164.

Iyanagi, T., 1990. On the mechanism of one-electron reduction of quinones by microsomal flavin enzymes: the kinetic analysis between cytochrome B5 and menadione. Free radical research communications 8, 259-268.

Iyanagi, T., Mason, H. S., 1973. Some properties of hepatic reduced nicotinamide adenine dinucleotide phosphate-cytochrome c reductase. Biochemistry 12, 2297-2308.

Kappus, H., Sies, H., 1981. Toxic drug effects associated with oxygen metabolism: redox cycling and lipid peroxidation. Experientia 37, 1233-1241.

Khalil, A. A., Davies, B., Castagnoli, N., Jr., 2006. Isolation and characterization of a monoamine oxidase B selective inhibitor from tobacco smoke. Bioorganic & medicinal chemistry 14, 3392-3398.

Khalil, A. A., Steyn, S., Castagnoli, N., Jr., 2000. Isolation and characterization of a monoamine oxidase inhibitor from tobacco leaves. Chemical research in toxicology 13, 31-35.

Kharitonov, S. A., Robbins, R. A., Yates, D., Keatings, V., Barnes, P. J., 1995. Acute and chronic effects of cigarette smoking on exhaled nitric oxide. American journal of respiratory and critical care medicine 152, 609-612.

Knowles, R. G., Palacios, M., Palmer, R. M., Moncada, S., 1989. Formation of nitric oxide from *L*-arginine in the central nervous system: a transduction mechanism for stimulation of the soluble guanylate cyclase. Proceedings of the National Academy of Sciences of the United States of America 86, 5159-5162.

Kumagai, Y., Nakajima, H., Midorikawa, K., Homma-Takeda, S., Shimojo, N., 1998. Inhibition of nitric oxide formation by neuronal nitric oxide synthase by quinones: nitric oxide synthase as a quinone reductase. Chem Res Toxicol 11, 608-613.

Kwon, N. S., Nathan, C. F., Gilker, C., Griffith, O. W., Matthews, D. E., Stuehr, D. J., 1990. *L*-citrulline production from *L*-arginine by macrophage nitric oxide synthase. The ureido oxygen derives from dioxygen. The Journal of biological chemistry 265, 13442-13445.

Lowe, E. R., Everett, A. C., Lee, A. J., Lau, M., Dunbar, A. Y., Berka, V., Tsai, A. L., Osawa, Y., 2005. Time-dependent inhibition and tetrahydrobiopterin depletion of endothelial nitric-oxide synthase caused by cigarettes. Drug metabolism and disposition: the biological fate of chemicals 33, 131-138.

Matsuda, H., Kimura, S., Iyanagi, T., 2000. One-electron reduction of quinones by the neuronal nitric-oxide synthase reductase domain. Biochimica et biophysica acta 1459, 106-116.

Mayer, B., John, M., Bohme, E., 1990. Purification of a Ca^{2+}/calmodulin-dependent nitric oxide synthase from porcine cerebellum. Cofactor-role of tetrahydrobiopterin. FEBS Lett 277, 215-219.

Miller, R. T., Martasek, P., Roman, L. J., Nishimura, J. S., Masters, B. S., 1997. Involvement of the reductase domain of neuronal nitric oxide synthase in superoxide anion production. Biochemistry 36, 15277-15284.

Nagafuji, T., Matsui, T., Koide, T., Asano, T., 1992. Blockade of nitric oxide formation by N omega-nitro-*L*-arginine mitigates ischemic brain edema and subsequent cerebral infarction in rats. Neuroscience letters 147, 159-162.

Nishimura, J. S., Narayanasami, R., Miller, R. T., Roman, L. J., Panda, S., Masters, B. S., 1999. The stimulatory effects of Hofmeister ions on the activities of neuronal nitric-oxide synthase. Apparent substrate inhibition by l-arginine is overcome in the presence of protein-destabilizing agents. The Journal of biological chemistry 274, 5399-5406.

Pollock, J. S., Forstermann, U., Mitchell, J. A., Warner, T. D., Schmidt, H. H., Nakane, M., Murad, F., 1991. Purification and characterization of particulate endothelium-derived relaxing factor synthase from cultured and native bovine aortic endothelial cells. Proceedings of the National Academy of Sciences of the United States of America 88, 10480-10484.

Roman, L. J., Sheta, E. A., Martasek, P., Gross, S. S., Liu, Q., Masters, B. S., 1995. High-level expression of functional rat neuronal nitric oxide synthase in Escherichia coli. Proceedings of the National Academy of Sciences of the United States of America 92, 8428-8432.

Scheele, J. S., Bruner, E., Kharitonov, V. G., Martasek, P., Roman, L. J., Masters, B. S., Sharma, V. S., Magde, D., 1999. Kinetics of NO ligation with nitric-oxide synthase by flash photolysis and stopped-flow spectrophotometry. The Journal of biological chemistry 274, 13105-13110.

Schmeltz, I., Tosk, J., Jacobs, G., Hoffmann, D., 1977. Redox potential and quinone content of cigarette smoke. Analytical chemistry 49, 1924-1929.

Spinnewyn, B., Cornet, S., Auguet, M., Chabrier, P. E., 1999. Synergistic protective effects of antioxidant and nitric oxide synthase inhibitor in transient focal ischemia. J Cereb Blood Flow Metab 19, 139-143.

Stedman, R. L., 1968. The chemical composition of tobacco and tobacco smoke. Chemical reviews 68, 153-207.

Stuehr, D. J., Nathan, C. F., 1989. Nitric oxide. A macrophage product responsible for cytostasis and respiratory inhibition in tumor target cells. The Journal of experimental medicine 169, 1543-1555.

Thom, S. R., Xu, Y. A., Ischiropoulos, H., 1997. Vascular endothelial cells generate peroxynitrite in response to carbon monoxide exposure. Chemical research in toxicology 10, 1023-1031.

Torikai, K., Uwano, Y., Nakamori, T., Tarora, W., Takahashi, H., 2005. Study on tobacco components involved in the pyrolytic generation of selected smoke constituents. Food Chem Toxicol 43, 559-568.

Vasquez-Vivar, J., Hogg, N., Pritchard, K. A., Jr., Martasek, P., Kalyanaraman, B., 1997. Superoxide anion formation from lucigenin: an electron spin resonance spin-trapping study. FEBS letters 403, 127-130.

Willmot, M., Gibson, C., Gray, L., Murphy, S., Bath, P., 2005. Nitric oxide synthase inhibitors in experimental ischemic stroke and their effects on infarct size and cerebral blood flow: a systematic review. Free radical biology & medicine 39, 412-425.

Winston, G. W., Church, D. F., Cueto, R., Pryor, W. A., 1993. Oxygen consumption and oxyradical production from microsomal reduction of aqueous extracts of cigarette tar. Archives of biochemistry and biophysics 304, 371-378.

Xie, Y., Garban, H., Ng, C., Rajfer, J., Gonzalez-Cadavid, N. F., 1997. Effect of long-term passive smoking on erectile function and penile nitric oxide synthase in the rat. The Journal of urology 157, 1121-1126.

Zhang, Z. G., Reif, D., Macdonald, J., Tang, W. X., Kamp, D. K., Gentile, R. J., Shakespeare, W. C., Murray, R. J., Chopp, M., 1996. ARL 17477, a potent and selective neuronal NOS inhibitor decreases infarct volume after transient middle cerebral artery occlusion in rats. J Cereb Blood Flow Metab 16, 599-604.

Zhao, X., Haensel, C., Araki, E., Ross, M. E., Iadecola, C., 2000. Gene-dosing effect and persistence of reduction in ischemic brain injury in mice lacking inducible nitric oxide synthase. Brain research 872, 215-218.

Chapter 2: Absence of Nitric Oxide Synthase in Sequentially Purified Rat Liver Mitochondria

2.1 Introduction

Nitric Oxide (NO•) is a highly diffusible, hydrophobic, gaseous free radical (Ignarro, 1989) that is responsible for autocrine and paracrine signaling activities (Shin *et al.*, 1992). NO• can readily partition into membranes (Ignarro *et al.*, 1988; Malinski *et al.*, 1993). Since NO• can diffuse across membranes (Thomas *et al.*, 2001), it influences biological functions such as blood pressure regulation, platelet aggregation and adhesion, neurotransmission and cellular defense (Forstermann *et al.*, 1991a; Furchgott and Vanhoutte, 1989; Hibbs *et al.*, 1988; Ignarro *et al.*, 1988; Knowles *et al.*, 1989; Murad *et al.*, 1992; Pollock *et al.*, 1991). The mechanism by which NO• influences biological functions is by binding to target proteins that contain heme or thiol(s) or alternatively, NO• can combine with $O_2^{\bullet-}$ to produce the toxic, and highly reactive species, peroxynitrite ($ONOO^-$).

Mitochondria are highly compartmentalized, membranous organelles which contain abundant amounts of reactive hemoproteins and thiols (Cadenas *et al.*, 2000; Radi *et al.*, 2002), to which NO• may bind reversibly (Moncada, 2000; Thomas *et al.*, 2003) or irreversibly (Ebel *et al.*, 1975; Nathan, 1992; Stuehr and Griffith, 1992). Mitochondria also generate copious amounts of $O_2^{\bullet-}$ during the process of cellular respiration (Boveris and Cadenas, 1975; Dionisi *et al.*, 1975). Studies conducted during the past decade have suggested that NO• can diffuse into mitochondria and cause mitochondrial dysfunction by reversibly inhibiting cytochrome-*c* oxidase (Brown *et al.*, 1995; Cleeter *et al.*, 1994; Moncada, 2000) and NADH dehydrogenase (Radi *et al.*, 1994). However, many toxic reactions that occur subsequent to NO• production,

are due to NO• reacting non-enzymatically with $O_2^{\bullet-}$ at an almost diffusion-limited reaction rate ($6.7 \times 10^9\ M^{-1}\ s^{-1}$) to produce the potent oxidant and ultimate toxicant, $ONOO^-$ (Huie and Padmaja, 1993). $ONOO^-$ can nitrate or oxidize mitochondrial proteins. Both nitration and oxidation reactions may inactivate mitochondrial matrix enzymes such as aconitase (Kennedy *et al.*, 1997), manganese superoxide dismutase (MacMillan-Crow *et al.*, 1998) and succinyl-CoA:3-oxoacid CoA-transferase (Turko *et al.*, 2001). Also, inhibition of mitochondrial respiration results in production of increased amounts of reactive oxygen species (ROS) and reactive nitrogen species (RNS) (Dedkova *et al.*, 2004), both of which may act as cytotoxicants resulting in cellular necrosis and/or apoptotic cell death (Brookes *et al.*, 2002; Moncada and Erusalimsky, 2002; Sarti *et al.*, 2003).

Physiologically, NO• is produced by three main isoforms of NOS: neuronal (nNOS), endothelial (eNOS) and inducible (iNOS) (Bredt and Snyder, 1990; Forstermann *et al.*, 1991a; Hibbs, 1991; Ignarro *et al.*, 1987b). Each NOS isoform consists of an N-terminal heme-containing oxygenase domain and a C-terminal flavin-containing reductase domain linked together by a calmodulin (CaM)-binding sequence (Sheta *et al.*, 1994). Reduced nicotinamide adenine dinucleotide phosphate (NADPH) is utilized as a co-substrate and each NOS isoform depends on (6*R*)-5,6,7,8-tetrahydro-*L*-biopterin (BH_4) and O_2 for the stoichiometric conversion of *L*-arginine to equimolar amounts of *L*-citrulline plus NO• (Kwon *et al.*, 1990).

In the mid-nineties, a putative variant of NOS was proposed to reside within mitochondria. Initially, the Kobzik (Kobzik *et al.*, 1995) and Hellsten (Frandsen *et al.*, 1996) groups observed an apparent eNOS immunoreactivity in skeletal muscle mitochondria. Simultaneously, Bates (Bates *et al.*, 1995, 1996) observed an apparent eNOS histochemical

reactivity in inner mitochondrial membrane preparations, isolated from rat liver, brain, heart, skeletal muscle and kidney. Tatoyan and Giulivi (37), acting on these initial observations, performed experiments in an attempt to confirm the identity of this putative mtNOS. Relying on immunochemical analysis, Tatoyan and Giulivi claimed that iNOS was the NOS isoform present in rat liver mitochondria (Tatoyan and Giulivi, 1998). Later, this same group presented mass spectrometric-derived data in support of the putative mtNOS being a variant of nNOS (Elfering *et al.*, 2002). Ghafourifar and co-workers (Ghafourifar and Richter, 1997) had previously reported that the putative mtNOS was calcium-sensitive and constitutive in nature. Since these reports, different groups have reported the presence of each of the three main isoforms of NOS within rat liver mitochondria (Elfering *et al.*, 2002; Kanai *et al.*, 2001; Lacza *et al.*, 2001). Interestingly, biochemical characterization of the putative mtNOS performed by the Giulivi group(Elfering *et al.*, 2002) revealed certain post-translational modifications (myristoylation and phosphorylation of the protein) that are thought to be unique to eNOS.

Throughout the late 1990's and early 2000's, many reports supported the presence of at least one of the 3 main isoforms of NOS residing in mitochondria. However, more recent reports tend to question this claim (Brookes, 2004; Lacza *et al.*, 2004; Lacza *et al.*, 2003; Tay *et al.*, 2004). Due to the contradictory reports regarding the existence of a putative mtNOS, Brookes (Brookes, 2004) compiled a critical and thorough review of the literature dealing with the putative mtNOS published up to 2003. This review brought to light the diverse technical issues involved in the aforementioned studies. Major issues were the degree of purity of mitochondrial preparations (Giulivi *et al.*, 1998; Kanai *et al.*, 2004), shortcomings of measurement methodology (Elfering *et al.*, 2002; Lopez-Figueroa *et al.*, 2000; Lopez-Figueroa *et al.*, 2002;

Zanella *et al.*, 2002), use of inappropriate, or total lack of, experimental controls and confusing technical practices. Lacza *et al.* (Lacza *et al.*, 2006) has reviewed the more recent developments in the area of putative mitochondrial NO• production and discussed some of the shortcomings of certain techniques still being used.

In light of this ongoing controversy regarding the presence or absence of a mtNOS, we designed and carefully conducted properly controlled studies to either confirm or refute the existence of any NOS isoform within mitochondria. Ultra pure rat liver mitochondria were isolated using repeated differential centrifugation followed by Percoll gradient purification. Proteomic analyses were then performed using a nanoHPLC-coupled nanospray LTQ-MS. To avoid the interfering factors that are rampant in NO• trapping assays (Schmidt *et al.*, 1994), the NOS-catalyzed conversion of [^{14}C]-*L*-arginine to [^{14}C]-*L*-citrulline was used to probe for NOS activity in mitochondria. Appropriate controls were employed and, for inhibition studies, high concentrations of *L*-thiocitrulline ((Narayanan and Griffith, 1994) denoted as TC, in figures) were used as the NOS inhibitor. Additionally, immuno-chemical analyses were performed with ultrapure mitochondria using nNOS, eNOS and CaM antibodies to validate the results obtained with the other approaches. Also, the problems faced with the commonly used techniques used in mtNOS studies are discussed.

2.2 Experimental Procedures

Chemicals and Biochemicals: 4-(2-hydroxyethyl)-1 piperazineethanesulfonic acid (HEPES), *L*-arginine·HCl, $CaCl_2 \cdot 4H_2O$, bovine brain CaM, (6*R)*-5,6,7,8-tetrahydro-*L*-biopterin (BH_4), NADPH, *L*-citrulline, ethylene diamine tetraacetic acid (EDTA), ethylene glycol tetraacetic acid (EGTA), dithiothreitol (DTT), iodoacetamide (IAA), sucrose, mannitol, acetone, *L*-thiocitrulline, N(ω)-nitro-*L*-arginine (*L*-NNA), monosodium- and disodium- phosphate, sodium dodecyl sulfate (SDS), alkaline phosphatase-conjugated anti-rabbit secondary antibody, horseradish peroxidase (HRP)-conjugated anti-rabbit and anti-mouse secondary antibodies. All of the above mentioned items were purchased from Sigma (St. Louis, MO). Dowex 50WX8 was obtained from Supelco (Bellefonte, PA). Acetonitrile (ACN) was purchased from Mallinckrodt-Baker, Inc. (Philipsburg, NJ). Trichloroacetic acid (TCA) was obtained from EMD Chemicals, Inc (San Diego, CA). Tris and nitrocellulose membranes were purchased from Bio-Rad (Hercules, CA). Super signal west pico chemiluminescent substrate was purchased from Pierce. Percoll and 2′, 5′-ADP Sepharose 4B were products of GE Healthcare (Uppsala, Sweden). cOmplete protease inhibitor cocktail tablets were purchased from Roche (Mannheim, Germany). Primary antibodies for the mitochondrial outer membrane marker, voltage dependent anion channel (VDAC) were obtained from Affinity Bioreagents (Golden, CO). Primary antibodies for glucose related protein (GRP 75)/mitochondrial heat shock protein 70 (mt hsp70) and CaM were purchased from Abcam Inc. (Cambridge, MA). nNOS and eNOS primary antibodies were generous gifts from Bettie Sue Masters Ph.D., University of Texas Health Science Center at San Antonio, TX. Tubulin antibody was a gift from Sukla Roychowdhary Ph.D., University of Texas

at El Paso, TX. All other chemicals and reagents were from common suppliers and were of the highest grade commercially available.

***Enzymes*:** Recombinant nNOS and eNOS (referred to as nNOSr and eNOSr, respectively) were over-expressed in *E. coli* and purified according to established methodology (Martasek *et al.*, 1996; Roman *et al.*, 1995). Superoxide dismutase (SOD) and catalase (CAT) were purchased from Sigma. The specific activities of SOD and CAT were 2,500-7,000 units/mg protein and ≥ 10,000 units/mg protein, respectively.

Animals: All experimental protocols involving animals were approved by University of Texas at El Paso Institutional Animal Care and Use Committee (IACUC). Male Sprague-Dawley (SD) rats (250–300 g; approx. 3 months of age) were obtained from Harlan (Houston, TX) and used in all studies.

***Preparation of Mitochondria*:** Pure rat liver mitochondria were obtained by repeated differential centrifugation followed by Percoll gradient purification. Expertise for the mitochondrial purification procedure was obtained first hand and adopted from the methodology used in the laboratory of James Geddes Ph.D., University of Kentucky, Lexington, KY. Initially, 2-4 rats were euthanized and the entire liver was excised and immersed in ice-cold mitochondrial isolation buffer (MIB) containing 215 mM mannitol, 75 mM sucrose, 1mM EGTA, 20 mM HEPES/KOH, pH 7.2. In addition, a serine- and cysteine-protease inhibiting cOmplete cocktail tablet was included. The liver lobes were blotted, washed 2-3 times with fresh MIB and minced into small pieces with scissors. The resulting minced pieces of liver were washed with MIB to remove blood. Then, 6-8 ml of ice-cold MIB was added to the washed and minced tissue. The tissue sample was placed in a glass dounce homogenizer in portions, immersed in ice and

homogenized gently with a loose-fitting teflon pestle (6 strokes) at 250 rpm, using a variable speed homogenizer (Glas-Col, Terre Haute, IN).

Following homogenization, both differential centrifugation and Percoll gradient freactionation steps were performed using a pre-cooled SM-24 rotor in a RC-5B Sorvall centrifuge at 4º C, for 10 min, unless specified otherwise. First, the tissue homogenate (referred to as CO, in figures) was suspended in ice-cold MIB and centrifuged at 800 x g. After the first 800 x g spin, the white fatty layer covering the supernatant was carefully removed using a lint-free wipe or a cotton wool. The 800 x g supernatant (M1) was then collected and the isolated pellet containing red spots of blood and cellular debris was discarded. M1 was spun at 10,000 x g to obtain a pellet containing mitochondria (M2). M2 was then gently resuspended by homogenization using a glass dounce homogenizer (4 strokes, 250 rpm). The differential centrifugation steps were then repeated with the MIB-resuspended M2 (at 800 x g (M3) and 10,000 x g (M4)) to obtain a relatively pure mitochondrial preparation. The mitochondrial pellet obtained after the 10,000 x g spin was resuspended in ice-cold MIB and then centrifuged at the lower speed of 9,000 x g. The pellet (M5) isolated during this step contained highly purified mitochondria

Mitochondria were further purified using Percoll gradient centrifugation as described previously (Brown *et al.*, 2006). Percoll was chosen as the gradient medium owing to its chemical inertness and negligible osmolarity (Pertoft *et al.*, 1978; Reinhart *et al.*, 1982). Ice cold-MIB without EGTA was used in all steps for preparing the Percoll gradient solutions as well as for washing. Mitochondria were supplemented with an equal volume of 30% Percoll (15% mitochondria containing Percoll). A discontinuous Percoll gradient was used, with the

bottom layer containing 40% Percoll, followed by 24% Percoll, and finally by 15% Percoll-containing mitochondria. The density gradient was spun at 30,400 x g and the band between 24% and 40% Percoll (containing the intact mitochondria) was carefully collected. The broken mitochondria at the bottom of the gradient were discarded. The intact mitochondrial sample was then suspended in MIB without EGTA and centrifuged at 16,700 x g for 15 min. Discarding the supernatant, the loose pellet obtained was resuspended in MIB without EGTA and subsequently centrifuged at 13,000 x g followed by a 10,000 x g spin. The intact mitochondrial pellet obtained after the final 10,000 x g spin, was collected and used for experimentation. These intact, pure mitochondria, obtained after repeated differential centrifugation and Percoll-gradient fractionation, are referred as 'MT' throughout the manuscript. The protein concentration of the pure mitochondria was measured using the Bradford protein assay (Bradford, 1976) using BSA as a standard.

***Isolation of Sub-Mitochondrial Particles*:** MT, were placed in a small glass vial residing within an ice-jacket and sonicated mildly for 20s, with alternating pulse and pause interval times of 5s each (amplitude - 25%) using an ultrasonic processor (Sonics and Materials, Inc.), equipped with a 1/8- inch diameter probe. For preparation of the positive control, sonication of MT was interrupted after 10s and nNOSr (200 femtomoles) was spiked into the half-sonicated MT sample and then the spiked samples were sonicated for the remaining 10s. Sub-mitochondrial particles were subsequently obtained from both the experimental and positive control samples by ultracentrifugation at 100,000 x g for 1hr at 4 ºC (TLA 100 rotor; Beckman Allegra 64 centrifuge). The supernatant fraction and the solubilized pellet (solubilized using 0.1% octyl β-*D*-glucopyranoside) were collected for further processing.

Affinity Purification of Sub-Mitochondrial Particles: Sub-mitochondrial particles (supernatant and solubilized pellet) of MT as well as positive controls were subjected to 2′, 5′-ADP Sepharose 4B chromatography to enrich samples with NADPH-binding proteins, including NOS, if present. Briefly, all sub-mitochondrial particle preparations, obtained from purified MT (initial amounts varied depending on the experiment) were incubated with 150 µl of the 2′, 5′-ADP Sepharose 4B bead slurry, equilibrated with ice-cold sodium phosphate buffer (50 mM, pH 7.4), and spun overnight (15 hrs) at 4º C. Mini-columns were then made in a 200 µl pipette tip, using the suspension of sub-mitochondrial particles that had been pre-incubated with 2′, 5′-ADP Sepharose 4B beads. The columns were then washed with ice- cold sodium phosphate buffer (5 x 100 µl). NADPH-dependent proteins bound to the columns were then eluted using 5 x 100 µl portions of 5 mM NADPH in 50 mM Tris containing 500 mM NaCl; pH 7.4.

Sample Processing for Mass Spectrometry: Protein precipitation was performed by treating the affinity-purified eluates of sub-mitochondrial particles and positive controls with 10% TCA for 30 min, on ice. Samples were vortexed every 10 min, and finally centrifuged at 16,000 x g for 20 min, at 4ºC. The TCA-precipitated samples were resuspended in acetone and centrifuged at 16,000 x g for 20 min, at 4ºC. Sample pellets were then dried using a centri-vap.

Dry, precipitated proteins were digested as described by Stone and Williams (Stone, 1996). Briefly, dried pellets from acetone washes were solubilized with a solution of 8 M urea/0.4 M NH_4HCO_3, and the sulfhydryls were reduced using DTT (9 mM) for 15 min at 50º C. The samples were cooled to room temperature and then treated with IAA (20 mM) for 15 min at RT. Subsequently, the IAA-treated samples were diluted with water to obtain a final concentration of 1 M urea. Finally, the samples were digested overnight with 1 µg of sequencing

grade trypsin (Promega) for every 50 µg of mitochondrial protein. Proteolysis was stopped by adding 1 µl of 100% formic acid (FA) (Sigma). The resulting samples were desalted using reverse-phase Ziptips manufactured with 200-µL micropipette tips and containing POROS 50 R2 beads (Applied Biosystems) (Jurado *et al.*, 2007). Next, strong cation exchange (SCX) chromatography was performed using POROS 50 HS beads (Rodrigues *et al.*, 2008) and the samples were fractionated by eluting with increasing concentrations of NaCl (0-500 mM). The eluates were again desalted using reverse phase ziptips and dried under vacuum centrifugation.

Each of the desalted SCX fractions were solubilized in 30 µL of 0.05% TFA and eight microliters were injected onto a trap column (C18, 0.25µL, OPTI-PAK). Separations were performed using a reverse-phase capillary column (Acclaim, 3 µm C18, 75 µm x 25 cm, LC Packings, Dionex) connected to a nanoHPLC system (nanoLC 1D plus, Eksigent). For elution, the mobile phases were A: 2% ACN, 0.1% FA; B: 80% ACN, 0.1% FA. A linear gradient from 0%-40% solvent B over 100 min was used. The eluting peptides were directly introduced into a linear ion trap-mass spectrometer equipped with a nanospray source (LTQ XL, Thermo Fisher Scientific). MS spectra were collected in centroid mode over the range of 400 to 1700 *m/z* and the five most abundant ions were submitted twice to collision-induced dissociation (CID) (35% normalized collision energy), before dynamically excluded for 120 s. All MS/MS spectra were from peptides of 600-4,000 Da and at least 15 fragments were converted into DTA files using Bioworks v.3.3.1 (Thermo Fisher Scientific). The DTA files were submitted for database searching using TurboSequest (Eng, 1994) (available in Bioworks v.3.3.1) against the rat sequences (v3.25) from the International Protein Index (www.ebi.ac.uk/IPI). All sequences were submitted in the forward as well as reverse orientations for calculating the false-positive rate

(FPR). The database search parameters included: i) trypsin cleavage in both peptide termini allowing one missed cleavage site; ii) carbamidomethylation of cysteine residues as a fixed modification; iii) oxidation of methionine residues as a variable modification; and iv) 2.0 Da and 1.0 Da for peptide and fragment mass tolerance, respectively. The following filters in Bioworks were applied: distinct peptides, consensus scores ≥ 10.2, DCn ≥ 0.1, protein probability ≤ $1x10^{-3}$, and Xcorr ≥ 1.5, 2.0 and 2.5 for singly-, doubly- and triply-charged peptides, respectively. To ensure the quality of the analyses, the FPR was calculated by dividing the number of hits matching the reverse sequences by the total number of identifications.

Assay for NOS Activity: The conversion of [^{14}C]-*L*-arginine to [^{14}C]-*L*-citrulline was used to estimate NOS activity (Nishimura *et al.*, 1999). Reaction mixtures consisted of 50 mM HEPES (pH 7.6), 400 μM NADPH, 400 μM $CaCl_2$, 5 μM BH_4, 20 μM *L*-arginine containing 0.5 μCi/ml [^{14}C]-*L*-arginine, and a 1.5-fold molar excess of CaM to nNOS (based on the positive control) in a total volume of 0.25 mL (Miller, 2002). MT (150 µg) were included in all assays, unless mentioned otherwise. A 4-fold excess of NADPH (400 μM *vs* the normal 100 μM assay concentration) was used to ensure that this co-substrate would not become a limiting factor in the reactions. In order to confirm that the NADPH concentration was indeed sufficient, an NADPH regenerating system, consisting of one unit of glucose 6-phosphate dehydrogenase, 125 mM glucose 6-phosphate and 12.5 mM $NADP^+$, was used in some pilot assays. The potent nNOS inhibitor for inhibition of NOS activity, *L*-thiocitrulline (800 µM) which is efficacious at this concentration towards any NOS isoform, was preincubated with MT samples for 10 min before initiating the reactions. The NOS inhibitor *L*-NNA (400 µM) was also used in some assays. Reactions were run for 10 min at 23°C.

Reaction mixtures were quenched with an ice-cold stop solution containing 1mM citrulline, 10 mM EDTA and 100 mM HEPES, pH 5.5 and then applied to 2 ml Dowex columns and [^{14}C]- *L*-citrulline was eluted with two x 1ml portions of water. To determine NOS activity, the entire eluates were used to quantify [^{14}C]-*L*-citrulline by liquid scintillation counting. Denatured MT (dMT), obtained by mild sonication for 5s (amplitude - 25 %), followed by incubation at 100 °C for 5 min, were used as negative mitochondrial controls. Controls consisted of complete reaction mix + MIB alone, complete reaction mix + dMT ± nNOSr, complete reaction mix + dMT – NADPH, complete reaction mix + dMT + *L*-thiocitrulline and complete reaction mix + *L*-thiocitrulline alone. Control values from incubations containing all ingredients except enzyme or MT, were subtracted from all data points. The positive controls consisted of MT (150 µg) spiked with 30 nM nNOSr. Data were analyzed using Sigma Plot 9.0 (Systat Software, Inc.) and expressed as the mean ± range of values, of experimental data points from two independent experiments, each run in duplicate.

***High Performance-Thin Layer Chromatography of Amino acids*:** Samples from [^{14}C]-*L*-arginine to [^{14}C]-*L*-citrulline conversion assay (eluted from Dowex columns or not exposed to Dowex) were treated with 80% acetone and the precipitation was enhanced with a freeze-thaw cycle at -80ºC for 36 hrs. The precipitated proteins were removed by centrifuging at 16,000 x g for 20 min.

Control experiments were performed to determine if there is any loss of radioactivity in the MT protein pellet. This was determined wherein all substrates and cofactors of [^{14}C]-*L*-arginine to [^{14}C]-*L*-citrulline conversion assay, except [^{14}C]-*L*-arginine were added to MT and quenched with STOP solution. [^{14}C]-*L*-arginine was then added which was followed with

acetone precipitation. Results from control experiments indicated that there was 0.01% percent loss of radioactivity in the pellet (data not shown).

The supernatants from 16000 x g spin, containing the amino acids, were collected separately and dried under a stream of nitrogen. The dried supernatant samples were then dissolved in 100 µl methanol:water (2:1) and 10 µl of each individual sample was loaded on HP-TLC silica 60 plate (EMB chemicals). Ten µl of 2 mg/ml *L*-arginine or *L*-citrulline or *L*-ornithine were used as standard. Butanol:acetic acid:water (60:20:20) was used as the mobile phase. HP-TLC was performed in a glass chamber using standard methodology and the plates were developed with a 2 % ninhydrin solution (in acetone). The plates were then placed on a hot plate (medium setting) for 1 min. After the non-radioactive *L*-arginine and *L*-citrulline control bands were identified visually, the plates were exposed to X-ray film (Kodak) for 108 hrs (4 1/2 days).

***SDS-PAGE and Western Analyses*:** Immunochemical analysis against MT as well as non-MT markers (GRP 75, VDAC and tubulin, respectively) were performed wherein 20 µg of rat liver samples (M1, M2, M3, M4, M5, MT and control tissue homogenate (CO)) were separated by SDS-PAGE (10 % polyacrylamide). Initially, samples were placed into 2X loading buffer containing 125 mM Tris-HCl (pH 6.8), 2% SDS, 20% glycerol, 0.2% bromophenol blue and 0.05% β-mercaptoethanol. Samples were then boiled for 3 min. Electrophoresis was performed using a Bio-Rad Mini Protean II gel apparatus at 100 V for 1.5 hrs. The separated proteins were then transferred from the gels onto nitrocellulose membranes (30 V) for 15 hrs, at 4°C.

Nitrocellulose membranes were then blocked with 5% non-fat dry milk in Tris-buffered saline (TBS; 0.3 M NaCl, 40 mM Tris-HCl; pH 7.6) containing 0.1% Tween 20 (TBST) for 1

hr. After washing for 30 min (3 x 10 min) with TBST, the membranes were incubated overnight at 4ºC with the primary antibodies against either mouse GRP 75 (1:1250), or rabbit VDAC (1:1,000) or mouse tubulin (1:250). The membranes were washed for 30 min (3 x 10 min) with TBST and incubated with the appropriate HRP-conjugated secondary antibody [anti-mouse (1:10,000 for GRP 75; 1:1,000 for tubulin) or anti-rabbit (1:10,000 for VDAC)]-for 1.5 hrs at 25 ºC. Membranes were then washed for 30 min (3 x 10 min) with TBST, incubated with chemiluminescent substrate (Pierce) for 5 min and developed using Kodak Biomax light film (Kodak).

Immunochemical analyses for NOS isoforms were performed using rat liver proteins (MT or CO). Positive controls consisted of nNOSr or eNOSr spiked MT. Samples (150 µg each) were placed into 2X loading buffer and incubated for 30 min at 37 ºC. Samples were loaded in wide lanes (using a 5 well comb) and SDS-PAGE was performed using 7.5% polyacrylamide and transferred to nitrocellulose membranes as mentioned previously. The membranes containing transferred proteins were blocked for 20 min with 1% non-fat dry milk plus 1% BSA in TBST. After thoroughly washing the membranes for 15 min (3 x 5 min) with TBST, Western blotting was performed for nNOS and eNOS. Briefly, the membranes were incubated with either rabbit polyclonal nNOS antibody (1:2,000) or monoclonal eNOS antibody (1:2,000) in TBST for 1hr at 4º C. Again, the membranes were washed for 15 min (3 x 5 min), with TBST, and subsequently, incubated for 1 hr with the appropriate alkaline phosphatase conjugated-anti-rabbit secondary antibody (1:2,000). After washing for 15 min (3 x 5 min) with TBST, the membranes were developed and proteins were visualized using the BCIP/NBT substrate (Sigma).

Immunochemical analyses against CaM were performed in which 150 µg of MT or 30 ng CaM-spiked in 150 µg MT (positive control) were separated by SDS-PAGE (15 % polyacrylamide) and transferred to nitrocellulose membranes as previously mentioned. The membranes were then blocked and incubated overnight with an anti-rabbit monoclonal antibody against CaM, diluted in TBST containing 5 % non-fat dry milk (1:10,000) at 4º C. After washing for 15 min (3 x 5 min) with TBST, the membranes were incubated with the anti-rabbit HRP-conjugated secondary antibody (1:5,000) for 1 hr. Membranes were washed for 15 min (3 x 5 min) with TBST, incubated with chemiluminescent substrate (Pierce) for 5 min and developed using a photo imager (Kodak).

Oxyhemoglobin capture assay: Assays, containing oxyhemoglobin (8 µM), *L*-arginine (100 µM), $CaCl_2$ (400 µM), CaM (25 nM), BH_4 (10 µM), NADPH (100µM) and HEPES (50 mM; pH 7.6) were conducted as previously described (Sheta *et al.*, 1994). MT (50 µg and 500 µg) were subjected to mild sonication for 5s, twice (amplitude - 25%) and added to the assay in place of nNOSr. In addition, 50 units each of superoxide dismutase (SOD) and catalase (CAT) were included in all assays to minimize interference from reactive oxygen species, $O_2^{\bullet-}$ & H_2O_2.

2.3 Results

Purity of Mitochondrial Preparations: Control tissue homogenate (CO) and fractions obtained during mitochondrial isolation steps (M2, M4, M5 and MT) were subjected to immunochemical analyses for mitochondrial and non-mitochondrial markers in order to document the purity of the preparation. Western blot analyses probing the mitochondrial matrix marker, GRP 75, indicated sequential enrichment of GRP 75 during purification (Fig. 2.1A). GRP 75 was neither detected in control tissue homogenate (Fig. 1.1A) nor in the crude supernatants (M1 or M3; data not shown). The mitochondrial outer membrane marker, VDAC was detected in the MT fraction, whereas it was not detected in control tissue homogenate (Fig. 2.1B). The non-mitochondrial, cytosolic marker tubulin, as a further test of purity, was detected in control tissue homogenate whereas it was absent in MT (Fig. 2.1C).

Proteomic Analyses of Mitochondria: Initially, purified intact rat liver MT (1.5 mg protein, Bradford) were TCA precipitated, acetone washed and processed for LTQ-MS analyses after digestion with trypsin as described ***(Experimental Procedures)***. A total of 300 proteins were identified, including several well-established mitochondrial proteins such as components of the respiratory complexes and other mitochondrial markers such as VDAC, NADH-ubiquinone oxidoreductase and ATP synthase subunits. However, there were no peptide signals in experimental samples to indicate the presence of any NOS isoform (Appendix 1).

As a next step, sub-mitochondrial particles were obtained from 2.9 mg of intact MT. Sub-mitochondrial particles were then subjected to affinity chromatography using 2′, 5′- ADP Sepharose 4B. The 2′, 5′- ADP Sepharose 4B eluates of both the supernatants as well as the solubilized pellets were processed as described ***(Experimental Procedures)*** and subjected to

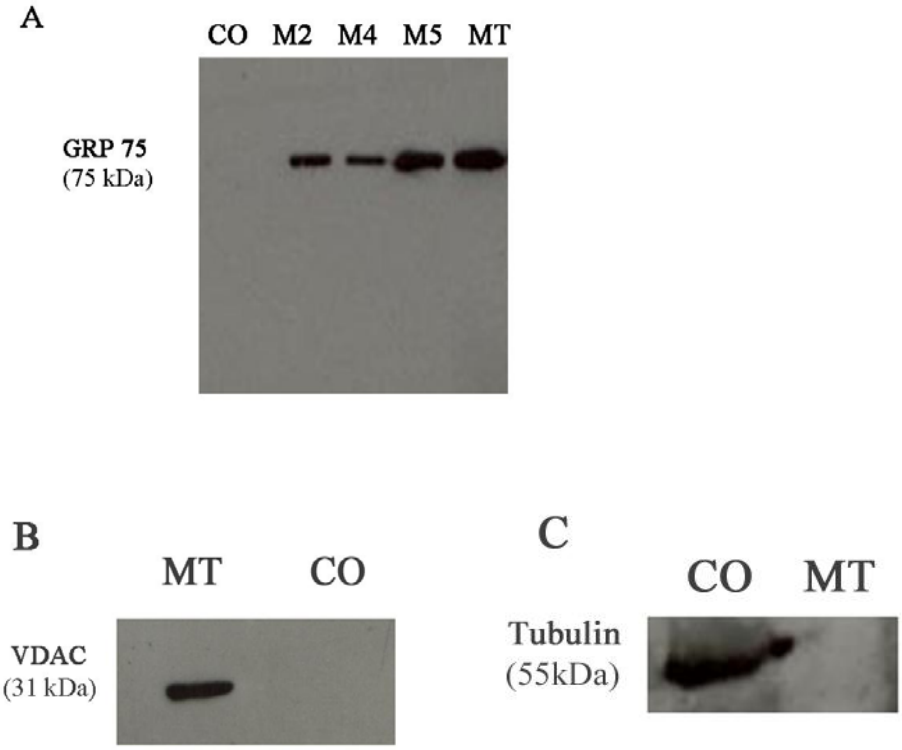

Fig. 2.1. Immunochemical analyses of rat liver mitochondrial fractions with antibodies against mitochondrial and non-mitochondrial markers. Proteins collected during mitochondrial isolation and purification steps (M2, 10,000 x g; M4, 10,000 x g; M5, 9,000 x g; MT, intact MT after repeated differential centrifugation and Percoll gradient purification and CO, control tissue homogenate) were separated by SDS-PAGE and transferred onto nitrocellulose membranes as described ***(Experimental Procedures)***. Western blotting was performed with antibodies against: A. the mitochondrial matrix marker, GRP 75, B. the mitochondrial outer membrane marker, VDAC or C. the cytosol marker, tubulin. The immunocomplexes were visualized by the HRP-conjugate reaction using a chemiluminescence substrate (Pierce). *Lane* MT, run on the same gel as other fractions, was cropped and pasted along side other fractions after removing the intervening lanes.

proteomic analyses. Positive-controls, consisting of sub-mitochondrial particles spiked with 200 femtomoles of nNOSr were run in parallel, as described ***(Experimental Procedures)***. LTQ-MS analyses of the affinity- purified eluates of supernatant from sub-mitochondrial particles led to the identification of 284 proteins with a false-positive rate of ~2% (Appendix 2). Again, MS analyses of the sub-mitochondrial particles failed to provide evidence for the existence of any NOS-derived peptide(s) (supernatant; Appendix 2 or pellet; data not shown).

However, two NOS-derived peptides could be detected in the MT samples spiked with nNOSr (positive control), even when one-fourth of the sample (as low as 50 femtomoles nNOSr) was analyzed by nanoLC-MS/MS (Appendix 3). Furthermore, neither CaM nor any known CaM-binding protein could be detected in MT samples or in samples of sub-mitochondrial particles. Thus, we conclude that NOS (any isoform) is absent from both intact MT as well as sub-mitochondrial particles, at least at levels that can be detected by the highly sensitive nanoLC-MS/MS analyses.

Assay for NOS activity: NOS activity was determined by measurement of the conversion of [^{14}C]-*L*-arginine to [^{14}C]-*L*-citrulline ***(Experimental Procedures),*** with intact MT (Fig. 2.2A) as well as with the supernatant fraction of sub-mitochondrial particles (Fig. 2.2B). The assay containing nNOSr (30 nM) alone, along all necessary substrates and co-factors, was used as a positive control. The positive control produced a substantial amount of [^{14}C]-*L*-citrulline (*Bar 1*; Fig. 2.2A and Fig. 2.2B). Addition of the NOS inhibitor, *L*-thiocitrulline (800 μM) abolished this activity by 98.5 % (*Bar 2*; Fig. 2.2A and Fig. 2.2B). Initially, when intact MT sample was added to the assay, a weak signal of radioactivity was observed (*Bar 3*; Fig. 2.2A). However, this signal could not be inhibited by thiocitrulline (Fig. 2.2A) or *L*-NNA (data not shown),

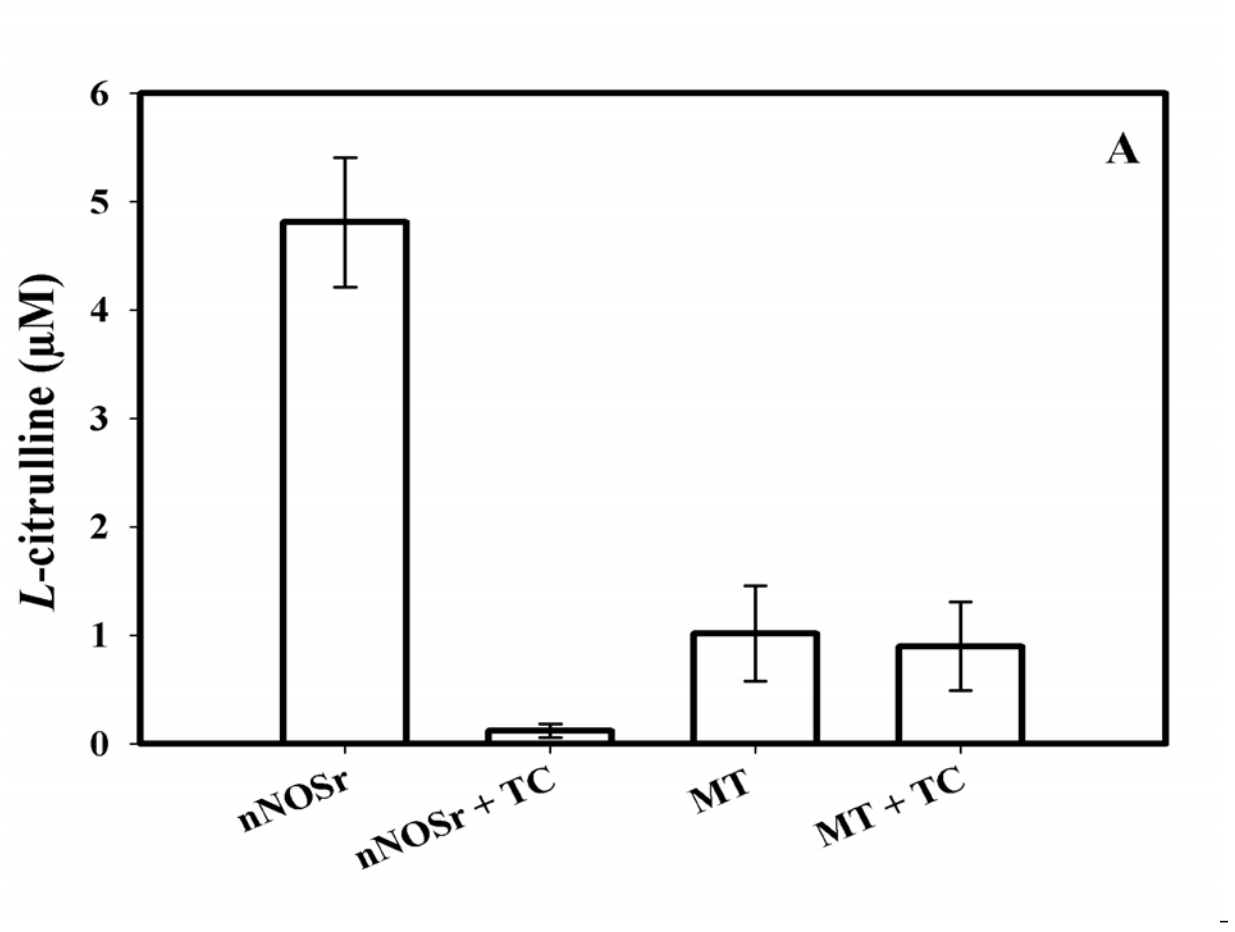

Fig. 2.2. [^{14}C]-*L*-arginine to [^{14}C]-*L*-citrulline conversion assay using MT. A. Measurement of the conversion of [^{14}C]-*L*-arginine to [^{14}C]-*L*-citrulline was performed on MT fractions. The positive control was nNOSr (30nM) in all experiments (*Bar 1*). [^{14}C]-*L*-citrulline production by nNOSr was almost completely inhibited by the NOS inhibitor, thiocitrulline (800 μM; denoted as TC; *Bar* 2). [^{14}C]-*L*-citrulline production by MT (150 μg; *Bar 3*); MT + TC (150 μg; *Bar 4*). Control values from incubation containing all ingredients except enzyme or MT, were subtracted from all data points. Data were expressed as the mean ± range of values, of experimental data points from two independent experiments, each run in duplicate.

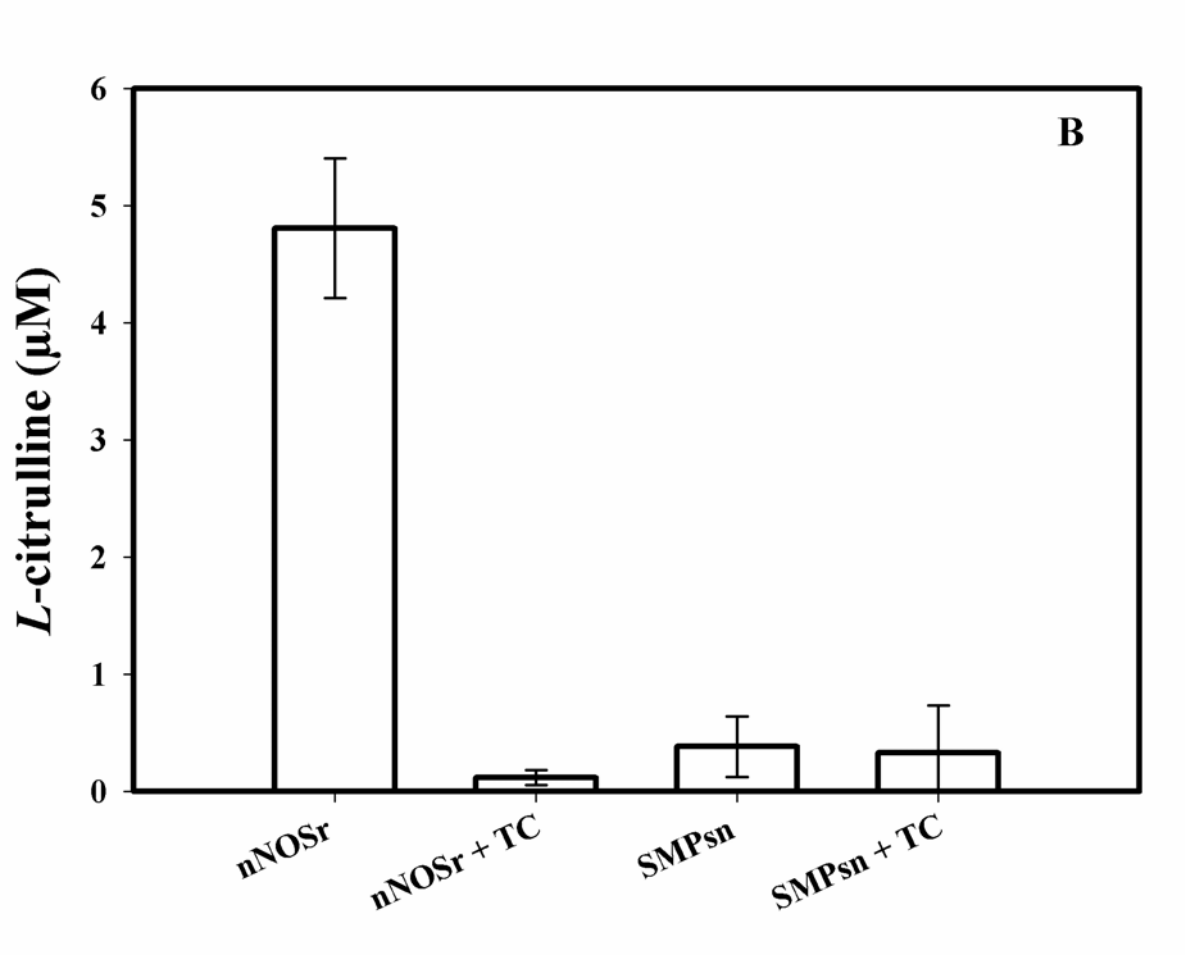

Fig. 2.2. [^{14}C]-*L*-arginine to [^{14}C]-*L*-citrulline conversion assay using MT. B. Measurement of the conversion of [^{14}C]-*L*-arginine to [^{14}C]-*L*-citrulline was performed on sub-mitochondrial particles (SMP). The positive control was nNOSr (30nM) in all experiments (*Bar 1*). [^{14}C]-*L*-citrulline production by nNOSr was almost completely inhibited by the NOS inhibitor, thiocitrulline (800 μM; denoted as TC; *Bar* 2). [^{14}C]-*L*-citrulline production by supernatant of sub-mitochondrial particle from 150 μg MT (denoted as SMPsn; *Bar 3*); SMPsn + TC (*Bar 4*). Control values from incubation containing all ingredients except enzyme or MT, were subtracted from all data points. Data were expressed as the mean ± range of values, of experimental data points from two independent experiments, each run in duplicate.

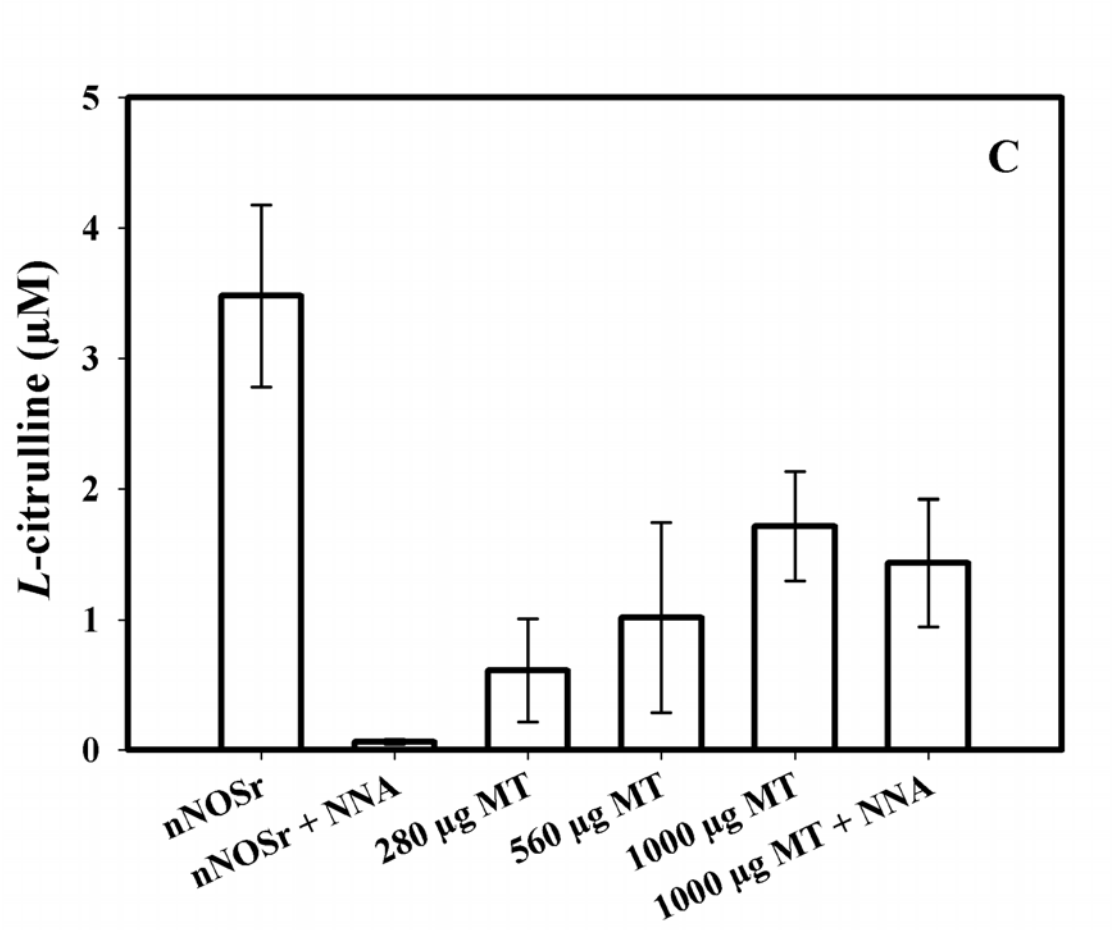

Fig. 2.2. [^{14}C]-*L*-arginine to [^{14}C]-*L*-citrulline conversion assay using MT. C. Measurement of the conversion of [^{14}C]-*L*-arginine to [^{14}C]-*L*-citrulline was performed on MT fractions. The positive control was nNOSr (30nM) in all experiments (*Bar 1)*. [^{14}C]-*L*-citrulline production by nNOSr was almost completely inhibited by the NOS inhibitors *L*-NNA (400 μM; *Bar 2*). [^{14}C]-*L*-citrulline production by intact MT of various amounts: 280 μg (*Bar 3*), 560 μg (*Bar 4*) and 1,000 μg (*Bar 5*) and 1,000 μg MT + *L*-NNA (*Bar 6*). Control values from incubation containing all ingredients except enzyme or MT, were subtracted from all data points. Data were expressed as the mean ± range of values, of experimental data points from two independent experiments, each run in duplicate.

providing evidence against a NOS-catalyzed reaction. Although *L*-thiocitrulline is a potent nNOS inhibitor, at 800 μM, it is non-specific, cross-reacting with all NOS isoforms and resulting in almost complete inhibition of NOS-catalyzed [^{14}C]-*L*-citrulline production.

Assays conducted with supernatants containing sub-mitochondrial particles, also showed a weaker radioactivity signal (Fig. 2.2B). As with the weak signal observed with intact MT, this signal could not be inhibited by *L*-thiocitrulline (800 μM). When this weak radioactive signal was investigated, it was found that assays performed with increasing amounts of intact MT protein produced a titratable increase in radioactive signal (Fig. 2.2C). Additionally, this radioactive signal could not be inhibited using the pure, commonly used NOS inhibitor, *L*-NNA (400 μM) when added to 1,000 μg MT (Fig. 2.2C). Thus, the radioactive signal obtained with MT or with supernatant containing sub-mitochondrial particle could not be inhibited by NOS inhibitors, indicating that the radioactive signal is probably not an enzymatic reaction catalyzed by NOS.

When assays were performed with increasing amounts of pure BSA (250, 500 and 750 μg) instead of MT, it did not result in appearance of any radioactive signal in the flow-through (< 3%) above control (data not shown). A NADPH regenerating system was included in some of the assays with MT in order to ensure that NADPH was not becoming a limiting factor. Again, nNOSr (30 nM) was used as the positive control. Results obtained with MT using the NADPH-regenerating system showed the same weak radioactive signal (Fig. 2.3). When nNOSr was spiked into MT, the [^{14}C]-*L*-citrulline signal dramatically increased (82% of the activity of the positive control).

Additional control assays using denatured MT (dMT) were performed in order to help us

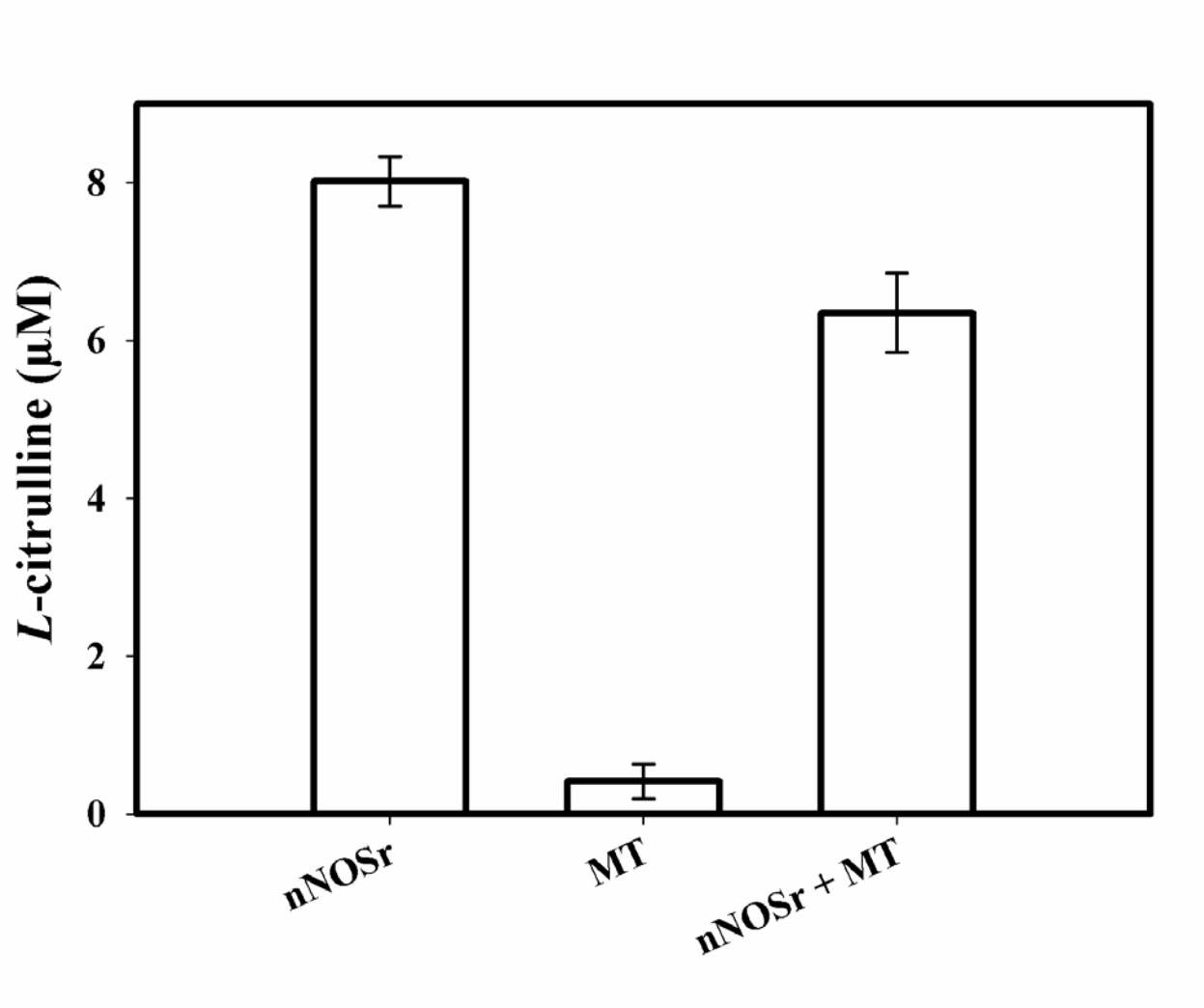

Fig. 2.3. [^{14}C]-*L*-citrulline production in the presence of NADPH regenerating system. Measurement of the conversion of [^{14}C]-*L*-arginine to [^{14}C]-*L*-citrulline was performed using a NADPH regenerating system containing glucose 6-phosphate (125 mM), NADP (12.5 mM) and 1 unit of glucose 6-phosphate dehydrogenase. *Bar 1:* The positive control, nNOSr (30 nM). *Bar 2:* MT (150 μg). *Bar 3:* MT (150 μg) + nNOSr (30 nM). Values from control incubations containing all ingredients except enzyme were subtracted from all data points. Data were expressed as the mean ± range of values, of experimental data points from two independent experiments, each run in duplicate.

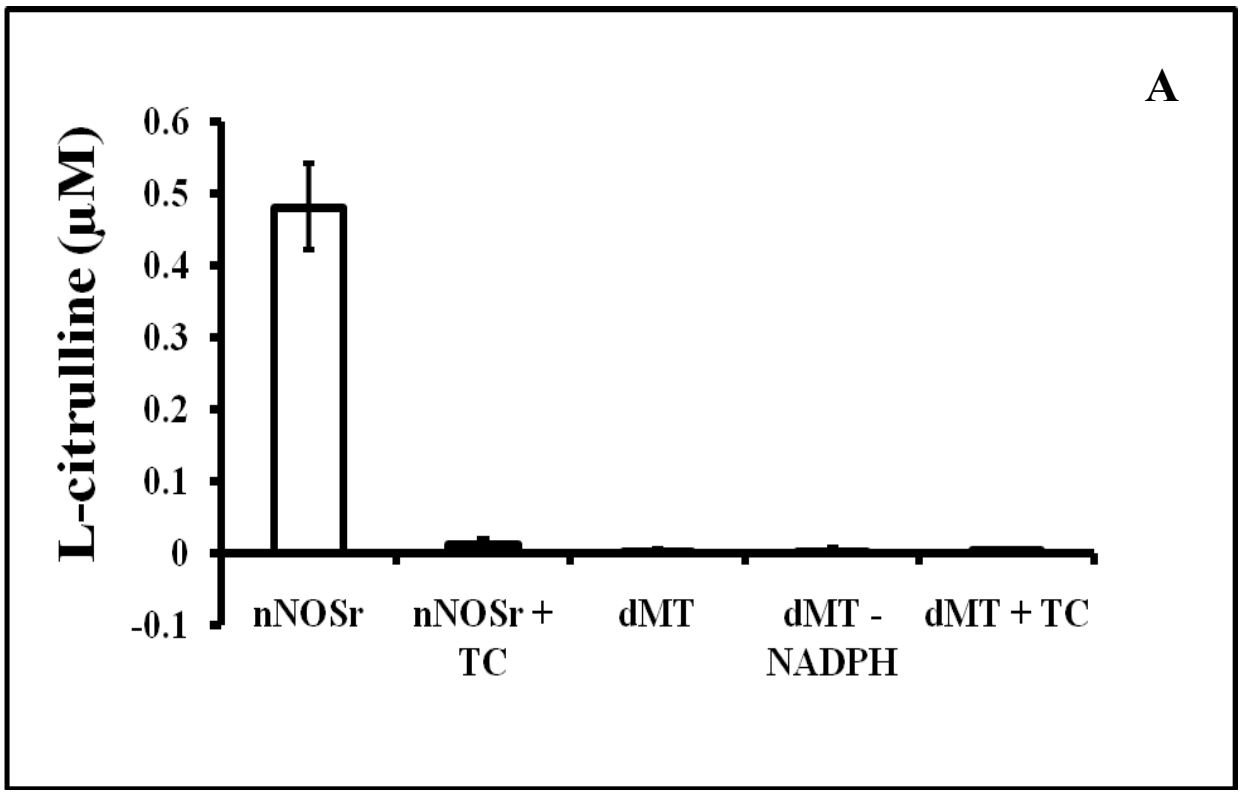

Fig. 2.4. [^{14}C]-*L*-citrulline production assay containing nNOSr with dMT. A. Measurement of the conversion of [^{14}C]-*L*-arginine to [^{14}C]-*L*-citrulline was performed on various amounts of dMT in the presence of nNOSr (30 nM). The incubates are as follows: *Bar 1:* nNOSr alone. *Bar 2:* nNOSr + TC. *Bar 3:* dMT alone. *Bar 4:* dMT without NADPH. *Bar 5*: dMT + TC. Values from control incubation containing all ingredients except enzyme were subtracted from all data points. Data were expressed as the mean ± range of values, of experimental data points from two independent experiments, each run in duplicate.

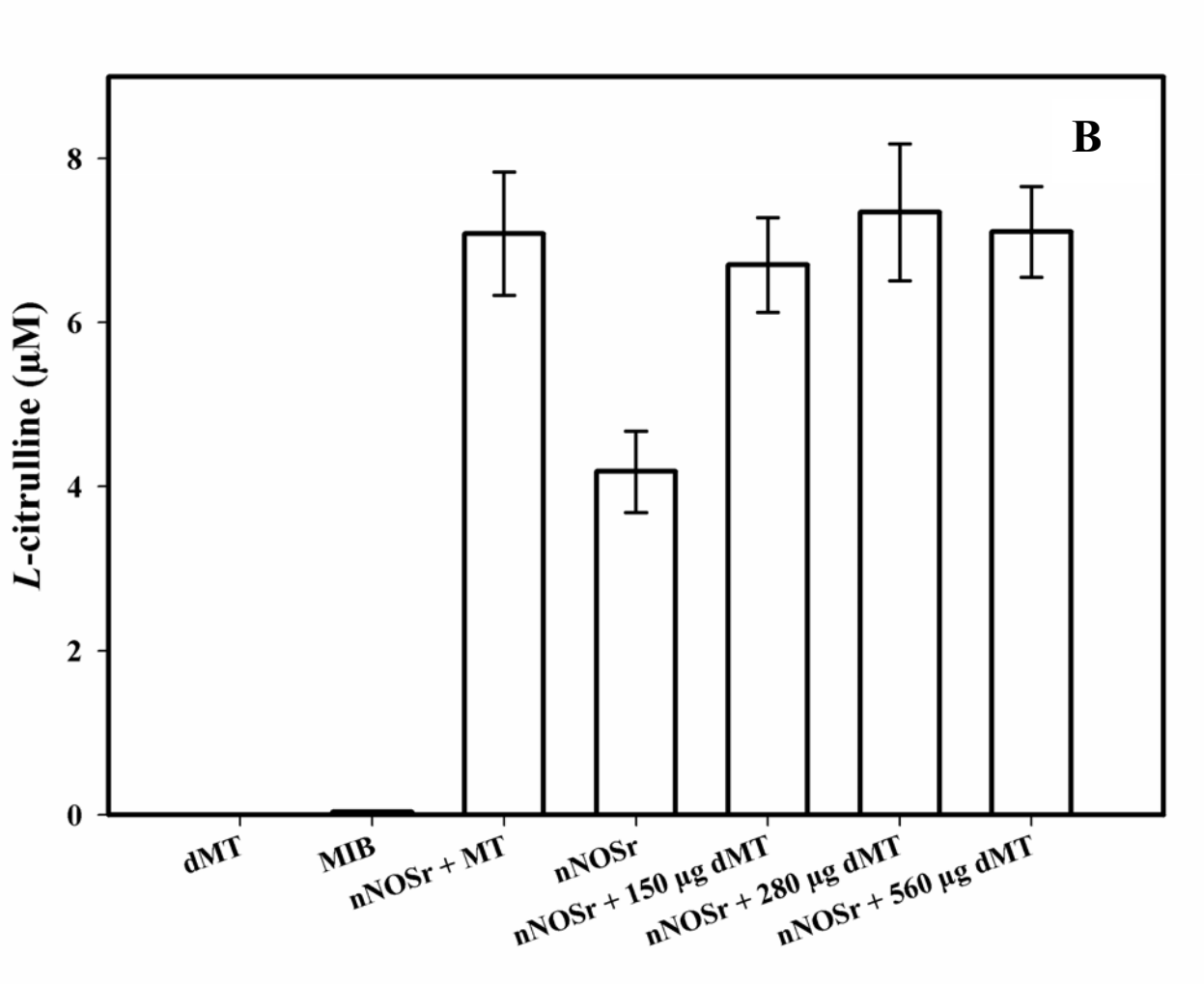

Fig. 2.4. [^{14}C]-*L*-citrulline production assay containing nNOSr with dMT. B. Measurement of the conversion of [^{14}C]-*L*-arginine to [^{14}C]-*L*-citrulline was performed on various amounts of dMT in the presence of nNOSr (30 nM). The incubates are as follows: *Bar 1:* dMT alone. *Bar 2:* MIB alone. *Bar 3:* nNOSr + intact 150 μg MT. *Bar 4:* nNOSr alone. *Bar 5*: nNOSr + 150 μg dMT. *Bar 6*: nNOSr + 280 μg dMT. *Bar 7:* nNOSr + 560 μg dMT. Values from control incubation containing all ingredients except enzyme were subtracted from all data points. Data were expressed as the mean ± range of values, of experimental data points from two independent experiments, each run in duplicate.

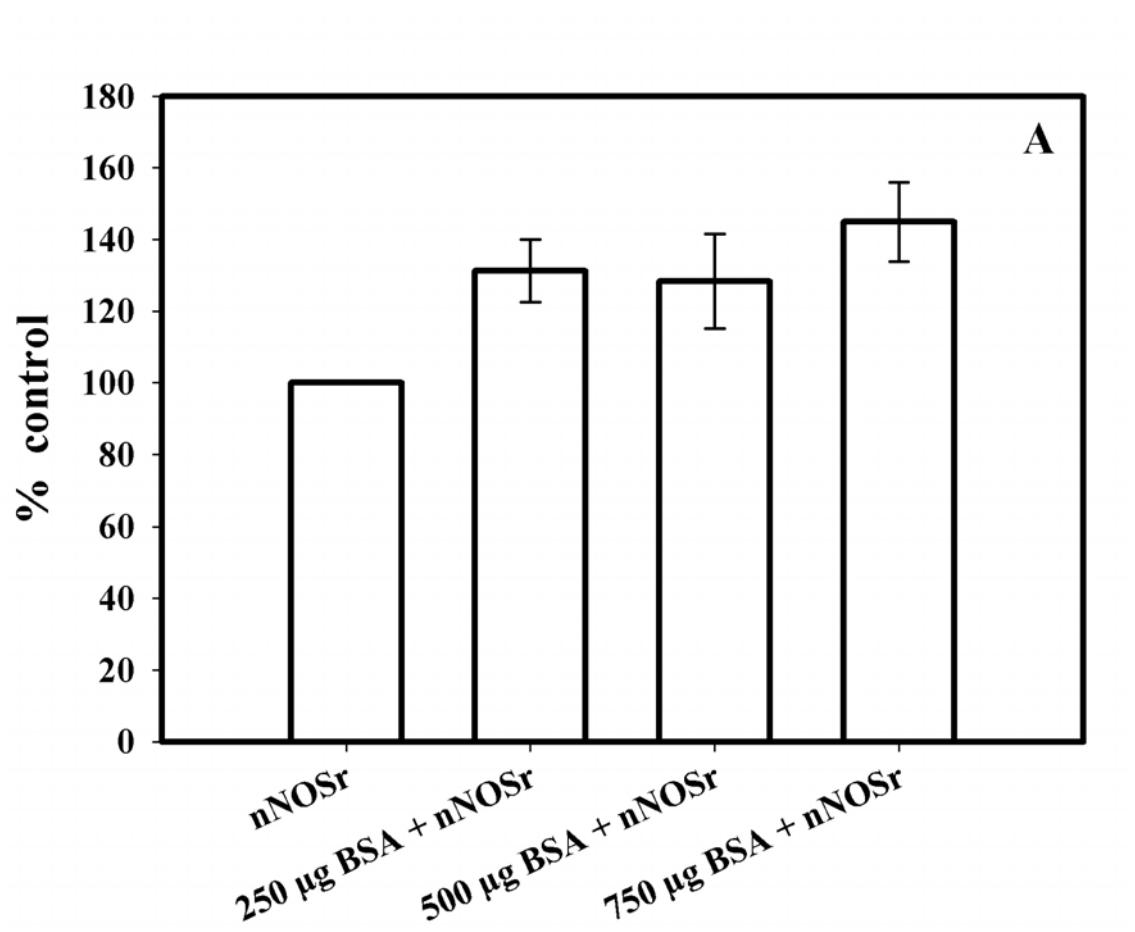

Fig. 2.5. Control experiments using [^{14}C]-*L*-citrulline production assays. A. Values from control incubation containing all ingredients except enzyme were subtracted from all data points. Data were expressed as the mean ± range of values, of experimental data points from two independent experiments, each run in duplicate. Measurement of conversion of [^{14}C]-*L*-arginine to [^{14}C]-*L*-citrulline was performed with various amounts of BSA (250, 500 and 750 µg) plus nNOSr (7.5 pmoles). Values are represented as the percentage change in relation to control radioactivity of nNOSr alone (shown as *Bar 1*).

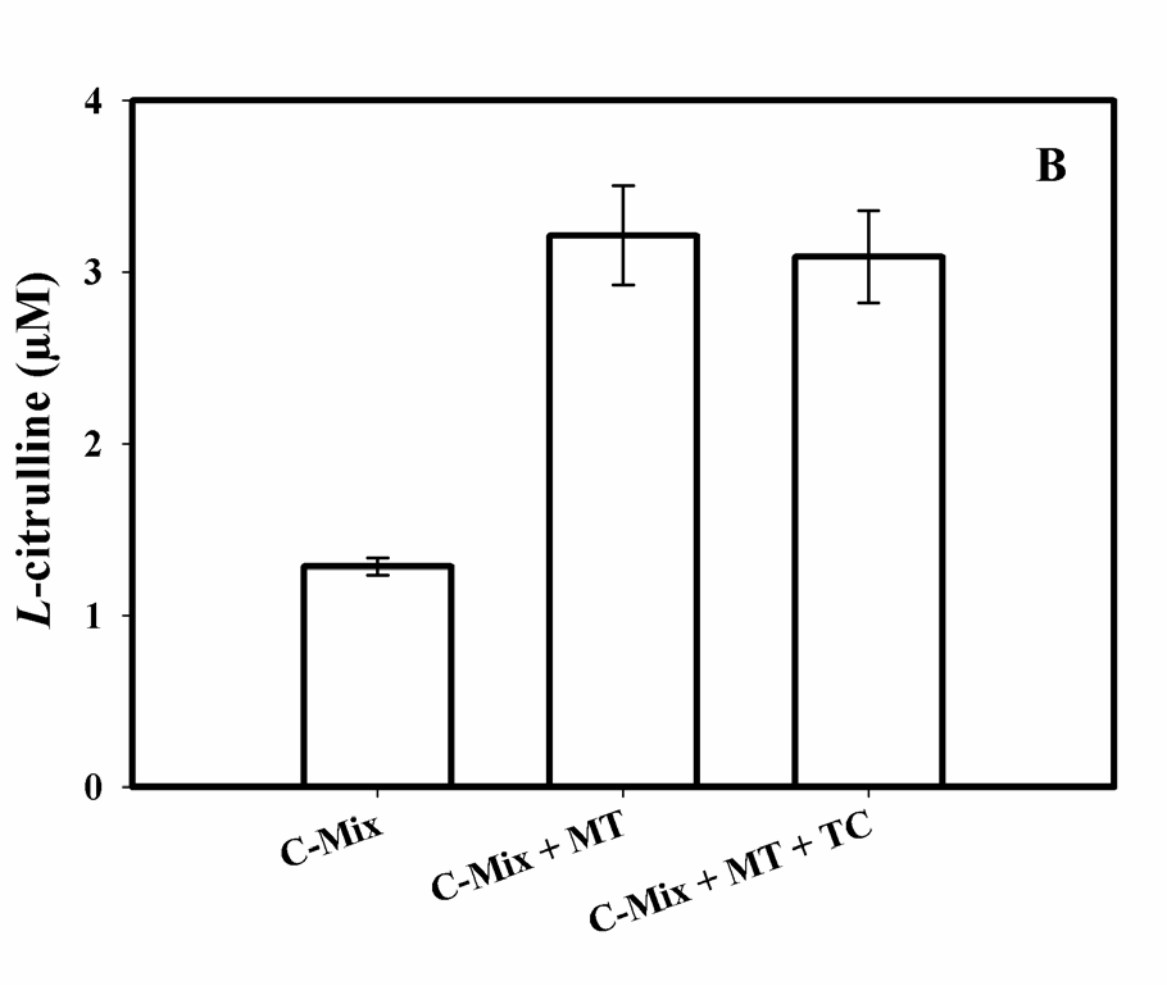

Fig. 2.5. Control experiments using [^{14}C]-*L*-citrulline production assays. B.Values from control incubation containing all ingredients except enzyme were subtracted from all data points. Data were expressed as the mean ± range of values, of experimental data points from two independent experiments, each run in duplicate. B. Measurement of the conversion of [^{14}C]-*L*-arginine to [^{14}C]-*L*-citrulline was performed with all substrates and cofactors (*L*-arginine, $CaCl_2$, CaM, [^{14}C]-*L*-arginine, HEPES) (C-Mix) in the absence of NADPH and BH_4. *Bar 1*: C-Mix. *Bar 2*: C-Mix + 150 µg MT. *Bar 3*: C-Mix + 150 µg MT + 800 µM *L*-thiocitrulline (denoted as TC). Incubates were eluted with Dowex column and scintillation counting was performed.

understand the reason(s) behind the weak signal that could not be inhibited by NOS inhibitors ***(Experimental Procedures)***. nNOSr (30 nM) was used as a positive control. dMT alone were used as a negative control. nNOSr-catalyzed [^{14}C]-*L*-citrulline production was measured in the presence of increasing amounts of dMT. Following incubation of 150 μg dMT with nNOSr plus all substrates and cofactors, the corresponding Dowex column eluates displayed a significant increase (63%) in radioactive signal when compared to the nNOSr signal in the absence of MT (*Bars 4 and 5;* Fig. 2.4A). dMT at concentration ≥ 150 μg protein plus nNOSr caused a concentration-dependent increase in [^{14}C] signal (*Bar 6* and *Bar 7*; Fig. 2.4A). Additional control assays were performed with: A) dMT minus NADPH and B) dMT plus *L*-thiocitrulline. These control assays were negative for a [^{14}C] signal in the eluates from the Dowex columns (Fig. 2.4B). Results from assays containing nNOSr with titrated amounts of dMT indicate that there is an nNOS-independent, but protein concentration-dependent increase in the [^{14}C]-radioactive signal in the Dowex column eluates. An important point to note is that, this effect occurs even with twice the amount of Dowex (2 ml) normally used in the literature (1 ml).

When assays were conducted with a pure protein BSA, increasing amounts of BSA (250, 500 and 750 μg) plus nNOSr (30 nM) slightly increased the radioactive "signal" that was produced when compared to nNOSr in the absence of BSA (Fig. 2.5A & RT. Miller Ph.D., unpublished observations). Furthermore, when C-Mix, which did not contain NADPH and BH_4, was incubated with MT , and then eluted from the Dowex columns, once again a titratable increase in [^{14}C] signal was observed (*Bar* 2, Fig. 2.5B) compared to the control, assayed in the absence of protein (*Bar* 1, Fig. 2.5B). This signal (*Bar* 2, Fig. 2.5B) could not be inhibited by *L*-thiocitrulline (800 μM; *Bar* 3; Fig. 2.5B). Results from Fig. 2.5B clearly indicate that this signal

is observed even in the absence of NADPH and BH_4, and is not due to a NOS-catalyzed reaction. Here, the control values from incubation containing all ingredients except enzyme or MT were not subtracted from all data points.

In order to identify the source of the weak radioactive signal emanating from the MT sample, we probed the conversion assay-eluates for amino acids, using HP-TLC (Fig. 2.6). [^{14}C]-*L*-arginine to [^{14}C]-*L*-citrulline conversion assay-eluates of the respective samples [nNOSr (30 nM; *lane* 1); nNOSr + *L*-thiocitrulline (800 μM; *lane* 2); MT (150 μg; *lane* 3); MT+ *L*-thiocitrulline (*lane* 4)] and the non-Dowex treated C-Mix (*lane* 5) were acetone-precipitated, centrifuged and the supernatants were subjected to HP-TLC followed by autoradiography (Fig. 2.6). On the other hand, C-Mix and the [^{14}C]-*L*-arginine to [^{14}C]-*L*-citrulline conversion assay-eluates of the MT sample (representing *lane* 6 and *lane* 7 respectively, in Fig. 2.6) were treated with Dowex columns, centrivapped and then subjected to acetone precipitation *(as described in Experimental Procedures)*. C-Mix which contained [^{14}C]-*L*-arginine, was used as a positive control (*lane* 5; Fig. 2.6).

In Fig. 2.6, the nNOSr containing sample was used as a positive control for validation of the assay. Both, the reaction substrate ([^{14}C]-*L*-arginine) and the product ([^{14}C]-*L*-citrulline) were present (*lane* 1). *L*-thiocitrulline was included in the conversion assay as negative control. Inhibition of nNOS prevented [^{14}C]-*L*-citrulline production (*lane* 2). Results from MT samples indicated no conversion of [^{14}C]-*L*-arginine to [^{14}C]-*L*-citrulline (*lane* 3). This result was in stark contrast to the band visualized in *lane* 9 that contained *L*-citrulline. When C-Mix alone was passed through Dowex column (*lane* 6), the positively charged [^{14}C]-*L*-arginine was completely bound to the Dowex resin, thus, no [^{14}C]-*L*-arginine signal was observed. Importantly, MT

sample eluates that were passed through Dowex (*lane* 7), did not show contain [^{14}C]-*L*-citrulline.

In order to identify if the fuzzy radioactive band that occurs at the top of lanes containing MT (lane 3, 4 and 5 in Fig. 2.7) was due to the action of *L*-arginase, TLC was performed wherein *L*-arginase inhibitor, *N*-hydroxy-*L*-arginine was used. Two sets of samples were used where one batch of [^{14}C]-*L*-arginine to [^{14}C]-*L*-citrulline conversion assay-eluates was passed through Dowex filtration and the other batch was not passed through Dowex filtration. Both set of samples were processed as mentioned earlier and TLC was performed ***(Experimental Procedures)***. Comparison of the eluates that were passed through Dowex filtration (Fig. 2.7A) and not through Dowex filtration (Fig. 2.7B) helped us understand if the radioactive bands are positively charged and also about the inference of *N*-OH-*L*-arginine with the fuzzy band formation. Each sample (lanes 1-9) contained all the substrates and the cofactors and the samples were loaded in the following order in both the TLC plates: No nNOSr/MT (*lane 1*); nNOSr (30 nM; *lane* 2); nNOSr + *L*-thiocitrulline (800 μM; *lane* 3); MT (150 μg; *lane 4*); MT+ *L*-thiocitrulline (*lane* 5), denatured MT (*lane 6*), MT + *N*-OH-*L*-arginine (40 μM; lane 7), nNOSr (30 nM) + *N*-OH-*L*-arginine (40 μM; lane 8), *N*-OH-*L*-arginine (40 μM; lane 9) (Fig. 2.7A, Dowex treated; Fig 7B, Dowex untreated. *Lanes 10, 11, 12* were loaded with *L*-arginine, *L*-citrulline and *L*-ornithine (10 μl of 2 mg/ml) alone. In Fig 2.7A, lane 6 containing denatured MT (boiled for 5 min) clearly indicated that the fuzzy band appeared only when the MT is active. In addition, *lane 7* containing MT + *N*-OH-*L*-arginine did not show any fuzzy band indicating that the product is arginase-dependent. Also, *lane 12* containing *L*-ornithine indicating that the fuzzy band in the MT samples were not *L*-ornithine as *L*-ornithine appeared at the lower level. In addition, the lane containing *N*-OH-*L*-Arginine (40 μM; *lane 9*) clearly showed that *N*-OH-*L*-

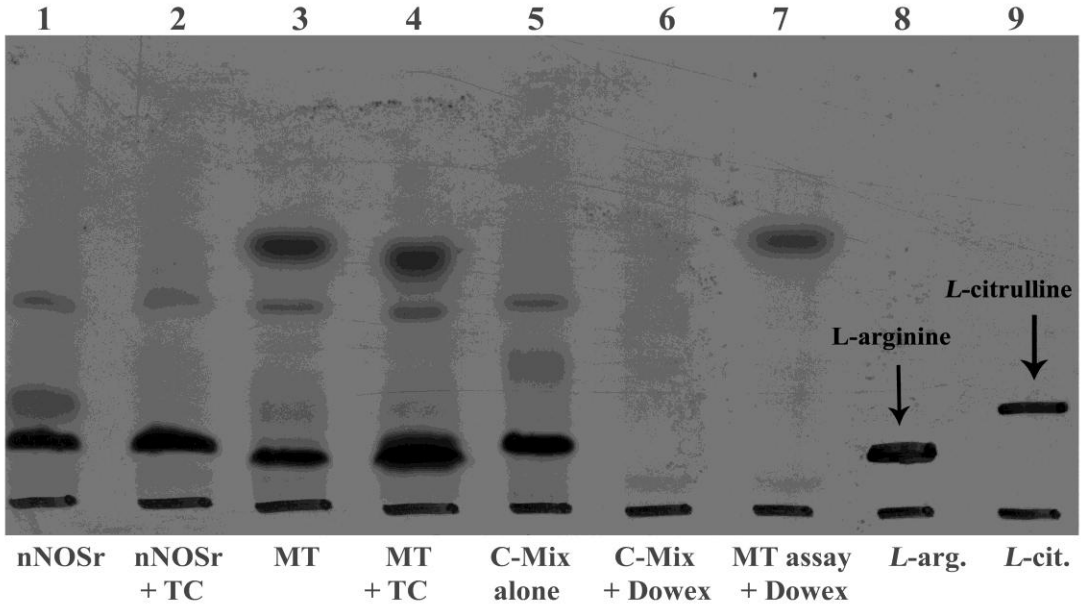

Fig. 2.6. HP-TLC of the acetone-precipitated supernatants of [^{14}C]-*L*-arginine to [^{14}C]-*L*-citrulline conversion assay eluates. Acetone precipitated [^{14}C]-*L*-arginine to [^{14}C]-*L*-citrulline conversion assay eluates (*lanes* 1-7) and the standards: *L*-arginine (*lane* 8) and *L*-citrulline (*lane* 9) were loaded on a plate coated with silica gel and, HP-TLC was performed and developed as described *(Experimental Procedures)*. The bottom most line under each lane is a sharpie-enhancement indicating the loading point. The lane pattern in HP-TLC, was as follows: 1) nNOSr, positive control detecting [^{14}C]-*L*-arginine (substrate) and [^{14}C]-*L*-citrulline (product); 2) nNOSr + *L*-thiocitrulline (denoted as TC), negative control for NOS reaction showing no conversion of [^{14}C]-*L*-arginine to [^{14}C]-*L*-citrulline; 3) MT included in the assay, no conversion of [^{14}C]-*L*-arginine to [^{14}C]-*L*-citrulline; 4) MT + TC included in the assay, no conversion of [^{14}C]-*L*-arginine to [^{14}C]-*L*-citrulline; 5) C-Mix standard without MT or nNOSr, negative control for [^{14}C]-*L*-citrulline; 6) C-Mix followed by Dowex chromatography, no [^{14}C]-*L*-arginine, no [^{14}C]-*L*-citrulline and no unidentified bands; 7) MT included in the assay followed by Dowex

chromatography, no conversion of [^{14}C]-*L*-arginine to [^{14}C]-*L*-citrulline; 8) Sharpie-enhanced *L*-arginine band (non radioactive) developed using 2% ninhydrin solution; 9) Sharpie-enhanced *L*-citrulline band (non radioactive) developed using 2% ninhydrin solution.

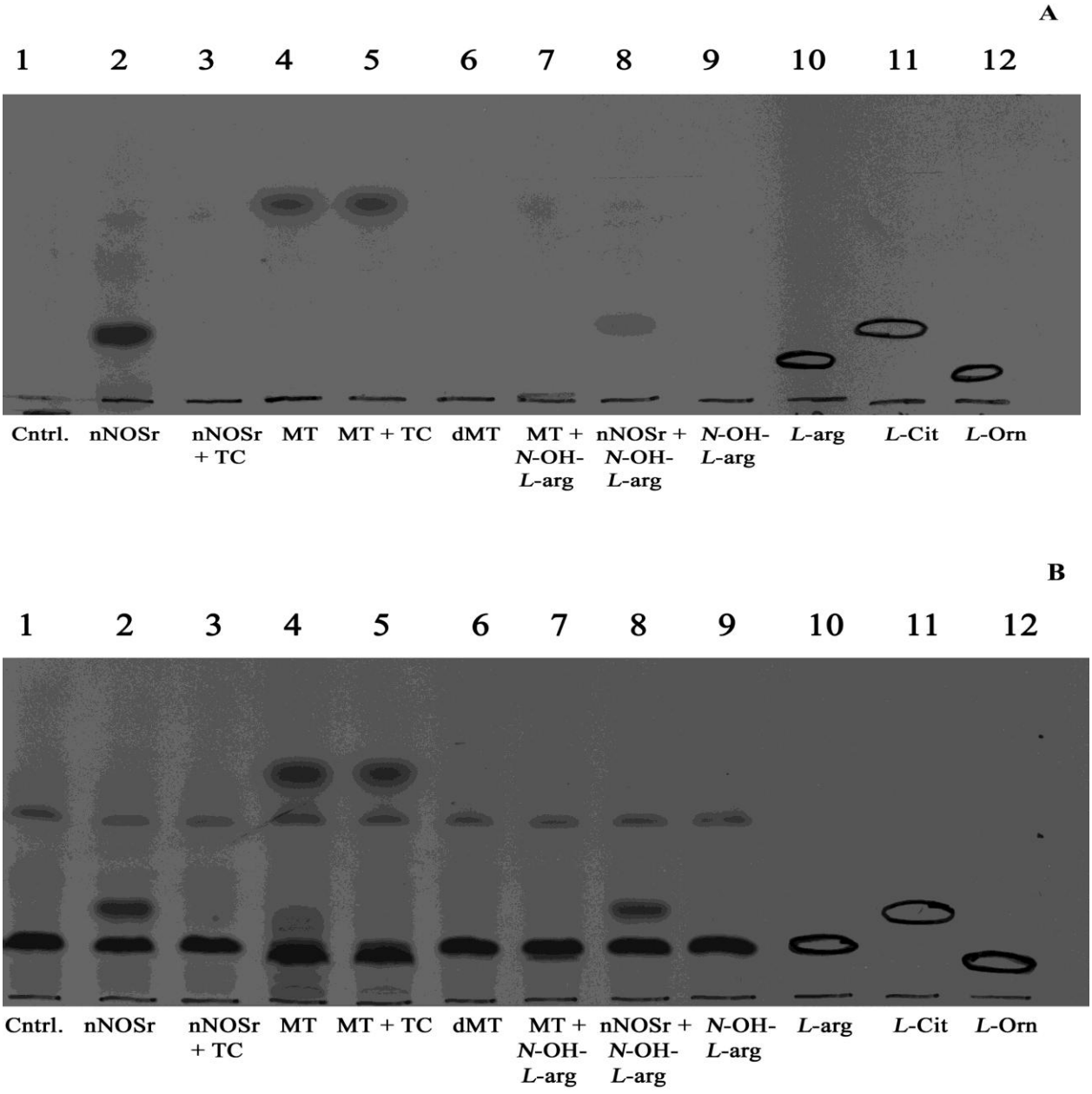

Fig. 2.7. HP-TLC of the acetone-precipitated supernatants of [^{14}C]-*L*-arginine to [^{14}C]-*L*-citrulline conversion assay eluates. Acetone precipitated [^{14}C]-*L*-arginine to [^{14}C]-*L*-citrulline conversion assay eluates treated through Dowex (Fig. 2.7A) and not passed through Dowex (Fig. 2.7B) (*lanes* 1-9 and the standards: *L*-arginine (lane 10), *L*-Citrulline (*lane 11*), *L*-Ornithine *(lane*

12) of Fig. 2.8A and 8B) were loaded on the plates coated with silica gel and, HP-TLC were performed and developed as described *(Experimental Procedures)*. Each sample contained all the substrates and the cofactors and the samples were in the following order: 1) No nNOSr/MT; 2) nNOSr (30 nM); 3) nNOSr + *L*-thiocitrulline (800 μM; denoted as TC); 4) MT (150 μg); 5) MT (150 μg)+ *L*-thiocitrulline ; 6) denatured MT(150 μg); 7) MT (150 μg) + *N*-OH-*L*-arginine (40 μM); 8) nNOSr (30 nM) + *N*-OH-*L*-arginine (40 μM); 9) *N*-OH-*L*-arginine (40 μM); 10) Sharpie-enhanced *L*-arginine band (non radioactive) developed using 2% ninhydrin solution; 11) Sharpie-enhanced *L*-citrulline band (non radioactive) developed using 2% ninhydrin solution; 12) Sharpie-enhanced *L*-Ornithine band (non radioactive) developed using 2% ninhydrin solution.

Arginine alone cannot interfere with the assay. However, the arginase dependent fuzzy band is not *L*-citrulline.

Thus, results obtained from assays measuring the conversion of [^{14}C]-*L*-arginine to [^{14}C]-*L*-citrulline confirmed that, the weak radioactive signal associated with MT sample does not represent NOS-catalyzed *L*-citrulline production. Furthermore, data from NOS activity assays validate one another and collectively, as well as individually, further support the contention that no NOS isoform is present in mitochondria.

Immunochemical analyses of MT using NOS and CaM antibodies: Immunochemical analyses were performed with MT using rabbit polyclonal anti- nNOS- and rabbit monoclonal anti-eNOS-antibodies. SDS-PAGE, gel transfer onto nitrocellulose membranes and Western blotting were performed as described ***(Experimental Procedures)***. Western blot analyses of MT (150 μg) using nNOS antibodies were negative for any NOS protein (Fig. 2.8A). Furthermore, no signal for any NOS protein was observed in the control tissue homogenate, confirming the lack of cellular contaminants in these preparations. However, when 30 ng of nNOSr was spiked into control samples consisting of 150 μg MT, a clear signal could be detected (Fig. 2.8A).

Western blot analyses, using a highly specific eNOS antibody also failed to detect the eNOS isoform in MT whereas the positive control sample containing 30 ng of eNOSr spiked in 150 μg mitochondria could be easily detected (Fig. 2.8B). Also, no signal for eNOS was detected in the control tissue homogenate. Although the nNOS antibody is 10-fold more specific towards detecting the nNOS isoform, at lower dilutions, it cross-reacts with other NOS isoforms, including iNOS (personal communication, B.S. Masters Ph.D.). In contrast, the eNOS antibody is absolutely specific in detecting eNOS (Jachymova *et al.*, 2005). Thus, immunochemical

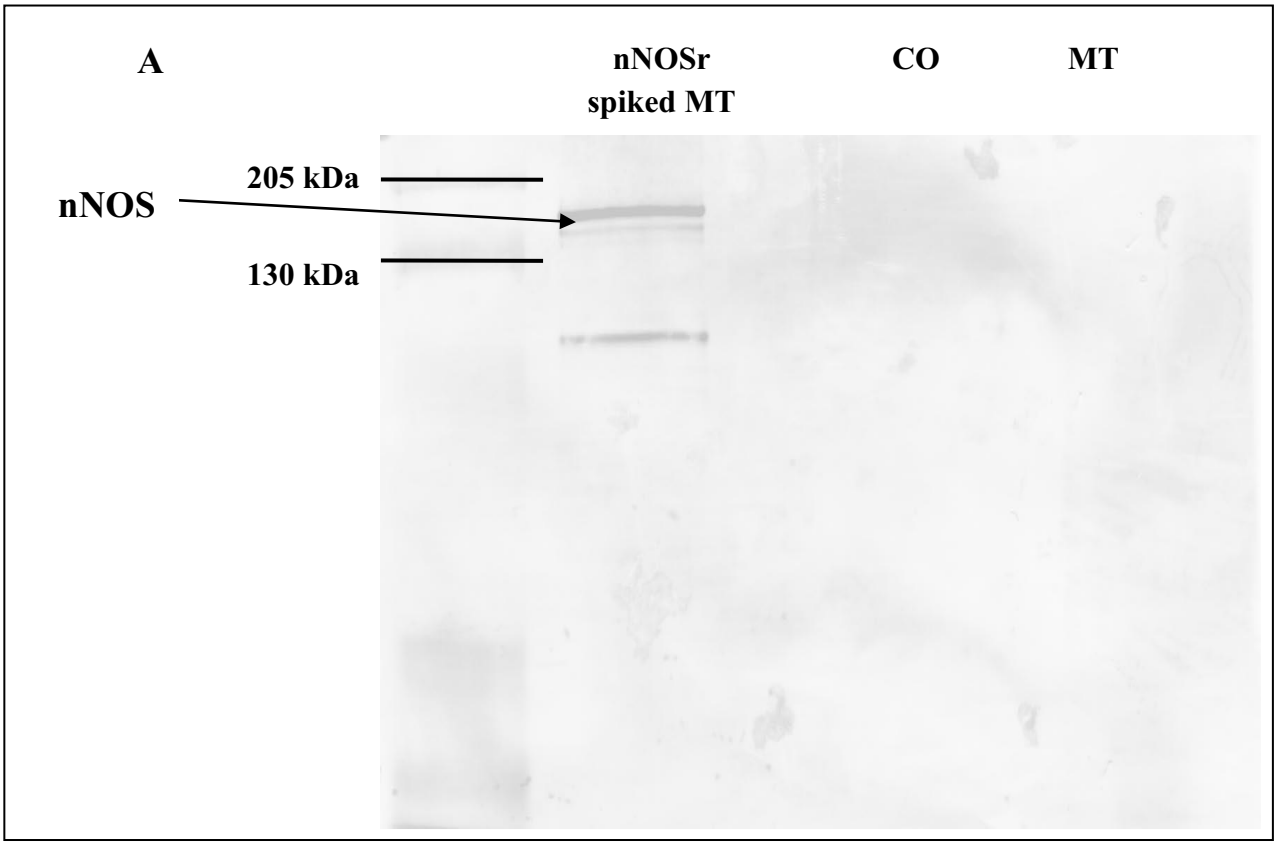

Fig. 2.8. Immunochemical analyses of MT using NOS and CaM antibodies. A. Proteins were separated with SDS-PAGE gel under the conditions described under '*Experimental Procedures*'. 8 µl of protein prestained standard (Biorad) was loaded (*Lane 1*). Western blots were performed with rabbit nNOS antibody. The positive control was 30 ng nNOSr spiked in 150 µg MT *(Lane 2)*. The immunocomplexes of A was developed by alkaline phosphatase reaction using BCIP/NBT substrate. The immunocomplexes were developed by HRP-conjugate using a chemiluminescence substrate (pierce) and MT denotes 150 µg purified mitochondria (*Lane 3*).

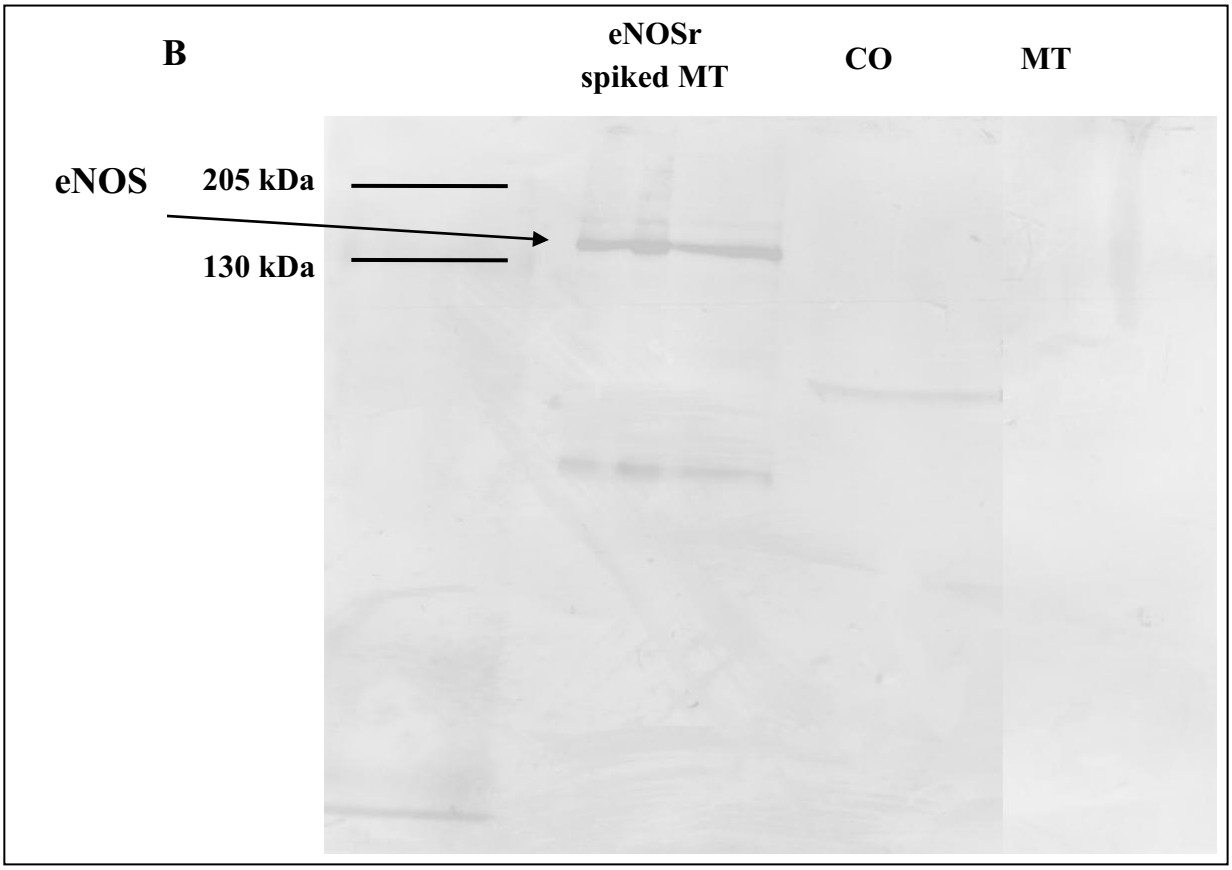

Fig. 2.8. Immunochemical analyses of MT using NOS and CaM antibodies. B. Proteins were separated with SDS-PAGE gel under the conditions described under '***Experimental Procedures***'. 8 µl of protein prestained standard (Biorad) was loaded (*Lane 1*). Western blots were performed with rabbit monoclonal eNOS antibody. The positive control was 30 ng eNOSr spiked in 150 µg MT *(Lane 2)*. The immunocomplexes of B was developed by alkaline phosphatase reaction using BCIP/NBT substrate. *Lane* MT, run on the same gel as other fractions, was cropped and pasted along with other fractions after removing intervening lanes; The immunocomplexes were developed by HRP-conjugate using a chemiluminescence substrate (pierce) and MT denotes 150 µg purified mitochondria (*Lane 3*).

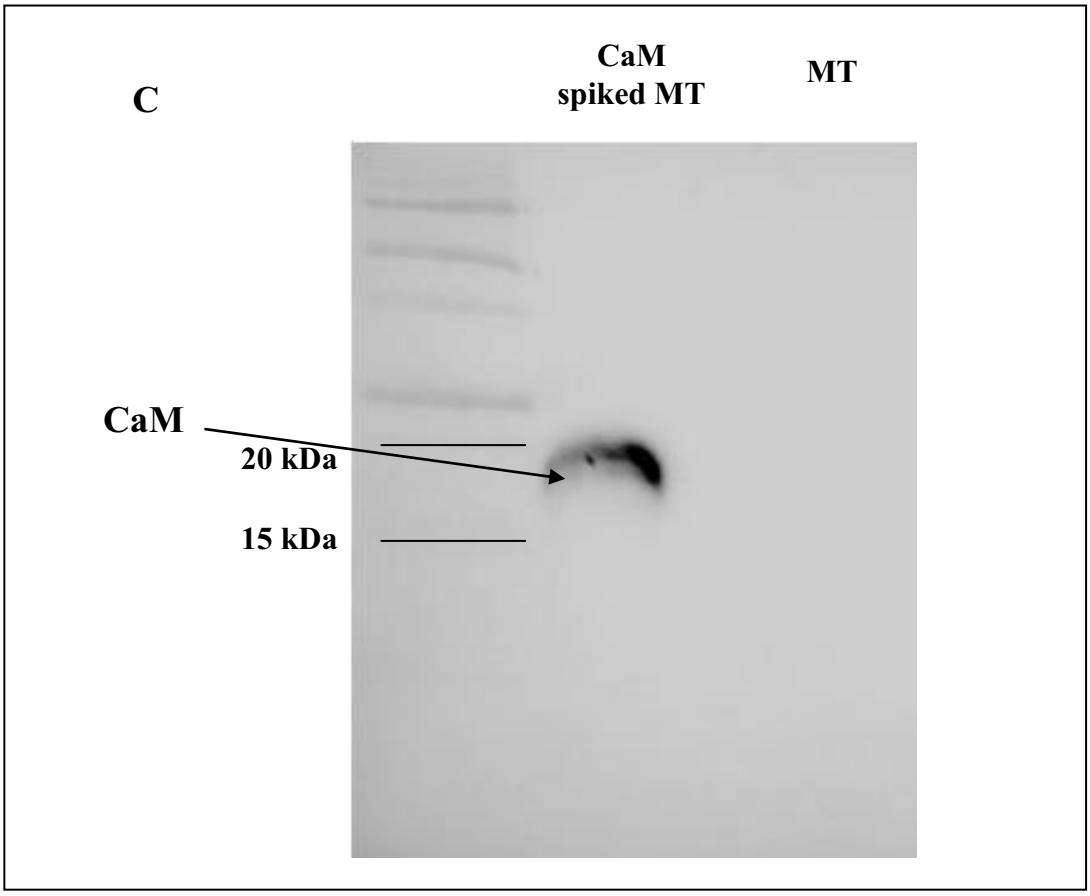

Fig. 2.8. Immunochemical analyses of MT using NOS and CaM antibodies. C. Proteins were separated with SDS-PAGE gel under the conditions described under '*Experimental Procedures*'. 8 µl of protein prestained standard (Biorad) was loaded (*Lane 1*). Western blots were performed with rabbit CaM antibody. The positive control was 30 ng CaM spiked in 150 µg MT (*Lane 2*). The immunocomplexes were developed by HRP-conjugate using a chemiluminescence substrate (pierce) and MT denotes 150 µg purified mitochondria (*Lane 3*).

analyses using NOS antibodies (with reactivities to nNOS, eNOS and iNOS) were negative for any NOS isoform in mitochondria. Additionally, Western blot analyses using a rabbit monoclonal antibody to CaM were negative for the presence of CaM in MT. However, the positive control sample containing 30 ng of CaM spiked into a sample of 150 μg MT could be easily detected (Fig. 2.8C).

2.4 Discussion

We have described carefully planned and executed studies, and present solid evidence, using several independent but complementary assays, to refute the presence of any NOS isoform in mitochondria.

We obtained highly-purified rat liver mitochondria and to our knowledge, we are the first group to have performed repeated differential centrifugation steps as well as a Percoll gradient purification to obtain this level of mitochondrial purity. These ultrapure mitochondria were then used to determine the presence or absence of any NOS isoform residing in or on mitochondria. We thank Jim Geddes Ph.D., for allowing us to learn this technique in his laboratory without which we could have not obtained the level of purity that we did. The Percoll gradient purification procedure was demonstrated by Brown *et al.* (47), to produce pure mitochondrial preparations devoid of contamination by other organelles. We took painstaking measures to avoid contamination and to obtain pure rat liver mitochondria. For example, use of an ice-jacketed tube during homogenization, avoidance of detergents for washing glassware, centrifuge tubes and all other containers, removal of the fatty layer floating above the supernatant of the various spins and avoidance of Mg^{2+} in MIB in order to prevent Mg^{2+} from inhibiting the putative mtNOS activity, as previously suggested (Ghafourifar *et al.*, 2005).

Western blot analyses were used to estimate mitochondrial purity. Increased enrichment of the mitochondrial matrix protein, GRP 75 was observed in sequential mitochondrial fractions collected during the mitochondrial isolation process (Fig. 2.1A). Additionally, the mitochondrial outer membrane marker, VDAC (Fig. 2.1B) was detected in MT, whereas it was not seen in the control tissue homogenate. Western blot analysis showed that, the cytoskeletal protein, tubulin

was also absent in MT which contrasted with results obtained with the control tissue homogenates (Fig. 2.1C). Furthermore, results from LTQ-MS analyses revealed that MT contains abundant mitochondrial proteins but only 0.006% cytosolic proteins and zero lysosomal proteins (Appendix 1 and 2). This supported the immunochemical data by clearly demonstrating only the negligible contamination of MT.

We next focused on designing experiments to confirm or refute the presence of a mtNOS. We began by using a logical, stepwise approach, namely, the use of nanoHPLC-coupled LTQ-MS utilizing a nanospray source. MS analyses of whole MT did not produce data to support the presence of any NOS isoform in MT (Appendix 1). To probe deeper, we prepared sub-mitochondrial particles from sonicated whole MT. The supernatant and solubilized-pellet were applied to a small column of 2′, 5′- ADP Sepharose 4B affinity resin. This affinity purification step enriched the supernatant and solubilized-pellet fractions with NADPH-binding. The eluted proteins were processed and analyzed using LTQ-MS. Even by using this enrichment step, we failed to detect any NOS isoform in the supernatant fraction (Appendix 2). Data collected from analyzing the fractions of the solubilized-MT pellet eluted from the 2′, 5′- ADP Sepharose 4B column also did not support the presence of any NOS protein residing in MT (data not shown). So that we did not miss anything, samples of the flow-through from both supernatant and solubilized pellet obtained during affinity purification, were tested and LTQ-MS failed to detect the presence of a NOS protein in these flow-through fractions (data not shown). Collectively and without exception, thorough examination of all MT fractions was, in every instance, negative for the presence of any NOS isoforms. On the other hand, nNOSr which was spiked into random MT samples and processed in parallel with the other samples could be detected at absolute levels

as low as ~ 50 femtomoles (Appendix 3). These positive control samples experiments confirmed that the chosen analytical methodology, LTQ-MS, possessed more than adequate sensitivity to detect NOS protein, if present.

We then used various other complimentary biochemical techniques to test for the presence of NOS in mitochondria. For enzyme activity, [^{14}C]-*L*-citrulline production assays (and not [^{3}H]-*L*-citrulline production assays) were performed with MT samples. The conversion of [^{14}C]-*L*-arginine to [^{14}C]-*L*-citrulline was used because it provides a more stable signal with little chance of isotope exchange thus, decreasing apparent false positives due to tritium exchange with water in an aqueous environment. At lower concentrations, thiocitrulline is somewhat selective for inhibiting nNOS, but at higher concentrations, it becomes a non-specific NOS inhibitor. Thus, this concentration used (800 μM) ensured non specificity, and inhibited all NOS isoforms. The background radioactive signal observed with MT samples which could not be inhibited using *L*-thiocitrulline (Fig. 2.2A) was also observed using *L*-NNA, a widely-used and non-specific NOS inhibitor (data not shown). However, control experiments using dMT (Fig. 2.4) as well as comparison of radioactive signals of C-Mix, MT and MT plus *L*-thiocitrulline (Fig. 2.5B) clearly demonstrated that the radioactive signal was not a NOS-catalyzed product.

Results from HP-TLC of the acetone precipitated-[^{14}C]-*L*-arginine to [^{14}C]-*L*-citrulline conversion assay eluates of MT, proved that there is no NOS-catalyzed [^{14}C]-*L*-citrulline production emanating from MT (*lane* 7; Fig. 2.6). However, a fuzzy band was seen at the topmost region of all the lanes that contained MT sample eluates (*lane* 3, 5 and 7) and this signal could not be inhibited by *L*-thiocitrulline (*lane* 4). In addition, studies using *N*-OH-*L*-arginine on MT sample indicates that this top-band is arginase-dependent. Currently, studies are underway

to identify this radioactive signal. Thus, results from NOS activity assays showed that the weak radioactive signal observed in the [^{14}C]-*L*-arginine to [^{14}C]-*L*-citrulline conversion assays which contained MT, did not represent NOS-catalyzed *L*-citrulline formation. Collectively, our data demonstrate that there is no NOS-catalyzed conversion of [^{14}C]-*L*-arginine to [^{14}C]-*L*-citrulline with MT samples.

Earlier studies have separately reported the presence of each NOS isoform within mitochondria (Bates *et al.*, 1995, 1996; Elfering *et al.*, 2002; Frandsen *et al.*, 1996; Ghafourifar and Richter, 1997; Kobzik *et al.*, 1995; Tatoyan and Giulivi, 1998). Several authors found immunoreactivity towards eNOS in the inner-mitochondrial membrane (Bates *et al.*, 1995, 1996; Hotta *et al.*, 1999; Lacza *et al.*, 2001), although some of those studies were not validated with confirmatory experiments using complementary methods. In some cases, the commercially obtained antibodies used have since been established to be somewhat non-specific depending on the source. For example, the Giulivi group used iNOS and nNOS antibodies to detect a 130 kDa mitochondrial protein, which they later claimed to have identified nNOSα using protein mass fingerprinting (Elfering *et al.*, 2002; Giulivi, 2003). However, the Lacza group has identified the same 130 kDa protein in nNOSα knockout mice using the same antibodies from the same source (Lacza *et al.*, 2006). We performed immunochemical analyses by using highly specific NOS antibodies that were characterized and proven specificity (59 and personal communication, B.S. Masters Ph.D.). Unlike the data presentation methods of many groups which consist of showing only cropped blots using NOS antibodies; we present the full immunoblot images showing that the nNOS and eNOS antibodies were unable to detect any sign of NOS in mitochondria. On the other hand, our positive controls nNOSr and eNOSr, when spiked into

mitochondrial samples, at levels as low as 30 ng, could be easily detected (Fig. 2.8A and 8B). The eNOS antibody was absolutely specific for detecting eNOS alone and no cross-reactivity with the other isoforms has been observed (Jachymova *et al.*, 2005). Although, at higher dilutions, the nNOS antibody is 10-fold more specific towards the nNOS isoform, but at these levels, it can cross-react with other isoforms (eNOS and iNOS) as well, when used at lower dilutions. Also, the protein CaM, required for NOS activity, was not detected by Western analyses in MT (Fig. 2.8C).

The oxyhemoglobin capture assay, which measures NO• production, was also performed. The oxymyogobin assay was avoided on purpose, as the extinction coefficient of oxymyoglobin (581-592 nm; 11.6 mM $^{-1}$cm^{-1}) (Tatoyan and Giulivi, 1998) is much less sensitive than that of oxyhemoglobin measured at 401 nm (59.9 mM^{-1}cm^{-1}) (Sheta *et al.*, 1994). Since hemoglobin or myoglobin cannot enter the mitochondrial matrix, and due to the considerable background present from the high light absorption and thus cloudiness of mitochondrial suspensions, we used sub-mitochondrial particles with the oxyhemoglobin assay as suggested previously by Ghafourifar (Ghafourifar, 2002). Mildly sonicated MT (50 µg and 500 µg) along with SOD and CAT (50 units each) were prepared and the assays were performed as previously described (Sheta *et al.*, 1994) ***(see Experimental Procedures)***. This reaction should produce a linear positive rate in the presence of NOS alone. Results clearly produced a negative rate of the reaction with increasing amounts of sub-mitochondrial particles (50 µg and 500 µg) (Fig. 2.9). Since the slope of the capture assay is normally positive when a flux of NO• is present, and normally negative when a flux of $O_2^{\bullet-}$ and/or H_2O_2 is present, these results indicated interference

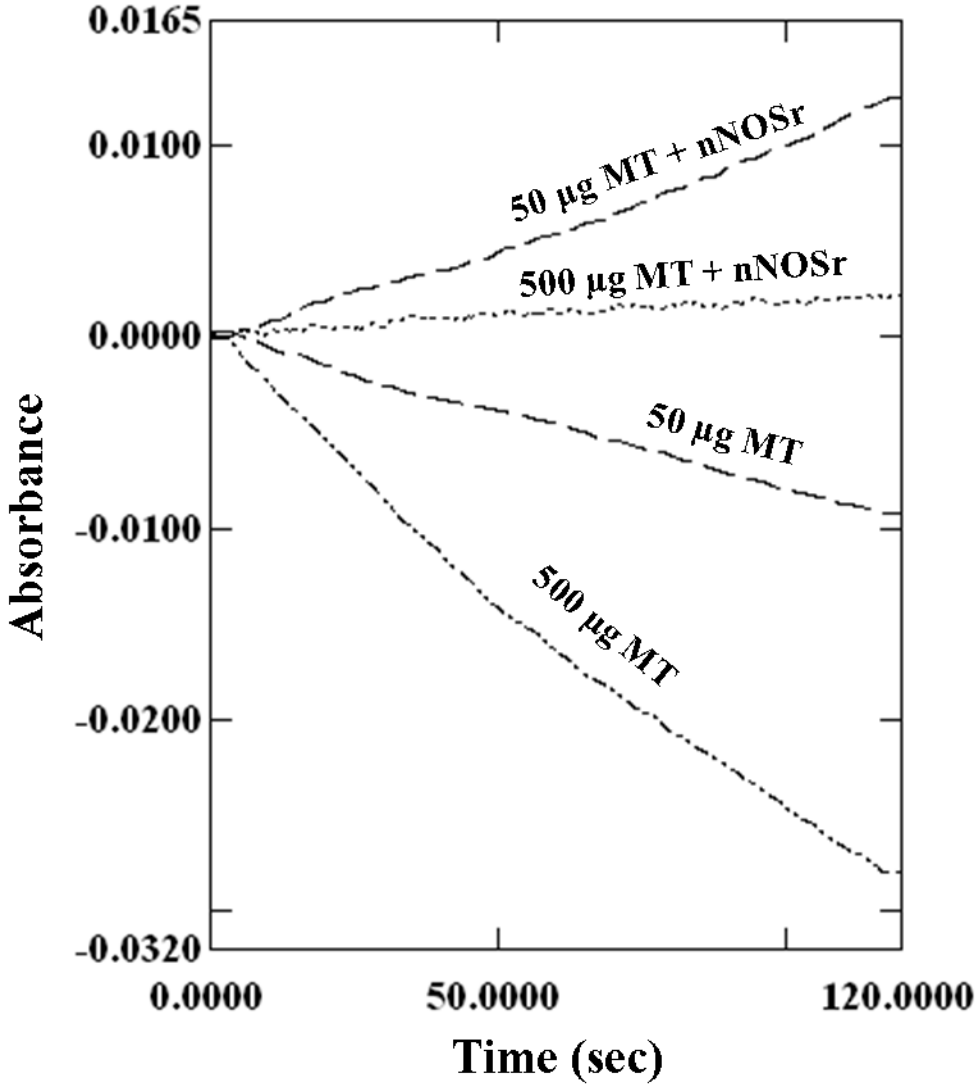

Fig. 2.9. Oxyhemoglobin capture assay with mildly sonicated MT. Mildly sonicated MT (50 µg and 500 µg) along with SOD and CAT (50 units each) were incubated and the assays were performed as mentioned (Sheta *et al.*, 1994). The rate of absorbance of mildly sonicated MT (50 µg and 500 µg) was negative in slope. When nNOSr (5 pmol) were spiked, the curves shifted positive.

of the assay by $O_2^{\bullet-}$ and H_2O_2, generated by the sub-mitochondrial particles. This effect was evident regardless of any low level NO• fluxes that may have been present. Assays performed using sub-mitochondrial particles in the absence of SOD and CAT, produced slightly even more negative rates, when compared to assays conducted in the presence of SOD and CAT (data not shown). When amounts of SOD and CAT were tripled (150 units each), there was no significant change in the negative slope of the reaction (data not shown). Upon spiking nNOSr (5 nM) into sub-mitochondrial particle samples, the rate of the oxy-hemoglobin capture assay shifted to the positive direction and demonstrated NO• production (Fig. 2.9). It should be of note that use of excessive amounts (1,000 U/ml) of SOD with sub-mitochondrial particles, as suggested previously (Ghafourifar *et al.*, 2005), may totally disregulate the mitochondrial enzyme systems and may result in interference with other protein structure and functions. Any effect observed with such high levels of SOD in techniques such as amperometry would likely be due to some non-specific protein effect. Therefore, using the oxyhemoglobin capture assay, production of NO• by sub-mitochondrial particles could not be confirmed in this laboratory due to the massive interfering factors which makes this assay useless in this model. These data support the results of Tay *et al.* (Tay *et al.*, 2004), who also could not detect NO• using the oxymyoglobin capture assay.

Electrochemical methodologies have been performed by many investigators in attempts to detect NO• in mitochondria. Results published by Kanai (Kanai *et al.*, 2001) and Schild (Schild *et al.*, 2003) using mouse heart and rat liver mitochondria, respectively, could not be reproduced by the Lacza or Tay groups (Lacza *et al.*, 2004; Tay *et al.*, 2004). This laboratory also failed to detect NO• production by sonicated MT (150 μg) using a NO• analyzer (Apollo

4000 NO analyzer). However, the electrode readily detected NO• flux by a positive control consisting of 2.5 nM nNOSr-spiked mitochondria samples or S-nitrosopenicillamine (250 nM) (data not shown). NOS requires several substrates and cofactors in order to generate NO•. These molecules include FAD, FMN, BH_4, O_2, *L*-arginine, Ca^{2+} and NADPH. Although many other proteins are present in mitochondria, the MS and immunochemical analyses failed to detect the presence of CaM, a protein that is absolutely required for NOS function (Appendix 1 and 2).

Although it has a limited lifetime, NO• is a diffusible radical (Thomas *et al.*, 2001) and there is no absolute requirement for it to be produced at the exact site of action (Brookes, 2004). Therefore, there is no requirement for NO• to be produced within mitochondria for it to exert its action on mitochondrial enzymes.

2.5 Conclusion

The existence of NOS within mitochondria has been questioned for the past 10 years or more. This situation may be due to: 1) differences in the purity of the mitochondria preparations used among groups, 2) failure to confirm results with complementary techniques, 3) lack of use of appropriate controls, as well as 4) poor reliability and reproducibility of certain techniques as suggested by Brookes (Brookes, 2004). Isolation of the purest mitochondria possible is absolutely necessary if we are to determine with any certainty whether there is a NOS isoform within mitochondria. Although the Lacza group initially identified eNOS in mitochondria (Lacza *et al.*, 2004; Lacza *et al.*, 2003), their subsequent studies conducted with brain, heart and liver mitochondria from mice, rats and pigs under stringent conditions did not support their original observations (Lacza *et al.*, 2001). Therefore, we performed experiments under stringently controlled conditions to isolate, purify and analyze mitochondria with appropriate controls and markers using a variety of complementary independent techniques. Results obtained, using LTQ-MS analyses complemented by other techniques, such as the [^{14}C]-*L*-arginine to [^{14}C]-*L*-citrulline conversion assay as well as immunochemical analyses, collectively and individually refute the claim that any NOS isoform resides within rat liver mitochondria.

2.6 Acknowledgements

I thank Dr. Igor C. Almeida and Ernesto S. Nakayasu for their valuable help and guidance in performing all the proteomics analyses. This publication was made possible by grant # ES 011982 to R.T. Miller from the National Institute of Environmental Health Sciences (NIEHS)/NIH. This project was also supported in part by grant # 5G12RR008124 to the Border Biomedical Research Center (BBRC)/University of Texas at El Paso from the National Center for Research Resources (NCRR)/NIH.

2.7 References

Bates, T. E., Loesch, A., Burnstock, G., Clark, J. B., 1995. Immunocytochemical evidence for a mitochondrially located nitric oxide synthase in brain and liver. Biochem Biophys Res Commun 213, 896-900.

Bates, T. E., Loesch, A., Burnstock, G., Clark, J. B., 1996. Mitochondrial nitric oxide synthase: a ubiquitous regulator of oxidative phosphorylation? Biochem Biophys Res Commun 218, 40-44.

Boveris, A., Cadenas, E., 1975. Mitochondrial production of superoxide anions and its relationship to the antimycin insensitive respiration. FEBS Lett 54, 311-314.

Bradford, M. M., 1976. A rapid and sensitive method for the quantitation of microgram quantities of protein utilizing the principle of protein-dye binding. Anal Biochem 72, 248-254.

Bredt, D. S., Snyder, S. H., 1990. Isolation of nitric oxide synthetase, a calmodulin-requiring enzyme. Proc Natl Acad Sci U S A 87, 682-685.

Brookes, P. S., 2004. Mitochondrial nitric oxide synthase. Mitochondrion 3, 187-204.

Brookes, P. S., Levonen, A. L., Shiva, S., Sarti, P., Darley-Usmar, V. M., 2002. Mitochondria: regulators of signal transduction by reactive oxygen and nitrogen species. Free Radic Biol Med 33, 755-764.

Brown, G. C., Bolanos, J. P., Heales, S. J., Clark, J. B., 1995. Nitric oxide produced by activated astrocytes rapidly and reversibly inhibits cellular respiration. Neurosci Lett 193, 201-204.

Brown, M. R., Sullivan, P. G., Geddes, J. W., 2006. Synaptic mitochondria are more susceptible to Ca^{2+}overload than nonsynaptic mitochondria. J Biol Chem 281, 11658-11668.

Cadenas, E., Poderoso, J. J., Antunes, F., Boveris, A., 2000. Analysis of the pathways of nitric oxide utilization in mitochondria. Free Radic Res 33, 747-756.

Cleeter, M. W., Cooper, J. M., Darley-Usmar, V. M., Moncada, S., Schapira, A. H., 1994. Reversible inhibition of cytochrome c oxidase, the terminal enzyme of the mitochondrial respiratory chain, by nitric oxide. Implications for neurodegenerative diseases. FEBS Lett 345, 50-54.

Dedkova, E. N., Ji, X., Lipsius, S. L., Blatter, L. A., 2004. Mitochondrial calcium uptake stimulates nitric oxide production in mitochondria of bovine vascular endothelial cells. American journal of physiology 286, C406-415.

Dionisi, O., Galeotti, T., Terranova, T., Azzi, A., 1975. Superoxide radicals and hydrogen peroxide formation in mitochondria from normal and neoplastic tissues. Biochim Biophys Acta 403, 292-300.

Ebel, R. E., O'Keefe, D. H., Peterson, J. A., 1975. Nitric oxide complexes of cytochrome P-450. FEBS Lett 55, 198-201.

Elfering, S. L., Sarkela, T. M., Giulivi, C., 2002. Biochemistry of mitochondrial nitric-oxide synthase. J Biol Chem 277, 38079-38086.

Eng, J. K., McCormack, A. L., and Yates, J. R. r. , 1994. J Am Soc Mass Spectrom 5, 976-989.

Forstermann, U., Pollock, J. S., Schmidt, H. H., Heller, M., Murad, F., 1991. Calmodulin-dependent endothelium-derived relaxing factor/nitric oxide synthase activity is present in the particulate and cytosolic fractions of bovine aortic endothelial cells. Proc Natl Acad Sci U S A 88, 1788-1792.

Frandsen, U., Lopez-Figueroa, M., Hellsten, Y., 1996. Localization of nitric oxide synthase in human skeletal muscle. Biochem Biophys Res Commun 227, 88-93.

Furchgott, R. F., Vanhoutte, P. M., 1989. Endothelium-derived relaxing and contracting factors. FASEB J 3, 2007-2018.

Ghafourifar, P., 2002. Characterization of mitochondrial nitric oxide synthase. Methods Enzymol 359, 339-350.

Ghafourifar, P., Asbury, M. L., Joshi, S. S., Kincaid, E. D., 2005. Determination of mitochondrial nitric oxide synthase activity. Methods Enzymol 396, 424-444.

Ghafourifar, P., Richter, C., 1997. Nitric oxide synthase activity in mitochondria. FEBS Lett 418, 291-296.

Giulivi, C., 2003. Characterization and function of mitochondrial nitric-oxide synthase. Free Radic Biol Med 34, 397-408.

Giulivi, C., Poderoso, J. J., Boveris, A., 1998. Production of nitric oxide by mitochondria. J Biol Chem 273, 11038-11043.

Hibbs, J. B., Jr., 1991. Synthesis of nitric oxide from L-arginine: a recently discovered pathway induced by cytokines with antitumour and antimicrobial activity. Res Immunol 142, 565-569; discussion 596-568.

Hibbs, J. B., Jr., Taintor, R. R., Vavrin, Z., Rachlin, E. M., 1988. Nitric oxide: a cytotoxic activated macrophage effector molecule. Biochem Biophys Res Commun 157, 87-94.

Hotta, Y., Otsuka-Murakami, H., Fujita, M., Nakagawa, J., Yajima, M., Liu, W., Ishikawa, N., Kawai, N., Masumizu, T., Kohno, M., 1999. Protective role of nitric oxide synthase against ischemia-reperfusion injury in guinea pig myocardial mitochondria. Eur J Pharmacol 380, 37-48.

Huie, R. E., Padmaja, S., 1993. The reaction of no with superoxide. Free Radic Res Commun 18, 195-199.

Ignarro, L. J., 1989. Endothelium-derived nitric oxide: actions and properties. FASEB J 3, 31-36.

Ignarro, L. J., Buga, G. M., Byrns, R. E., Wood, K. S., Chaudhuri, G., 1988. Endothelium-derived relaxing factor and nitric oxide possess identical pharmacologic properties as relaxants of bovine arterial and venous smooth muscle. J Pharmacol Exp Ther 246, 218-226.

Ignarro, L. J., Byrns, R. E., Buga, G. M., Wood, K. S., 1987. Endothelium-derived relaxing factor from pulmonary artery and vein possesses pharmacologic and chemical properties identical to those of nitric oxide radical. Circ Res 61, 866-879.

Jachymova, M., Martasek, P., Panda, S., Roman, L. J., Panda, M., Shea, T. M., Ishimura, Y., Kim, J. J., Masters, B. S., 2005. Recruitment of governing elements for electron transfer in the nitric oxide synthase family. Proc Natl Acad Sci U S A 102, 15833-15838.

Jurado, J. D., Rael, E. D., Lieb, C. S., Nakayasu, E., Hayes, W. K., Bush, S. P., Ross, J. A., 2007. Complement inactivating proteins and intraspecies venom variation in Crotalus oreganus helleri. Toxicon 49, 339-350.

Kanai, A., Epperly, M., Pearce, L., Birder, L., Zeidel, M., Meyers, S., Greenberger, J., de Groat, W., Apodaca, G., Peterson, J., 2004. Differing roles of mitochondrial nitric oxide synthase in cardiomyocytes and urothelial cells. Am J Physiol Heart Circ Physiol 286, H13-21.

Kanai, A. J., Pearce, L. L., Clemens, P. R., Birder, L. A., VanBibber, M. M., Choi, S. Y., de Groat, W. C., Peterson, J., 2001. Identification of a neuronal nitric oxide synthase in isolated cardiac mitochondria using electrochemical detection. Proc Natl Acad Sci U S A 98, 14126-14131.

Kennedy, M. C., Antholine, W. E., Beinert, H., 1997. An EPR investigation of the products of the reaction of cytosolic and mitochondrial aconitases with nitric oxide. J Biol Chem 272, 20340-20347.

Knowles, R. G., Palacios, M., Palmer, R. M., Moncada, S., 1989. Formation of nitric oxide from L-arginine in the central nervous system: a transduction mechanism for stimulation of the soluble guanylate cyclase. Proc Natl Acad Sci U S A 86, 5159-5162.

Kobzik, L., Stringer, B., Balligand, J. L., Reid, M. B., Stamler, J. S., 1995. Endothelial type nitric oxide synthase in skeletal muscle fibers: mitochondrial relationships. Biochem Biophys Res Commun 211, 375-381.

Kwon, N. S., Nathan, C. F., Gilker, C., Griffith, O. W., Matthews, D. E., Stuehr, D. J., 1990. L-citrulline production from L-arginine by macrophage nitric oxide synthase. The ureido oxygen derives from dioxygen. J Biol Chem 265, 13442-13445.

Lacza, Z., Horn, T. F., Snipes, J. A., Zhang, J., Roychowdhury, S., Horvath, E. M., Figueroa, J. P., Kollai, M., Szabo, C., Busija, D. W., 2004. Lack of mitochondrial nitric oxide production in the mouse brain. J Neurochem 90, 942-951.

Lacza, Z., Pankotai, E., Csordas, A., Gero, D., Kiss, L., Horvath, E. M., Kollai, M., Busija, D. W., Szabo, C., 2006. Mitochondrial NO and reactive nitrogen species production: does mtNOS exist? Nitric Oxide 14, 162-168.

Lacza, Z., Puskar, M., Figueroa, J. P., Zhang, J., Rajapakse, N., Busija, D. W., 2001. Mitochondrial nitric oxide synthase is constitutively active and is functionally upregulated in hypoxia. Free Radic Biol Med 31, 1609-1615.

Lacza, Z., Snipes, J. A., Zhang, J., Horvath, E. M., Figueroa, J. P., Szabo, C., Busija, D. W., 2003. Mitochondrial nitric oxide synthase is not eNOS, nNOS or iNOS. Free Radic Biol Med 35, 1217-1228.

Lopez-Figueroa, M. O., Caamano, C., Morano, M. I., Ronn, L. C., Akil, H., Watson, S. J., 2000. Direct evidence of nitric oxide presence within mitochondria. Biochem Biophys Res Commun 272, 129-133.

Lopez-Figueroa, M. O., Caamano, C. A., Morano, M. I., Akil, H., Watson, S. J., 2002. Fluorescent imaging of mitochondrial nitric oxide in living cells. Methods Enzymol 352, 296-303.

MacMillan-Crow, L. A., Crow, J. P., Thompson, J. A., 1998. Peroxynitrite-mediated inactivation of manganese superoxide dismutase involves nitration and oxidation of critical tyrosine residues. Biochemistry 37, 1613-1622.

Malinski, T., Taha, Z., Grunfeld, S., Patton, S., Kapturczak, M., Tomboulian, P., 1993. Diffusion of nitric oxide in the aorta wall monitored in situ by porphyrinic microsensors. Biochem Biophys Res Commun 193, 1076-1082.

Martasek, P., Liu, Q., Liu, J., Roman, L. J., Gross, S. S., Sessa, W. C., Masters, B. S., 1996. Characterization of bovine endothelial nitric oxide synthase expressed in E. coli. Biochem Biophys Res Commun 219, 359-365.

Miller, R. T., 2002. Dinitrobenzene-mediated production of peroxynitrite by neuronal nitric oxide synthase. Chem Res Toxicol 15, 927-934.

Moncada, S., 2000. Nitric oxide and cell respiration: physiology and pathology. Verh K Acad Geneeskd Belg 62, 171-179; discussion 179-181.

Moncada, S., Erusalimsky, J. D., 2002. Does nitric oxide modulate mitochondrial energy generation and apoptosis? Nat Rev Mol Cell Biol 3, 214-220.

Murad, F., Forstermann, U., Nakane, M., Schmidt, H., Pollock, J., Sheng, H., Matsumoto, T., Warner, T., Mitchell, J., Tracey, R., *et al.*, 1992. The nitric oxide-cyclic GMP signal transduction pathway in vascular smooth muscle preparations and other tissues. Jpn J Pharmacol 58 Suppl 2, 150P-157P.

Narayanan, K., Griffith, O. W., 1994. Synthesis of L-thiocitrulline, L-homothiocitrulline, and S-methyl-L-thiocitrulline: a new class of potent nitric oxide synthase inhibitors. Journal of medicinal chemistry 37, 885-887.

Nathan, C., 1992. Nitric oxide as a secretory product of mammalian cells. FASEB J 6, 3051-3064.

Nishimura, J. S., Narayanasami, R., Miller, R. T., Roman, L. J., Panda, S., Masters, B. S., 1999. The stimulatory effects of Hofmeister ions on the activities of neuronal nitric-oxide synthase. Apparent substrate inhibition by l-arginine is overcome in the presence of protein-destabilizing agents. J Biol Chem 274, 5399-5406.

Pertoft, H., Laurent, T. C., Laas, T., Kagedal, L., 1978. Density gradients prepared from colloidal silica particles coated by polyvinylpyrrolidone (Percoll). Anal Biochem 88, 271-282.

Pollock, J. S., Forstermann, U., Mitchell, J. A., Warner, T. D., Schmidt, H. H., Nakane, M., Murad, F., 1991. Purification and characterization of particulate endothelium-derived relaxing factor synthase from cultured and native bovine aortic endothelial cells. Proc Natl Acad Sci U S A 88, 10480-10484.

Radi, R., Cassina, A., Hodara, R., 2002. Nitric oxide and peroxynitrite interactions with mitochondria. Biol Chem 383, 401-409.

Radi, R., Rodriguez, M., Castro, L., Telleri, R., 1994. Inhibition of mitochondrial electron transport by peroxynitrite. Archives of biochemistry and biophysics 308, 89-95.

Reinhart, P. H., Taylor, W. M., Bygrave, F. L., 1982. A procedure for the rapid preparation of mitochondria from rat liver. Biochem J 204, 731-735.

Rodrigues, M. L., Nakayasu, E. S., Oliveira, D. L., Nimrichter, L., Nosanchuk, J. D., Almeida, I. C., Casadevall, A., 2008. Extracellular vesicles produced by Cryptococcus neoformans contain protein components associated with virulence. Eukaryot Cell 7, 58-67.

Roman, L. J., Sheta, E. A., Martasek, P., Gross, S. S., Liu, Q., Masters, B. S., 1995. High-level expression of functional rat neuronal nitric oxide synthase in Escherichia coli. Proc Natl Acad Sci U S A 92, 8428-8432.

Sarti, P., Giuffre, A., Barone, M. C., Forte, E., Mastronicola, D., Brunori, M., 2003. Nitric oxide and cytochrome oxidase: reaction mechanisms from the enzyme to the cell. Free Radic Biol Med 34, 509-520.

Schild, L., Reinheckel, T., Reiser, M., Horn, T. F., Wolf, G., Augustin, W., 2003. Nitric oxide produced in rat liver mitochondria causes oxidative stress and impairment of respiration after transient hypoxia. FASEB J 17, 2194-2201.

Schmidt, K., Klatt, P., Mayer, B., 1994. Reaction of peroxynitrite with oxyhaemoglobin: interference with photometrical determination of nitric oxide. Biochem J 301 (Pt 3), 645-647.

Sheta, E. A., McMillan, K., Masters, B. S., 1994. Evidence for a bidomain structure of constitutive cerebellar nitric oxide synthase. J Biol Chem 269, 15147-15153.

Shin, W. S., Sasaki, T., Kato, M., Hara, K., Seko, A., Yang, W. D., Shimamoto, N., Sugimoto, T., Toyo-oka, T., 1992. Autocrine and paracrine effects of endothelium-derived relaxing factor on intracellular Ca^{2+} of endothelial cells and vascular smooth muscle cells. Identification by two-dimensional image analysis in coculture. J Biol Chem 267, 20377-20382.

Stone, K. L., and Williams, K. R. , 1996. Enzymatic digestion of proteins in solution and in SDS polyacrilamide gel. In: Walker, J. M. (ed). . The protein protocol handbook., Humana Press Inc., Totowa, NJ.

Stuehr, D. J., Griffith, O. W., 1992. Mammalian nitric oxide synthases. Adv Enzymol Relat Areas Mol Biol 65, 287-346.

Tatoyan, A., Giulivi, C., 1998. Purification and characterization of a nitric-oxide synthase from rat liver mitochondria. J Biol Chem 273, 11044-11048.

Tay, Y. M., Lim, K. S., Sheu, F. S., Jenner, A., Whiteman, M., Wong, K. P., Halliwell, B., 2004. Do mitochondria make nitric oxide? no? Free Radic Res 38, 591-599.

Thomas, D. D., Liu, X., Kantrow, S. P., Lancaster, J. R., Jr., 2001. The biological lifetime of nitric oxide: implications for the perivascular dynamics of NO and O2. Proc Natl Acad Sci U S A 98, 355-360.

Thomas, D. D., Miranda, K. M., Colton, C. A., Citrin, D., Espey, M. G., Wink, D. A., 2003. Heme proteins and nitric oxide (NO): the neglected, eloquent chemistry in NO redox signaling and regulation. Antioxid Redox Signal 5, 307-317.

Turko, I. V., Marcondes, S., Murad, F., 2001. Diabetes-associated nitration of tyrosine and inactivation of succinyl-CoA:3-oxoacid CoA-transferase. Am J Physiol Heart Circ Physiol 281, H2289-2294.

Zanella, B., Calonghi, N., Pagnotta, E., Masotti, L., Guarnieri, C., 2002. Mitochondrial nitric oxide localization in H9c2 cells revealed by confocal microscopy. Biochem Biophys Res Commun 290, 1010-1014.

Chapter 3: Effect of Redox-Cycling Agents on Modulation of Protein or Gene Expression *in vivo*

3.1 Paraquat-Induced Early Phase Protein Expression Changes in Rat Liver Tissue and Mitochondria

3.1.1 Introduction

Paraquat (1, 1-dimethyl-4,4-bipyridinium ion; PQ) is a fast acting, potent, synthetic herbicide that is used in over 120 countries in the world. First described in 1882 (Weidel, 1882), PQ is hydrophilic in nature and belongs to a class of bipyridyl derivatives. As an herbicide, the mechanism of action of PQ is through redox-cycling. Normally, in the plant, the electrons are transferred from plastocyanin of photosystem I to ferrodoxin and then to $NADP^+$ to create NADPH. When a green plant is exposed to PQ, it accepts an electron from photosystem 1 to form $PQ^{\cdot+}$, a monocation-free radical and then autoxidizes by donating its electron to molecular O_2, generating superoxide anion radical ($O_2^{\cdot-}$). This cycle can then repeat. This continuous redox-cycling process of PQ continues until there is insufficient electron flux for the normal physiological processes to operate. This is due to depletion of NADPH and generation of reactive oxygen species (ROS) (Adam *et al.*, 1990; Farrington *et al.*, 1973; Zweig *et al.*, 1965).

In man, the toxicity of paraquat was first reported by Clark *et al.* (1966)(Clark *et al.*, 1966) and the affected organs were lung, liver, kidney and thymus. However, the lung is the major site of toxicity in rat and humans. Preferential accumulation of PQ is observed in lungs through the polyamine uptake system which recognizes PQ as a substrate (Lewis *et al.*, 1989; Smith, 1982; Wyatt *et al.*, 1988), making lung the most common target organ for PQ toxicity (Rose *et al.*, 1974). However, the actual death is most commonly due to the result of multisystem failure and includes acute pulmonary edema, hepato-renal failure and myocarditis (Conradi *et al.*, 1983). These data are substantiated by various occupational exposure case reports where PQ

exposure had resulted in PQ toxicity in various organs such as lung, liver, kidney, brain and heart (Cantor and Young-Holt, 2002).

Since the 80's, many case reports have been published indicating liver may also be a major target of PQ toxicity (Burk *et al.*, 1980; Matsumoto *et al.*, 1980; Mullick *et al.*, 1981; Takegoshi *et al.*, 1988). These studies describe PQ induced hepatotoxicity that consisted of jaundice and abnormal liver function tests including increases in serum levels of lactate dehydrogenase, serum glutamic oxaloacetic transaminase, serum glutamic pyruvic transaminase, alkaline phosphatase and decreases in serum albumin and globulin (Erickson *et al.*, 1997; Hong *et al.*, 2000). Predominantly, liver injury is manifested in the form of cholestasis (Bataller *et al.*, 2000) and cholangiocellular damage (Conradi *et al.*, 1983; Mullick *et al.*, 1981).

Although PQ is known to possess the redox-cycling property allowing it to potentially produce ROS, the mechanism of toxicity is not fully established. Previous studies found that the ROS-mediated PQ-toxicity is preceded by altered mitochondrial respiratory function. Specifically, disrupted oxidative phosphorylation occurred at very early stages of PQ exposure in alveolar epithelial cells, liver cells as well as in skeletal tissue of rats (Hirai *et al.*, 1985; Ueda *et al.*, 1985; Yamamoto *et al.*, 1987) and later in the brain (Tawara *et al.*, 1996). The involvement of mitochondria was studied initially in rat liver by Fukoshima and co-workers who showed that PQ may generate ROS by accepting electrons from purified complex I (NADH-dehydrogenase) of the respiratory chain producing increased $O_2^{\bullet-}$ radicals (Fukushima *et al.*, 1993). Palmeira *et al.* (1997) (Palmeira *et al.*, 1995) reported that PQ impaired the function of mitochondria in rat liver by uncoupling oxidative phosphorylation, inhibiting complex III, IV and a causing a direct effect on ATP synthase. In addition, PQ was also found to induce a Ca^{2+} dependent permeability increase of inner mitochondrial membrane in rat liver mitochondria (Costantini *et al.*, 1995).

Subsequently, Complex I of the outer mitochondrial membrane was reported to play a role in PQ cytotoxicity (Shimada *et al.*, 1998).

While the mechanism of PQ-induced toxicity is not fully understood, some compounds including nicotinamide, captopril and ethyl pyruvate (Fukushima *et al.*, 1997; Ghazi-Khansari *et al.*, 2005; Lee *et al.*, 1998) were identified to reduce PQ-induced toxicity. PQ-toxicity in the brain was thought to be linked with Parkinson's disease as it depletes dopaminergic neurons as well as the dopamine in substantia nigra of dopamine (Brooks *et al.*, 1999; McCormack *et al.*, 2002; Tawara *et al.*, 1996). Recent studies have also shown that the mitochondria are major sources of PQ-induced ROS such as $O_2^{\cdot-}$ and H_2O_2 (Castello *et al.*, 2007; Mukhopadhyay *et al.*, 2007).

Although mitochondria are considered to be involved in PQ-induced toxicity, studies exploring the role of mitochondria, the mechanism of toxicity and the proteins involved after acute PQ-exposure are limited. Recently, it was shown that the paraquat-exposed rats demonstrated the majority of gene expression changes in the lung tissue at 2 hr time point when compared to 8 and 18 hours (Mainwaring *et al.*, 2006). Also, gene expressions was affected and resulted in onset of pulmonary injury at 3 hr time point in rats (Tomita *et al.*, 2004). Therefore, we performed experiments to identify the protein expression changes during the early phase of PQ-treatment (as early as 3 hrs), in liver tissue as well as in mitochondria of rats. Here, we performed a quantitative proteomic analysis using ^{18}O labeling approach to analyze tissue homogenate and isolated mitochondria sample from PQ-treated rats. The samples were digested with trypsin in buffer prepared in ^{16}O-water (control) or ^{18}O-water (PQ-treated), mixed in a proportion 1:1 and analyzed liquid chromatography coupled linear ion-trap mass spectrometry (LTQ-MS).

3.1.2 Experimental Procedures

Biochemicals: Paraquat (PQ), ammonium bicarbonate, 4-(2-hydroxyethyl)-1 piperazineethanesulfonic acid (HEPES), *L*-arginine·HCl, $CaCl_2 \cdot 4H_2O$, bovine brain CaM, (6*R)*-5,6,7,8-tetrahydro-*L*-biopterin (BH_4), NADPH, *L*-citrulline, ethylene diamine tetraacetic acid (EDTA), ethylene glycol tetraacetic acid (EGTA), dithiothreitol (DTT), iodoacetamide (IAA), sucrose, mannitol, acetone, *L*-thiocitrulline, N(ω)-nitro-*L*-arginine (*L*-NNA), monosodium- and disodium- phosphate, sodium dodecyl sulfate (SDS), alkaline phosphatase (ALP)-conjugated anti-rabbit secondary antibody, horseradish peroxidase (HRP)-conjugated anti-rabbit and anti-mouse secondary antibodies. All of the above mentioned items were purchased from Sigma (St. Louis, MO). Dowex 50WX8 was obtained from Supelco (Bellefonte, PA). Acetonitrile (ACN) was purchased from Mallinckrodt-Baker, Inc. (Philipsburg, NJ). Trichloroacetic acid (TCA) was obtained from EMD Chemicals, Inc (San Diego, CA). Tris-HCl and nitrocellulose membranes were purchased from Bio-Rad (Hercules, CA). Super Signal West Pico chemiluminescent substrate was purchased from Pierce. Percoll and 2′, 5′- ADP Sepharose-4B were products of GE Healthcare (Uppsala, Sweden). Complete protease inhibitor cocktail tablets were purchased from Roche (Mannheim, Germany). All other chemicals and reagents were from common suppliers and were of the highest grade commercially available.

Animals: All experimental protocols involving animals were approved by University of Texas at El Paso Institutional Animal Care and Use Committee (IACUC). Male Sprague-Dawley (SD) rats (250–300 g; approx. 3 months of age) were obtained from Harlan (Houston, TX) and used in all studies.

Treatment: A pair of SD rats was treated with PQ at a dose of 40 mg/ kg body weight and the control pair received no treatment. Both the pairs of rats were euthanized 3hrs after dosing and all the liver lobes were collected. This experiment was performed once more in duplicate for a total of two-independent experiment.

Preparation of Mitochondria: Pure rat liver mitochondria from the control and PQ-treated rats were obtained by repeated differential centrifugation followed by Percoll gradient purification as described previously (Venkatakrishnan *et al.*, 2008, publication in progress). Expertise for the mitochondrial purification procedure was obtained first hand and adopted from the methodology used in the laboratory of James Geddes Ph. D., University of Kentucky, Lexington, KY. Initially, the livers from each rat were excised and immersed in ice-cold mitochondrial isolation buffer (MIB) containing 215 mM mannitol, 75 mM sucrose, 1mM EGTA, 20 mM HEPES/KOH, pH 7.2. In addition, a serine- and cysteine-protease inhibiting complete cocktail tablet was included in this buffer. The liver lobes were blotted dry, washed 2-3 times with fresh MIB and minced into small pieces with scissors. The resulting minced pieces of liver were washed with MIB to remove blood. Then, 6-8 ml of ice-cold MIB was added to the washed and minced tissue. The tissue sample was placed in a glass dounce homogenizer in portions, immersed in ice and homogenized gently with a loose-fitting teflon pestle (6 strokes) at 250 rpm, using a variable speed homogenizer (Glas-Col, Terre Haute, IN).

Following homogenization, both differential centrifugation and Percoll gradient fractionation steps were performed using a pre-cooled SM-24 rotor in a RC-5B Sorvall centrifuge at 4º C, for 10 min, unless specified otherwise. First, the tissue homogenate (referred to as CO, in figures) was suspended in ice-cold MIB and centrifuged at 800 x g. After the first 800 x g spin, the white fatty layer covering the supernatant was carefully removed using a lint-

free wipe or a cotton wool. The 800 x g supernatant (M1) was then collected and the isolated pellet containing red spots of blood and cellular debris was discarded. M1 was spun at 10,000 x g to obtain a pellet containing mitochondria (M2). M2 was then gently resuspended by homogenization using a glass dounce homogenizer (4 strokes, 250 rpm). The differential centrifugation steps were then repeated with the MIB-resuspended M2 (at 800 x g (M3) and 10,000 x g (M4)) to obtain a relatively pure mitochondrial preparation. The mitochondrial pellet obtained after the 10,000 x g spin was resuspended in ice-cold MIB and then centrifuged at the lower speed of 9,000 x g. The pellet (M5) isolated during this step contained highly purified mitochondria.

Mitochondria were further purified using Percoll gradient centrifugation as described previously (Brown *et al.*, 2006). Percoll was chosen as the gradient medium due to its chemical inertness and negligible osmolarity (Pertoft *et al.*, 1978; Reinhart *et al.*, 1982). Ice cold-MIB without EGTA was used in all steps for preparing the Percoll gradient solutions as well as for washing. Mitochondria were supplemented with an equal volume of 30% Percoll (15% mitochondria containing Percoll). A discontinuous Percoll gradient was used, with the bottom layer containing 40% Percoll, followed by 24% Percoll, and finally by 15% Percoll-containing mitochondria. The density gradient was spun at 30,400 x g and the band between 24% and 40% Percoll (containing the intact mitochondria) was carefully collected. The broken mitochondria at the bottom of the gradient were discarded. The intact mitochondrial sample was then suspended in MIB without EGTA and centrifuged at 16,700 x g for 15 min. Discarding the supernatant, the loose pellet obtained was resuspended in MIB without EGTA and subsequently centrifuged at 13,000 x g followed by a 10,000 x g spin. The intact mitochondrial pellet obtained after the final

10,000 x g spin, was collected and used for experimentation. The protein concentration of the pure mitochondria was measured using the Bradford protein assay using BSA as a standard.

Sample Processing for Mass Spectrometry: Protein precipitation was performed by treating 150 µg of mitochondria and 100 µg of the liver tissue homogenate from the control and paraquat-treated rats with 10% TCA for 30 min, on ice. Samples were vortexed every 10 min, and finally centrifuged at 16,000 x g for 20 min, at 4ºC. The TCA-precipitated samples were washed in acetone and centrifuged at 16,000 x g for 20 min, at 4ºC. Sample pellets were then dried using a vacuum centrifuge.

Dry, precipitated proteins were digested as described by Stone and Williams (Stone, 1996). Briefly, dried pellets from acetone washes were solubilized with a solution of 8 M urea/0.4 M NH_4HCO_3, and the sulfhydryls were reduced using DTT (9 mM) for 15 min at 50° C. The samples were cooled to room temperature and then treated with IAA (20 mM) for 15 min at RT. Subsequently, the IAA-treated samples were diluted with water to obtain a final concentration of 1 M urea. The samples were then digested overnight with 1 µg of sequencing grade trypsin (Promega) for every 50 µg of mitochondrial protein. Proteolysis was stopped by adding 1 µl of 100 % formic acid (FA). The resulting samples were desalted using a reverse phase ziptip manufactured with 200-µL micropipette tips and containing POROS 50 R2 beads (Applied Biosystems) (Jurado *et al.*, 2007) and dried using vacuum centrifugation.

^{18}O labeling and Trypsin Digestion: The desalted samples of mitochondria and the tissue homogenate from the control and paraquat-treated rats were dried with 100 µl of methanol twice, using a vaccum centrifuge. The methanol dried samples of mitochondria and the tissue homogenate from paraquat-treated rats were incubated with 10 µl of ^{18}O water. After 15 hrs of

incubation at 4°C, these samples were dried under vacuum centrifugation, resuspended 100 µl of NH_4HCO_3 buffer made in O^{18} water, and digested trypsin dissolved in ^{18}O buffer for 24 hrs at 37°C. Proteolysis was stopped by adding 2 µl of 100% formic acid (FA) (Sigma). Samples of mitochondria and the tissue homogenate from the control rats were processed exactly in the same manner as like paraquat treated rat samples except for the use of HPLC-grade ^{16}O water instead of ^{18}O water. Two samples of 0.5 nmoles of BSA were also prepared in the same conditions and used as the labeling control. Wherein one sample was ^{18}O labeled and the other was treated with trypsin in buffer prepared with HPLC-grade ^{16}O water. All the trypsin-digested and neutralized samples (from BSA, mitochondria and tissue homogenates of control and paraquat-treated rats) were desalted using a reverse-phase Ziptips (Jurado *et al.*, 2007) dried under vacuum centrifugation. Alternatively, tissue homogenate samples were fractionated by strong cation-exchange (SCX) as described by Rodrigues *et al.* (2008)(Rodrigues *et al.*, 2008).

Parameters of liquid chromatography-tandem mass spectrometry (LC-MS/MS) analysis: Each of the desalted fractions were solubilized in 30 µL of 0.05% TFA and eight microliters were injected onto a lab-manufactured trap column (5 µm C18, 1 cm x 75 µm, Luna, Phenomenex), using the vented column approach (Licklider *et al.*, 2002). Separations were performed using a lab-manufactured reverse-phase capillary column (5 µm C18, 12.5 cm x 75 µm, Luna, Phenomenex) connected to a nanoHPLC system (nanoLC 1D plus, Eksigent). For elution, the mobile phases were A: 2% ACN, 0.1% FA; B: 80% ACN, 0.1% FA. A linear gradient from 0-40% solvent B over 200 min was used. The eluting peptides were directly introduced into a linear ion trap-mass spectrometer (LTQ XL, Thermo Fisher Scientific) equipped with a Triversa Nanomate system(Adivion). MS spectra were collected in centroid mode over the range of 400 to 1700 *m/z* and the 10 most abundant ions were submitted twice to collision-induced

dissociation (CID) (35% normalized collision energy), before dynamically excluded for 60 s. All MS/MS spectra were from peptides of 600-4,000 Da and at least 15 fragments were converted into DTA files using Bioworks v.3.3.1 (Thermo Fisher Scientific). The DTA files were submitted for database searching using TurboSequest (Eng, 1994) (available in Bioworks v.3.3.1) against the rat sequences (v3.47) from the International Protein Index (www.ebi.ac.uk/IPI), and human keratin and porcine trypsin from GenBank (http://www.ncbi.nlm.nih.gov/sites/entrez?db=Protein&itool=toolbar) (March 17th, 2008). All sequences were set in the forward as well as reverse orientations for calculating the false-positive rate (FPR) forming a database with 82106 protein sequences. The database search parameters included: i) trypsin cleavage in both peptide termini allowing one missed cleavage site; ii) carbamidomethylation of cysteine residues as a fixed modification; iii) oxidation of methionine residues as a variable modification; and iv) 2.0 Da and 1.0 Da for peptide and fragment mass tolerance, respectively v) ^{18}O labeling at the C-terminus. Quantification of ^{18}O labeling was done with ICAT/c-ICAT function at the C-terminus with a shift of 4 Da, mass tolerance of 1.5, threshold of 100000 and smoothing points of 13. The following filters in Bioworks were applied: distinct peptides, consensus scores $\geq$ 10, DCn $\geq$ 0.1, protein probability $\leq 5 \times 10^{-4}$, and Xcorr $\geq$ 1.5, 2.2 and 2.7 for singly-, doubly- and triply-charged peptides, respectively. To ensure the quality of the analyses, the FPR was calculated by dividing the number of hits matching the reverse sequences by the total number of identifications.

To verify the ^{18}O-labeling efficiency, BSA standards were run in a nanoHPLC (Ultimate Plus, Dionex LC Packings, Sunnyvale, CA) equipped with a Famos autosampler (Dionex LC Packings, Sunnyvale, CA) and coupled to a Qtof-MS (Micromass Qtof-1, Waters, Framingham, MA). Peptides were separated in a lab-manufactured reverse phase capillary column (C18 5µm,

75µm x 20cm, Luna, Phenomenex) with a flow rate of 300 nL/min and the following gradient: 100% solvent A for 5 min, 0-50% solvent B in 25 min, 50-90% solvent B in 1 min, and 90% solvent B for 5 min (solvent A = 5% ACN/0.1% FA; solvent B = 80% ACN/0.1% FA). The mass spectrometry (MS) spectra were collected for 2 sec each in the 400-1,800 *m/z* range.

Functional annotation of PQ-affected proteins: In order to annotate the possible functions and involved processes of all proteins affected by PQ (up- or down-regulated), we applied a combination of gene ontology (GO) mapping using GOblet and Interpro scan using Blast2go tool to the subset of proteins that were responsive to PQ. The Goblet analyses were performed on 10-20-2008 using the rodent database with a maximum *e*-value of 1e-10. The Interpro analysis was performed to identify a specific domain or protein families of the sequences in the PQ-responsive proteins using Blast 2 GO software.

3.1.3 Results

Mass Spectrometric analyses of mitochondria and liver tissue homogenate from PQ-treated and untreated rats: Ultra-pure rat liver mitochondria and the whole liver homogenate from the PQ-treated and untreated rats, were subjected to TCA precipitation followed by acetone washes. The samples were then digested with trypsin, desalted and dried using vacuum centrifugation as described in ***Experimental Procedures*****.** Subsequently, the mitochondria and liver homogenates from the PQ-treated rats were labeled with ^{18}O, whereas the untreated mitochondria and the liver homogenate protein samples were labeled with ^{16}O at the C-terminus **(*Experimental Procedures*)**. In parallel, BSA (0.5 nmoles) was used as a control for ^{18}O labeling. Both the mitochondria and the tissue homogenate samples of PQ-treated and untreated rats were desalted, dried and analyzed by LC-MS as described **(*Experimental Procedures*)**. Quantitative measurement of the abundance of the mitochondria and the tissue homogenate proteins was obtained by calculating the fold-change ratio of O^{18}/O^{16} (PQ and the untreated) labeled samples.

A total of 335 proteins were identified in the mitochondria sample with a false-positive rate of ~2.5 % (Appendix 4). Initially, in the tissue homogenate, data indicated a total of 498 proteins with a false-positive rate of 1.4 % (data not shown). However, in order to increase the proteome coverage, the tissue homogenate sample was fractionated through a strong-cation exchange zip tip, desalted and analyzed again using LC-MS ***(Experimental Procedures)***. Then, a total of 994 proteins were identified with a false-positive rate of ~2.5 % (Appendix 5).

The abundances of the proteins in the mitochondria and the tissue homogenates were analyzed by plotting histograms with the log fold ratio of $^{18}O/^{16}O$ (PQ-treated/untreated). The

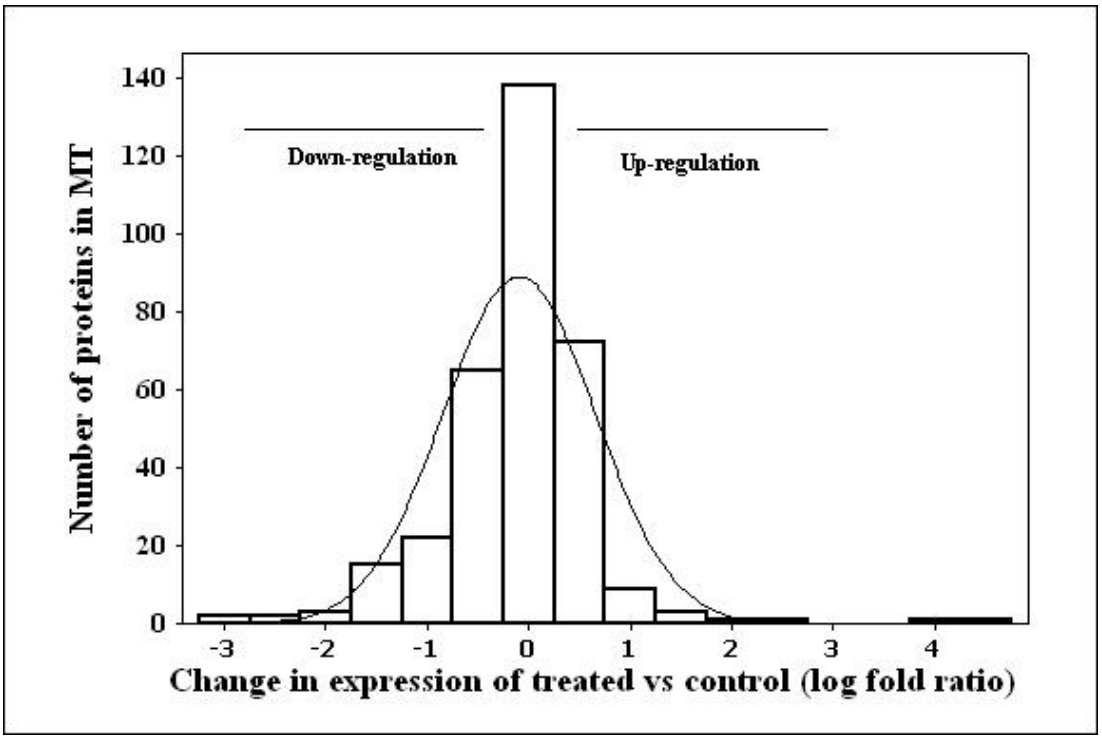
Number of proteins in MT
140
120
100
80
60
40
20
0
Down-regulation
Up-regulation
-3
-2
-1
0
1
2
3
4
Change in expression of treated vs control (log fold ratio)

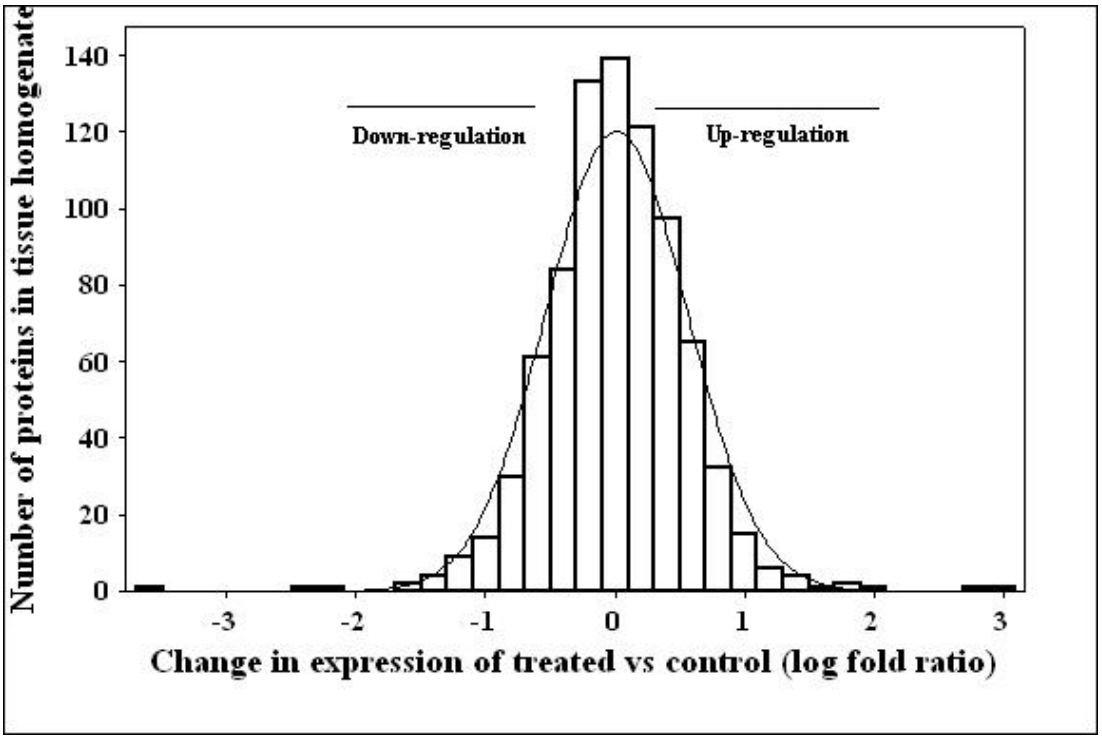

Fig. 3.1.1. Normal distribution log ratio of expression of proteins (PQ-treated/ un-treated) in A. mitochondria and B. liver tissue homogenate identified by LTQ-MS, using ^{18}O labeling.

normal distribution curves, with a peak at 0 (ratio=1) (Fig. 3.1.1A and 3.1.1B) clearly indicated that the ^{18}O labeling was complete in both the mitochondria and tissue homogenates, meaning also that most of the proteins remained unchanged with PQ-treatment. The control, BSA used for as a standard for ^{18}O labeling, also indicated a highly efficient labeling showing a 4 dalton-difference between PQ-treated and un-treated BSA (Fig. 3.1.2).

Table 3.1.1 and 3.1.2 show the list of proteins whose levels were changed (up- or down-regulated) by atleast 2-fold, in mitochondria and tissue homogenate samples, respectively, 3 hr following PQ administration. In mitochondria, a total of 29 proteins were down-regulated and 8 proteins were up-regulated, whereas in the tissue homogenate, containing proteins from cytosol as well as from various organelles (ribosomes, endoplasmic reticulum and mitochondria), 20 were down-regulated and 17 were up-regulated. Notably, in mitochondria, two complex 1 subunits (Ndufs5/Ndufs7) were found to be down-regulated. Interpro-scan was performed with the sequences of the down- and up-regulated proteins in mitochondria and tissue homogenate using Blast2GO software in order to identify the protein domain/family of those proteins (***Experimental Procedures***). The results of the Interpro scan of the various modulated proteins were also added to Table 3.1.1 and 3.1.2.

GO annotation and InterPro scan analyses of early-phase expression changes following PQ treatment: In order to identify the molecular functions and the biological roles of the modulated proteins, identified using mass spectrometric analyses, in mitochondria as well as in tissue homogenate samples, the modulated proteins were analyzed using gene ontology terminology and clustered using the GOblet GO browser software.

Mitochondria samples: The GO-annotations describing the 'molecular function', 'biological processes' and the 'cellular localization' of the down- and up-regulated proteins in mitochondria

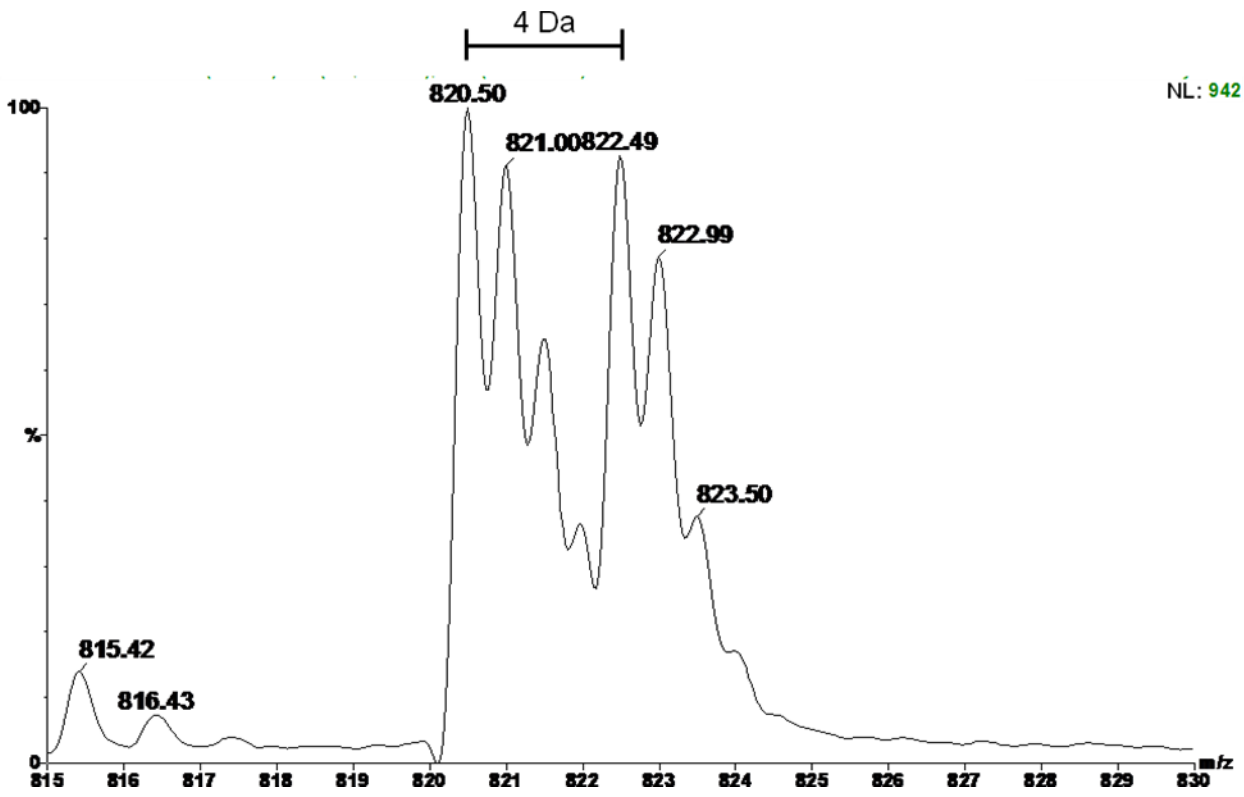

Fig. 3.1.2. ^{18}O labeling spectrum of the control sample, bovine serum albumin (BSA)

are listed in Tables 3.1.3 and 3.1.4, respectively. Out of the 29 proteins that were down-regulated in mitochondria, the 'molecular function' of 62 % of the proteins and the 'biological processes' of 58 % of the proteins were identified using GO annotation analyses. In terms of 'molecular function' of the down-regulated proteins, a majority of the total proteins belonged to the class of 'oxido-reductase (Prxd6; Ndufs5/7; Pah; Cryz; mdh1, Retsat; CYP2C6; Dhrs7; Cisd1; Table 3.1.1 and 3) followed by 'hydrolases and 'transferases' (level 3; Table 3.1.3). Notably, peroxyredoxin 6 (Prxd 6), an antioxidant protein was down-regulated by > 9.5 fold following a 3 hr PQ-exposure. In addition, ATP1a2, a sodium/ potassium transporting protein involved in ATP binding and hydrolysis was down-regulated.

Of the 8 proteins that were up-regulated in mitochondria, the 'molecular function' and the 'biological processes' of the 75 % of the proteins were identified (Table 3.1.4). Notably, glutathione-S-transferase theta 1(Gstt1) was increased by 23-fold and was the protein that exhibited the maximum fold-change ratio. Also, NACHT, a leucine rich repeat and PYD (pyrin domain) containing 1a (Nrlp1a), a caspase recruitment domain protein was up-regulated by 15-fold. Nrlp1a activates the transcription factor NFkB, functions in ATP binding, cytokine production and is thought to function through the Toll signaling pathway (Table 3.1.4).

Tissue homogenate samples: The GO-annotations identifying the 'molecular function', 'biological processes' and 'cellular localization' of the down- and up-regulated proteins in the tissue homogenate are listed, in Tables 3.1.5 and 3.1.6. Of the 20 proteins that were down-regulated, the 'molecular function' of 80 % of the proteins and the 'biological processes' of 80 % of the proteins were identified using GO annotation analyses (Table 3.1.5).

The predominant 'molecular function' of the down-regulated proteins in the whole liver homogenate samples include 'oxido-reductases' (Mao, Bckdha, Pdia, Hsd17b13) as well in 'transferases' (Gstm3, gstt1, Nnmt) (Table 3.1.4). Hsd17b13, a protein involved in estrogen biosynthesis was down-regulated. Interestingly, thioredoxin 1 (Txn 1), an anti-oxidant protein was also down-regulated (Table 3.1.5). In addition, two serine protease inhibitor proteins, Serpin a3L and Serpin a3K, were down regulated.

Of the 17 proteins that were up-regulated in the tissue homogenate samples, the 'molecular function' of 71 % and the 'biological processes' of 53 % of the proteins were identified using GO annotation analyses (Table 3.1.6). In terms of 'molecular function', the majority of the PQ-responsive proteins were involved in a 'binding' (41%) function. In particular, the up-regulated binding proteins are involved in functions such as ribonucleotide synthesis, nucleic acid binding/metabolism, ATP-dependent helicase activity, RNA polymerase II transcription factor activity and unfolded protein binding. In addition, some of the upregulated proteins are involved in 'transferase activity' (Ak3l1, tymp, Gnmt and Phyh). Proteins involved in biosynthesis such as Ctsg (protein biosynthesis) and Ak3l1 (ribonucleotide biosynthesis) were also drastically up-regulated. Proteins involved in the degradation pathway such as proteosomal subunit beta 3 (Psmb) and ubiquitin-activating enzyme E1 (Ube1y1) were also up-regulated. Dc2, a protein that is thought to be involved in (glycosylation *via* asparagine) was significantly up-regulated (Table 3.1.6).

Table 3.1.1. LTQ-MS analyses showing rat liver mitochondrial proteins that were regulated after PQ-treatment.

S.N	Reference	avg Ratio (Heavy/Light)		InterPro	Interpro Ontology
	Protein/Full name	PQ/Untreated	Regulation		
1	Prdx6 Peroxiredoxin-6	0.11	Down	IPR000866	Alkyl hydroperoxide reductase/ Thiol specific antioxidant/ Mal allergen
2	Dbi Acyl-CoA-binding protein	0.11	Down	IPR000582	Acyl-CoA-binding protein, ACBP
3	Atp1a2 Sodium/potassium-transporting ATPase subunit alpha-2	0.15	Down	IPR001757	ATPase, P-type, K/Mg/Cd/Cu/Zn/Na/Ca/Na/H-transporter
4	Ppia Peptidyl-prolyl cis-trans isomerase A	0.18	Down	IPR002130	Peptidyl-prolyl cis-trans isomerase, cyclophilin-type
6	Hmgcs1 Hydroxymethylglutaryl-CoA synthase, cytoplasmic	0.25	Down	IPR010122	Hydroxymethylglutaryl-CoA synthase, eukaryotic
7	Hspe1 Hspd1 10 kDa heat shock protein, mitochondrial	0.26	Down	IPR001476	Chaperonin Cpn10
8	Sult1b1 Sulfotransferase family cytosolic 1B member 1	0.26	Down	IPR000863	Sulphotransferase
9	Nfx1 124 kDa protein	0.30	Down	IPR001374	Single-stranded nucleic acid binding R3H
10	Ndufs5 NADH dehydrogenase (ubiquinone) Fe-S protein 5b	0.31	Down	nil	nil
11	Arf2 ADP-ribosylation factor 2	0.32	Down	IPR006688	ADP-ribosylation factor
12	Ttr Transthyretin	0.33	Down	IPR000895	Transthyretin
13	Ndufs7 NADH dehydrogenase (Ubiquinone) Fe-S protein 7	0.33	Down	IPR006138	NADH dehydrogenase (ubiquinone), 20 kDa subunit
14	Lonp1 Lon protease homolog, mitochondrial	0.34	Down	IPR004815	Peptidase S16, ATP-dependent protease La
15	Pah Phenylalanine-4-hydroxylase	0.34	Down	IPR005961	Phenylalanine-4-hydroxylase, tetrameric form
16	Mdh1 Malate dehydrogenase, cytoplasmic	0.35	Down	IPR011274	Malate dehydrogenase, NAD-dependent, cytosolic
17	Cryz Quinone oxidoreductase	0.36	Down	IPR002085	Alcohol dehydrogenase superfamily, zinc-containing
18	Atad5 similar to chromosome fragility associated gene 1	0.37	Down	IPR003593	AAA+ ATPase, core
20	Cisd1 CDGSH iron sulfur domain 1	0.39	Down	IPR006622	Iron sulphur domain-containing, CDGSH-type
21	Fetub Fetub protein	0.39	Down	IPR000010	Proteinase inhibitor I25, cystatin
22	Slc25a1 Tricarboxylate transport protein, mitochondrial	0.40	Down	IPR002113	Adenine nucleotide translocator 1
23	Retsat All-trans-retinol 13,14-reductase	0.40	Down	IPR003953	Fumarate reductase/succinate dehydrogenase flavoprotein, N-terminal
24	Hsd11b1 Isoform 11-HSD1A of Corticosteroid 11-beta-dehydrogenase isozyme 1	0.41	Down	IPR002198	Short-chain dehydrogenase/reductase SDR
25	Dlst Dihydrolipoyllysine-residue succinyltransferase component of 2-oxoglutarate dehydrogenase complex, mitochondrial	0.42	Down	IPR006255	Dihydrolipoamide succinyltransferase
26	Cyp2c6 Cytochrome P450PB-1	0.45	Down	IPR002401	Cytochrome P450, E-class, group I
27	Rps27a Ribosomal protein S27a	0.48	Down	IPR002906	Ribosomal protein S27a
28	Psap Sulfated glycoprotein 1	0.48	Down	IPR008373	Saposin
29	Dhrs7 Down in nephrectomized rat kidney #3	0.48	Down	IPR002198	Short-chain dehydrogenase/reductase SDR
30	Gstt1 28 kDa protein	23.94	Up	IPR004045/IPR004046	Glutathione S-transferase, N-terminal/C-terminal
31	Nlrp1a similar to NACHT, leucine rich repeat and PYD containing 1	15.62	Up	IPR007111/IPR001315	NACHT nucleoside triphosphatase/Caspase

					Recruitment
32	Ctbs Di-N-acetylchitobiase	4.81	Up	IPR013781	Glycoside hydrolase, subgroup, catalytic core
33	Tpp1 Tripeptidyl-peptidase 1	4.62	Up	IPR009020	Proteinase inhibitor, propeptide
34	Gcsh Glycine cleavage system H protein, mitochondrial	2.92	Up	IPR002930	Glycine cleavage H-protein
35	Ivd Isovaleryl-CoA dehydrogenase, mitochondrial	2.85	Up	IPR013764	Acyl-CoA oxidase/dehydrogenase, type1/2, C-terminal
36	Lactb2 Beta-lactamase-like protein 2	2.64	Up	IPR001279	Beta-lactamase-like
37	Slc27a2 Very long-chain acyl-CoA synthetase	2.05	Up	IPR000873	AMP-dependent synthetase and ligase

Table 3.1.2. LTQ-MS analyses showing the whole liver tissue homogenate proteins that were regulated after PQ-treatment.

	Protein/ Full name Reference	PQ/Untreated avg Ratio (Heavy/Light)	Regulation	InterPro	Interpro Ontology Family/ Domain)
1	Hsd17b13 17-beta hydroxysteroid dehydrogenase 13	0.08	Down	IPR002198	Short-chain dehydrogenase/reductase SDR
2	34 kDa protein	0.19	Down	IPR000941	Enolase
3	Nnmt nicotinamide N-methyltransferase	0.22	Down	IPR000940	Methyltransferase, NNMT/PNMT/TEMT
4	Mpst 3-mercaptopyruvate sulfurtransferase	0.34	Down	IPR001763	Rhodanese-like
5	Glutathione transferase class alpha chain 10 (Fragment)	0.34	Down	IPR003080	Glutathione S-transferase, alpha class
6	Eef1g Elongation factor 1-gamma	0.36	Down	IPR001662	Translation elongation factor EF1B, gamma chain, conserved
7	Maoa similar to Amine oxidase [flavin-containing] A	0.38	Down	IPR001613	Flavin-containing amine oxidase
8	Hnrpd Isoform 1 of Heterogeneous nuclear ribonucleoprotein D0	0.39	Down	IPR000504	RNA recognition motif, RNP-1
9	Ppa2 similar to inorganic pyrophosphatase 2	0.40	Down	IPR008162	Inorganic pyrophosphatase
10	Mtch2 mitochondrial carrier homolog 2	0.41	Down	IPR001993	Mitochondrial substrate carrier
11	Bckdha branched chain ketoacid dehydrogenase E1, alpha polypeptide	0.41	Down	IPR001017	Dehydrogenase, E1 component
12	Txn1 Thioredoxin	0.41	Down	IPR015467	Thioredoxin family
13	Serpina3k Serine protease inhibitor A3K	0.42	Down	IPR000215	Protease inhibitor I4, serpin
14	Pdia4 Protein disulfide-isomerase A4	0.42	Down	IPR017068	Protein disulphide-isomerase A4
15	Atp5c1 ATP synthase gamma chain	0.42	Down	Nil	Nil
16	Gstm3 Glutathione S-transferase Yb4	0.45	Down	IPR003081	Glutathione S-transferase, Mu class
17	Gcs1 Mannosyl-oligosaccharide glucosidase	0.46	Down	IPR004888	Glycoside hydrolase, family 63
18	LOC299282 Serine protease inhibitor A3L	0.48	Down	IPR000215	Protease inhibitor I4, serpin
19	Rplp1 60S acidic ribosomal protein P1	0.49	Down	IPR001813	Ribosomal protein 60S
20	Ndufa6 similar to NADH dehydrogenase (ubiquinone) 1 alpha subcomplex, 6	0.50	Down	IPR016488	NADH dehydrogenase [ubiquinone] (complex I), alpha subcomplex, subunit 6
21	Dc2 DC2 protein	7.72	Up	noIPR	Unintegrated
22	Ctsg 30 kDa protein	7.28	Up	IPR004038	Ribosomal protein L7Ae/L30e/S12e/Gadd45
23	Ak3l1 Adenylate kinase isoenzyme 4, mitochondrial	3.81	Up	IPR006259	Adenylate kinase, subfamily
24	LOC688869;Cox6b1 similar to cytochrome c oxidase, subunit VIb polypeptide 1	3.55	Up	IPR009432	Protein of unknown function DUF1075
25	Psmb3 Proteasome subunit beta type-3	3.15	Up	IPR001353	20S proteasome, A and B subunits
26	Phyh Phytanoyl-CoA dioxygenase, peroxisomal	2.82	Up	IPR008775	Phytanoyl-CoA dioxygenase
27	Bphl Biphenyl hydrolase-like	2.68	Up	IPR000073	Alpha/beta hydrolase fold-1
28	Gnmt Glycine N-methyltransferase	2.55	Up	IPR014369	Glycine N-methyltransferase
29	LOC688869;Cox6b1 similar to cytochrome c oxidase, subunit VIb polypeptide 1	2.51	Up	IPR003213	Cytochrome c oxidase, subunit VIb
30	Tymp Thymidine phosphorylase	2.27	Up	IPR000312/IPR000053	Glycosyl transferase, family 3
31	LOC246266 60 kDa lysophospholipase	2.24	Up	IPR006034	Asparaginase/glutaminase
32	Myl6l Myosin light polypeptide 6	2.23	Up	IPR002048	Calcium-binding EF-hand
33	Abat 50 kDa protein	2.22	Up	IPR004631	4-aminobutyrate aminotransferase, eukaryotic
34	Ube1y1 Ubiquitin-activating enzyme E1	2.18	Up	IPR000011/IPR000594	Ubiquitin-activating enzyme, E1

35	Mcfd2 Multiple coagulation factor deficiency protein 2 homolog	2.12	Up	IPR002048	Calcium-binding EF-hand
36	Ywhae 14-3-3 protein epsilon	2.05	Up	IPR000308	14-3-3 protein
37	57 kDa protein	2.03	Up	IPR001404	Heat shock protein Hsp90

Table 3.1.3. GO ontology analyses of the down-regulated proteins in liver mitochondria after PQ-treatment.

N	Level	GO	Name	Count	% Proteins (Total =29)	Proteins
1	1	GO:0003674	molecular_function	17	58.6	Hspe1, Ppia, Retsat, Nfx1, Cryz, Atad5, Pah, Fetub, Dbi, Hmgcs1, Mdh1, Atp1a2, Cyp2c6, Dlst, Sult1b1, Arf2, Lonp1
2	2	GO:0003824	catalytic activity	10	34.5	Ppia, Retsat, Pah, Dbi, Hmgcs1, Mdh1, Atp1a2, Cyp2c6, Dlst, Sult1b1, Lonp1
3	3	GO:0016491	oxidoreductase activity	4	13.8	Retsat, Pah, Mdh1, Cyp2c6
4	3	GO:0016740	transferase activity	3	10.3	Hmgcs1, Dlst,Sult1b1
5	3	GO:0016787	hydrolase activity	2	6.9	Atp1a2,Lonp4
6	3	GO:0016853	isomerase activity	2	6.9	Ppia, Dbi
7	2	GO:0005215	transporter activity	1	3.4	Atp1a2
8	3	GO:0005386	carrier activity	1	3.4	Atp1a2
9	3	GO:0015075	ion transporter activity	1	3.4	Atp1a2
10	3	GO:0043492	ATPase activity, coupled to movement of substances	1	3.4	Atp1a2
11	2	GO:0005488	binding	9	31.0	Hspe1, Nfx1, Cryz, Pah,Dbi, Atp1a2, Cyp2c6, Arf2, Lonp2
12	3	GO:0000166	nucleotide binding	4	13.8	Hspe1, Atp1a2, Arf2, Lonp3
13	3	GO:0003676	nucleic acid binding	1	3.4	Nfx1
14	3	GO:0005515	protein binding	3	10.3	Hspe1, Nfx1, Cryz
15	3	GO:0008289	lipid binding	1	3.4	Dbi
16	3	GO:0043167	ion binding	3	10.3	Nfx1, Pah,Cyp2c6
17	3	GO:0043176	amine binding	1	3.4	Pah
18	3	GO:0046906	tetrapyrrole binding	1	3.4	Cyp2c6
19	3	GO:0048037	cofactor binding	1	3.4	Dbi
20	2	GO:0030234	enzyme regulator activity	1	3.4	Fetub
21	3	GO:0004857	enzyme inhibitor activity	1	3.4	Fetub
22	2	GO:0030528	transcription regulator activity	2	6.9	Nfx1,Atad5
23	3	GO:0003700	transcription factor activity	1	3.4	Nfx1
24	3	GO:0016564	transcriptional repressor activity	1	3.4	Atad5
25	1	GO:0005575	cellular_component	14	48.3	Retsat, Nfx1, Atp1a2, Cyp2c6, Dlst, Lonp1, Ndufs5, Ndufs7, Prdx6, Slc25a1, Psap, Ttr, Hsd11b1, Cisd1
26	2	GO:0005576	extracellular region	1	3.4	Cyp2c6
27	3	GO:0005615	extracellular space	1	3.4	Cyp2c6
28	2	GO:0005623	cell	14	48.3	Retsat, Nfx1, Atp1a2, Cyp2c6, Dlst, Lonp1, Ndufs5, Ndufs7, Prdx6, Slc25a1, Psap, Ttr, Hsd11b1, Cisd1
29	3	GO:0005622	intracellular	12	41.4	Retsat, Nfx1, Dlst, Lonp1, Ndufs5, Ndufs7, Slc25a1, Psap, Ttr, Cisd1,Hsd11b1,Prdx6
30	3	GO:0016020	membrane	7	24.1	Retsat,Dlst, Ndufs7, Slc25a1, Ttr, Prdx6,Atp1a2
31	2	GO:0031974	membrane-enclosed lumen	1	3.4	Dlst

32	3	GO:0043233	organelle lumen	1	3.4	Dlst
33	2	GO:0031975	envelope	5	17.2	Retsat,Dlst, Ndufs7, Slc25a1,Prdx6
34	3	GO:0031967	organelle envelope	5	17.2	Retsat,Dlst, Ndufs7, Slc25a1,Prdx6
35	2	GO:0043226	organelle	12	41.4	Retsat, Nfx1, Dlst, Lonp1, Psap, Ndufs5, Ndufs7, Slc25a1, Ttr, Cisd1,Hsd11b1,Prdx6
36	3	GO:0043227	membrane-bound organelle	12	41.4	Retsat, Nfx1, Dlst, Lonp1, Psap, Ndufs5, Ndufs7, Slc25a1, Ttr, Cisd1,Hsd11b1,Prdx6
37	3	GO:0043229	intracellular organelle	12	41.4	Retsat, Nfx1, Dlst, Lonp1, Psap, Ndufs5, Ndufs7, Slc25a1, Ttr, Cisd1,Hsd11b1,Prdx6
38	3	GO:0043233	organelle lumen	1	3.4	Dlst
39	2	GO:0043234	protein complex	1	3.4	Dlst
40	3	GO:0045254	pyruvate dehydrogenase complex	1	3.4	Dlst
41	1	GO:0008150	biological_process	16	55.2	Hspe1, Ppia, Retsat, Nfx1, Cryz, Pah, Dbi, Hmgcs1, Mdh1, Atp1a2, Cyp2c6,Lonp1, Psap,Slc25a1,Rps27a, Dhrs7,
42	2	GO:0007582	physiological process	16	55.2	Hspe1, Ppia, Retsat, Nfx1, Cryz, Pah,Dbi, Hmgcs1, Mdh1, Atp1a2, Cyp2c6,Lonp1, Psap,Slc25a1,Rps27a, Dhrs7,
43	3	GO:0008152	metabolism	15	51.7	Hspe1, Ppia, Retsat, Nfx1, Cryz, Pah, Dbi, Hmgcs1, Mdh1, Cyp2c6,Lonp1, Psap,Slc25a1,Rps27a, Dhrs7
44	3	GO:0050791	regulation of physiological process	1	3.4	Nfx1
45	3	GO:0050874	organismal physiological process	1	3.4	Psap
46	3	GO:0050875	cellular physiological process	14	48.3	Hspe1, Ppia, Retsat, Nfx1, Cryz, Pah, Hmgcs1, Mdh1, Atp1a2, Cyp2c6,Lonp1, Psap,Slc25a1,Rps27a
47	3	GO:0051179	localization	3	10.3	Retsat, Atp1a2, Cyp2c6
48	2	GO:0009987	cellular process	14	48.3	Hspe1, Ppia, Retsat, Nfx1, Cryz, Pah, Hmgcs1, Mdh1, Atp1a2, Cyp2c6, Lonp1, Psap, Slc25a1, Rps27a
49	3	GO:0050794	regulation of cellular process	1	3.4	Nfx1
50	3	GO:0050875	cellular physiological process	14	48.3	Hspe1, Ppia, Retsat, Nfx1, Cryz, Pah, Hmgcs1, Mdh1, Atp1a2, Cyp2c6, Lonp1, Psap, Slc25a1, Rps27a
51	2	GO:0050789	regulation of biological process	1	3.4	Nfx 1
52	3	GO:0050791	regulation of physiological process	1	3.4	Nfx 1
53	3	GO:0050794	regulation of cellular process	1	3.4	Nfx 1

Table 3.1.4. GO ontology analyses of the up-regulated proteins in liver mitochondria after PQ-treatment.

N	Level	GO	Name	Count	% Proteins (Total =8)	Proteins
1	1	GO:0003674	molecular_function	6	75	Ctbs,Nlrp1a,Gstt1,Slc27a2, Tpp1, Ivd
2	2	GO:0003824	catalytic activity	4	50	Ctbs,Gstt1,Slc27a2, Tpp1
3	3	GO:0016740	transferase activity	1	12.5	Gstt1
4	3	GO:0016787	hydrolase activity	2	25	Ctbs,Tpp1
5	3	GO:0016874	ligase activity	1	12.5	Slc27a2
6	2	GO:0005488	binding	3	37.5	Ctbs,Nlrp1a,Ivd
7	3	GO:0000166	nucleotide binding	1	12.5	Nlrp1a
8	3	GO:0001871	pattern binding	1	12.5	Ctbs
9	3	GO:0003676	nucleic acid binding	1	12.5	Ivd
10	3	GO:0030246	carbohydrate binding	1	12.5	Ctbs
11	2	GO:0030528	transcription regulator activity	1	12.5	Ivd
12	3	GO:0003700	transcription factor activity	1	12.5	Ivd
13	1	GO:0005575	cellular_component	4	50	Lactb2,Ctbs,Gcsh,Ivd
14	2	GO:0005576	extracellular region	1	12.5	Ctbs
15	3	GO:0005615	extracellular space	1	12.5	Ctbs
16	2	GO:0005623	Cell	3	37.5	Lactb2,Gcsh,Ivd
17	3	GO:0005622	intracellular	3	37.5	Lactb2, Gcsh,Ivd
18	3	GO:0016020	membrane	1	12.5	Ivd
19	2	GO:0031975	envelope	1	12.5	Ivd
20	3	GO:0031967	organelle envelope	1	12.5	Ivd
21	2	GO:0043226	organelle	2	25	Lactb2, Ivd
22	3	GO:0043227	membrane-bound organelle	2	25	Lactb2, Ivd
23	3	GO:0043229	intracellular organelle	2	25	Lactb2, Ivd
24	2	GO:0043234	protein complex	1	12.5	Gcsh
25	3	GO:0005960	glycine cleavage complex	1	12.5	Gcsh
26	1	GO:0008150	biological_process	6	75	Ctbs,Nlrp1a,Gcsh,Slc27a2, Tpp1, Ivd
27	2	GO:0007582	physiological process	6	75	Ctbs,Nlrp1a,Gcsh,Slc27a2, Tpp1, Ivd
28	3	GO:0008152	metabolism	6	75	Ctbs,Nlrp1a,Gcsh,Slc27a2, Tpp1, Ivd
29	3	GO:0050791	regulation of physiological process	2	25	Nlrp1a,Ivd
30	3	GO:0050874	organismal physiological process	2	25	Ctbs,Nlrp1a
31	3	GO:0050875	cellular physiological process	5	62.5	Ctbs,Nlrp1a,Gcsh,Tpp1, Ivd
32	2	GO:0009987	cellular process	5	62.5	Ctbs,Nlrp1a,Gcsh,Tpp1, Ivd
33	3	GO:0007154	cell communication	1	12.5	Nlrp1a
34	3	GO:0050794	regulation of cellular process	2	25	Nlrp1a,Ivd

35	3	GO:0050875	cellular physiological process	5	62.5	Ctbs,Nlrp1a,Gcsh,Tpp1, Ivd
36	2	GO:0050789	regulation of biological process	2	25	Nlrp1a,Ivd
37	3	GO:0050791	regulation of physiological process	2	25	Nlrp1a,Ivd
38	3	GO:0050794	regulation of cellular process	2	25	Nlrp1a,Ivd
39	2	GO:0050896	response to stimulus	2	25	Ctbs,Nlrp1a,
40	3	GO:0006950	response to stress	1	12.5	Ctbs
41	3	GO:0009607	response to biotic stimulus	2	25	Ctbs,Nlrp1a,
42	3	GO:0009628	response to abiotic stimulus	1	12.5	Ctbs

Table 3.1.5. GO ontology analyses of the down-regulated proteins in liver tissue homogenate after PQ-treatment.

Level	GO	Name	Count	% Proteins (Total =20)	Proteins
1	GO:0003674	molecular_function	16	80	LOC680351, Gstm3, Gcs1, Rplp1, Serpina3k, GST-alpha, 34 kDa, Maoa, Txn1, Mtch2, Nnmt, Bckdha, Hnrpd, Pdia4, Ppa2, Hsd17b13
2	GO:0003824	catalytic activity	10	50	Gstm3,Gcs1,Gst alpha,34 kDa,Maoa,Nnmt,Bckdha,Pdia4,Ppa2,Hsd17b13
3	GO:0016491	oxidoreductase activity	4	20	Maoa,Bckdha,Hsd17b13,Pdia4
3	GO:0016740	transferase activity	3	15	Gstm3, Gst alpha, Nnmt
3	GO:0016787	hydrolase activity	2	10	Gcs1,Ppa2
3	GO:0016829	lyase activity	1	5	34 kDa
3	GO:0016853	isomerase activity	1	5	Pdia4
2	GO:0005198	structural molecule activity	1	5	Rplp1
3	GO:0003735	structural constituent of ribosome	1	5	Rplp1
2	GO:0005215	transporter activity	2	10	Txn1,Pdia4
3	GO:0005386	carrier activity	2	10	Txn1,Pdia4
3	GO:0005489	electron transporter activity	2	10	Txn1,Pdia4
2	GO:0005488	binding	4	20	Hnrpd,Pdia4,Ppa2,Mtch2
3	GO:0003676	nucleic acid binding	1	5	Hnrpd
3	GO:0043167	ion binding	2	10	Pdia4,Ppa2
2	GO:0030234	enzyme regulator activity	2	10	LOC680351,Serpina3k
3	GO:0004857	enzyme inhibitor activity	2	10	LOC680351,Serpina3k
1	GO:0005575	cellular_component	7	35	Eef1g, Rplp1, 34 kDa,Mtch2,Hnrpd, Pdia4, Ndufa6
2	GO:0005576	extracellular region	1	5	Pdia4
3	GO:0005615	extracellular space	1	5	Pdia4
2	GO:0005623	cell	7	35	Eef1g, Rplp1, 34kDa,Mtch2,Hnrpd, Pdia4, Ndufa6
3	GO:0005622	intracellular	6	30	Eef1g, Rplp1, 34kDa,Hnrpd, Pdia4, Ndufa6
3	GO:0016020	membrane	1	5	Mtch2
2	GO:0043226	organelle	5	25	Eef1g, Rplp1, Hnrpd, Pdia4, Ndufa6
3	GO:0043227	membrane-bound organelle	4	20	Eef1g, Hnrpd, Pdia4, Ndufa6
3	GO:0043228	non-membrane-bound organelle	1	5	Rplp1
3	GO:0043229	intracellular organelle	5	25	Eef1g, Rplp1, Hnrpd, Pdia4, Ndufa6
2	GO:0043234	protein complex	3	15	Rplp1, Hnrpd, 34 kDa
3	GO:0000015	phosphopyruvate hydratase complex	2	10	Hnrpd, 34 kDa
3	GO:0030529	ribonucleoprotein complex	2	10	Rplp1, Hnrpd
1	GO:0008150	biological_process	16	80	LOC680351, Gstm3, Gcs1, Rplp1, Gst alpha, 34 kDa, Mpst, Maoa, Txn1, Mtch2, Nnmt, Bckdha, Hnrpd, Pdia4, Ppa2, Hsd17b13
2	GO:0007582	physiological process	16	80	LOC680351, Gstm3, Gcs1, Rplp1, Gst alpha, 34 kDa, Mpst, Maoa, Txn1, Mtch2, Nnmt, Bckdha, Hnrpd, Pdia4, Ppa2, Hsd17b14

3	GO:0008152	metabolism	14	70	Gstm3, Gcs1, Rplp1, Gst alpha, 34 kDa, Mpst, Maoa, Txn1, Mtch2, Nnmt, Bckdha, Hnrpd, Ppa2, Hsd17b15
3	GO:0016265	death	1	5	Pdia4
3	GO:0050791	regulation of physiological process	2	10	Hnrpd, Pdia4
3	GO:0050874	organismal physiological process	1	5	Nnmt
3	GO:0050875	cellular physiological process	11	55	LOC680351, 34 kDa, Rplp1, Mpst, Maoa, Txn1, Mtch2, Nnmt, Hnrpd, Pdia4, Hsd17b19
3	GO:0051179	localization	3	15	Maoa, Txn1, Mtch2,
2	GO:0009987	cellular process	11	55	LOC680351, Rplp1, 34 kDa, Mpst, Maoa, Txn1, Nnmt, Hnrpd,Mtch2, Pdia4, Hsd17b21
3	GO:0007154	cell communication	1	5	Nnmt
3	GO:0050794	regulation of cellular process	2	10	Hnrpd, Pdia4
3	GO:0050875	cellular physiological process	11	55	LOC680351, Rplp1, 34 kDa, Mpst, Maoa, Txn1, Nnmt, Hnrpd,Mtch2, Pdia4, Hsd17b21
2	GO:0050789	regulation of biological process	2	10	Hnrpd, Pdia4
3	GO:0048518	positive regulation of biological process	1	5	Pdia4
3	GO:0050791	regulation of physiological process	2	10	Hnrpd, Pdia4
3	GO:0050794	regulation of cellular process	2	10	Hnrpd, Pdia4

Table 3.1.6. GO ontology analyses of upregulated proteins in liver tissue homogenate after PQ-treatment.

N	Level	GO	Name	Count	% Proteins (Total =17)	Proteins
1	1	GO:0003674	molecular_function	12	70.6	Ak3l1, Mcfd2, Ube1y1,Ywhae,LOC246266,Psmb3,57 kDa, Myl6l,Tymp,Ctsg,Gnmt, Phyh
2	2	GO:0003824	catalytic activity	7	41.2	Ak3l1, Ube1y1,Ywhae,Psmb3, Tymp,Gnmt, Phyh
3	3	GO:0008641	small protein activating enzyme activity	1	5.9	Ube1y1
4	3	GO:0016491	oxidoreductase activity	1	5.9	Ywhae
5	3	GO:0016740	transferase activity	4	23.5	Ak3l1,Tymp,Gnmt, Phyh
6	3	GO:0016787	hydrolase activity	1	5.9	Psmb3
7	2	GO:0005198	structural molecule activity	1	5.9	Ctsg
8	3	GO:0003735	structural constituent of ribosome	1	5.9	Ctsg
9	2	GO:0005488	binding	7	41.2	Ak3l1, Mcfd2, Ywhae,LOC246266,57 kDa, Myl6l, Phyh
10	3	GO:0000166	nucleotide binding	2	11.8	Ak3l1,57 kDa
11	3	GO:0003676	nucleic acid binding	1	5.9	LOC246266
12	3	GO:0005515	protein binding	3	17.6	Ywhae,57 kDa, Phyh
13	3	GO:0043167	ion binding	2	11.8	Mcfd2, Myl6l
14	2	GO:0030528	transcription regulator activity	1	5.9	LOC246266
15	3	GO:0003700	transcription factor activity	1	5.9	LOC246266
16	1	GO:0005575	cellular_component	8	47.1	Ak3l1,Abat,Bphl,Psmb3,57 kDa,Ctsg,Cox6b1,Phyh
17	2	GO:0005576	extracellular region	2	11.8	Ak3l1,57 kDa
18	3	GO:0005615	extracellular space	2	11.8	Ak3l1,57 kDa
19	2	GO:0005623	cell	8	47.1	Ak3l1,Abat,Bphl,Psmb3,57 kDa,Ctsg,Cox6b1,Phyh
20	3	GO:0005622	intracellular	8	47.1	Ak3l1,Abat,Bphl,Psmb3,57 kDa,Ctsg,Cox6b1,Phyh
21	3	GO:0016020	membrane	1	5.9	Cox6b1
22	2	GO:0031975	envelope	1	5.9	Cox6b1
23	3	GO:0031967	organelle envelope	1	5.9	Cox6b1
24	2	GO:0043226	organelle	7	41.2	Ak3l1,Abat,Bphl,57 kDa,Ctsg,Cox6b1,Phyh
25	3	GO:0043227	membrane-bound organelle	6	35.3	Ak3l1,Abat,Bphl,57 kDa,Cox6b1,Phyh
26	3	GO:0043228	non-membrane-bound organelle	2	11.8	Ctsg
27	3	GO:0043229	intracellular organelle	7	41.2	Ak3l1,Abat,Bphl,57 kDa,Ctsg,Cox6b1,Phyh
28	2	GO:0043234	protein complex	2	11.8	Psmb3,Ctsg
29	3	GO:0000502	proteasome complex (sensu Eukaryota)	1	5.9	Psmb3,
30	3	GO:0030529	ribonucleoprotein complex	1	5.9	Ctsg
31	1	GO:0008150	biological_process	9	52.9	Ak3l1, Ube1y1,LOC246266,Psmb3,57 kDa, Dc2, Tymp,Ctsg, Phyh
32	2	GO:0007275	development	1	5.9	Tymp
33	3	GO:0009653	morphogenesis	1	5.9	Tymp
34	3	GO:0048513	organ development	1	5.9	Tymp
35	2	GO:0007582	physiological process	8	47.1	Ak3l1, Ube1y1,LOC246266,Psmb3,57 kDa, Dc2,Ctsg, Phyh
36	3	GO:0008152	metabolism	8	47.1	Ak3l1, Ube1y1,LOC246266,Psmb3,57 kDa, Dc2,Ctsg, Phyh

37	3	GO:0050791	regulation of physiological process	1	5.9	LOC246266
38	3	GO:0050875	cellular physiological process	8	47.1	Ak3l1, Ube1y1,LOC246266,Psmb3,57 kDa, Dc2,Ctsg, Phyh
39	2	GO:0009987	cellular process	8	47.1	Ak3l1, Ube1y1,LOC246266,Psmb3,57 kDa, Dc2,Ctsg, Phyh
40	3	GO:0050794	regulation of cellular process	1	5.9	LOC246266
41	3	GO:0050875	cellular physiological process	8	47.1	Ak3l1, Ube1y1,LOC246266,Psmb3,57 kDa, Dc2,Ctsg, Phyh
42	2	GO:0050789	regulation of biological process	1	5.9	LOC246266
43	3	GO:0050791	regulation of physiological process	1	5.9	LOC246266
44	3	GO:0050794	regulation of cellular process	1	5.9	LOC246266
45	2	GO:0050896	response to stimulus	2	11.8	57 kDa,Tymp
46	3	GO:0006950	response to stress	1	5.9	57 kDa
47	3	GO:0007610	behavior	1	5.9	Tymp
48	3	GO:0009605	response to external stimulus	1	5.9	Tymp
49	3	GO:0009628	response to abiotic stimulus	2	11.8	57 kDa,Tymp

3.1.4 Discussion

PQ, one of the most widely applied herbicides in the world, exerts its toxic action by generating ROS. PQ can also produce ROS within neurons, leading to the production of malondialdehyde (lipid peroxidation), protein carbonylation (protein oxidation) and DNA fragmentation (DNA damage) (Peng *et al.*, 2005; Thiruchelvam *et al.*, 2005; Yang and Tiffany-Castiglioni, 2005). Some of the redox-enzymes are also thought to be involved in PQ-mediated toxicity. They include CYPOR (Clejan and Cederbaum, 1989), microsomal NADP(H)-dependent reductases (Dicker and Cederbaum, 1991), NADH:ubiquitin oxidoreductase (Fukushima *et al.*, 1993), NADPH ferridoxin oxidoreductase (Liochev *et al.*, 1994), nitric oxide synthase (Day *et al.*, 1999), NADPH oxidase (Bonneh-Barkay *et al.*, 2005), ubiquitin: cytochrome *c* oxido reductase (Castello *et al.*, 2007) and thioredoxin reductase (Gray *et al.*, 2007). However, complimentary studies have to be performed to validate some of these results.

Recent reports suggest that mitochondria are involved in ROS generation for PQ-mediated toxicity. Most of the studies were conducted by incubating mitochondria with PQ at different amounts (*ex-vivo*). However, the mechanism of PQ-toxicity can be understood better by *in vivo* models. Rats were treated with a single dose of PQ (40 mg/kg) and changes in protein expression in liver tissue homogenate and mitochondria were measured. In order to understand the initial changes in protein expression and the involvement of mitochondria, we performed proteomic analyses 3 hr following PQ-exposure. In addition to the LC-MS analyses, the proteins identified as being down- or up-regulated in liver mitochondria and liver tissue homogenates were subjected to 'GO annotation' using GOblet and 'protein domain or protein family annotation' from Interpro database using the Blast2go tool.

In the mitochondria samples, two sub-units of NADH dehydrogenase (complex 1; Ndufs5, Ndufs7) were observed to be down-regulated after PQ-exposure. Previously, reduction of the complex 1 gene expression level was observed in rat liver and brain following 2 hrs of PQ exposure (Tawara *et al.*, 1996). In addition, complex 1 was reported to be the major factor involved in $O_2^{\bullet-}$ production in PQ-toxicity (Cocheme and Murphy, 2008). Though complex 3 is also thought to be affected (Castello *et al.*, 2007), no significant changes in its fold-ratio (≤ 2 fold) were observed at this early time point. Peroxyredoxin 6 (Prdx 6), a protein that functions in antioxidant defense was down-regulated by 89%. Prdx6 is found to be expressed in all major organs with a particularly high level in lung and functions in phospholipid metabolism (Manevich and Fisher, 2005), which may also be considered to account for the specific targeting of PQ to lungs. In addition, a lipid-metabolism protein, acyl CoA-binding protein (Dbi) was down-regulated to large extent (11%). A majority of the down-regulated proteins in mitochondria were involved in fatty acid or amino-acid metabolism (36.7%), though not specific to any single process (Tables 3.1.3 and 3.1.4).

PQ, a redox cycling compound is thought to exert its toxic actions by interacting with enzymes involved in oxidation-reduction reactions. In mitochondria, we observed 4 proteins with oxido-reductase activity to be down-regulated (Retsat, Pah, Mdh1, Cyp2c6) (Table 3.1.3). However, each protein has to be investigated by various techniques to confirm these results. Next to the oxidoreductase activity, proteins that were involved in transferase activity were signifiacantly modulated. Hydroxymethylglutaryl-CoA synthase (Hmgcs1) was down-regulated significantly followed by the sulfotransferase family cytosolic 1B member 1(sult1b1) and dihydrolipoyllysine-residue succinyltransferase component of 2-oxoglutarate dehydrogenase complex (dlst). Down-regulation of sult1b1 and cyp2c6 indicate that the metabolism and

detoxification processes are affected in PQ-exposure toxicity. On the other hand, upregulation of glutathione-S-transferase theta 1 (Gstt1) suggest that the glutathione metabolism pathway and the detoxification pathway may be modulated in an inverse manner. But by observing a decrease in Cyp2c6, it can be suspected that some other system is activating PQ and the glutathione S transferase is being up-regulated by increased output from this system. Further studies have to be performed to support this notion.

Interestingly, Lonp1, an ATPase dependent protease, Tpp1, a peptidase and Fetub, a proteinase-inhibitor were down-regulated indicating that the protein degradation pathway were subjected to be affected. Down-regulation of ADP ribosylation factor and the up-regulation of Slc27a2, an AMP dependent synthetase and ligase protein suggest the possibility of DNA damage and the involvement of DNA repair pathway. In addition, ATP1a2, a sodium/potassium transporting ATPase subunit alpha 2 proteins was down-regulated. Also, slc25a1, a citrate transmembrane transporter protein and adenine nucleotide translocator protein was down-regulated at this early time point which may lead to mitochondrial damage and generation of ROS. Thus, results from the mitochondria sample clearly demonstrate that many mitochondrial proteins are affected at this early phase of PQ-exposure. Also, the proteins that were affected were involved in various functions including metabolism, oxidoreductase activity, mitochondrial transport, mitochondrial function and DNA repair.

In the liver homogenate sample, levels of 37 proteins were modulated wherein 20 were down-regulated and 17 were up-regulated (Tables 3.1.4 and 3.1.5). Among that, 5 proteins involved in transferase activity were down-regulated (Gstm3, Gst α, Nnmt) and 5 were up-regulated (Ak3II, Ak2, Tymp, Gnmt, Phyh). Although, the proteins were involved in various transferase activities, the down-regulation of the subunits of glutathione-S-transferase (Gstm3,

Gst α) in the tissue clearly suggest the involvement of glutathione metabolism pathway. In addition, thioredoxin- 1 (Txn 1) an antioxidant and a thiol protein, were down-regulated. Furthermore, 5 oxido-reductase activity proteins were down-regulated (Mao-a, Bckdha, Hsd17b13, and Pdia4) and only one is up-regulated (Ywhae).

In brain, PQ exposure is thought to be linked with Parkinsons disease. PQ, which is structuraly similar to MPP^+, also depletes dopaminergic neurons in substantia nigra (Brooks *et al.*, 1999; McCormack *et al.*, 2002), reduces nicotinic receptor-induced dopamine release in monkey striatum (O'Leary *et al.*, 2008) causing Parkinson's like symptoms (Brooks *et al.*, 1999; McCormack *et al.*, 2002; Thiruchelvam *et al.*, 2005; Wesseling *et al.*, 2001; Yang and Tiffany-Castiglioni, 2005). Our results showing down-regulation of monoamine oxidase a (Mao-a) in the tissue homogenate suggest that further investigation has to be performed to substantiate its relation to dopamine levels.

Downregulation of serine protease inhibitors (Serpina a3L, a3k) and the upregulation of proteosomal subunit, Psmb3 and the ubiquitin activating enzyme (Ubeye1) suggest that the protein degradation pathway is greatly affected 3 hrs following PQ-administration in the liver tissue. Moreover, Tymp, a protein that is thought to be up-regulated before liver damage due to stress was found to be increased in the liver homogenate. Also, it is observed recently that PQ produces apoptosis in human neuroblastoma SH-SY5y cells causing decrease in complex 1 activity, caspase 9 and 3 activation (Yang and Tiffany-Castiglioni, 2008). In addition, a number of proteins with binding functions were modulated wherein 4 were down-regulated (Hnrpd, Pdia4, Ppa2, Mtch2) and 7 were up-regulated (Ak3l1, Mcfd2, Ywhae, LOC246266, 57 kDa, Myl6l, Phyh) (Table 3.1.6). In addition, cytochrome-*c* oxidase was up-regulated and mitochondrial substrate carrier protein (Mtch2) was down-regulated indicating that mitochondria

function may be affected by the proteins in the cytosol. Also, Ca^{2+}-binding proteins, myosin light polypeptide 6 (Myl 6) and multiple coagulation factor deficiency protein 2 homolog (Mcfd2) were up-regulated in the liver homogenate.

3.1.5 Conclusion

It is to be mentioned that many of the proteins in the mitochondria and the liver homogenate that were modulated after PQ-exposure are involved in oxidation-reduction processes. The present proteomic analyses have explored a number of proteins that may be involved in the early stage of PQ-induced toxicity. However, further studies are needed to determine and verify the exact mechanisms and the pathways involved in PQ-induced toxicity. Each factor will then have to be considered in relation to the overall global picture, because only rarely is just one pathway or factor involved in a toxic response.

3.1.6 Acknowlegments

I thank Dr. Igor C. Almeida and Ernesto S. Nakayasu for their valuable help, suggestions and guidance in performing all the proteomics analyses. This publication was made possible by grant # ES 011982 to R.T. Miller from the National Institute of Environmental Health Sciences (NIEHS)/NIH. This project was also supported in part by grant # 5G12RR008124 to the Border Biomedical Research Center (BBRC)/University of Texas at El Paso from the National Center for Research Resources (NCRR)/NIH.

3.1.7 References

Adam, A., Smith, L. L., Cohen, G. M., 1990. An assessment of the role of redox cycling in mediating the toxicity of paraquat and nitrofurantoin. Environmental health perspectives 85, 113-117.

Bataller, R., Bragulat, E., Nogue, S., Gorbig, M. N., Bruguera, M., Rodes, J., 2000. Prolonged cholestasis after acute paraquat poisoning through skin absorption. The American journal of gastroenterology 95, 1340-1343.

Bonneh-Barkay, D., Reaney, S. H., Langston, W. J., Di Monte, D. A., 2005. Redox cycling of the herbicide paraquat in microglial cultures. Brain Res Mol Brain Res 134, 52-56.

Brooks, A. I., Chadwick, C. A., Gelbard, H. A., Cory-Slechta, D. A., Federoff, H. J., 1999. Paraquat elicited neurobehavioral syndrome caused by dopaminergic neuron loss. Brain research 823, 1-10.

Brown, M. R., Sullivan, P. G., Geddes, J. W., 2006. Synaptic mitochondria are more susceptible to Ca2+overload than nonsynaptic mitochondria. J Biol Chem 281, 11658-11668.

Burk, R. F., Lawrence, R. A., Lane, J. M., 1980. Liver necrosis and lipid peroxidation in the rat as the result of paraquat and diquat administration. Effect of selenium deficiency. J Clin Invest 65, 1024-1031.

Cantor, A., Young-Holt, B., 2002. Pesticide-related symptoms among farm workers in rural Honduras. International journal of occupational and environmental health 8, 41-45.

Castello, P. R., Drechsel, D. A., Patel, M., 2007. Mitochondria are a major source of paraquat-induced reactive oxygen species production in the brain. J Biol Chem 282, 14186-14193.

Clark, D. G., McElligott, T. F., Hurst, E. W., 1966. The toxicity of paraquat. British journal of industrial medicine 23, 126-132.

Clejan, L., Cederbaum, A. I., 1989. Synergistic interactions between NADPH-cytochrome P-450 reductase, paraquat, and iron in the generation of active oxygen radicals. Biochem Pharmacol 38, 1779-1786.

Cocheme, H. M., Murphy, M. P., 2008. Complex I is the major site of mitochondrial superoxide production by paraquat. J Biol Chem 283, 1786-1798.

Conradi, S. E., Olanoff, L. S., Dawson, W. T., Jr., 1983. Fatality due to paraquat intoxication: confirmation by postmortem tissue analysis. American journal of clinical pathology 80, 771-776.

Costantini, P., Petronilli, V., Colonna, R., Bernardi, P., 1995. On the effects of paraquat on isolated mitochondria. Evidence that paraquat causes opening of the cyclosporin A-sensitive permeability transition pore synergistically with nitric oxide. Toxicology 99, 77-88.

Day, B. J., Patel, M., Calavetta, L., Chang, L. Y., Stamler, J. S., 1999. A mechanism of paraquat toxicity involving nitric oxide synthase. Proc Natl Acad Sci U S A 96, 12760-12765.

Dicker, E., Cederbaum, A. I., 1991. NADH-dependent generation of reactive oxygen species by microsomes in the presence of iron and redox cycling agents. Biochem Pharmacol 42, 529-535.

Eng, J. K., McCormack, A. L., and Yates, J. R. r. , 1994. J Am Soc Mass Spectrom 5, 976-989.

Erickson, T., Brown, K. M., Wigder, H., Gillespie, M., 1997. A case of paraquat poisoning and subsequent fatality presenting to an emergency department. The Journal of emergency medicine 15, 649-652.

Farrington, J. A., Ebert, M., Land, E. J., Fletcher, K., 1973. Bipyridylium quaternary salts and related compounds. V. Pulse radiolysis studies of the reaction of paraquat radical with oxygen. Implications for the mode of action of bipyridyl herbicides. Biochim Biophys Acta 314, 372-381.

Fukushima, T., Gao, T., Tawara, T., Hojo, N., Isobe, A., Yamane, Y., 1997. Inhibitory effect of nicotinamide to paraquat toxicity and the reaction site on complex I. Archives of toxicology 71, 633-637.

Fukushima, T., Yamada, K., Isobe, A., Shiwaku, K., Yamane, Y., 1993. Mechanism of cytotoxicity of paraquat. I. NADH oxidation and paraquat radical formation via complex I. Exp Toxicol Pathol 45, 345-349.

Ghazi-Khansari, M., Nasiri, G., Honarjoo, M., 2005. Decreasing the oxidant stress from paraquat in isolated perfused rat lung using captopril and niacin. Archives of toxicology 79, 341-345.

Gray, J. P., Heck, D. E., Mishin, V., Smith, P. J., Hong, J. Y., Thiruchelvam, M., Cory-Slechta, D. A., Laskin, D. L., Laskin, J. D., 2007. Paraquat increases cyanide-insensitive respiration in murine lung epithelial cells by activating an NAD(P)H:paraquat oxidoreductase: identification of the enzyme as thioredoxin reductase. J Biol Chem 282, 7939-7949.

Hirai, K., Witschi, H., Cote, M. G., 1985. Mitochondrial injury of pulmonary alveolar epithelial cells in acute paraquat intoxication. Experimental and molecular pathology 43, 242-252.

Hong, S. Y., Yang, D. H., Hwang, K. Y., 2000. Associations between laboratory parameters and outcome of paraquat poisoning. Toxicology letters 118, 53-59.

Jurado, J. D., Rael, E. D., Lieb, C. S., Nakayasu, E., Hayes, W. K., Bush, S. P., Ross, J. A., 2007. Complement inactivating proteins and intraspecies venom variation in Crotalus oreganus helleri. Toxicon 49, 339-350.

Lee, H. S., Kim, K., Kim, J. H., Do, K. S., Lee, S. K., 1998. On-line sample preparation of paraquat in human serum samples using high-performance liquid chromatography with column switching. Journal of chromatography 716, 371-374.

Lewis, C. P., Haschek, W. M., Wyatt, I., Cohen, G. M., Smith, L. L., 1989. The accumulation of cystamine and its metabolism to taurine in rat lung slices. Biochem Pharmacol 38, 481-488.

Liochev, S. I., Hausladen, A., Beyer, W. F., Jr., Fridovich, I., 1994. NADPH: ferredoxin oxidoreductase acts as a paraquat diaphorase and is a member of the soxRS regulon. Proc Natl Acad Sci U S A 91, 1328-1331.

Mainwaring, G., Lim, F. L., Antrobus, K., Swain, C., Clapp, M., Kimber, I., Orphanides, G., Moggs, J. G., 2006. Identification of early molecular pathways affected by paraquat in rat lung. Toxicology 225, 157-172.

Manevich, Y., Fisher, A. B., 2005. Peroxiredoxin 6, a 1-Cys peroxiredoxin, functions in antioxidant defense and lung phospholipid metabolism. Free Radic Biol Med 38, 1422-1432.

Matsumoto, T., Matsumori, H., Kuwabara, N., Fukuda, Y., Ariwa, R., 1980. A histopathological study of the liver in paraquat poisoning--an analysis of fourteen autopsy cases with emphasis on bile duct injury. Acta pathologica japonica 30, 859-870.

McCormack, A. L., Thiruchelvam, M., Manning-Bog, A. B., Thiffault, C., Langston, J. W., Cory-Slechta, D. A., Di Monte, D. A., 2002. Environmental risk factors and Parkinson's disease: selective degeneration of nigral dopaminergic neurons caused by the herbicide paraquat. Neurobiology of disease 10, 119-127.

Mukhopadhyay, P., Rajesh, M., Yoshihiro, K., Hasko, G., Pacher, P., 2007. Simple quantitative detection of mitochondrial superoxide production in live cells. Biochem Biophys Res Commun 358, 203-208.

Mullick, F. G., Ishak, K. G., Mahabir, R., Stromeyer, F. W., 1981. Hepatic injury associated with paraquat toxicity in humans. Liver 1, 209-221.

O'Leary, K. T., Parameswaran, N., Johnston, L. C., McIntosh, J. M., Di Monte, D. A., Quik, M., 2008. Paraquat exposure reduces nicotinic receptor-evoked dopamine release in monkey striatum. J Pharmacol Exp Ther 327, 124-129.

Palmeira, C. M., Moreno, A. J., Madeira, V. M., 1995. Mitochondrial bioenergetics is affected by the herbicide paraquat. Biochim Biophys Acta 1229, 187-192.

Peng, J., Stevenson, F. F., Doctrow, S. R., Andersen, J. K., 2005. Superoxide dismutase/catalase mimetics are neuroprotective against selective paraquat-mediated dopaminergic neuron death in the substantial nigra: implications for Parkinson disease. J Biol Chem 280, 29194-29198.

Pertoft, H., Laurent, T. C., Laas, T., Kagedal, L., 1978. Density gradients prepared from colloidal silica particles coated by polyvinylpyrrolidone (Percoll). Anal Biochem 88, 271-282.

Reinhart, P. H., Taylor, W. M., Bygrave, F. L., 1982. A procedure for the rapid preparation of mitochondria from rat liver. Biochem J 204, 731-735.

Rodrigues, M. L., Nakayasu, E. S., Oliveira, D. L., Nimrichter, L., Nosanchuk, J. D., Almeida, I. C., Casadevall, A., 2008. Extracellular vesicles produced by Cryptococcus neoformans contain protein components associated with virulence. Eukaryot Cell 7, 58-67.

Rose, M. S., Smith, L. L., Wyatt, I., 1974. Evidence for energy-dependent accumulation of paraquat into rat lung. Nature 252, 314-315.

Shimada, H., Hirai, K., Simamura, E., Pan, J., 1998. Mitochondrial NADH-quinone oxidoreductase of the outer membrane is responsible for paraquat cytotoxicity in rat livers. Archives of biochemistry and biophysics 351, 75-81.

Smith, L. L., 1982. Young Scientists Award lecture 1981: The identification of an accumulation system for diamines and polyamines into the lung and its relevance to paraquat toxicity. Archives of toxicology. Supplement. = Archiv fur Toxikologie 5, 1-14.

Stone, K. L., and Williams, K. R. , 1996. Enzymatic digestion of proteins in solution and in SDS polyacrilamide gel. In: Walker, J. M. (ed). . The protein protocol handbook., Humana Press Inc., Totowa, NJ.

Takegoshi, K., Nakanuma, Y., Ohta, M., Thoyama, T., Okuda, K., Kono, N., 1988. Light and electron microscopic study of the liver in paraquat poisoning. Liver 8, 330-336.

Tawara, T., Fukushima, T., Hojo, N., Isobe, A., Shiwaku, K., Setogawa, T., Yamane, Y., 1996. Effects of paraquat on mitochondrial electron transport system and catecholamine contents in rat brain. Archives of toxicology 70, 585-589.

Thiruchelvam, M., Prokopenko, O., Cory-Slechta, D. A., Richfield, E. K., Buckley, B., Mirochnitchenko, O., 2005. Overexpression of superoxide dismutase or glutathione peroxidase protects against the paraquat + maneb-induced Parkinson disease phenotype. J Biol Chem 280, 22530-22539.

Tomita, M., Okuyama, T., Hidaka, K., Ishikawa, T., Adachi, J., Nohno, T., 2004. Early differential gene expression of rat lung after exposure to paraquat. Free Radic Res 38, 821-829.

Ueda, T., Hirai, K., Ogawa, K., 1985. Effects of paraquat on the mitochondrial structure and Ca-ATPase activity in rat hepatocytes. Journal of electron microscopy 34, 85-91.

Weidel, H., Rosso, M., 1882. Studien uber das pyridin. Monatshefte für Chemie 3, 850-885.

Wesseling, C., van Wendel de Joode, B., Ruepert, C., Leon, C., Monge, P., Hermosillo, H., Partanen, T. J., 2001. Paraquat in developing countries. International journal of occupational and environmental health 7, 275-286.

Wyatt, I., Soames, A. R., Clay, M. F., Smith, L. L., 1988. The accumulation and localisation of putrescine, spermidine, spermine and paraquat in the rat lung. In vitro and in vivo studies. Biochem Pharmacol 37, 1909-1918.

Yamamoto, T., Anno, M., Sato, T., 1987. Effects of paraquat on mitochondria of rat skeletal muscle. Comparative biochemistry and physiology 86, 375-378.

Yang, W., Tiffany-Castiglioni, E., 2005. The bipyridyl herbicide paraquat produces oxidative stress-mediated toxicity in human neuroblastoma SH-SY5Y cells: relevance to the dopaminergic pathogenesis. Journal of toxicology and environmental health 68, 1939-1961.

Yang, W., Tiffany-Castiglioni, E., 2008. Paraquat-induced apoptosis in human neuroblastoma SH-SY5Y cells: involvement of p53 and mitochondria. Journal of toxicology and environmental health 71, 289-299.

Zweig, G., Shavit, N., Avron, M., 1965. Diquat (I,I'-ethylene-2,2'-dipyridylium dibromide) in photo-reactions of isolated chloroplasts. Biochim Biophys Acta 109, 332-346.

3.2 Antioxidant Gene Expression Changes in Brain Regions that are susceptible to 1, 3-Dinitrobenzene-mediated Toxicity

3.2.1 Introduction

Neuronal nitric oxide synthase (nNOS) is a modular enzyme consisting of a heme containing oxygenase domain (McMillan *et al.*, 1992; Stuehr and Ikeda-Saito, 1992; White and Marletta, 1992) and a flavin containing reductase domain (Bredt *et al.*, 1991) fused by a calmodulin binding sequence. nNOS catalyses the conversion of *L*-arginine to *L*-citrulline plus nitric oxide (NO•) (Furchgott and Vanhoutte, 1989; Ignarro *et al.*, 1987b; Moncada *et al.*, 1989). NOS has been shown to interact with small molecules that are redox-active such as the dinitrobenzenes (Miller, 2002) and quinones (Kumagai *et al.*, 1998). 1, 3-Dinitrobenzene (1, 3-DNB) is a putative CNS-toxicant in rats (Philbert *et al.*, 1987). Studies in rats have shown that 1, 3-DNB is metabolized in the liver by cytochrome P450 leading to hydroxylated metabolites and by NADPH-cytochrome P450 reductase (CYPOR) *via* reductive metabolism (Cossum and Rickert, 1985; Nystrom and Rickert, 1987). Furthermore, it is proposed that the metabolism of 1, 3-DNB to reactive intermediates is involved in mediating CNS toxicity. The interaction of 1, 3-DNB with nNOS generates superoxide anion radical ($O_2^{\bullet-}$) *via* similar reductive metabolism. Previously, our laboratory (Miller, 2002) provided evidence for the simultaneous production of $O_2^{\bullet-}$ and NO• leading to peroxynitrite ($ONOO^-$) formation (Huie and Padmaja, 1993). In rat and mouse brainstem and cortical astrocytes, 1, 3-DNB was shown to inhibit the complex II of mitochondria, a $O_2^{\bullet-}$ generating organelle, (Phelka *et al.*, 2003).

Evidence has been presented implicating the increased energy metabolism, altered cellular redox status, free radical formation and oxidative stress in the toxicity of 1, 3-DNB. In parallel to our studies on the formation of DNB metabolites and DNB-induced $ONOO^-$

production *via* interaction with nNOS, studies were initiated to investigate the possible changes in gene expression of the antioxidant enzymes, Cu/Zn superoxide dismutase (SOD1) and glutathione peroxidase (GSH-Px) in nNOS localized areas of brain (i.e cerebellum and brainstem (pons and medulla)) in response to 1, 3-DNB administration.

3.2.2 Experimental Procedures

Materials: 1, 3-DNB was purchased from Sigma-Aldrich. TRI reagent for RNA isolation was purchased from Molecular Research Center. Reverse transcription was performed using MMLV reverse transcriptase (BD Biosciences). For PCR, primers for SODI and GSH-Px sequences were purchased from Gibco. Taq polymerase was purchased from Promega.

Animals and 1, 3-DNB treatment: Male Sprague Dawley rats weighing between 275- 350 gms were used. Rats were injected with (10 mg/kg, i.p) 1, 3-DNB dissolved in corn oil (every 12hrs for 3 doses). Control received only corn oil vehicle. Brain samples from the 1, 3-DNB treated rats were collected at specified time points (0, 6, 12, 24 hrs) after the final dose. There were two rats under each time point. Brain samples from the controls were collected at 0 hr time point (after the final dose of corn-oil). The samples were snap-frozen in liquid nitrogen and stored at -80 ºC until used. The tissue samples consisted of the lower half of the cerebellum and the pons and the medulla.

Reverse Transcription-Polymerase Chain Reaction (RTPCR) assay: Individual samples of total RNA were extracted using TRI reagent under the guidance of Dr. Thomas Getchell at the University of Kentucky. The total RNA was estimated spectrophotometrically at 260 nm and the purity of the RNA was estimated by measuring the ratio of the absorbance of RNA / protein (A_{260}/A_{280}) > 1.8. The quality of RNA was confirmed by running 1% agarose gel electrophoresis which showed that the isolated RNA is highly pure.

Five µg of total RNA was reverse-transcribed using 1µl of 20 µM Oligo dT. RNA was transcribed into cDNA using the MMLV reverse transcriptase, included in BD biosciences kit (#K1402-1). The total volume was adjusted to 20 µl with diethylpyrocarbonate (DEPC)-treated

water. The reactions were carried out for 1 hr at 42 °C followed by a 5 min incubation at 94 °C. For the PCR reaction, 3.2 µl of the RT-reaction mixture was used. In addition to the RT-reaction mixture, the PCR reaction mixture (20 µl) contained 0.5 units of Taq polymerase, 0.2 mM dNTP mix, 1.5 mM $MgCl_2$, PCR buffer and 2.5 pmol of the oligonucleotide primers. The primers were designed based on the methodology of Agardh *et al.* (2002) (Agardh *et al.*, 2002) and are shown in Table 3.1.1. Denaturation, annealing and polymerase extension were performed for 45 seconds at 94 °C, 30 seconds at 62 °C, and 60 seconds at 72 °C for a total of 35 cycles. Controls were carried through each step of the RT and PCR. In RT, the reaction mix minus RNA was used as a control and in PCR, the controls consisted of reaction mix minus RNA as well as just water alone.

One-half of the PCR reaction product (10 µL) was separated on a 1% agarose gel containing ethidium bromide (EtBr), and the products were visualized on a UV light source. The gene expression was semi-quantified by measuring the densities of their bands using *quantity one* software.

Table 3.2.1. Oligonucleotide Sequences of 5' and 3' Primers of SOD1 and GSH-Px

Based on Agardh et al., 2002

5' Primers	3' Primers
CuZnSOD (exon1) 5'-CAGGATTAACTGAAGGCGAGCATG-3'	*5' CAATCACACCACAAGCCAAGCGGC-3'*
GSH-Px (exon 1-2) 5'-GTTCGGACATCAGGAGAATGGCAA-3'	*5'-GGTTGCTAGGCTGCTTGGACAGCA-3'*

3.2.3 Results and Discussion

Rats were exposed to 1, 3-DNB (10 mg/kg; 3 * 12 hrs) and the brains regions (cerebellum, pons and medulla) were obtained at different time points after the final dose (0 hrs, 6 hrs, 12 hrs and 24 hrs) as mentioned ***(experimental procedures)***. RNA was isolated from the brain regions and RTPCR was performed using primers for SOD1 and GSH-Px (Table 3.1.1). The PCR products were separated using a 1% agarose gel. The expression was semi-quantified by measuring the densities of the bands using *quantity one* software. For each gene, the ratio of the density of the gene expression of the treated groups and the control group were calculated and tabulated.

Six hours following 3 doses of 1, 3-DNB, GSH-Px gene expression levels exhibited only a minor increase in expression (8 %) at 6 hr point (Table 3.2.2). At 12 and 24 hrs, GSH-Px gene expression levels increased by 35 % (Fig. 3.2.1). These data indicate that the nNOS-rich regions in brain are suited for handling free radicals and the enzymes present may be involved in a protective mechanism to prevent toxicity of not only free radicals but also reactive intermediates like 1,3-DNB. This preliminary data shows that there is a specific difference in the regulation of the GSH-Px gene in response to 1, 3-DNB administration. On the other hand, SOD1 gene expression levels were increased (17 %) at the 6 hr time point compared to control (Table 3.2.3). At the 12 hrs time point, gene expression levels of SOD1 dropped back down to the control value and remained that way through the 24 hour time point (Fig. 3.2.2).

Table 3.2.2. Density ratios of GSH-Px expression *vs* control at various time points after 1, 3-DNB treatment.

Groups (time after exposure)	**1 (0 hrs)**	**2 (6 hrs)**	**3 (12 hrs)**	**4 (24 hrs)**
GSH-Px density ratio (treated/control)	1.01	1.1	1.36	1.35

Table 3.2.3. Density ratios of SOD1 expression *vs* control at various time points after 1, 3-DNB treatment.

Groups (time after exposure)	**1 (0 hrs)**	**2 (6 hrs)**	**3 (12 hrs)**	**4 (24 hrs)**
SOD1 density ratio (treated/control)	0.96	1.13	0.97	1.01

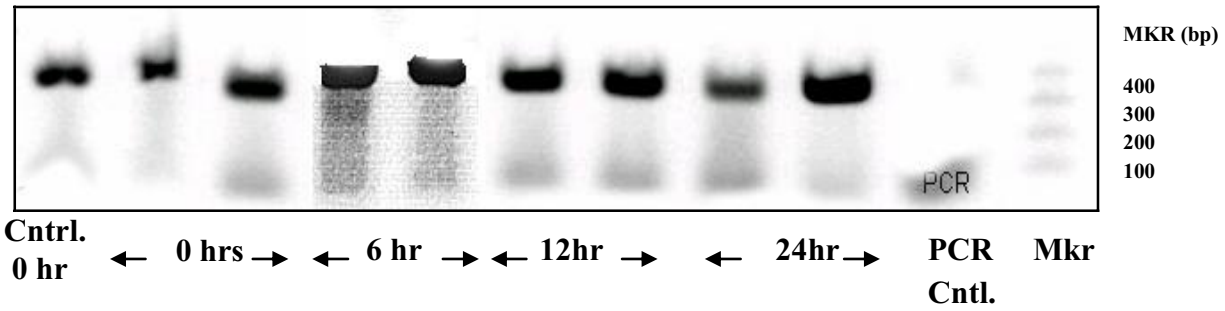

Fig. 3.2.1. GSH-Px gene expression levels after treatment of rats with 1, 3-DNB. Groups consists of two rats and the brains of each group of rats were collected at 0, 6, 12, 24 hrs after the treatment of 1, 3-DNB (10 mg/kg, every 12 hrs for 3 doses). RTPCR was performed and processed as described in ***Experimental Procedures***. Agarose gels (1%) were run to visualize gene expression levels of GSH-Px in response to 1, 3-DNB treatment. Brain sample from corn oil treated rat as well as a PCR control consisting of dH_2O were used as a control.

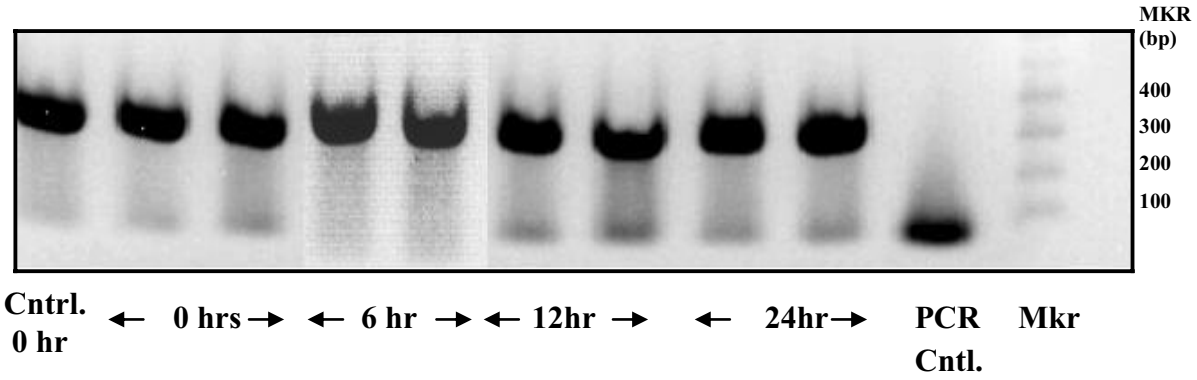

Fig. 3.2.2. SOD1 gene expression levels after treatment of rats with 1, 3-DNB (10 mg/kg) every 12 hrs for 3 doses. Groups consists of two rats and the brains of each group of rats were collected at 0, 6, 12, 24 hrs after the treatment of 1, 3-DNB (10 mg/kg, every 12 hrs for 3 doses).. RTPCR was performed and processed as described in ***Experimental Procedures***. Agarose gels (1%) were run to visualize gene expression levels of SOD1 in response to 1, 3-DNB treatment. Brain sample from corn oil treated rat as well as a PCR control consisting of dH_2O were used as a control.

In order to understand the changes in the levels of antioxidants, other enzymes that evolved to handle free radicals and reactive intermediates have to be investigated. Of course, those experiments would compare tissues from corn oil treated rats to that of the 1, 3-DNB-treated rats. As reports from other groups (Philbert *et al.*, 1987; Phelka *et al.*, 2003) suggested, mitochondrial damage and the resulting dysfunction of energy production due to 1, 3-DNB treatment is a real possibility. Studies on the gene expression changes of MT enzymes including, the mitochondrial antioxidant, manganese-superoxide dismutase, could provide further insight into 1, 3-DNB mediated neuro/glial toxicity.

3.2.4 Conclusion

These results indicate that GSH-Px gene expression was increased at both the 12 hr and 24 hr time points following the last of 3 doses of 1, 3-DNB. These data also point to a possible maximum level of GSH-Px gene expression at 12 hr. However, it is necessary to study the GSH-Px gene-expression levels in relation to various time points after 1, 3-DNB exposure, in order to fully understand the pattern of GSH-Px gene modulation. In addition, other antioxidant enzymes and various redox-active proteins should be examined in these brain regions in order to understand the mechanism of toxicity and the overall global effect of 1, 3-DNB administration in relation to neuro/glial toxicity.

3.2.5 Acknowledgements

I thank Dr. Tom Getchell and Ms. Radhika Vaishnav for their guidance on RNA isolation. Also, we thank Dr. Chotiros Daosukho for her guidance in performing RTPCR. Support for initial pilot studies was provided by the Kentucky Science and Engineering Foundation (grant # KSEF- 03-RDE-005). This report was made possible by grant # ES 011982 to R.T. Miller from the National Institute of Environmental Health Sciences (NIEHS)/NIH. This project was also supported in part by grant # 5G12RR008124 to the Border Biomedical Research Center (BBRC)/University of Texas at El Paso from the National Center for Research Resources (NCRR)/NIH.

3.2.6 References

Agardh, C. D., Israelsson, B., Thuesen-Olesen, B., Agardh, E., 2002. Application of quantitative competitive polymerase chain reaction for measurements of mRNA from antioxidative enzymes in the diabetic rat retina and kidney. Metabolism 51, 1279-1284.

Bredt, D. S., Hwang, P. M., Glatt, C. E., Lowenstein, C., Reed, R. R., Snyder, S. H., 1991. Cloned and expressed nitric oxide synthase structurally resembles cytochrome P-450 reductase. Nature 351, 714-718.

Cossum, P. A., Rickert, D. E., 1985. Metabolism of dinitrobenzenes by rat isolated hepatocytes. Drug Metab Dispos 13, 664-668.

Furchgott, R. F., Vanhoutte, P. M., 1989. Endothelium-derived relaxing and contracting factors. FASEB J 3, 2007-2018.

Huie, R. E., Padmaja, S., 1993. The reaction of no with superoxide. Free Radic Res Commun 18, 195-199.

Ignarro, L. J., Byrns, R. E., Buga, G. M., Wood, K. S., 1987. Endothelium-derived relaxing factor from pulmonary artery and vein possesses pharmacologic and chemical properties identical to those of nitric oxide radical. Circ Res 61, 866-879.

Kumagai, Y., Nakajima, H., Midorikawa, K., Homma-Takeda, S., Shimojo, N., 1998. Inhibition of nitric oxide formation by neuronal nitric oxide synthase by quinones: nitric oxide synthase as a quinone reductase. Chem Res Toxicol 11, 608-613.

McMillan, K., Bredt, D. S., Hirsch, D. J., Snyder, S. H., Clark, J. E., Masters, B. S., 1992. Cloned, expressed rat cerebellar nitric oxide synthase contains stoichiometric amounts of heme, which binds carbon monoxide. Proc Natl Acad Sci U S A 89, 11141-11145.

Miller, R. T., 2002. Dinitrobenzene-mediated production of peroxynitrite by neuronal nitric oxide synthase. Chem Res Toxicol 15, 927-934.

Moncada, S., Palmer, R. M., Higgs, E. A., 1989. The biological significance of nitric oxide formation from L-arginine. Biochem Soc Trans 17, 642-644.

Nystrom, D. D., Rickert, D. E., 1987. Metabolism and excretion of dinitrobenzenes by male Fischer-344 rats. Drug Metab Dispos 15, 821-825.

Phelka, A. D., Beck, M. J., Philbert, M. A., 2003. 1,3-Dinitrobenzene inhibits mitochondrial complex II in rat and mouse brainstem and cortical astrocytes. Neurotoxicology 24, 403-415.

Philbert, M. A., Gray, A. J., Connors, T. A., 1987. Preliminary investigations into the involvement of the intestinal microflora in CNS toxicity induced by 1,3-dinitrobenzene in male F-344 rats. Toxicol Lett 38, 307-314.

Stuehr, D. J., Ikeda-Saito, M., 1992. Spectral characterization of brain and macrophage nitric oxide synthases. Cytochrome P-450-like hemeproteins that contain a flavin semiquinone radical. J Biol Chem 267, 20547-20550.

White, K. A., Marletta, M. A., 1992. Nitric oxide synthase is a cytochrome P-450 type hemoprotein. Biochemistry 31, 6627-6631.

Chapter 4: An Easy and Efficient Method for Production and Purification of Polyclonal Anti-nitrotyrosine Antibodies from Chicken

4.1 Introduction

Tyrosine nitration is the process of addition of a nitro (NO_2) group to the carbon ortho to the hydroxyl group on the tyrosine ring (Scheme 4.1). If a tyrosine is a residue within a protein, covalent modification of the protein will occur. Covalent modification of tyrosine or other protein residues may be silent or may lead to loss of function of the protein. Although a topic of debate, the nitrating species most often implicated in protein nitration are peroxynitrite ($ONOO^-$), nitrous acid (HNO_2) and nitrogen dioxide ($NO_2\bullet$) radical (Ischiropoulos *et al.*, 1992).

In almost all instances, $ONOO^-$ is the main nitrating species (Koppenol *et al.*, 1992; Pryor and Squadrito, 1995) and is formed by the near-diffusion limited reaction between nitric oxide ($NO\bullet$) and superoxide anion radical ($O_2^{\bullet-}$) ($k = 6.7 \times 10^9\ M^{-1}\ s^{-1}$; (Huie and Padmaja, 1993). Subsequent reaction of $ONOO^-$ with CO_2 leads to the formation of an intermediate, peroxonitrocarbonate ($ONOOCO_2^-$) (Ischiropoulos *et al.*, 1992). $ONOOCO_2^-$ then decomposes to form a carbonate radical $CO_3\bullet^-$, an oxidating species that initially oxidizes the tyrosine to form a tyrosine radical, and $NO_2\bullet$, a nitrating species that nitrates the tyrosine radical to form the covalent modification product, 3-nitrotyrosine. Thus, $ONOOCO_2^-$ can nitrate tyrosine residues in proteins. $ONOO^-$ can also be protonated to form peroxynitrous acid (ONOOH) which yields $OH\bullet$, an oxidating species that can oxidize tyrosine to form a phenolic tyrosine radical. ONOOH has been shown to cause lipid peroxidation of low density lipoproteins in membranes (Darley-Usmar *et al.*, 1992; Haddad *et al.*, 1993; Radi *et al.*, 1991a; Van der Vliet *et al.*, 1994). In addition, formation of HNO_2 by the acidification of nitrite is thought to play a role in nitration of tyrosine residues in

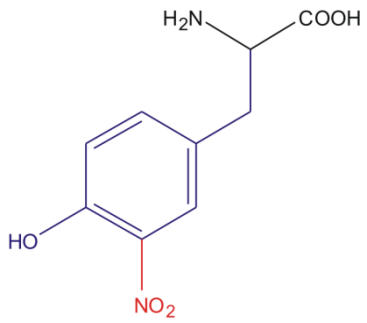

Scheme 4.1. Structure of 3-nitrotyrosine

certain tissues (Knowles *et al.*, 1974). Although this process requires a significant drop in pH (pH<6.0), nevertheless, HNO_2 can nitrate protein slowly. Oxidation of nitrite by peroxidases and hydrogen peroxide was also found to produce tyrosine nitration *in vivo* in mice (Brennan *et al.*, 2002; Gaut *et al.*, 2002b). Enzyme studies indicate that myeloperoxidase, eosinophil peroxidase as well as certain hemoproteins (myoglobin, cytochrome P450) may catalyze the oxidation of nitrite (Cohen *et al.*, 1964; Heppel and Porterfield, 1948) to nitrogen dioxides (Brennan *et al.*, 2002; van der Vliet *et al.*, 1997; Wu *et al.*, 1999). The resulting nitrogen dioxides are capable of nitrating tyrosine residues. These oxidizing pathways are also capable of oxidizing tyrosine to dityrosine. However, 3-nitrotyrosine formation is more often used as a stable biomarker for $ONOO^-$ production. *In vitro* and *in vivo* studies continue to be conducted, to sort-out and identify the various nitrating species as well as their specificity in nitrating tyrosine residues in proteins of only certain tissues; a phenomenon that occurs during the course of different disease conditions. Nevertheless, in support of a role for NOS in protein nitration, it has been established that NO• provides the source of nitrogen for the various nitrating species identified to date (Ischiropoulos, 1998). Interestingly, 3-nitrotyrosine can be accumulated slowly without an apparent need for $O_2^{\bullet-}$ or hydrogen peroxide (Turko and Murad, 2002). This indicates that a number of biological reactions and processes beginning with the formation of NO• may be responsible for nitration of tyrosine residues and can result in formation of 3-nitrotyrosine.

3-nitrotyrosine is a stable end-product with a pH-dependent absorbance between 350 nm and 450 nm and can be easily measured using a spectrophotometer. The absorbance maximum is dependent on pH as it shifts from 365 nm in acidic pH to 428 nm in pH greater than 8.0. 3-nitrotyrosine can be analyzed using various techniques such as gas chromatography (Ohshima *et al.*, 1990), mass spectrometry (Crowley *et al.*, 1998; Frost *et al.*, 2000; Gaut *et al.*, 2002a; Jiang

and Balazy, 1998; Yi *et al.*, 2000), high performance liquid chromatography combined with electrochemical detection as well as immunohistochemistry (Crow, 1999; Ishida *et al.*, 2002; Shigenaga, 1999; Shigenaga *et al.*, 1997).

Nitrated proteins have been detected in most organ systems under physiological conditions and also in a number of cellular models, but the majority of the studies have been focused on disease states (Greenacre and Ischiropoulos, 2001; Turko and Murad, 2002). Tyrosine nitration has been associated with oxidative stress including Alzheimer's disease (Hensley *et al.*, 1998; Smith *et al.*, 1997; Teunissen *et al.*, 2002; Tohgi *et al.*, 1999), Parkinson's disease (Ferrante *et al.*, 1999; Giasson *et al.*, 2000; Good *et al.*, 1998; Good *et al.*, 1996; Pennathur *et al.*, 1999) and Amylotropic Lateral Sclerosis(ALS) (Abe *et al.*, 1995). Nitration of tyrosine residues has been visualized using immunological techniques in atherosclerotic plaques of human coronary vessels (Beckmann *et al.*, 1994), in lungs of infants with acute lung injury, in tissues of patients with sepsis and during ARDS (Haddad *et al.*, 1994; Kooy *et al.*, 1995). Examination of nitrated tissue samples has revealed intriguing sub-cellular localization of nitrated proteins within asymmetric synapses in dendritic spines, synaptic vesicles in axon terminals, and astrocytic processes in the brain (Bolan *et al.*, 2000).

The commercial nitrotyrosine antibodies are extremely expensive for small quantities and not-so specific for use in immunochemistry, and excess effort have to be performed to identify the modified proteins (Ye *et al.*, 1996). Therefore, we developed a simpler method to obtain enormous amounts of pure, nitrotyrosine antibodies from chicken for laboratory use. The polyclonal nitrotyrosine antibodies were raised in chicken and purified using 3-nitrotyrosine immuno-affinity chromatography. The antibodies were validated using nitrated BSA and visualized at different dilutions by SDS-PAGE and Western blotting. In addition, a nitrated

protein ladder was developed for use as a tool for detecting nitration of the tyrosines in tissues containing complex cellular proteins.

4.2 Experimental Procedures

Chemicals and reagents*:* 3-Nitro-*L*-tyrosine, sodium chloride, bovine serum albumin, superoxide dismutase, catalase, cytochrome P450 reductase, β-galactosidase, Cytochrome-*c* were purchased from Sigma Chemical Company (St Louis, MO). Affi-Gel 15 was purchased from Bio-Rad (Hercules, CA). Ultrapure Tris Base was obtained from Research Products International (Mt. Prospect, IL). Centriprep-50 centrifugal concentrators were purchased from Millipore Corporation (Bedford, MA).

Treatment with antigen and Serum Collection*:* Five mg of KLH was nitrated on sequential additions using peroxynitrite (Beckman *et al.*, 1994) and sent to Alpha diagnostics International (San Antonio, TX). Two hundred µg of nitrated KLH was injected to chickens on day 1, 14, 28, 42 day and serum of each respective bleed was collected over a total time period of 77 days. Preimmune serum was collected on day 1 and bleeds I, bleed II and bleed III were collected on the 49^{th}, 63^{rd} and 77^{th} day respectively. Booster injections were given between bleeds on the 56^{th} and 70^{th} days. Thus, preimmune serum as well as the first, second and third bleeds were obtained.

Preparation of Peroxynitrite*:* Peroxynitrite was prepared as previously described (Beckman *et al.*, 1994).

Nitration of protein ladder or BSA*:* The protein ladder used for nitration contained 100 µg of bovine serum albumin (66 kDa), catalase, NADPH-cytochrome P450 reductase, β-galactosidase and cytochrome-*c* were weighed and dissolved together in 50 µl of 1M potassium phosphate buffer (made from monobasic and dibasic). For nitration of the BSA, 20 µg of BSA was dissolved in 50 µl of potassium phosphate buffer. $ONOO^-$ was used as the nitrating agent for

all nitration. The UV-VIS spectrum was collected between 200-800 nm. Two μM additions of $ONOO^-$ were added to the cuvette containing 400 μl protein mixture or BSA, and the absorbance resulting from nitration was measured at 360 nm. The pH of the solution was measured after every addition, using a thin strip of pH paper. Additions were stopped after adding 28 μM $ONOO^-$, when the pH of the sample in the cuvette turned slightly basic (pH ~8). Equimolar amounts of acid to that of the peroxynitrite added were included to bring the sample back to neutral pH. The nitrated protein mixture and the nitrated BSA were made into aliquots of smaller volumes and stored at -80ºC.

SDS-PAGE and Western Analyses*:* One to ten μg of nitrated BSA or nitrated protein ladder, were loaded in different lanes on a 10 % polyacrylamide gel, depending on the experiment. Non-nitrated BSA (1 μg) was used as a negative control. Initially, samples were placed into 2X loading buffer containing 125 mM Tris-HCl (pH 6.8), 2% SDS, 20% glycerol, 0.2% bromophenol blue and 0.05% β-mercaptoethanol. Samples were then boiled in a water-bath for 3 min. SDS-PAGE was performed using a Bio-Rad Mini Protean II gel apparatus at 100 V for 1.5 hrs. The separated proteins were then transferred from the gels onto nitrocellulose membranes (30 V) for 1 hr at 18 V using a Bio-Rad semi-dry electrophoretic transfer cell.

Nitrocellulose membranes containing the transferred proteins were then blocked with 5 % non-fat dry milk (carnation) in Tris-buffered saline (TBS; 0.3 M NaCl, 40 mM Tris-HCl; pH 7.6) containing 0.1% Tween 20 (TBST) for 1 hr. After washing with TBST for 30 min (3 x 10 min), the membranes were incubated overnight at 4ºC with the purified primary anti-3-nitrotyrosine antibodies of appropriate dilutions as needed for the experiment. The membranes were washed with TBST for 1 hr (4 x 15 min) and incubated with an alkaline phosphatase-conjugated secondary antibody raised in goat (1:15,000 dilution) for 1.5 hrs at 25 ºC.

Membranes were then washed with TBST for 1 hr (4 x 15 min) and the proteins were visualized using the BCIP/NBT substrate (Sigma).

4.3 Results

Pre-immune serum and the serum from bleeds I, II and III from chicken were obtained from Alpha Diagnostics by injecting the nitrated KLH as described in ***experimental procedures***. We developed an immunoaffinity purification method and optimized the conditions to obtain the anti-nitrotyrosine antibodies from chicken serum bleeds. The method, optimization and the validation are as follows:

Coupling of Nitrotyrosine with Agarose Gel Beads*:* Each ml of affi-gel-15, the activated immuno-affinity support consisting of agarose gel beads, contained 15 μmoles of active ester. An excess of 3-nitrotyrosine (20 mg/ ml of gel) was incubated with the affigel beads for 4 hrs. After incubation, the suspension was filtered using a Buchner funnel and Whatman papers and packed into a nickel- nitrilotriacetic acid (Ni-NTA) column of 2.5 - 3.0 cm diameter.

Immuno-Affinity Purification of Chicken Serum*:* The column, packed with 3-nitrotyrosine coupled agarose beads, was washed with 2 bed volumes of Tris buffer. Tris buffer (10 mM; pH 7.4) was used for serum dilution as well as for column washing during the process of immune-affinity purification, unless mentioned otherwise. The chicken serum from bleed I was diluted in Tris buffer (1: 1 v/v). Serum from bleeds II and III were diluted (1:2 v/v). The diluted serum was loaded by gradual pipetting along the walls into the column. The column flow-throughs of the serum from each bleed were collected and saved. After loading, the column was washed with 2 bed volumes of Tris buffer(10 mM; pH 7.4). One-half ml fractions were collected from the column washes and the decrease in the peak in every fraction was observed at 280 nm using a UV-VIS spectrophotometer. The absorbance at 280 nm gradually decreased in the later fractions and finally dropped to an insignificant value. Then, the column was washed with 1 bed volume of Tris buffer(10 mM; pH 7.4) containing 0.5% NaCl. One-half ml fractions were collected

during the wash step and monitored for a decrease in absorbance at 280 nm. Weak absorbance values at 280 nm were observed in the initial wash fractions and this value dropped down to an insignificant value with the later fractions. The column was next washed again with 1 bed volume of Tris. Yet again, the wash fractions were observed for the decrease in the peak at 280 nm. After washing, the bound antibody was eluted with 2-3 bed volumes of 100 mM glycine, pH 1.9. The 0.5 ml eluate-fractions were collected and those with the highest absorbance at 280 nm were pooled. The eluted antibody from each collected fraction was neutralized immediately with 1M Tris, pH 8.0, to prevent protein denaturation.

The pooled eluates were buffer-exchanged by centrifuging in centriprep-50 concentrators using a Beckmann Coultry centrifuge (JA 10) at 3,000 x g, 35 min x 5, every time disposing the filtered liquid and diluting the remaining sample in 1:1 v/v ratio with phosphate buffered saline (PBS) 1M, pH 7.4. The amount of protein (antibodies) present was estimated using the biorad protein assay. Sodium Azide (NaN_3; 0.2 %) was added to the antibodies and aliquots (0.5 µg/ µl) were made and frozen at 80 ºC. The column was stored in a solution of PBS buffer pH 7.4 containing 0.2% sodium azide, at -4 ºC.

Validation of the anti-nitrotyrosine antibodies using western blotting: Using SDS-PAGE and Western blotting, the selectivity and the specificity of the anti-nitrotyrosine antibodies were compared to that of the serum of respective bleeds.

A 10 % polyacrylamide gel was loaded with 1 µg of nitrated BSA in all the 4 lanes. After the SDS-PAGE and transfer, nitrocellulose membranes corresponding to each lane were cut into thin strips. Western blotting was performed wherein the 3 strips of the gel containing nitrated BSA were incubated with either, the pre immune serum or the serum of bleed II or bleed

III (0.5 µg/ul, 1:500 dilution for each). The three other strips from the gel were incubated with the purified anti-nitrotyrosine antibodies (0.5 µg/ul, 1:500 dilution). After washes, the strips were incubated with anti-chicken IgG secondary antibody (1: 15,000) and developed as described ***(experimental procedures).***

Results indicated that there is no specific band corresponding to the nitrated BSA using the serum bleeds (Fig. 4.1). There was a heavy smudge immediately after exposure to the BCIP-NBT substrate. In order to identify the best working dilution for identifying the nitrated tyrosines, a dot blot was performed as an initial step using bleed II antibodies (Fig. 4.2). 1µg of nitrated BSA was placed on all the 1 cm^2 nitrocellulose membranes and the membranes were incubated with the primary anti-3-nitrotyrosine antibodies (0.5 µg/µl; 1: 250; 1: 500; 1:1000). The negative controls loaded were the BSA and pre-immune serum, and were incubated with 1:500 anti-3-nitrotyrosine antibody. Then, after washing with TBS-T for 5 min x 3, the membranes were incubated with anti-chicken secondary IgG antibodies (1:15,000). The membranes were finally incubated with alkaline phosphatase conjugated BCIP/NBT substrate.

A sharp, purplish blue color spot was observed in membranes spotted with various antibody dilutions with different intensities. The negative control, BSA and the preimmune serum did not produce any purplish blue color spot indicating that the antibodies are specific to nitrated proteins. The membrane with the 1: 250 dilution appeared to show a darker spot, when compared to other dilutions. However, as the spots do not help extensively to determine the exact dilution, we decided to perform Western analyses using the bleed II and III anti-3-nitrotyrosine antibodies.

P.I B-1 B-2 B-3

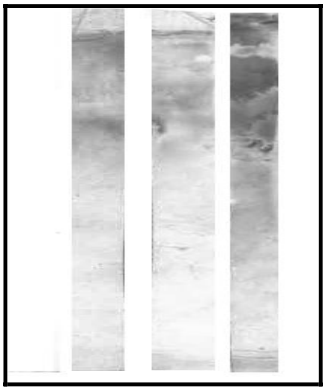

Fig. 4.1. Western blotting analyses of nitrated BSA using the serum bleeds. SDS-PAGE was performed wherein the lanes were loaded with nitrated BSA (1 μg) on a 10% polyacrylamide gel and the gel was transferred onto the nitrocellulose membrane ***(experimental procedures)***. The membrane was cut into strips and western blotting was performed by incubating either with pre-immune serum (P.I) or the anti-nitrotyrosine serum bleeds, bleed I (B-1), Bleed II (B-2), Bleed III (B-3) (0.5 μg/μl, 1:500 dilution). The membranes were then incubated with secondary anti-chicken IgG antibodies (1: 15,000) and developed with alkaline phosphatase-conjugated BCIP/NBT substrate.

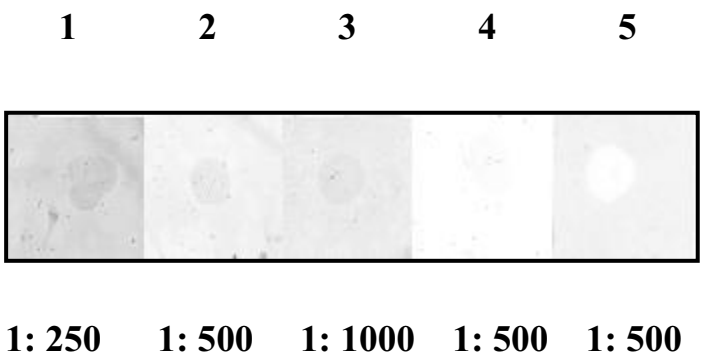

Fig. 4.2. Dot-blot analysis of the nitrated BSA incubated using anti-nitrotyrosine antibodies. *Lanes* 1-3 contained nitrated BSA spots and were incubated with anti-nitrotyrosine antibodies at various dilutions 1) 1: 250 2) 1: 500 3) 1: 1000. *Lane* 4 (spotted with pre-immune serum (1:500)) and *lane* 5 (spotted with BSA) were incubated with anti-nitrotyrosine antibody (1:500). The membranes were then incubated with secondary anti-chicken IgG antibodies (1: 15,000) and developed with alkaline phosphatase-conjugated BCIP/NBT substrate.

1 2 3 4

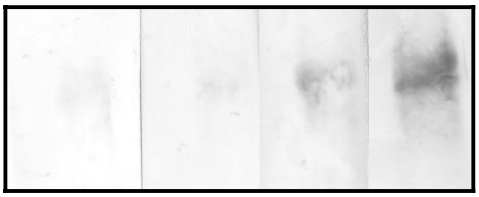

1: 2000 1:1000 1:500 1: 250

Fig. 4.3. Western blotting analyses of nitrated BSA using anti-nitrotyrosine antibodies. SDS-PAGE was performed wherein the lanes were loaded with nitrated BSA (1 μg) on a 10% polyacrylamide gel and the gel was transferred onto the nitrocellulose membrane ***(experimental procedures)***. The membrane was cut into strips and Western blotting was performed by incubating with different dilutions of the anti-nitrotyrosine antibodies (bleed III; 0.5 μg/μl). The dilutions used were 1) 1: 2000 2) 1: 1000 3) 1: 500 4) 1: 250. The membranes were incubated with secondary anti-chicken IgG antibodies (1: 15,000) and developed with alkaline phosphatase-conjugated BCIP/NBT substrate.

SDS-PAGE and Western blotting were performed with the anti-3-nitrotyrosine antibody (bleed III) using different dilutions (Fig. 4.3). Each lane contained 1μg nitrated BSA and the nitrocellulose membrane blot strips were incubated with different dilutions of bleed III anti-nitrotyrosine antibody (0.5 μg/μl; 1:125; 1:250; 1:500; 1:1000; 1:2000).

Results indicate that the band intensity decreases with increases in dilution of the antibodies. However, a band was observed even with 1:2000 dilution and the band was very intense at a 1: 250 dilution.

Validation of nitrated protein ladder: 5.5, 11 and 16.5 μg of the nitrated protein mixture (containing catalase, β-galactosidase, BSA, SOD and cytochrome c), prepared as mentioned in ***experimental procedures***, were loaded on a 10% gel and SDS-PAGE was performed as described. 24 μg of the non-nitrated BSA was loaded on the last lane. After, electrophoresis and transfer, western blotting was performed wherein the membrane was incubated with our anti-nitrotyrosine antibodies (1:500), subsequently with anti-chicken alkaline phosphatase conjugated IgG antibodies (1:25,000) and developed as described in ***experimental procedures***. Results in Fig. 4.4 clearly indicate the nitrated tyrosine bands of catalase (*band* 1), β-galactosidase (*band* 2), BSA (*band* 3), SOD (*band* 4) and cytochrome c (*band* 5) in all the three lanes containing nitrated protein mixture. On the other hand, the non-nitrated BSA did not show any band indicating that the antibody is highly selective to nitration of the tyrosine.

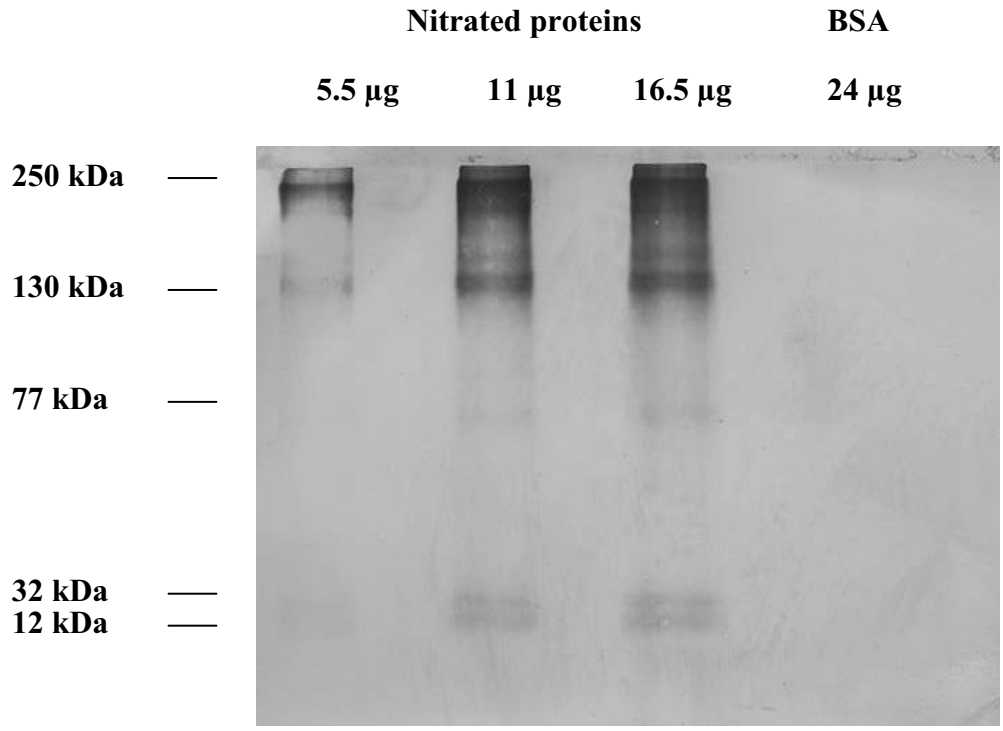

Fig. 4.4. Western blotting analyses of the nitrated protein ladder. 5.5, 11 and 16.5 µg of the nitrated protein mixture (containing catalase, β-galactosidase, BSA, SOD and cytochrome c) were loaded on a 10% polyacrylamide gel and SDS-PAGE was performed and the gel was transferred onto the nitrocellulose membrane ***(experimental procedures)***. Western blotting was performed by incubating with the anti-nitrotyrosine antibody (1:500). The membranes were incubated with secondary anti-chicken IgG antibodies (1: 25,000) and developed with alkaline phosphatase-conjugated BCIP/NBT substrate.

4.4 Discussion

In this manuscript, we describe an easy procedure to obtain and purify 3-nitrotyrosine antibodies from chicken. The conditions for immuno-affinity purification of the serum of bleeds were optimized by repeated trial and error. Initially, MOPS (100 mM; pH 7.4) was the buffer of choice. 100 mM MOPS plus 1 M NaCl was used to wash the column, the fractions were collected and monitored. Under these conditions, the antibodies were washed off the column and resulted in almost no recovery of the antibody during elution. Therefore, the concentration of the NaCl was reduced to 500 mM and 250 mM, and tested again. When 250 mM NaCl was used for washing, it did not strip the proteins off the column. Furthermore, when MOPS was replaced with Tris (10 mM), the non-specifically bound proteins were effectively washed free and there was a better elution of antibody. We also found that an additional wash with Tris alone (10 mM; pH 7.4), after washing the column with Tris (10 mM; pH 7.4) plus NaCl (0.5%) , helped in removing the unbound antibodies before elution. Contrary to what was originally believed, tyrosine nitration is now being recognized as a selective process that modifies only specific proteins *in vivo*. The factors that may contribute to the selectivity are: 1. proximity of those proteins to the site of generation of the nitrating agents, 2. availability and abundance of proteins that contain a large number of tyrosine residues and, 3. presence of proteins that contain tyrosine residues in a specific environment that promotes nitration (Zhang *et al.*, 2003).

Protein nitration has widely been utilized as a densitometric biological marker to monitor disease onset, progression and outcome. Many specific proteins such as Mn-superoxide dismutase (MnSOD) in rejected human kidney allographs (MacMillan-Crow *et al.*, 1996), low density lipoprotein in human atherosclerotic lesions (Leeuwenburgh *et al.*, 1997), prostacyclin synthase in bovine atherosclerotic lesions (Zou *et al.*, 1999), SERCA2a in aged rat skeletal

muscle (Viner *et al.*, 1999), succinyl coA:3-oxoacid CoA transferase in a rat model of diabetes after endotoxin challenges (Marcondes *et al.*, 2001; Turko *et al.*, 2001), mitochondrial proteins in liver and lung of rat tissue after endotoxin challenge (Aulak *et al.*, 2001), actin in kidney and hepatic tissue of mice with sickle cell disease (Aslan *et al.*, 2003), tyrosine hydroxylase (Ara *et al.*, 1998) and α-synuclein (Przedborski *et al.*, 2001) in the 1-methyl-4-phenyl-1, 2, 3, 6-tetrahydropyridine (MPTP) model of Parkinson's disease (Giasson *et al.*, 2000) are modified. In addition, several plasma proteins are modified by nitration in patients with acute lung injury and lung cancer (Gole *et al.*, 2000; Pignatelli *et al.*, 2001).

We used chicken to obtain anti-3-nitrotyrosine antibodies for many reasons. The major reasons for using chicken antibodies are: Chickens produce rich antibodies and there is less cross reactivity of the antibodies, when other animals give poor or no response. Also, the concentration of the antibodies in the egg yolk and that in the chicken sera are comparable, thus providing two good sources of antibody from the same animal. Other reasons for using chickens to raise antibodies are that chicken antibodies do not bind with mammalian rheumatoid factors or Fc-receptors or with proteins A or G. Therefore, the chicken antibodies are less likely to produce false positive reactions in certain immunochemical assays. Above all, chickens lay eggs regularly, providing a continual source of antibody without having to employ invasive techniques for antibody collection. Conversely, since chicken antibodies don't bind proteins A or G like most other species' antibodies, one needs to be creative in planning a purification scheme.

Furthermore, our innovation is that, we have come up with the concept of preparing nitrated protein marker ladders in our laboratory. So far, there have been no literature reports regarding the use of nitrated protein marker ladders. This ladder will be of immense value in

identifying nitrated proteins in tissue samples which contain innumerable proteins. This information will help other laboratories prepare an inexpensive nitrated protein ladder.

4.5 Conclusion

Although there are many other techniques to quantify nitrated tyrosines, we have detailed a relatively inexpensive approach to identify nitrated tyrosines in biological samples. Though anti-nitrotyrosine antibodies are available commercially, they are extremely expensive. The anti-nitrotyrosine antibodies produced and purified in our lab were found to be selective, specific and could be used at very low dilutions. We hope this article will be of immense use for laboratories which would want to use anti-nitrotyrosine antibodies frequently due to the fact that they are both less expensive, and more specific compared to what is on the market. Hopefully we can help others bypass pitfalls we previously encountered.

4.6 Acknowledgements

We thank Josh Tobias for assistance with the purification technique. Support for initial pilot studies was provided by the Kentucky Science and Engineering Foundation (grant # KSEF-03-RDE-005). This report was made possible by grant # ES 011982 to R.T. Miller from the National Institute of Environmental Health Sciences (NIEHS)/NIH. This project was also supported in part by grant # 5G12RR008124 to the Border Biomedical Research Center (BBRC)/University of Texas at El Paso from the National Center for Research Resources (NCRR)/NIH.

4.7 References

Abe, K., Pan, L. H., Watanabe, M., Kato, T., Itoyama, Y., 1995. Induction of nitrotyrosine-like immunoreactivity in the lower motor neuron of amyotrophic lateral sclerosis. Neurosci Lett 199, 152-154.

Ara, J., Przedborski, S., Naini, A. B., Jackson-Lewis, V., Trifiletti, R. R., Horwitz, J., Ischiropoulos, H., 1998. Inactivation of tyrosine hydroxylase by nitration following exposure to peroxynitrite and 1-methyl-4-phenyl-1,2,3,6-tetrahydropyridine (MPTP). Proc Natl Acad Sci U S A 95, 7659-7663.

Aslan, M., Ryan, T. M., Townes, T. M., Coward, L., Kirk, M. C., Barnes, S., Alexander, C. B., Rosenfeld, S. S., Freeman, B. A., 2003. Nitric oxide-dependent generation of reactive species in sickle cell disease. Actin tyrosine induces defective cytoskeletal polymerization. J Biol Chem 278, 4194-4204.

Aulak, K. S., Miyagi, M., Yan, L., West, K. A., Massillon, D., Crabb, J. W., Stuehr, D. J., 2001. Proteomic method identifies proteins nitrated in vivo during inflammatory challenge. Proc Natl Acad Sci U S A 98, 12056-12061.

Beckman, J. S., Chen, J., Ischiropoulos, H., Crow, J. P., 1994. Oxidative chemistry of peroxynitrite. Methods in enzymology 233, 229-240.

Beckmann, J. S., Ye, Y. Z., Anderson, P. G., Chen, J., Accavitti, M. A., Tarpey, M. M., White, C. R., 1994. Extensive nitration of protein tyrosines in human atherosclerosis detected by immunohistochemistry. Biol Chem Hoppe Seyler 375, 81-88.

Bolan, E. A., Gracy, K. N., Chan, J., Trifiletti, R. R., Pickel, V. M., 2000. Ultrastructural localization of nitrotyrosine within the caudate-putamen nucleus and the globus pallidus of normal rat brain. J Neurosci 20, 4798-4808.

Brennan, M. L., Wu, W., Fu, X., Shen, Z., Song, W., Frost, H., Vadseth, C., Narine, L., Lenkiewicz, E., Borchers, M. T., Lusis, A. J., Lee, J. J., Lee, N. A., Abu-Soud, H. M., Ischiropoulos, H., Hazen, S. L., 2002. A tale of two controversies: defining both the role of peroxidases in nitrotyrosine formation in vivo using eosinophil peroxidase and myeloperoxidase-deficient mice, and the nature of peroxidase-generated reactive nitrogen species. J Biol Chem 277, 17415-17427.

Cohen, G., Martinez, M., Hochstein, P., 1964. Generation of Hydrogen Peroxide during the Reaction of Nitrate with Oxyhemoglobin. Biochemistry 3, 901-903.

Crow, J. P., 1999. Measurement and significance of free and protein-bound 3-nitrotyrosine, 3-chlorotyrosine, and free 3-nitro-4-hydroxyphenylacetic acid in biologic samples: a high-performance liquid chromatography method using electrochemical detection. Methods Enzymol 301, 151-160.

Crowley, J. R., Yarasheski, K., Leeuwenburgh, C., Turk, J., Heinecke, J. W., 1998. Isotope dilution mass spectrometric quantification of 3-nitrotyrosine in proteins and tissues is facilitated by reduction to 3-aminotyrosine. Anal Biochem 259, 127-135.

Darley-Usmar, V. M., Hogg, N., O'Leary, V. J., Wilson, M. T., Moncada, S., 1992. The simultaneous generation of superoxide and nitric oxide can initiate lipid peroxidation in human low density lipoprotein. Free Radic Res Commun 17, 9-20.

Ferrante, R. J., Hantraye, P., Brouillet, E., Beal, M. F., 1999. Increased nitrotyrosine immunoreactivity in substantia nigra neurons in MPTP treated baboons is blocked by inhibition of neuronal nitric oxide synthase. Brain Res 823, 177-182.

Frost, M. T., Halliwell, B., Moore, K. P., 2000. Analysis of free and protein-bound nitrotyrosine in human plasma by a gas chromatography/mass spectrometry method that avoids nitration artifacts. Biochem J 345 Pt 3, 453-458.

Gaut, J. P., Byun, J., Tran, H. D., Heinecke, J. W., 2002a. Artifact-free quantification of free 3-chlorotyrosine, 3-bromotyrosine, and 3-nitrotyrosine in human plasma by electron capture-negative chemical ionization gas chromatography mass spectrometry and liquid chromatography-electrospray ionization tandem mass spectrometry. Anal Biochem 300, 252-259.

Gaut, J. P., Byun, J., Tran, H. D., Lauber, W. M., Carroll, J. A., Hotchkiss, R. S., Belaaouaj, A., Heinecke, J. W., 2002b. Myeloperoxidase produces nitrating oxidants in vivo. J Clin Invest 109, 1311-1319.

Giasson, B. I., Duda, J. E., Murray, I. V., Chen, Q., Souza, J. M., Hurtig, H. I., Ischiropoulos, H., Trojanowski, J. Q., Lee, V. M., 2000. Oxidative damage linked to neurodegeneration by selective alpha-synuclein nitration in synucleinopathy lesions. Science (New York, N.Y 290, 985-989.

Gole, M. D., Souza, J. M., Choi, I., Hertkorn, C., Malcolm, S., Foust, R. F., 3rd, Finkel, B., Lanken, P. N., Ischiropoulos, H., 2000. Plasma proteins modified by tyrosine nitration in acute respiratory distress syndrome. Am J Physiol Lung Cell Mol Physiol 278, L961-967.

Good, P. F., Hsu, A., Werner, P., Perl, D. P., Olanow, C. W., 1998. Protein nitration in Parkinson's disease. J Neuropathol Exp Neurol 57, 338-342.

Good, P. F., Werner, P., Hsu, A., Olanow, C. W., Perl, D. P., 1996. Evidence of neuronal oxidative damage in Alzheimer's disease. Am J Pathol 149, 21-28.

Greenacre, S. A., Ischiropoulos, H., 2001. Tyrosine nitration: localisation, quantification, consequences for protein function and signal transduction. Free Radic Res 34, 541-581.

Haddad, I. Y., Ischiropoulos, H., Holm, B. A., Beckman, J. S., Baker, J. R., Matalon, S., 1993. Mechanisms of peroxynitrite-induced injury to pulmonary surfactants. Am J Physiol 265, L555-564.

Haddad, I. Y., Pataki, G., Hu, P., Galliani, C., Beckman, J. S., Matalon, S., 1994. Quantitation of nitrotyrosine levels in lung sections of patients and animals with acute lung injury. J Clin Invest 94, 2407-2413.

Hensley, K., Maidt, M. L., Yu, Z., Sang, H., Markesbery, W. R., Floyd, R. A., 1998. Electrochemical analysis of protein nitrotyrosine and dityrosine in the Alzheimer brain indicates region-specific accumulation. J Neurosci 18, 8126-8132.

Heppel, L. A., Porterfield, V. T., 1948. Enzymatic dehalogenation of certain brominated and chlorinated compounds. J Biol Chem 176, 763-769.

Huie, R. E., Padmaja, S., 1993. The reaction of no with superoxide. Free Radic Res Commun 18, 195-199.

Ischiropoulos, H., 1998. Biological tyrosine nitration: a pathophysiological function of nitric oxide and reactive oxygen species. Arch Biochem Biophys 356, 1-11.

Ischiropoulos, H., Zhu, L., Chen, J., Tsai, M., Martin, J. C., Smith, C. D., Beckman, J. S., 1992. Peroxynitrite-mediated tyrosine nitration catalyzed by superoxide dismutase. Arch Biochem Biophys 298, 431-437.

Ishida, N., Hasegawa, T., Mukai, K., Watanabe, M., Nishino, H., 2002. Determination of nitrotyrosine by HPLC-ECD and its application. J Vet Med Sci 64, 401-404.

Jiang, H., Balazy, M., 1998. Detection of 3-nitrotyrosine in human platelets exposed to peroxynitrite by a new gas chromatography/mass spectrometry assay. Nitric Oxide 2, 350-359.

Knowles, M. E., McWeeny, D. J., Couchman, L., Thorogood, M., 1974. Interaction of nitrite with proteins at gastric pH. Nature 247, 288-289.

Kooy, N. W., Royall, J. A., Ye, Y. Z., Kelly, D. R., Beckman, J. S., 1995. Evidence for in vivo peroxynitrite production in human acute lung injury. Am J Respir Crit Care Med 151, 1250-1254.

Koppenol, W. H., Moreno, J. J., Pryor, W. A., Ischiropoulos, H., Beckman, J. S., 1992. Peroxynitrite, a cloaked oxidant formed by nitric oxide and superoxide. Chem Res Toxicol 5, 834-842.

Leeuwenburgh, C., Hardy, M. M., Hazen, S. L., Wagner, P., Oh-ishi, S., Steinbrecher, U. P., Heinecke, J. W., 1997. Reactive nitrogen intermediates promote low density lipoprotein oxidation in human atherosclerotic intima. J Biol Chem 272, 1433-1436.

MacMillan-Crow, L. A., Crow, J. P., Kerby, J. D., Beckman, J. S., Thompson, J. A., 1996. Nitration and inactivation of manganese superoxide dismutase in chronic rejection of human renal allografts. Proc Natl Acad Sci U S A 93, 11853-11858.

Marcondes, S., Turko, I. V., Murad, F., 2001. Nitration of succinyl-CoA:3-oxoacid CoA-transferase in rats after endotoxin administration. Proc Natl Acad Sci U S A 98, 7146-7151.

Ohshima, H., Friesen, M., Brouet, I., Bartsch, H., 1990. Nitrotyrosine as a new marker for endogenous nitrosation and nitration of proteins. Food Chem Toxicol 28, 647-652.

Pennathur, S., Jackson-Lewis, V., Przedborski, S., Heinecke, J. W., 1999. Mass spectrometric quantification of 3-nitrotyrosine, ortho-tyrosine, and o,o'-dityrosine in brain tissue of 1-methyl-4-

phenyl-1,2,3, 6-tetrahydropyridine-treated mice, a model of oxidative stress in Parkinson's disease. J Biol Chem 274, 34621-34628.

Pignatelli, B., Li, C. Q., Boffetta, P., Chen, Q., Ahrens, W., Nyberg, F., Mukeria, A., Bruske-Hohlfeld, I., Fortes, C., Constantinescu, V., Ischiropoulos, H., Ohshima, H., 2001. Nitrated and oxidized plasma proteins in smokers and lung cancer patients. Cancer research 61, 778-784.

Pryor, W. A., Squadrito, G. L., 1995. The chemistry of peroxynitrite: a product from the reaction of nitric oxide with superoxide. Am J Physiol 268, L699-722.

Przedborski, S., Chen, Q., Vila, M., Giasson, B. I., Djaldatti, R., Vukosavic, S., Souza, J. M., Jackson-Lewis, V., Lee, V. M., Ischiropoulos, H., 2001. Oxidative post-translational modifications of alpha-synuclein in the 1-methyl-4-phenyl-1,2,3,6-tetrahydropyridine (MPTP) mouse model of Parkinson's disease. Journal of neurochemistry 76, 637-640.

Radi, R., Beckman, J. S., Bush, K. M., Freeman, B. A., 1991. Peroxynitrite-induced membrane lipid peroxidation: the cytotoxic potential of superoxide and nitric oxide. Arch Biochem Biophys 288, 481-487.

Shigenaga, M. K., 1999. Quantitation of protein-bound 3-nitrotyrosine by high-performance liquid chromatography with electrochemical detection. Methods Enzymol 301, 27-40.

Shigenaga, M. K., Lee, H. H., Blount, B. C., Christen, S., Shigeno, E. T., Yip, H., Ames, B. N., 1997. Inflammation and NO(X)-induced nitration: assay for 3-nitrotyrosine by HPLC with electrochemical detection. Proc Natl Acad Sci U S A 94, 3211-3216.

Smith, M. A., Richey Harris, P. L., Sayre, L. M., Beckman, J. S., Perry, G., 1997. Widespread peroxynitrite-mediated damage in Alzheimer's disease. J Neurosci 17, 2653-2657.

Teunissen, C. E., de Vente, J., Steinbusch, H. W., De Bruijn, C., 2002. Biochemical markers related to Alzheimer's dementia in serum and cerebrospinal fluid. Neurobiol Aging 23, 485-508.

Tohgi, H., Abe, T., Yamazaki, K., Murata, T., Ishizaki, E., Isobe, C., 1999. Alterations of 3-nitrotyrosine concentration in the cerebrospinal fluid during aging and in patients with Alzheimer's disease. Neurosci Lett 269, 52-54.

Turko, I. V., Marcondes, S., Murad, F., 2001. Diabetes-associated nitration of tyrosine and inactivation of succinyl-CoA:3-oxoacid CoA-transferase. American journal of physiology 281, H2289-2294.

Turko, I. V., Murad, F., 2002. Protein nitration in cardiovascular diseases. Pharmacol Rev 54, 619-634.

van der Vliet, A., Eiserich, J. P., Halliwell, B., Cross, C. E., 1997. Formation of reactive nitrogen species during peroxidase-catalyzed oxidation of nitrite. A potential additional mechanism of nitric oxide-dependent toxicity. J Biol Chem 272, 7617-7625.

Van der Vliet, A., Smith, D., O'Neill, C. A., Kaur, H., Darley-Usmar, V., Cross, C. E., Halliwell, B., 1994. Interactions of peroxynitrite with human plasma and its constituents: oxidative damage and antioxidant depletion. Biochem J 303 (Pt 1), 295-301.

Viner, R. I., Ferrington, D. A., Williams, T. D., Bigelow, D. J., Schoneich, C., 1999. Protein modification during biological aging: selective tyrosine nitration of the SERCA2a isoform of the sarcoplasmic reticulum Ca^{2+}-ATPase in skeletal muscle. Biochem J 340 (Pt 3), 657-669.

Wu, W., Chen, Y., Hazen, S. L., 1999. Eosinophil peroxidase nitrates protein tyrosyl residues. Implications for oxidative damage by nitrating intermediates in eosinophilic inflammatory disorders. J Biol Chem 274, 25933-25944.

Ye, Y. Z., Strong, M., Huang, Z. Q., Beckman, J. S., 1996. Antibodies that recognize nitrotyrosine. Methods in enzymology 269, 201-209.

Yi, D., Ingelse, B. A., Duncan, M. W., Smythe, G. A., 2000. Quantification of 3-nitrotyrosine in biological tissues and fluids: generating valid results by eliminating artifactual formation. J Am Soc Mass Spectrom 11, 578-586.

Zhang, H., Bhargava, K., Keszler, A., Feix, J., Hogg, N., Joseph, J., Kalyanaraman, B., 2003. Transmembrane nitration of hydrophobic tyrosyl peptides. Localization, characterization, mechanism of nitration, and biological implications. J Biol Chem 278, 8969-8978.

Zou, M. H., Leist, M., Ullrich, V., 1999. Selective nitration of prostacyclin synthase and defective vasorelaxation in atherosclerotic bovine coronary arteries. The American journal of pathology 154, 1359-1365.

Discussion

Redox-cycling agents such as quinones and nitroarenes can get reduced by the nNOS reductase domain (Abu-Soud *et al.*, 1994; Klatt *et al.*, 1992; Kumagai *et al.*, 1998; Sheta *et al.*, 1994; Workman, 1992). The one-electron reduced nitroarene or quinone reoxidizes, regenerating the starting material donating the spare electron to O_2, thereby reducing O_2 to form the superoxide anion radical ($O_2^{\bullet-}$). This reduction-oxidation cycle is termed as redox-cycling. Previous studies indicate that the redox-cycling agents such as nitroarenes and quinones can change the products of the nNOS reaction from NO• and *L*-citrulline to peroxynitrite ($ONOO^-$) and *L*-citrulline (Miller, 2002). Generation of reactive nitrogen species (RNS) such as $ONOO^-$ and the release of the end-product inhibition (expected on NOS by NO•), by redox-cyclers may result in cellular toxicity and even cell death (Miller, 2002).

Earlier studies reported that the aqueous extracts of cigarette tar contained a quinone-semiquinone-hydroquinone cycling system. The auto-oxidizable compounds present in this redox-cycling system of cigarette tar (Schmeltz *et al.*, 1977) was suggested to act as a source for the production of ROS, such as $O_2^{\bullet-}$, *via* NAD(P)H-dependent mechanisms (Winston *et al.*, 1993). Studies utilizing tobacco leaves as a targeted library for identifying possible treatments for Parkinson's disease have uncovered an inhibitor (2,3,6-trimethyl-1,4-naphthoquinone (TMN) of the flavoenzyme, monoamine oxidase-A (Khalil *et al.*, 2000). We performed studies using various varieties of tobacco to identify if there were any constituent(s) that could interact with the flavoenzyme, nNOS. Results from [^{14}C]-*L*-arginine to [^{14}C]-*L*-citrulline conversion assays that incorporated extracts from different varieties of tobacco indicate that there are nNOS inhibitory constituent(s) in tobacco (Figs. 1.1, 1.2, 1.3; Chapter 1). The nNOS inactivator(s)

were found to be non-polar, lipophilic and non-volatile in nature. However, the exact number and nature of the tobacco constituent(s) responsible for inactivating nNOS remain unknown. Tobacco extracts can vary widely in their chemical composition, depending on the variety of tobacco. Variation in content of the major tobacco constituents was evident from comparing HPLC profiles of the various inhibitory hexane extracts. In addition, we showed that there are both activators as well as inactivators of nNOS present in non-burned tobacco. Results from experiments with pooled hexane sub-fractions of TI-1565 tobacco extracts provided support for the contention that more than one bioactive compound was present in certain extracts, as nNOS inhibition was produced by multiple fractions of HPLC eluate which spanned a time period of several mins (Fig. 1.5, chapter 1). We speculate that there are countless other compounds possessing activity towards nNOS which remain to be identified. Future studies will attempt to identify the exact chemical nature of the compound(s) contained within the hexane extracts of TI-1565 responsible for producing nNOS inhibition. Furthermore, studies into the mechanism of action of these tobacco constituents will be required in order to ascertain the isoform-selectivity (if any) of nNOS inhibition. Our studies in which the tobacco-derived redox-active compounds such as TMN or menadione were individually incorporated into the [^{14}C]-*L*-arginine to [^{14}C]-*L*-citrulline conversion assay indicated that single compounds can produce either stimulation or inhibition of *L*-citrulline production by nNOS with the particular effect being dependent on the concentration of the compound used as well as the compound's electrochemical characteristics.

Generally, quinones are modulatory of nNOS activity. Production of NO$^{\bullet}$ and $O_2^{\bullet-}$ is possible with certain quinones and nitroarenes, wherein the electron flux is sufficient enough through NOS to accommodate electron transfer to some exogenous electron acceptor yet

maintain sufficient electron flux to the heme in the nNOS oxygenase domain to maintain *L*-citrulline and NO• production (Miller *et al.*, 1997; Nishimura *et al.*, 1999).

$ONOO^-$, produced by the combination of NO• with $O_2^{\bullet-}$ at an almost diffusion-limited reaction rate ($6.7 \times 109\ M^{-1}\ s^{-1}$) (Huie and Padmaja, 1993), can nitrate or oxidize mitochondrial proteins. Mitochondria are highly compartmentalized, membranous organelles which contain abundant amounts of reactive hemoproteins, iron-sulfur proteins and thiols (Cadenas *et al.*, 2000; Radi *et al.*, 2002), to which NO• may bind reversibly (Moncada, 2000; Thomas *et al.*, 2003) or irreversibly (Ebel *et al.*, 1975; Nathan, 1992; Stuehr and Griffith, 1992). Mitochondria also generate copious amounts of $O_2^{\bullet-}$ during the process of cellular respiration (Boveris and Cadenas, 1975; Dionisi *et al.*, 1975). Both nitration and oxidation reactions mediated by $ONOO^-$ may inactivate mitochondrial matrix enzymes such as aconitase (Kennedy *et al.*, 1997), manganese superoxide dismutase (MacMillan-Crow *et al.*, 1998) and succinyl-CoA:3-oxoacid CoA-transferase (Turko *et al.*, 2001). Also, inhibition of mitochondrial respiration results in production of increased amounts of ROS and RNS (Dedkova *et al.*, 2004), both of which may act as cytotoxicants promoting cell death by cellular necrosis and/or apoptotis (Brookes *et al.*, 2002; Moncada and Erusalimsky, 2002; Sarti *et al.*, 2003).

The existence of NOS within mitochondria has been questioned for over a decade. However, we were unable to repeat or reproduce the studies claiming NOS in mitochondria. This situation may be due to: 1) differences in the purity of the mitochondria preparations used among groups, 2) failure to confirm results with complementary or redundant techniques, 3) failure to use appropriate controls, as well as 4) poor reliability and reproducibility of certain techniques as suggested by Brookes (Brookes, 2004). Isolation of the purest mitochondria

possible is imperative to determine with any certainty whether there is a NOS isoform within mitochondria. Although the Lacza group initially identified eNOS in mitochondria (Lacza *et al.*, 2004; Lacza *et al.*, 2003), subsequent studies conducted with brain, heart and liver mitochondria from mice, rats and pigs under stringent conditions did not support their original observations (Lacza *et al.*, 2001). Therefore, we performed experiments under stringently controlled conditions to isolate, purify and analyze mitochondria with appropriate controls and markers. This was accompanied by using a variety of complementary independent techniques. Results obtained, using LTQ-MS analyses complemented by other techniques, such as the [^{14}C]-*L*-arginine to [^{14}C]-*L*-citrulline conversion assay as well as immunochemical analyses, collectively, as well as individually, refute the claim that any NOS isoform resides within rat liver mitochondria (chapter 2). However, studies conducted during the past decade have suggested that NO• can diffuse into mitochondria and cause mitochondrial dysfunction by reversibly inhibiting certain enzyme. For example, cytochrome-*c* oxidase (Brown *et al.*, 1995; Cleeter *et al.*, 1994; Moncada, 2000) and NADH dehydrogenase (Radi *et al.*, 1994). Although NO• has a limited lifetime (4-5s) that is concentration-dependent, NO• is a gas and a diffusible radical (Thomas *et al.*, 2001). Thus, there is no absolute requirement for NO• to be produced at the exact site of action (Brookes, 2004). Therefore, there is no requirement for NO• to be produced within mitochondria for it to exert its action on mitochondrial enzymes.

Nevertheless, mitochondria are thought to be involved in the toxicity of redox-active compounds. For example, paraquat, a fast acting, synthetic herbicide that is used in over 120 countries in the world is a well-known redox-cycling agent. In addition to the lung damage reported due to paraquat accumulation, many case reports have been published indicating that liver may also be a major target of PQ toxicity (Burk *et al.*, 1980; Matsumoto *et al.*, 1980;

Mullick *et al.*, 1981; Takegoshi *et al.*, 1988). Previous studies found that the ROS-mediated PQ-toxicity is preceded by altered mitochondrial respiratory function. The involvement of mitochondria was studied initially in rat liver by Fukoshima and co-workers who showed that PQ may generate ROS by accepting electrons from purified complex I (NADH-dehydrogenase) of the respiratory chain producing increased $O_2^{\bullet}$ radicals (Fukushima *et al.*, 1993). Although mitochondria are considered to be involved in PQ-induced toxicity, studies exploring the role of mitochondria, the mechanism of toxicity and the proteins involved after acute PQ-exposure are limited. Therefore, we initiated our own studies, in order to identify the proteins that are modulated during the early stage of PQ exposure dose (40 mg/kg, i.p) and to more clearly understand the role that mitochondria may in PQ toxicity. Proteomic analyses were performed with mitochondria as well as with liver tissue homogenate of PQ-treated rats. Analyses were carried out using nanospray coupled-linear ion trap mass spectrometry (LTQ-MS) employing ^{18}O labeling. Mass analyses of mitochondria, identified 29 and 8 proteins to be down- and up regulated above 2 folds, respectively. This includes down-regulation of complex 1 subunits (Ndufs5, Ndufs7). GO ontology and Interpro analyses of these modulated mitochondrial proteins indicated that they were involved in various processes including oxidoreductase activity, transferase activity, hydrolase activity and transport (Table 3.1.3 and 3.1.4; chapter 3.1). Analyses on the whole liver tissue homogenate identified 20 and 17 proteins to be down- and up regulated above 2 folds, respectively. With whole liver tissue homogenate, proteins involved in metabolism and binding function were mainly affected (Table 3.1.5 and 3.1.6; chapter 3.1). In addition, proteins involved in ubiquitination and the proteolytic pathway as well as oxidoreductase and transferase activities were modulated.

Another redox-cycler, 1, 3-dinitrobenzene, a putative central nervous system toxicant is currently being studied in our laboratory. Our laboratory has established that in the presence of the dinitrobenzene isomers, electron transfer through NOS may be altered, resulting in the production of $ONOO^-$. In addition to the biochemical studies, we also initiated studies investigating possible changes in gene expression levels of the antioxidant enzymes, Cu/Zn superoxide dismutase (SODI) and glutathione peroxidase (GSH-Px) in nNOS rich areas of brain (cerebellum and brainstem) using RTPCR. GSH-Px gene expression was increased at both the 12 hr and 24 hr time points following 3 doses of 1, 3-DNB. These data also point to a possible maximum level of GSH-Px gene expression happening at or before at 12 hr. However, it is necessary to study the GSH-Px gene-expression levels in relation to various time points after 1, 3-DNB exposure, in order to fully understand the pattern of GSH-Px gene modulation. In addition, other antioxidant enzymes and various redox-active proteins should be examined in the nNOS-rich brain regions in order to understand the mechanism of toxicity and the overall global effect of 1, 3-DNB administration in relation to neuro/glial toxicity.

Damage and dysfunction of sub-cellular organelles like mitochondria (Bolanos *et al.*, 1995) are caused predominantly by inactivation of enzymes *via* nitration and/or oxidation. Although a topic of debate, the nitrating species most often implicated in protein nitration is $ONOO^-$. $ONOO^-$ thus formed is known to target tyrosine residues in proteins, causing tyrosine nitration (Ischiropoulos *et al.*, 1992) which is a stable marker for past $ONOO^-$ production.

Although there are many other techniques to quantify nitrated tyrosines, we have detailed a relatively inexpensive approach to identify nitrated tyrosines in biological samples. Though anti-nitrotyrosine antibodies are available commercially, they are extremely expensive. The anti-

nitrotyrosine antibodies produced and purified in our lab were found to be selective, specific and could be used at very low dilutions.

References

Abu-Soud, H. M., Yoho, L. L., Stuehr, D. J., 1994. Calmodulin controls neuronal nitric-oxide synthase by a dual mechanism. Activation of intra- and interdomain electron transfer. J Biol Chem 269, 32047-32050.

Bolanos, J. P., Heales, S. J., Land, J. M., Clark, J. B., 1995. Effect of peroxynitrite on the mitochondrial respiratory chain: differential susceptibility of neurones and astrocytes in primary culture. J Neurochem 64, 1965-1972.

Boveris, A., Cadenas, E., 1975. Mitochondrial production of superoxide anions and its relationship to the antimycin insensitive respiration. FEBS Lett 54, 311-314.

Brookes, P. S., 2004. Mitochondrial nitric oxide synthase. Mitochondrion 3, 187-204.

Brookes, P. S., Levonen, A. L., Shiva, S., Sarti, P., Darley-Usmar, V. M., 2002. Mitochondria: regulators of signal transduction by reactive oxygen and nitrogen species. Free Radic Biol Med 33, 755-764.

Brown, G. C., Bolanos, J. P., Heales, S. J., Clark, J. B., 1995. Nitric oxide produced by activated astrocytes rapidly and reversibly inhibits cellular respiration. Neurosci Lett 193, 201-204.

Burk, R. F., Lawrence, R. A., Lane, J. M., 1980. Liver necrosis and lipid peroxidation in the rat as the result of paraquat and diquat administration. Effect of selenium deficiency. J Clin Invest 65, 1024-1031.

Cadenas, E., Poderoso, J. J., Antunes, F., Boveris, A., 2000. Analysis of the pathways of nitric oxide utilization in mitochondria. Free Radic Res 33, 747-756.

Cleeter, M. W., Cooper, J. M., Darley-Usmar, V. M., Moncada, S., Schapira, A. H., 1994. Reversible inhibition of cytochrome c oxidase, the terminal enzyme of the mitochondrial

respiratory chain, by nitric oxide. Implications for neurodegenerative diseases. FEBS Lett 345, 50-54.

Dedkova, E. N., Ji, X., Lipsius, S. L., Blatter, L. A., 2004. Mitochondrial calcium uptake stimulates nitric oxide production in mitochondria of bovine vascular endothelial cells. American journal of physiology 286, C406-415.

Dionisi, O., Galeotti, T., Terranova, T., Azzi, A., 1975. Superoxide radicals and hydrogen peroxide formation in mitochondria from normal and neoplastic tissues. Biochim Biophys Acta 403, 292-300.

Ebel, R. E., O'Keefe, D. H., Peterson, J. A., 1975. Nitric oxide complexes of cytochrome P-450. FEBS Lett 55, 198-201.

Fukushima, T., Yamada, K., Isobe, A., Shiwaku, K., Yamane, Y., 1993. Mechanism of cytotoxicity of paraquat. I. NADH oxidation and paraquat radical formation via complex I. Exp Toxicol Pathol 45, 345-349.

Huie, R. E., Padmaja, S., 1993. The reaction of no with superoxide. Free Radic Res Commun 18, 195-199.

Ischiropoulos, H., Zhu, L., Chen, J., Tsai, M., Martin, J. C., Smith, C. D., Beckman, J. S., 1992. Peroxynitrite-mediated tyrosine nitration catalyzed by superoxide dismutase. Archives of biochemistry and biophysics 298, 431-437.

Kennedy, M. C., Antholine, W. E., Beinert, H., 1997. An EPR investigation of the products of the reaction of cytosolic and mitochondrial aconitases with nitric oxide. J Biol Chem 272, 20340-20347.

Khalil, A. A., Steyn, S., Castagnoli, N., Jr., 2000. Isolation and characterization of a monoamine oxidase inhibitor from tobacco leaves. Chemical research in toxicology 13, 31-35.

Klatt, P., Heinzel, B., Mayer, B., Ambach, E., Werner-Felmayer, G., Wachter, H., Werner, E. R., 1992. Stimulation of human nitric oxide synthase by tetrahydrobiopterin and selective binding of the cofactor. FEBS Lett 305, 160-162.

Kumagai, Y., Nakajima, H., Midorikawa, K., Homma-Takeda, S., Shimojo, N., 1998. Inhibition of nitric oxide formation by neuronal nitric oxide synthase by quinones: nitric oxide synthase as a quinone reductase. Chem Res Toxicol 11, 608-613.

Lacza, Z., Horn, T. F., Snipes, J. A., Zhang, J., Roychowdhury, S., Horvath, E. M., Figueroa, J. P., Kollai, M., Szabo, C., Busija, D. W., 2004. Lack of mitochondrial nitric oxide production in the mouse brain. J Neurochem 90, 942-951.

Lacza, Z., Puskar, M., Figueroa, J. P., Zhang, J., Rajapakse, N., Busija, D. W., 2001. Mitochondrial nitric oxide synthase is constitutively active and is functionally upregulated in hypoxia. Free Radic Biol Med 31, 1609-1615.

Lacza, Z., Snipes, J. A., Zhang, J., Horvath, E. M., Figueroa, J. P., Szabo, C., Busija, D. W., 2003. Mitochondrial nitric oxide synthase is not eNOS, nNOS or iNOS. Free Radic Biol Med 35, 1217-1228.

MacMillan-Crow, L. A., Crow, J. P., Thompson, J. A., 1998. Peroxynitrite-mediated inactivation of manganese superoxide dismutase involves nitration and oxidation of critical tyrosine residues. Biochemistry 37, 1613-1622.

Matsumoto, T., Matsumori, H., Kuwabara, N., Fukuda, Y., Ariwa, R., 1980. A histopathological study of the liver in paraquat poisoning--an analysis of fourteen autopsy cases with emphasis on bile duct injury. Acta pathologica japonica 30, 859-870.

Miller, R. T., 2002. Dinitrobenzene-mediated production of peroxynitrite by neuronal nitric oxide synthase. Chem Res Toxicol 15, 927-934.

Miller, R. T., Martasek, P., Roman, L. J., Nishimura, J. S., Masters, B. S., 1997. Involvement of the reductase domain of neuronal nitric oxide synthase in superoxide anion production. Biochemistry 36, 15277-15284.

Moncada, S., 2000. Nitric oxide and cell respiration: physiology and pathology. Verh K Acad Geneeskd Belg 62, 171-179; discussion 179-181.

Moncada, S., Erusalimsky, J. D., 2002. Does nitric oxide modulate mitochondrial energy generation and apoptosis? Nat Rev Mol Cell Biol 3, 214-220.

Mullick, F. G., Ishak, K. G., Mahabir, R., Stromeyer, F. W., 1981. Hepatic injury associated with paraquat toxicity in humans. Liver 1, 209-221.

Nathan, C., 1992. Nitric oxide as a secretory product of mammalian cells. FASEB J 6, 3051-3064.

Nishimura, J. S., Narayanasami, R., Miller, R. T., Roman, L. J., Panda, S., Masters, B. S., 1999. The stimulatory effects of Hofmeister ions on the activities of neuronal nitric-oxide synthase. Apparent substrate inhibition by l-arginine is overcome in the presence of protein-destabilizing agents. J Biol Chem 274, 5399-5406.

Radi, R., Cassina, A., Hodara, R., 2002. Nitric oxide and peroxynitrite interactions with mitochondria. Biol Chem 383, 401-409.

Radi, R., Rodriguez, M., Castro, L., Telleri, R., 1994. Inhibition of mitochondrial electron transport by peroxynitrite. Archives of biochemistry and biophysics 308, 89-95.

Sarti, P., Giuffre, A., Barone, M. C., Forte, E., Mastronicola, D., Brunori, M., 2003. Nitric oxide and cytochrome oxidase: reaction mechanisms from the enzyme to the cell. Free Radic Biol Med 34, 509-520.

Schmeltz, I., Tosk, J., Jacobs, G., Hoffmann, D., 1977. Redox potential and quinone content of cigarette smoke. Analytical chemistry 49, 1924-1929.

Sheta, E. A., McMillan, K., Masters, B. S., 1994. Evidence for a bidomain structure of constitutive cerebellar nitric oxide synthase. J Biol Chem 269, 15147-15153.

Stuehr, D. J., Griffith, O. W., 1992. Mammalian nitric oxide synthases. Adv Enzymol Relat Areas Mol Biol 65, 287-346.

Takegoshi, K., Nakanuma, Y., Ohta, M., Thoyama, T., Okuda, K., Kono, N., 1988. Light and electron microscopic study of the liver in paraquat poisoning. Liver 8, 330-336.

Thomas, D. D., Liu, X., Kantrow, S. P., Lancaster, J. R., Jr., 2001. The biological lifetime of nitric oxide: implications for the perivascular dynamics of NO and O2. Proc Natl Acad Sci U S A 98, 355-360.

Thomas, D. D., Miranda, K. M., Colton, C. A., Citrin, D., Espey, M. G., Wink, D. A., 2003. Heme proteins and nitric oxide (NO): the neglected, eloquent chemistry in NO redox signaling and regulation. Antioxid Redox Signal 5, 307-317.

Turko, I. V., Marcondes, S., Murad, F., 2001. Diabetes-associated nitration of tyrosine and inactivation of succinyl-CoA:3-oxoacid CoA-transferase. Am J Physiol Heart Circ Physiol 281, H2289-2294.

Winston, G. W., Church, D. F., Cueto, R., Pryor, W. A., 1993. Oxygen consumption and oxyradical production from microsomal reduction of aqueous extracts of cigarette tar. Archives of biochemistry and biophysics 304, 371-378.

Workman, P., 1992. Bioreductive mechanisms. International journal of radiation oncology, biology, physics 22, 631-637.

Appendix

Appendix 1: LTQ-MS Analyses of Intact MT Proteins

	IPI accession numbers - protein description Intact MT		MW
1	IPI:IPI00210644.1	Carbamoyl-phosphate synthase [ammonia], mitochondrial precursor	164474.80
2	IPI:IPI00231742.4	Catalase	59588.55
3	IPI:IPI00324633.2	Glutamate dehydrogenase 1, mitochondrial precursor	61377.36
4	IPI:IPI00551812.1	ATP synthase subunit beta, mitochondrial precursor	56318.59
5	IPI:IPI00326948.2	Hsd17b4 protein	81037.99
6	IPI:IPI00201413.1	3-ketoacyl-CoA thiolase, mitochondrial	41844.49
7	IPI:IPI00232011.8	Peroxisomal bifunctional enzyme	78477.41
8	IPI:IPI00205561.1	Acyl-coenzyme A oxidase 2, peroxisomal	76750.05
9	IPI:IPI00207010.2	Bile acid CoA:amino acid N-acyltransferase	46435.08
10	IPI:IPI00188989.1	Long-chain-fatty-acid--CoA ligase 1	78128.34
11	IPI:IPI00207941.1	Dimethylglycine dehydrogenase, mitochondrial precursor	95987.51
12	IPI:IPI00231365.4	Uricase	34780.86
13	IPI:IPI00210920.1	Aspartate aminotransferase, mitochondrial precursor	47284.15
14	IPI:IPI00205018.2	Methylmalonate-semialdehyde dehydrogenase [acylating], mitochondrial precursor	57882.70
15	IPI:IPI00197696.2	Malate dehydrogenase, mitochondrial precursor	35660.82
16	IPI:IPI00396910.1	ATP synthase subunit alpha, mitochondrial precursor	59716.74
17	IPI:IPI00209045.2	93 Tax_Id=10116 76 kDa protein	75810.41
18	IPI:IPI00197770.1	Aldehyde dehydrogenase, mitochondrial precursor	56452.72
19	IPI:IPI00210435.1	Pyruvate carboxylase, mitochondrial precursor	129607.80
20	IPI:IPI00358163.3	similar to Calcium-binding mitochondrial carrier protein Aralar2	74351.98
21	IPI:IPI00475676.3	60 kDa protein	59604.52
22	IPI:IPI00210444.5	Hydroxymethylglutaryl-CoA synthase, mitochondrial precursor	56875.68
23	IPI:IPI00211510.1	Isoform 1 of Acyl-coenzyme A oxidase 1, peroxisomal	74631.41
24	IPI:IPI00191737.5	Serum albumin precursor	68674.16
25	IPI:IPI00200659.1	Succinate dehydrogenase [ubiquinone] flavoprotein subunit, mitochondrial precursor	71569.76
26	IPI:IPI00339148.2	60 kDa heat shock protein, mitochondrial precursor	60917.48
27	IPI:IPI00210139.1	Ornithine carbamoyltransferase, mitochondrial precursor	39860.83

28	IPI:IPI00206624.1	78 kDa glucose-regulated protein precursor	72302.52
29	IPI:IPI00198887.1	Protein disulfide-isomerase precursor	56915.78
30	IPI:IPI00231253.4	3-hydroxyacyl-CoA dehydrogenase type-2	27097.53
31	IPI:IPI00211225.1	Long-chain specific acyl-CoA dehydrogenase, mitochondrial precursor	47842.46
32	IPI:IPI00480620.1	3-hydroxybutyrate dehydrogenase	38308.38
33	IPI:IPI00395281.1	Electron transfer flavoprotein-ubiquinone oxidoreductase, mitochondrial precursor	68154.77
34	IPI:IPI00209807.2	Tax_Id=10116 Sarcosine dehydrogenase, mitochondrial precursor	101578.90
35	IPI:IPI00363265.3	Stress-70 protein, mitochondrial precursor	73811.90
36	IPI:IPI00208917.4	similar to aldehyde dehydrogenase family 7, member A1	58711.46
37	IPI:IPI00358005.1	Choline dehydrogenase	66346.48
38	IPI:IPI00213584.3	Alanine--glyoxylate aminotransferase 2, mitochondrial precursor	57395.82
39	IPI:IPI00324741.2	Protein disulfide-isomerase A3 precursor	57043.07
40	IPI:IPI00212622.1	Trifunctional enzyme subunit alpha, mitochondrial precursor	82460.70
41	IPI:IPI00207601.1	similar to Hydroxyacid oxidase 1	40942.25
42	IPI:IPI00205332.4	Electron transfer flavoprotein subunit alpha, mitochondrial precursor	34929.47
43	IPI:IPI00364925.3	Dehydrogenase E1 and transketolase domain containing 1	102576.50
44	IPI:IPI00193153.1	2-hydroxyphytanoyl-CoA lyase	63575.34
45	IPI:IPI00231359.3	Acetyl-Coenzyme A dehydrogenase, short chain	44939.09
46	IPI:IPI00366293.2	Thiosulfate sulfurtransferase	33254.73
47	IPI:IPI00193279.1	Ornithine aminotransferase, mitochondrial precursor	48302.11
48	IPI:IPI00193485.2	Isocitrate dehydrogenase [NADP], mitochondrial precursor	50934.94
49	IPI:IPI00367281.2	Similar to bile acid Coenzyme A: amino acid N-acyltransferase; glycine N-choloyltransferase	45980.94
50	IPI:IPI00365545.1	Dihydrolipoyl dehydrogenase, mitochondrial precursor	54004.15
51	IPI:IPI00326195.3	Peroxisomal trans-2-enoyl-CoA reductase	32830.77
52	IPI:IPI00231860.4	ATP-binding cassette sub-family D member 3	75136.23
53	IPI:IPI00365985.4	93 kDa protein	92474.11
54	IPI:IPI00231245.4	Hydroxyacid oxidase 2	39045.39
55	IPI:IPI00769236.1	similar to butyryl Coenzyme A synthetase 1	65489.71
56	IPI:IPI00201262.1	Alpha-1-inhibitor 3 precursor	163669.20
57	IPI:IPI00205157.1	Hydroxyacyl-coenzyme A dehydrogenase, mitochondrial precursor	34425.90

58	IPI:IPI00195423.1	UDP-glucuronosyltransferase 2B5 precursor	60553.29
59	IPI:IPI00324302.3	Acetyl-CoA acetyltransferase, mitochondrial precursor	44666.50
60	IPI:IPI00325136.5	Isoform SCPx of Nonspecific lipid-transfer protein	58775.50
61	IPI:IPI00208203.2	Peroxisomal delta3, delta2-enoyl-Coenzyme A isomerase	42994.03
62	IPI:IPI00326972.6	Carboxylesterase 3 precursor	62107.82
63	IPI:IPI00382228.1	Ab2-132	39427.87
64	IPI:IPI00200466.2	ADP/ATP translocase 2	32749.11
65	IPI:IPI00196656.2	Ba1-667	107383.30
66	IPI:IPI00191728.1	Calreticulin precursor	47965.90
67	IPI:IPI00364321.2	Electron transfer flavoprotein subunit beta	27539.02
68	IPI:IPI00231662.6	diaphorase 1	34152.73
69	IPI:IPI00188858.3	Alpha-methylacyl-CoA racemase	41670.45
70	IPI:IPI00327781.1	Cytochrome P450 2C11	57144.53
71	IPI:IPI00209690.1	Epoxide hydrolase 1	52547.88
72	IPI:IPI00213057.2	Very-long-chain specific acyl-CoA dehydrogenase, mitochondrial precursor	71244.98
73	IPI:IPI00564133.1	Kynurenine aminotransferase III	51011.37
74	IPI:IPI00557975.1	similar to acyl-Coenzyme A dehydrogenase family, member 11	87315.77
75	IPI:IPI00195123.1	ATP synthase O subunit, mitochondrial precursor	23382.78
76	IPI:IPI00360618.3	similar to glycine-N-acyltransferase	33964.06
77	IPI:IPI00421539.3	Aconitate hydratase, mitochondrial precursor	85380.08
78	IPI:IPI00231774.5	Amine oxidase [flavin-containing] B	58221.31
79	IPI:IPI00198966.3	50 kDa protein	50222.72
80	IPI:IPI00207217.1	Enoyl-CoA hydratase, mitochondrial precursor	31496.19
81	IPI:IPI00393599.3	similar to MOCO sulphurase C-terminal domain containing 1	37766.40
82	IPI:IPI00188924.4	Ubiquinol-cytochrome-c reductase complex core protein 2, mitochondrial precursor	48366.24
83	IPI:IPI00230838.4	ATP synthase D chain, mitochondrial	18620.56
84	IPI:IPI00231013.1	Isoform Short of Cytochrome b5	11268.60
85	IPI:IPI00205745.3	Isoform Mitochondrial of Peroxiredoxin-5, mitochondrial precursor	22164.57
86	IPI:IPI00231106.4	3-mercaptopyruvate sulfurtransferase	32788.41
87	IPI:IPI00212110.1	UDP-glucuronosyltransferase 2B2 precursor	60945.65
88	IPI:IPI00358033.1	NADH-ubiquinone oxidoreductase 75 kDa subunit, mitochondrial precursor	79361.70

89	**IPI:IPI00370596.2**	**3-ketoacyl-CoA thiolase B, peroxisomal precursor**	**43792.71**
90	**IPI:IPI00202658.1**	**3-hydroxyisobutyrate dehydrogenase, mitochondrial precursor**	**35279.60**
91	**IPI:IPI00471577.1**	**Ubiquinol-cytochrome-c reductase complex core protein 1, mitochondrial precursor**	**52815.46**
92	**IPI:IPI00373331.2**	**similar to lactamase, beta**	**60410.13**
93	**IPI:IPI00231473.4**	**Cytochrome P450 2D26**	**57392.14**
94	**IPI:IPI00195593.1**	**Carnitine O-palmitoyltransferase 2, mitochondrial precursor**	**74063.50**
95	**IPI:IPI00205374.1**	**Hydroxymethylglutaryl-CoA lyase, mitochondrial precursor**	**34169.71**
96	**IPI:IPI00327879.1**	**Cytochrome P450 27, mitochondrial precursor**	**60694.86**
97	**IPI:IPI00364948.3**	**Fatty aldehyde dehydrogenase**	**54047.38**
98	**IPI:IPI00212316.1**	**similar to Microsomal triglyceride transfer protein large subunit precursor**	**99124.76**
99	**IPI:IPI00454288.1**	**LRRGT00199**	**67677.30**
100	**IPI:IPI00197555.6**	**Suclg1 protein**	**36125.00**
101	**IPI:IPI00192078.2**	**Biphenyl hydrolase-like**	**32802.13**
102	**IPI:IPI00208288.4**	**similar to succinate dehydrogenase Ip subunit**	**31808.93**
103	**IPI:IPI00212014.2**	**Transitional endoplasmic reticulum ATPase**	**89477.95**
104	**IPI:IPI00364134.1**	**similar to Protein NipSnap1**	**33325.04**
105	**IPI:IPI00332027.7**	**Betaine--homocysteine S-methyltransferase**	**44947.86**
106	**IPI:IPI00231028.2**	**ES1 protein homolog, mitochondrial precursor**	**28154.87**
107	**IPI:IPI00195109.3**	**Serine hydroxymethyl transferase 2**	**55729.75**
108	**IPI:IPI00421874.3**	**Voltage-dependent anion-selective channel protein 1**	**30605.53**
109	**IPI:IPI00193919.4**	**sulfite oxidase**	**60767.94**
110	**IPI:IPI00230897.4**	**Hemoglobin subunit beta-1**	**15838.20**
111	**IPI:IPI00555278.2**	**L-gulonolactone oxidase**	**50451.34**
112	**IPI:IPI00231864.4**	**Cytochrome c, somatic**	**11466.98**
113	**IPI:IPI00212015.1**	**Medium-chain specific acyl-CoA dehydrogenase, mitochondrial precursor**	**46525.83**
114	**IPI:IPI00215574.5**	**3,2-trans-enoyl-CoA isomerase, mitochondrial precursor**	**32234.02**
115	**IPI:IPI00193221.2**	**similar to Maleylacetoacetate isomerase (MAAI) (Glutathione S-transferase zeta 1) (GSTZ1-1) isoform 2**	**19169.87**
116	**IPI:IPI00366020.2**	**similar to butyryl Coenzyme A synthetase 1**	**27846.13**
117	**IPI:IPI00192301.1**	**Glutathione peroxidase 1**	**22244.37**
118	**IPI:IPI00421374.1**	**LRRGT00016**	**89698.71**

119	IPI:IPI00191711.1	Major urinary protein precursor	20723.51
120	IPI:IPI00231782.6	3 beta-hydroxysteroid dehydrogenase type 5	42048.65
121	IPI:IPI00189203.3	similar to Protein C10orf70	17528.89
122	IPI:IPI00365929.1	thioredoxin domain containing 7	48729.69
123	IPI:IPI00361193.5	similar to aldehyde dehydrogenase 1 family, member L2	101674.90
124	IPI:IPI00205749.1	Liver carboxylesterase 3 precursor	61675.54
125	IPI:IPI00204774.1	Liver carboxylesterase B-1 precursor	62454.86
126	IPI:IPI00209115.2	Slc25a3 protein	39595.54
127	IPI:IPI00231148.7	Glycerol-3-phosphate dehydrogenase [NAD+], cytoplasmic	37297.21
128	IPI:IPI00208215.2	Thioredoxin-dependent peroxide reductase, mitochondrial precursor	28277.46
129	IPI:IPI00360501.3	similar to Glutaryl-CoA dehydrogenase, mitochondrial precursor	49283.34
130	IPI:IPI00205036.1	hemoglobin alpha 2 chain	15274.78
131	IPI:IPI00471539.4	similar to succinate-Coenzyme A ligase, GDP-forming, beta subunit isoform 4	46958.84
132	IPI:IPI00211756.1	Prohibitin	29801.90
133	IPI:IPI00372796.5	similar to Mitochondrial carrier homolog 2	51422.39
134	IPI:IPI00230889.4	Microsomal glutathione S-transferase 1	17329.19
135	IPI:IPI00196764.1	Cytochrome P450 3A2	57694.40
136	IPI:IPI00555265.1	Nicotinamide nucleotide transhydrogenase	113796.40
137	IPI:IPI00326433.10	10 kDa heat shock protein, mitochondrial	10763.82
138	IPI:IPI00327626.1	UDP-glucuronosyltransferase 2B3 precursor	60485.04
139	IPI:IPI00198467.1	Trifunctional enzyme subunit beta, mitochondrial precursor	51381.60
140	IPI:IPI00365813.3	similar to Voltage-dependent anion-selective channel protein 1	35017.96
141	IPI:IPI00364431.2	similar to succinate-Coenzyme A ligase, ADP-forming, beta subunit	50274.26
142	IPI:IPI00194042.3	Cytochrome c oxidase polypeptide VIa-liver, mitochondrial precursor	12293.25
143	IPI:IPI00214373.1	Kynurenine/alpha-aminoadipate aminotransferase mitochondrial precursor	47753.74
144	IPI:IPI00209363.1	Mitochondrial dicarboxylate carrier	31434.09
145	IPI:IPI00231200.4	NADPH--cytochrome P450 reductase	76783.27
146	IPI:IPI00327079.4	Glutathione S-transferase kappa 1	25345.24
147	IPI:IPI00213659.3	2,4-dienoyl-CoA reductase, mitochondrial precursor	36109.73
148	IPI:IPI00231204.4	Peroxisomal membrane protein 2	22431.20
149	IPI:IPI00389152.4	similar to cytochrome c oxidase, subunit VIb polypeptide 1	10064.88

150	**IPI:IPI00198325.1**	**Cytochrome P450 2D4**	**56661.35**
151	**IPI:IPI00203690.5**	**4-trimethylaminobutyraldehyde dehydrogenase**	**56432.66**
152	**IPI:IPI00195585.1**	**Retinol dehydrogenase 3**	**35639.48**
153	**IPI:IPI00210029.1**	**Peroxisomal 2,4-dienoyl-CoA reductase**	**31272.29**
154	**IPI:IPI00189813.1**	**Actin, alpha skeletal muscle**	**42023.86**
155	**IPI:IPI00194324.2**	**Pyruvate dehydrogenase E1 component subunit beta, mitochondrial precursor**	**38957.08**
156	**IPI:IPI00196107.1**	**ATP synthase B chain, mitochondrial precursor**	**28850.49**
157	**IPI:IPI00202580.2**	**Tax_Id=10116 Cytochrome P450 2D3**	**57105.55**
158	**IPI:IPI00193716.1**	**Isovaleryl-CoA dehydrogenase, mitochondrial precursor**	**46405.80**
159	**IPI:IPI00190701.5**	**Apolipoprotein E precursor**	**35731.37**
160	**IPI:IPI00211096.1**	**Isoform 11-HSD1A of Corticosteroid 11-beta-dehydrogenase isozyme 1**	**31862.52**
161	**IPI:IPI00476550.4**	**similar to Propionyl-CoA carboxylase alpha chain, mitochondrial precursor**	**79804.14**
162	**IPI:IPI00327694.3**	**Tricarboxylate transport protein, mitochondrial precursor**	**33813.84**
163	**IPI:IPI00192572.1**	**Phytanoyl-CoA dioxygenase, peroxisomal precursor**	**38563.52**
164	**IPI:IPI00205163.3**	**Similar to MIR-interacting saposin-like protein**	**20696.26**
165	**IPI:IPI00204118.1**	**Apoptosis-inducing factor 1, mitochondrial precursor**	**66680.92**
166	**IPI:IPI00194222.1**	**Cytochrome c oxidase subunit 4 isoform 1, mitochondrial precursor**	**19502.08**
167	**IPI:IPI00207474.3**	**Glycine C-acetyltransferase**	**45194.23**
168	**IPI:IPI00189819.1**	**Actin, cytoplasmic 1**	**41709.74**
169	**IPI:IPI00207933.2**	**dehydrogenase/reductase (SDR family) member 4**	**29802.84**
170	**IPI:IPI00192246.1**	**Cytochrome c oxidase subunit 5A, mitochondrial precursor**	**16119.31**
171	**IPI:IPI00327991.3**	**Cytochrome P450 2C23**	**56396.72**
172	**IPI:IPI00196748.3**	**Cytochrome P450 2C7**	**56150.69**
173	**IPI:IPI00202370.3**	**similar to Amine oxidase [flavin-containing] A**	**98012.69**
174	**IPI:IPI00470304.1**	**Serum paraoxonase/lactonase 3**	**39433.25**
175	**IPI:IPI00471911.6**	**Fructose-bisphosphate aldolase B**	**39462.19**
176	**IPI:IPI00214454.2**	**Glycine cleavage system H protein, mitochondrial precursor**	**18473.39**
177	**IPI:IPI00231264.5**	**Serum paraoxonase/arylesterase 1**	**39340.16**
178	**IPI:IPI00213569.1**	**UDP-glucuronosyltransferase 1-1 precursor**	**59623.84**
179	**IPI:IPI00204316.1**	**ATP synthase coupling factor 6, mitochondrial precursor**	**12486.58**
180	**IPI:IPI00560967.1**	**hypothetical protein**	**35126.32**

181	IPI:IPI00558154.1	60 kDa protein	59976.52
182	IPI:IPI00198039.1	similar to ETHE1 protein	27659.00
183	IPI:IPI00373418.3	similar to Lipoamide acyltransferase component of branched-chain alpha-keto acid dehydrogenase complex, mitochondrial precursor (Dihydrolipoyllysine-residue (2-methylpropanoyl)transferase) (E2) (Dihydrolipoamide branched chain transacylase) (BCKAD ..	53240.08
184	IPI:IPI00194045.1	Isocitrate dehydrogenase [NADP] cytoplasmic	46704.57
185	IPI:IPI00201307.1	similar to ubiquinol-cytochrome c reductase binding protein	13549.92
186	IPI:IPI00373134.2	similar to fumarylacetoacetate hydrolase domain containing 2A	40314.03
187	IPI:IPI00358757.3	similar to Histidine triad nucleotide-binding protein 2	17369.26
188	IPI:IPI00371236.3	similar to Tu translation elongation factor, mitochondrial	49491.04
189	IPI:IPI00211593.1	Superoxide dismutase [Mn], mitochondrial precursor	24658.58
190	IPI:IPI00372191.2	Methylcrotonoyl-Coenzyme A carboxylase 1	79279.50
191	IPI:IPI00212104.7	RGD1306809_predicted protein	31605.03
192	IPI:IPI00214152.1	Hydroxyacylglutathione hydrolase	28877.78
193	IPI:IPI00365663.1	branched chain ketoacid dehydrogenase E1, alpha polypeptide	50636.22
194	IPI:IPI00480820.3	Membrane-associated progesterone receptor component 1	21453.66
195	IPI:IPI00209480.5	Propionyl-CoA carboxylase beta chain, mitochondrial precursor	58589.15
196	IPI:IPI00192043.2	Methylcrotonoyl-Coenzyme A carboxylase 2	61956.70
197	IPI:IPI00201636.3	similar to 2-oxoisovalerate dehydrogenase beta subunit, mitochondrial precursor	42795.88
198	IPI:IPI00193765.2	Dipeptidyl-peptidase 1 precursor	52201.72
199	IPI:IPI00190557.2	Prohibitin-2	33291.91
200	IPI:IPI00207110.1	Acyl-coenzyme A thioesterase 8	35980.30
201	IPI:IPI00382270.1	Ab1-114	36896.87
202	IPI:IPI00204311.1	Adenylate kinase isoenzyme 4, mitochondrial	25187.26
203	IPI:IPI00421711.1	Similar to CG6105-PA	11453.09
204	IPI:IPI00360229.4	similar to CG6432-PA	74627.66
205	IPI:IPI00213538.5	Carnitine O-palmitoyltransferase I, liver isoform	88082.81
206	IPI:IPI00390435.1	76 kDa protein	75771.79
207	IPI:IPI00358481.3	Alcohol dehydrogenase, iron containing, 1	50365.61
208	IPI:IPI00199636.1	Calnexin precursor	67212.71
209	IPI:IPI00366416.2	similar to cytochrome c-1	35411.98
210	IPI:IPI00187918.4	80 kDa protein	80446.53

211	IPI:IPI00198324.1	Cytochrome P450 2B3	56348.04
212	IPI:IPI00203473.3	UDP-glucuronosyltransferase 2B4 precursor	61020.25
213	IPI:IPI00361686.5	Complement component 1 Q subcomponent-binding protein, mitochondrial precursor	30977.52
214	IPI:IPI00393883.3	56 kDa protein	56419.17
215	IPI:IPI00778252.1	Protein	53222.95
216	IPI:IPI00210975.1	150 kDa oxygen-regulated protein precursor	111220.10
217	IPI:IPI00372804.2	Probable saccharopine dehydrogenase	47058.14
218	IPI:IPI00215093.1	2-oxoglutarate dehydrogenase E1 component, mitochondrial precursor	116221.50
219	IPI:IPI00551702.2	Dihydrolipoyllysine-residue succinyltransferase component of 2- oxoglutarate dehydrogenase complex, mitochondrial precursor	48894.45
220	IPI:IPI00191176.4	Cytochrome P450PB-1	42247.14
221	IPI:IPI00231941.1	Isoform 2 of Acyl-coenzyme A oxidase 1, peroxisomal	74643.30
222	IPI:IPI00471872.1	Aldehyde dehydrogenase X, mitochondrial precursor	57588.52
223	IPI:IPI00197371.4	similar to Glutathione S-transferase Mu 6	25609.96
224	IPI:IPI00382126.1	Aa2-174	106824.80
225	IPI:IPI00358196.3	similar to cytochrome P450, family 2, subfamily J, polypeptide 4	51583.62
226	IPI:IPI00200883.2	Isoform 2 of Glutaminase liver isoform, mitochondrial precursor	59165.78
227	IPI:IPI00189773.1	Short/branched chain specific acyl-CoA dehydrogenase, mitochondrial precursor	47793.35
228	IPI:IPI00205107.4	Proline oxidase-like protein (Fragment)	50970.21
229	IPI:IPI00326225.2	D-amino-acid oxidase	38942.70
230	IPI:IPI00362963.1	Similar to RIKEN cDNA 1810022C23	33665.14
231	IPI:IPI00764950.1	similar to ubiquinol-cytochrome c reductase complex 7.2kDa protein isoform a	7456.85
232	IPI:IPI00556929.4	Isoform 1 of Voltage-dependent anion-selective channel protein 3	30778.38
233	IPI:IPI00559296.2	similar to ATP-binding cassette sub-family D member 1	81885.95
234	IPI:IPI00339123.2	Acyl-coenzyme A oxidase 3, peroxisomal	78396.07
235	IPI:IPI00198750.1	Acyl-coenzyme A thioesterase 12	61978.86
236	IPI:IPI00231611.7	Isoform Mitochondrial of Fumarate hydratase, mitochondrial precursor	54429.11
237	IPI:IPI00471545.5	Kidney expressed gene 1	33994.32
238	IPI:IPI00197986.1	MIPP65	49282.30
239	IPI:IPI00204128.2	similar to microsomal glutathione S-transferase 3	16752.52
240	IPI:IPI00202584.1	Cytochrome P450 2D10	57039.44

241	IPI:IPI00565267.1	Dimethylaniline monooxygenase [N-oxide-forming] 3	59921.54
242	IPI:IPI00195860.1	Cytochrome c oxidase polypeptide VIIa-liver/heart, mitochondrial precursor	9346.94
243	IPI:IPI00208209.1	PRx IV	30988.08
244	IPI:IPI00327518.4	Arginase-1	36480.91
245	IPI:IPI00204365.2	Ribophorin I	68358.76
246	IPI:IPI00230832.6	Cytochrome c oxidase polypeptide VIc-2	8318.41
247	IPI:IPI00212731.1	Cathepsin D precursor	44651.93
248	IPI:IPI00365904.4	similar to glutaredoxin 5	16421.55
249	IPI:IPI00779445.1	40 kDa protein	40076.55
250	IPI:IPI00231714.3	Dihydrolipoyllysine-residue acetyltransferase component of pyruvate dehydrogenase complex, mitochondrial precursor	67123.58
251	IPI:IPI00337099.2	similar to very-long-chain acyl-CoA dehydrogenase VLCAD homolog isoform 1	68799.78
252	IPI:IPI00561751.1	NADH dehydrogenase (ubiquinone) Fe-S protein 5b	12691.50
253	IPI:IPI00371518.1	Succinate dehydrogenase complex, subunit C, integral membrane protein	18190.66
254	IPI:IPI00362243.6	GTP:AMP phosphotransferase mitochondrial	25291.42
255	IPI:IPI00200145.1	60S acidic ribosomal protein P1	11490.69
256	IPI:IPI00203214.5	Elongation factor 2	95091.98
257	IPI:IPI00199426.8	4-aminobutyrate aminotransferase, mitochondrial precursor	56419.52
258	IPI:IPI00211779.1	Peroxiredoxin-1	22095.32
259	IPI:IPI00208281.1	UDP-glucuronosyltransferase 2B8 precursor	60050.08
260	IPI:IPI00191112.1	similar to Acyl carrier protein, mitochondrial precursor	17503.07
261	IPI:IPI00360993.3	similar to glycine decarboxylase	113846.50
262	IPI:IPI00213735.2	Sideroflexin-1	35392.19
263	IPI:IPI00515762.1	Dimethylglycine dehydrogenase	95917.41
264	IPI:IPI00204597.1	similar to NADH dehydrogenase (ubiquinone) 1 beta subcomplex, 2	11834.86
265	IPI:IPI00679201.2	Mitochondrial import inner membrane translocase subunit Tim9	10369.15
266	IPI:IPI00475946.2	Isoform 2 of Serotransferrin precursor	54488.86
267	IPI:IPI00230857.6	Adenylate kinase isoenzyme 2, mitochondrial	26231.51
268	IPI:IPI00326561.3	Tax_Id=10116 Delta(3,5)-Delta(2,4)-dienoyl-CoA isomerase, mitochondrial precursor	36148.43
269	IPI:IPI00209286.2	Hydroxy-delta-5-steroid dehydrogenase, 3 beta-and steroid delta- isomerase 1	41930.74
270	IPI:IPI00358872.2	Aminomethyltransferase	44035.90

271	IPI:IPI00360061.3	Hypothetical protein LOC313840	47187.46
272	IPI:IPI00327469.1	Alpha-2-HS-glycoprotein precursor	37958.24
273	IPI:IPI00767019.1	similar to trophinin isoform 1	180377.20
274	IPI:IPI00364850.1	similar to NADH dehydrogenase (ubiquinone) 1 beta subcomplex, 6, 17kDa isoform 1	15628.29
275	IPI:IPI00371385.3	similar to Hypothetical transthyretin-like protein R09H10.3 in chromosome IV	15000.45
276	IPI:IPI00211897.3	Glutathione S-transferase alpha-5	25200.12
277	IPI:IPI00390086.3	similar to ATP synthase, H+ transporting, mitochondrial F0 complex, subunit f, isoform 2	10445.56
278	IPI:IPI00373250.4	similar to aminoadipate-semialdehyde synthase precursor	102622.50
279	IPI:IPI00212499.1	Iodotyrosine dehalogenase 1 precursor	32825.25
280	IPI:IPI00369093.1	Ubiquinol-cytochrome c reductase complex 11 kDa protein, mitochondrial precursor	10416.97
281	IPI:IPI00212980.1	Isoform Long of Brain protein 44	14248.61
282	IPI:IPI00764232.2	similar to translocase of inner mitochondrial membrane 50 homolog isoform 1	14257.50
283	IPI:IPI00213436.2	similar to NADH-ubiquinone oxidoreductase MLRQ subunit	9320.87
284	IPI:IPI00205076.1	Lon protease homolog, mitochondrial precursor	105726.40
285	IPI:IPI00368844.3	similar to sarcosine dehydrogenase	24616.93
286	IPI:IPI00382223.1	Ab2-305	43539.42
287	IPI:IPI00372377.1	similar to Putative dimethylaniline monooxygenase [N-oxide-forming] 6	60077.29
288	IPI:IPI00471647.1	NADH dehydrogenase (Ubiquinone) Fe-S protein 2	52527.64
289	IPI:IPI00231978.4	ATP synthase e chain, mitochondrial	8118.43
290	IPI:IPI00198897.1	similar to NADH dehydrogenase (ubiquinone) 1 alpha subcomplex, 6	15214.07
291	IPI:IPI00212811.1	Cathepsin B precursor	37445.62
292	IPI:IPI00200760.6	similar to cDNA sequence BC027342 isoform 2	75750.16
293	IPI:IPI00369339.3	similar to apical protein 2	92720.16
294	IPI:IPI00388687.3	similar to solute carrier family 25 (mitochondrial carrier, Aralar), member 12	50560.04
295	IPI:IPI00324041.1	Long-chain-fatty-acid--CoA ligase 6	78129.98
296	IPI:IPI00370931.3	similar to acyl-Coenzyme A dehydrogenase family, member 10	35283.31
297	IPI:IPI00213045.3	CYP2J4	57840.98
298	IPI:IPI00411230.2	Glutathione S-transferase Mu 2	25554.93
299	IPI:IPI00213231.5	Long-chain-fatty-acid--CoA ligase 5	76355.69
300	IPI:IPI00190402.1	UDP-glucuronosyltransferase 2B1 precursor	60445.31

Appendix 2: LTQ-MS Analyses of Affinity-Purified MT Proteins

	IPI accession numbers - protein description Affinity purified MT		MW
1	IPI:IPI00210644.1	Carbamoyl-phosphate synthase [ammonia], mitochondrial precursor	164474.80
2	IPI:IPI00324633.2	Glutamate dehydrogenase 1, mitochondrial precursor	61377.36
3	IPI:IPI00326948.2	Hsd17b4 protein	81037.99
4	IPI:IPI00231742.4	Catalase	59588.55
5	IPI:IPI00324741.2	Protein disulfide-isomerase A3 precursor	57043.07
6	IPI:IPI00361193.5	similar to aldehyde dehydrogenase 1 family, member L2	101674.90
7	IPI:IPI00206624.1	78 kDa glucose-regulated protein precursor	72302.52
8	IPI:IPI00232011.8	Peroxisomal bifunctional enzyme	78477.41
9	IPI:IPI00212014.2	Transitional endoplasmic reticulum ATPase	89477.95
10	IPI:IPI00196725.5	10-formyltetrahydrofolate dehydrogenase	99063.85
11	IPI:IPI00205561.1	Acyl-coenzyme A oxidase 2, peroxisomal	76750.05
12	IPI:IPI00209690.1	Epoxide hydrolase 1	52547.88
13	IPI:IPI00480639.3	Complement C3 precursor	186341.70
14	IPI:IPI00365985.4	93 kDa protein	92474.11
15	IPI:IPI00188989.1	Long-chain-fatty-acid--CoA ligase 1	78128.34
16	IPI:IPI00557975.1	similar to acyl-Coenzyme A dehydrogenase family, member 11	87315.77
17	IPI:IPI00359647.2	similar to hexose-6-phosphate dehydrogenase	89783.37
18	IPI:IPI00210435.1	Pyruvate carboxylase, mitochondrial precursor	129607.80
19	IPI:IPI00325136.5	Isoform SCPx of Nonspecific lipid-transfer protein	58775.50
20	IPI:IPI00231200.4	NADPH--cytochrome P450 reductase	76783.27
21	IPI:IPI00326195.3	Peroxisomal trans-2-enoyl-CoA reductase	32830.77
22	IPI:IPI00192572.1	Phytanoyl-CoA dioxygenase, peroxisomal precursor	38563.52
23	IPI:IPI00364318.2	Putative L-aspartate dehydrogenase	31240.22
24	IPI:IPI00326140.3	Alpha-1-macroglobulin precursor	167018.90
25	IPI:IPI00190701.5	Apolipoprotein E precursor	35731.37
26	IPI:IPI00196656.2	Ba1-667	107383.30
27	IPI:IPI00193379.1	NADPH:adrenodoxin oxidoreductase, mitochondrial precursor	54328.83
28	IPI:IPI00382191.1	Cc2-27	120448.80
29	IPI:IPI00551812.1	ATP synthase subunit beta, mitochondrial precursor	56318.59

30	IPI:IPI00555161.1	Aa1064	535688.10
31	IPI:IPI00212220.2	Protein disulfide-isomerase A4 precursor	72674.80
32	IPI:IPI00211225.1	Long-chain specific acyl-CoA dehydrogenase, mitochondrial precursor	47842.46
33	IPI:IPI00767154.1	similar to glyoxylate reductase/hydroxypyruvate reductase	35784.76
34	IPI:IPI00198750.1	Acyl-coenzyme A thioesterase 12	61978.86
35	IPI:IPI00370815.3	similar to T-complex protein 1 subunit theta	59708.64
36	IPI:IPI00205018.2	Methylmalonate-semialdehyde dehydrogenase [acylating], mitochondrial precursor	57882.70
37	IPI:IPI00195585.1	Retinol dehydrogenase 3	35639.48
38	IPI:IPI00210444.5	Hydroxymethylglutaryl-CoA synthase, mitochondrial precursor	56875.68
39	IPI:IPI00207010.2	Bile acid CoA:amino acid N-acyltransferase	46435.08
40	IPI:IPI00396910.1	ATP synthase subunit alpha, mitochondrial precursor	59716.74
41	IPI:IPI00363265.3	Stress-70 protein, mitochondrial precursor	73811.90
42	IPI:IPI00231365.4	Uricase	34780.86
43	IPI:IPI00211096.1	Isoform 11-HSD1A of Corticosteroid 11-beta-dehydrogenase isozyme 1	31862.52
44	IPI:IPI00365929.1	thioredoxin domain containing 7	48729.69
45	IPI:IPI00209045.2	93 Tax_Id=10116 76 kDa protein	75810.41
46	IPI:IPI00210029.1	Peroxisomal 2,4-dienoyl-CoA reductase	31272.29
47	IPI:IPI00205519.4	UDP-glucose:glycoprotein glucosyltransferase 1 precursor	176477.40
48	IPI:IPI00207933.2	dehydrogenase/reductase (SDR family) member 4	29802.84
49	IPI:IPI00201262.1	Alpha-1-inhibitor 3 precursor	163669.20
50	IPI:IPI00215093.1	2-oxoglutarate dehydrogenase E1 component, mitochondrial precursor	116221.50
51	IPI:IPI00196764.1	Cytochrome P450 3A2	57694.40
52	IPI:IPI00211392.1	Formimidoyltransferase-cyclodeaminase	58876.71
53	IPI:IPI00208203.2	Peroxisomal delta3, delta2-enoyl-Coenzyme A isomerase	42994.03
54	IPI:IPI00189813.1	Actin, alpha skeletal muscle	42023.86
55	IPI:IPI00213057.2	Very-long-chain specific acyl-CoA dehydrogenase, mitochondrial precursor	71244.98
56	IPI:IPI00367281.2	Similar to bile acid Coenzyme A: amino acid N-acyltransferase; glycine N-choloyltransferase	45980.94
57	IPI:IPI00364286.3	similar to T-complex protein 1 subunit eta	59620.29
58	IPI:IPI00211510.1	Isoform 1 of Acyl-coenzyme A oxidase 1, peroxisomal	74631.41
59	IPI:IPI00195423.1	UDP-glucuronosyltransferase 2B5 precursor	60553.29

60	IPI:IPI00364948.3	Fatty aldehyde dehydrogenase	54047.38
61	IPI:IPI00366218.2	T-complex protein 1 subunit beta	57291.22
62	IPI:IPI00231356.8	C-1-tetrahydrofolate synthase, cytoplasmic	100801.20
63	IPI:IPI00200847.1	T-complex protein 1 subunit alpha	60321.84
64	IPI:IPI00198324.1	Cytochrome P450 2B3	56348.04
65	IPI:IPI00363176.1	similar to zinc binding alcohol dehydrogenase, domain containing 2	40450.14
66	IPI:IPI00565267.1	Dimethylaniline monooxygenase [N-oxide-forming] 3	59921.54
67	IPI:IPI00372388.1	T-complex protein 1 subunit gamma	60608.46
68	IPI:IPI00213659.3	2,4-dienoyl-CoA reductase, mitochondrial precursor	36109.73
69	IPI:IPI00193153.1	2-hydroxyphytanoyl-CoA lyase	63575.34
70	IPI:IPI00196118.4	Isoform 1 of Thioredoxin reductase 2, mitochondrial precursor	56492.04
71	IPI:IPI00191176.4	Cytochrome P450PB-1	42247.14
72	IPI:IPI00195593.1	Carnitine O-palmitoyltransferase 2, mitochondrial precursor	74063.50
73	IPI:IPI00230889.4	Microsomal glutathione S-transferase 1	17329.19
74	IPI:IPI00205135.6	Transglutaminase 2, C polypeptide	76887.20
75	IPI:IPI00198887.1	Protein disulfide-isomerase precursor	56915.78
76	IPI:IPI00470301.1	T-complex protein 1 subunit epsilon	59498.89
77	IPI:IPI00371634.1	B-cell receptor-associated protein 31	27894.02
78	IPI:IPI00555278.2	L-gulonolactone oxidase	50451.34
79	IPI:IPI00364321.2	Electron transfer flavoprotein subunit beta	27539.02
80	IPI:IPI00190531.3	glutathione reductase	45934.69
81	IPI:IPI00231473.4	Cytochrome P450 2D26	57392.14
82	IPI:IPI00208209.1	PRx IV	30988.08
83	IPI:IPI00231148.7	Glycerol-3-phosphate dehydrogenase [NAD+], cytoplasmic	37297.21
84	IPI:IPI00327781.1	Cytochrome P450 2C11	57144.53
85	IPI:IPI00198039.1	similar to ETHE1 protein	27659.00
86	IPI:IPI00210139.1	Ornithine carbamoyltransferase, mitochondrial precursor	39860.83
87	IPI:IPI00372377.1	similar to Putative dimethylaniline monooxygenase [N-oxide-forming] 6	60077.29
88	IPI:IPI00231264.5	Serum paraoxonase/arylesterase 1	39340.16
89	IPI:IPI00205036.1	hemoglobin alpha 2 chain	15274.78
90	IPI:IPI00194925.1	Ribonuclease 4 precursor	16892.29

91	IPI:IPI00207184.1	Endoplasmic reticulum protein ERp29 precursor	28556.95
92	IPI:IPI00192076.3	100 kDa protein	100174.60
93	IPI:IPI00470304.1	Serum paraoxonase/lactonase 3	39433.25
94	IPI:IPI00327079.4	Glutathione S-transferase kappa 1	25345.24
95	IPI:IPI00231662.6	diaphorase 1	34152.73
96	IPI:IPI00358005.1	Choline dehydrogenase	66346.48
97	IPI:IPI00212110.1	UDP-glucuronosyltransferase 2B2 precursor	60945.65
98	IPI:IPI00206948.1	All-trans-retinol 13,14-reductase precursor	67487.41
99	IPI:IPI00205374.1	Hydroxymethylglutaryl-CoA lyase, mitochondrial precursor	34169.71
100	IPI:IPI00201564.4	Dimethylaniline monooxygenase [N-oxide-forming] 1	59786.84
101	IPI:IPI00231782.6	3 beta-hydroxysteroid dehydrogenase type 5	42048.65
102	IPI:IPI00231774.5	Amine oxidase [flavin-containing] B	58221.31
103	IPI:IPI00189819.1	Actin, cytoplasmic 1	41709.74
104	IPI:IPI00230897.4	Hemoglobin subunit beta-1	15838.20
105	IPI:IPI00212015.1	Medium-chain specific acyl-CoA dehydrogenase, mitochondrial precursor	46525.83
106	IPI:IPI00327991.3	Cytochrome P450 2C23	56396.72
107	IPI:IPI00191416.1	Bile acyl-CoA synthetase	76217.12
108	IPI:IPI00209570.2	similar to malic enzyme 2, NAD(+)-dependent, mitochondrial	65309.87
109	IPI:IPI00231860.4	ATP-binding cassette sub-family D member 3	75136.23
110	IPI:IPI00188111.1	Chaperonin subunit 6a	57980.80
111	IPI:IPI00362963.1	Similar to RIKEN cDNA 1810022C23	33665.14
112	IPI:IPI00207601.1	similar to Hydroxyacid oxidase 1	40942.25
113	IPI:IPI00231637.4	Glucose-6-phosphate 1-dehydrogenase	59206.89
114	IPI:IPI00207110.1	Acyl-coenzyme A thioesterase 8	35980.30
115	IPI:IPI00198325.1	Cytochrome P450 2D4	56661.35
116	IPI:IPI00213033.2	15 kDa protein	15243.07
117	IPI:IPI00369774.1	Methyltransferase-like protein 7B precursor	27885.51
118	IPI:IPI00193485.2	Isocitrate dehydrogenase [NADP], mitochondrial precursor	50934.94
119	IPI:IPI00324912.5	Cytochrome P450 2E1	56459.77
120	IPI:IPI00390975.3	57 kDa protein	57462.17
121	IPI:IPI00454559.2	Txnrd1 protein	62962.64

122	IPI:IPI00231359.3	Acetyl-Coenzyme A dehydrogenase, short chain	44939.09
123	IPI:IPI00205417.5	Very-long-chain acyl-CoA synthetase	70648.55
124	IPI:IPI00392676.3	similar to biliverdin reductase B	22083.29
125	IPI:IPI00364506.4	similar to thioredoxin reductase 3	80889.86
126	IPI:IPI00195372.1	Elongation factor 1-alpha 1	50082.16
127	IPI:IPI00373331.2	similar to lactamase, beta	60410.13
128	IPI:IPI00464794.1	Quinone oxidoreductase	34953.15
129	IPI:IPI00364866.1	BWK4	46848.43
130	IPI:IPI00196696.5	Cytochrome P450 2A1	55973.20
132	IPI:IPI00210120.2	Aa1018	55924.79
133	IPI:IPI00210975.1	150 kDa oxygen-regulated protein precursor	111220.10
134	IPI:IPI00190402.1	UDP-glucuronosyltransferase 2B1 precursor	60445.31
135	IPI:IPI00202584.1	Cytochrome P450 2D10	57039.44
136	IPI:IPI00231245.4	Hydroxyacid oxidase 2	39045.39
137	IPI:IPI00201528.1	similar to tissue specific transplantation antigen P35B	35773.93
138	IPI:IPI00370596.2	3-ketoacyl-CoA thiolase B, peroxisomal precursor	43792.71
139	IPI:IPI00231253.4	3-hydroxyacyl-CoA dehydrogenase type-2	27097.53
140	IPI:IPI00360954.1	NAD(P) dependent steroid dehydrogenase-like	40386.03
141	IPI:IPI00193716.1	Isovaleryl-CoA dehydrogenase, mitochondrial precursor	46405.80
142	IPI:IPI00475676.3	60 kDa protein	59604.52
143	IPI:IPI00198467.1	Trifunctional enzyme subunit beta, mitochondrial precursor	51381.60
144	IPI:IPI00324272.1	Apolipoprotein A-IV precursor	44428.77
145	IPI:IPI00202325.1	UDP-glucuronosyltransferase 1-2 precursor	60005.94
146	IPI:IPI00764168.1	similar to Glucosylceramidase precursor (Beta-glucocerebrosidase) (Acid beta-glucosidase) (D-glucosyl-N-acylsphingosine glucohydrolase) isoform 1	57455.18
147	IPI:IPI00210874.1	Synaptic glycoprotein SC2	36098.81
148	IPI:IPI00212651.1	Mitochondrial import inner membrane translocase subunit Tim13	10450.95
149	IPI:IPI00206395.2	Granzyme J	27455.09
150	IPI:IPI00231064.6	Aldehyde dehydrogenase, dimeric NADP-preferring	50175.70
151	IPI:IPI00188804.1	60S acidic ribosomal protein P2	11684.86
152	IPI:IPI00421874.3	Voltage-dependent anion-selective channel protein 1	30605.53

153	IPI:IPI00201413.1	3-ketoacyl-CoA thiolase, mitochondrial	41844.49
154	IPI:IPI00366293.2	Thiosulfate sulfurtransferase	33254.73
155	IPI:IPI00366079.1	46 kDa protein	46324.02
156	IPI:IPI00208205.1	Heat shock cognate 71 kDa protein	70827.34
157	IPI:IPI00388209.2	similar to Glucosidase II beta subunit precursor	59181.21
158	IPI:IPI00212622.1	Trifunctional enzyme subunit alpha, mitochondrial precursor	82460.70
159	IPI:IPI00197770.1	Aldehyde dehydrogenase, mitochondrial precursor	56452.72
160	IPI:IPI00371036.1	Mitochondrial fission 1 protein	16983.95
161	IPI:IPI00202580.2	Tax_Id=10116 Cytochrome P450 2D3	57105.55
162	IPI:IPI00339148.2	60 kDa heat shock protein, mitochondrial precursor	60917.48
163	IPI:IPI00213644.3	Peptidyl-prolyl cis-trans isomerase B precursor	23787.54
164	IPI:IPI00191707.4	Pyruvate dehydrogenase E1 component alpha subunit, somatic form, mitochondrial precursor	43198.64
165	IPI:IPI00332027.7	Betaine--homocysteine S-methyltransferase	44947.86
166	IPI:IPI00231368.4	Thioredoxin	11534.62
167	IPI:IPI00194324.2	Pyruvate dehydrogenase E1 component subunit beta, mitochondrial precursor	38957.08
168	IPI:IPI00554264.2	37 kDa protein	37401.43
169	IPI:IPI00193233.1	Cytochrome b5 type B precursor	16254.83
170	IPI:IPI00327335.3	Sulfotransferase family cytosolic 1B member 1	34812.77
171	IPI:IPI00198947.1	Cytochrome P450 1A2	58256.52
172	IPI:IPI00421539.3	Aconitate hydratase, mitochondrial precursor	85380.08
173	IPI:IPI00208215.2	Thioredoxin-dependent peroxide reductase, mitochondrial precursor	28277.46
174	IPI:IPI00191385.3	Phosphoinositide phosphatase SAC1	66996.11
175	IPI:IPI00211897.3	Glutathione S-transferase alpha-5	25200.12
176	IPI:IPI00201333.4	similar to alpha glucosidase 2 alpha neutral subunit	109363.00
177	IPI:IPI00327626.1	UDP-glucuronosyltransferase 2B3 precursor	60485.04
178	IPI:IPI00203106.5	Dimethylaniline monooxygenase [N-oxide-forming] 5	59886.23
179	IPI:IPI00325610.5	Haptoglobin precursor	38524.56
180	IPI:IPI00199636.1	Calnexin precursor	67212.71
181	IPI:IPI00231013.1	Isoform Short of Cytochrome b5	11268.60
182	IPI:IPI00480820.3	Membrane-associated progesterone receptor component 1	21453.66

183	IPI:IPI00471911.6	Fructose-bisphosphate aldolase B	39462.19
184	IPI:IPI00326972.6	Carboxylesterase 3 precursor	62107.82
185	IPI:IPI00371043.2	similar to arginine-rich, mutated in early stage tumors	20374.61
186	IPI:IPI00194404.5	Nucleoside diphosphate kinase A	17181.81
187	IPI:IPI00191728.1	Calreticulin precursor	47965.90
188	IPI:IPI00188967.1	Ig kappa chain C region, A allele	11724.61
189	IPI:IPI00207146.1	Zero beta-1 globin	16012.26
190	IPI:IPI00373250.4	similar to aminoadipate-semialdehyde synthase precursor	102622.50
191	IPI:IPI00393599.3	similar to MOCO sulphurase C-terminal domain containing 1	37766.40
192	IPI:IPI00325765.2	Aflatoxin B1 aldehyde reductase member 2	40649.32
193	IPI:IPI00193049.1	Sulfotransferase 1A1	33884.02
194	IPI:IPI00191711.1	Major urinary protein precursor	20723.51
195	IPI:IPI00231786.3	malic enzyme 1	65522.91
196	IPI:IPI00195160.1	Sulfated glycoprotein 1 precursor	61083.70
197	IPI:IPI00210423.4	Peroxisomal biogenesis factor 14	40911.64
198	IPI:IPI00203090.1	Flavin-containing monooxygenase 4 shortened form	55927.49
199	IPI:IPI00195109.3	Serine hydroxymethyl transferase 2	55729.75
200	IPI:IPI00199203.1	similar to glyceraldehyde-3-phosphate dehydrogenase	35832.84
201	IPI:IPI00191897.4	similar to Nucleoside diphosphate kinase B	16179.14
202	IPI:IPI00193765.2	Dipeptidyl-peptidase 1 precursor	52201.72
203	IPI:IPI00365861.3	Angiogenin ribonuclease 1	16095.09
204	IPI:IPI00371893.3	similar to Cystatin S precursor	15900.72
205	IPI:IPI00197555.6	Suclg1 protein	36125.00
206	IPI:IPI00371106.2	similar to vacuolar protein sorting 29 isoform 2	20876.86
207	IPI:IPI00189203.3	similar to Protein C10orf70	17528.89
208	IPI:IPI00365087.3	similar to endoplasmic reticulum protein ERp19	28721.63
209	IPI:IPI00213231.5	Long-chain-fatty-acid--CoA ligase 5	76355.69
210	IPI:IPI00208111.5	Estradiol 17-beta-dehydrogenase 2	41939.54
211	IPI:IPI00780394.1	Coatomer protein complex, subunit gamma	98468.99
212	IPI:IPI00326561.3	Tax_Id=10116 Delta(3,5)-Delta(2,4)-dienoyl-CoA isomerase, mitochondrial precursor	36148.43
213	IPI:IPI00205693.1	Sodium/potassium-transporting ATPase alpha-2 chain precursor	112145.60

214	IPI:IPI00209286.2	Hydroxy-delta-5-steroid dehydrogenase, 3 beta-and steroid delta- isomerase 1	41930.74
215	IPI:IPI00188858.3	Alpha-methylacyl-CoA racemase	41670.45
216	IPI:IPI00393340.2	Hypothetical protein	59212.74
217	IPI:IPI00202658.1	3-hydroxyisobutyrate dehydrogenase, mitochondrial precursor	35279.60
218	IPI:IPI00200489.1	Isoform Mitochondrial of Malonyl-CoA decarboxylase, mitochondrial precursor	54727.34
219	IPI:IPI00358987.3	similar to Zinc finger SWIM domain containing protein 5	131330.00
220	IPI:IPI00365545.1	Dihydrolipoyl dehydrogenase, mitochondrial precursor	54004.15
221	IPI:IPI00559296.2	similar to ATP-binding cassette sub-family D member 1	81885.95
222	IPI:IPI00209480.5	Propionyl-CoA carboxylase beta chain, mitochondrial precursor	58589.15
223	IPI:IPI00205076.1	Lon protease homolog, mitochondrial precursor	105726.40
224	IPI:IPI00198620.1	ATP synthase delta chain, mitochondrial precursor	17584.18
225	IPI:IPI00198327.2	Voltage-dependent anion-selective channel protein 2	31725.62
226	IPI:IPI00382202.1	Ba1-647	42447.49
227	IPI:IPI00210900.1	AMBP protein precursor	38825.96
228	IPI:IPI00187967.1	similar to CG32512-PA	21171.21
229	IPI:IPI00212666.2	Isoform 1 of Murinoglobulin-1 precursor	165220.90
230	IPI:IPI00197579.1	Tubulin beta-5 chain	49639.01
231	IPI:IPI00190759.2	Isoform Gamma-B of Fibrinogen gamma chain precursor	50600.47
232	IPI:IPI00373140.2	similar to destrin	18507.48
233	IPI:IPI00372804.2	Probable saccharopine dehydrogenase	47058.14
234	IPI:IPI00206330.1	Cytochrome P450 4F4	60011.33
235	IPI:IPI00190499.5	Tripeptidyl-peptidase 1 precursor	61293.95
236	IPI:IPI00210384.3	14 kDa protein	13544.47
237	IPI:IPI00207355.3	Heat shock-related 70 kDa protein 2	69485.71
238	IPI:IPI00231659.3	Transmembrane emp24 domain-containing protein 10 precursor	24841.85
239	IPI:IPI00364124.2	Alpha-2-macroglobulin receptor-associated protein precursor	42006.10
240	IPI:IPI00231150.4	Glutathione S-transferase alpha (Fragment)	25971.69
241	IPI:IPI00189549.2	79 kDa protein	78888.05
242	IPI:IPI00208281.1	UDP-glucuronosyltransferase 2B8 precursor	60050.08
243	IPI:IPI00365813.3	similar to Voltage-dependent anion-selective channel protein 1	35017.96
244	IPI:IPI00326433.10	10 kDa heat shock protein, mitochondrial	10763.82

245	IPI:IPI00198988.1	Nucleoside diphosphate kinase DR-nm23	19076.89
246	IPI:IPI00207217.1	Enoyl-CoA hydratase, mitochondrial precursor	31496.19
247	IPI:IPI00194045.1	Isocitrate dehydrogenase [NADP] cytoplasmic	46704.57
248	IPI:IPI00209042.1	3'(2'),5'-bisphosphate nucleotidase 1	33153.06
249	IPI:IPI00213538.5	Carnitine O-palmitoyltransferase I, liver isoform	88082.81
250	IPI:IPI00365390.1	similar to histidine triad protein 4	19722.80
251	IPI:IPI00190557.2	Prohibitin-2	33291.91
252	IPI:IPI00324443.1	Cytochrome P450 2D1	57138.68
253	IPI:IPI00400739.1	Ectonucleoside triphosphate diphosphohydrolase 5	47342.86
254	IPI:IPI00369954.2	Pipecolic acid oxidase	43862.61
255	IPI:IPI00372796.5	similar to Mitochondrial carrier homolog 2	51422.39
256	IPI:IPI00230874.10	Biliverdin reductase A precursor	33544.52
257	IPI:IPI00360993.3	similar to glycine decarboxylase	113846.50
258	IPI:IPI00769119.1	similar to UDP-glucuronosyltransferase 2B5 precursor	49498.36
259	IPI:IPI00464485.1	HBS1-like protein	74727.25
260	IPI:IPI00212478.1	Epsilon 1 globin	16094.46
261	IPI:IPI00566093.3	Lanosterol synthase	83485.31
262	IPI:IPI00365891.4	similar to Endoribonuclease Dicer	216818.50
263	IPI:IPI00210494.1	Steryl-sulfatase precursor	62638.46
264	IPI:IPI00421711.1	Similar to CG6105-PA	11453.09
265	IPI:IPI00364138.4	74 kDa protein	73668.34
266	IPI:IPI00365149.2	Ubiquinone biosynthesis protein COQ9, mitochondrial precursor	35123.48
267	IPI:IPI00204311.1	Adenylate kinase isoenzyme 4, mitochondrial	25187.26
268	IPI:IPI00359623.3	similar to aldehyde dehydrogenase 8 family, member A1 isoform 2	53387.29
269	IPI:IPI00197982.1	Oxidative 17 beta hydroxysteroid dehydrogenase type 6	37116.13
270	IPI:IPI00203400.1	similar to 60S ribosomal protein L9	21806.43
271	IPI:IPI00203054.2	Hypothetical protein LOC619561	67842.92
272	IPI:IPI00215451.3	92 kDa protein	92303.57
273	IPI:IPI00188924.4	Ubiquinol-cytochrome-c reductase complex core protein 2, mitochondrial precursor	48366.24
274	IPI:IPI00364856.3	similar to DEAD/H box polypeptide RIG-I	105903.10
275	IPI:IPI00212767.1	Anionic trypsin-1 precursor	25942.68

276	**IPI:IPI00196748.3**	**Cytochrome P450 2C7**	**56150.69**
277	**IPI:IPI00360356.1**	**similar to cytoplasmic beta-actin**	**41935.92**
278	**IPI:IPI00210158.1**	**26S protease regulatory subunit 6B**	**47378.66**
279	**IPI:IPI00554086.4**	**Cytochrome P450 2C24 (Fragment)**	**49917.21**
280	**IPI:IPI00778660.1**	**33 kDa protein**	**32833.91**
281	**IPI:IPI00189753.3**	**Cytochrome P450 4F1**	**59830.03**
282	**IPI:IPI00337123.3**	**similar to Myomesin-1 (190 kDa titin-associated protein) (190 kDa connectin-associated protein) isoform 3**	**175393.40**
283	**IPI:IPI00361190.2**	**Transmembrane channel-like gene family 5**	**87930.96**
284	**IPI:IPI00382295.1**	**Ac2-125**	**97458.27**

Appendix 3: LTQ-MS Analyses of nNOS-spiked MT Proteins

	IPI/SwissProt accession numbers - protein description nNOS spiked MT	MW
1	IPI:IPI00324633.2 Glutamate dehydrogenase 1, mitochondrial precursor	61377.36
2	IPI:IPI00232011.8 Peroxisomal bifunctional enzyme	78477.41
3	IPI:IPI00231742.4 Catalase	59588.55
4	IPI:IPI00324741.2 Protein disulfide-isomerase A3 precursor	57043.07
5	IPI:IPI00361193.5 similar to aldehyde dehydrogenase 1 family, member L2	101674.90
6	IPI:IPI00210644.1 Carbamoyl-phosphate synthase [ammonia], mitochondrial precursor	164474.80
7	IPI:IPI00193379.1 NADPH:adrenodoxin oxidoreductase, mitochondrial precursor	54328.83
8	IPI:IPI00326948.2 Hsd17b4 protein	81037.99
9	IPI:IPI00206624.1 78 kDa glucose-regulated protein precursor	72302.52
10	IPI:IPI00326195.3 Peroxisomal trans-2-enoyl-CoA reductase	32830.77
11	IPI:IPI00231200.4 NADPH--cytochrome P450 reductase	76783.27
12	IPI:IPI00209570.2 similar to malic enzyme 2, NAD(+)-dependent, mitochondrial	65309.87
13	IPI:IPI00359647.2 similar to hexose-6-phosphate dehydrogenase	89783.37
14	IPI:IPI00557975.1 similar to acyl-Coenzyme A dehydrogenase family, member 11	87315.77
15	IPI:IPI00364318.2 Putative L-aspartate dehydrogenase	31240.22
16	IPI:IPI00205561.1 Acyl-coenzyme A oxidase 2, peroxisomal	76750.05
17	IPI:IPI00210029.1 Peroxisomal 2,4-dienoyl-CoA reductase	31272.29
18	IPI:IPI00212220.2 Protein disulfide-isomerase A4 precursor	72674.80
19	IPI:IPI00196725.5 10-formyltetrahydrofolate dehydrogenase	99063.85
20	IPI:IPI00207010.2 Bile acid CoA:amino acid N-acyltransferase	46435.08
21	IPI:IPI00211225.1 Long-chain specific acyl-CoA dehydrogenase, mitochondrial precursor	47842.46
22	IPI:IPI00190701.5 Apolipoprotein E precursor	35731.37
23	IPI:IPI00192572.1 Phytanoyl-CoA dioxygenase, peroxisomal precursor	38563.52
24	IPI:IPI00209690.1 Epoxide hydrolase 1	52547.88
25	IPI:IPI00210435.1 Pyruvate carboxylase, mitochondrial precursor	129607.80
26	IPI:IPI00767154.1 similar to glyoxylate reductase/hydroxypyruvate reductase	35784.76
27	IPI:IPI00213644.3 Peptidyl-prolyl cis-trans isomerase B precursor	23787.54
28	IPI:IPI00365985.4 93 kDa protein	92474.11
29	IPI:IPI00390975.3 57 kDa protein	57462.17

30	**IPI:IPI00325136.5**	**Isoform SCPx of Nonspecific lipid-transfer protein**	**58775.50**
31	**IPI:IPI00231245.4**	**Hydroxyacid oxidase 2**	**39045.39**
32	**IPI:IPI00198887.1**	**Protein disulfide-isomerase precursor**	**56915.78**
33	**IPI:IPI00213659.3**	**2,4-dienoyl-CoA reductase, mitochondrial precursor**	**36109.73**
34	**IPI:IPI00207601.1**	**similar to Hydroxyacid oxidase 1**	**40942.25**
35	**IPI:IPI00209045.2**	**93 Tax_Id=10116 76 kDa protein**	**75810.41**
36	**IPI:IPI00210444.5**	**Hydroxymethylglutaryl-CoA synthase, mitochondrial precursor**	**56875.68**
37	**IPI:IPI00215093.1**	**2-oxoglutarate dehydrogenase E1 component, mitochondrial precursor**	**116221.50**
38	**IPI:IPI00190531.3**	**glutathione reductase**	**45934.69**
39	**IPI:IPI00363176.1**	**similar to zinc binding alcohol dehydrogenase, domain containing 2**	**40450.14**
40	**IPI:IPI00207933.2**	**dehydrogenase/reductase (SDR family) member 4**	**29802.84**
41	**IPI:IPI00212014.2**	**Transitional endoplasmic reticulum ATPase**	**89477.95**
42	**IPI:IPI00193153.1**	**2-hydroxyphytanoyl-CoA lyase**	**63575.34**
43	**IPI:IPI00365929.1**	**thioredoxin domain containing 7**	**48729.69**
44	**IPI:IPI00213033.2**	**15 kDa protein**	**15243.07**
45	**IPI:IPI00339148.2**	**60 kDa heat shock protein, mitochondrial precursor**	**60917.48**
46	**IPI:IPI00198750.1**	**Acyl-coenzyme A thioesterase 12**	**61978.86**
47	**IPI:IPI00382191.1**	**Cc2-27**	**120448.80**
48	**IPI:IPI00764168.1**	**similar to Glucosylceramidase precursor (Beta-glucocerebrosidase) (Acid beta-glucosidase) (D-glucosyl-N-acylsphingosine glucohydrolase) isoform 1**	**57455.18**
49	**IPI:IPI00367281.2**	**Similar to bile acid Coenzyme A: amino acid N-acyltransferase; glycine N-choloyltransferase**	**45980.94**
51	**IPI:IPI00211096.1**	**Isoform 11-HSD1A of Corticosteroid 11-beta-dehydrogenase isozyme 1**	**31862.52**
52	**IPI:IPI00454559.2**	**Txnrd1 protein**	**62962.64**
53	**IPI:IPI00326433.10**	**10 kDa heat shock protein, mitochondrial**	**10763.82**
54	**IPI:IPI00201413.1**	**3-ketoacyl-CoA thiolase, mitochondrial**	**41844.49**
55	**IPI:IPI00191728.1**	**Calreticulin precursor**	**47965.90**
56	**IPI:IPI00196656.2**	**Ba1-667**	**107383.30**
57	**IPI:IPI00480639.3**	**Complement C3 precursor**	**186341.70**
58	**IPI:IPI00555278.2**	**L-gulonolactone oxidase**	**50451.34**
59	**IPI:IPI00464794.1**	**Quinone oxidoreductase**	**34953.15**
60	**IPI:IPI00230889.4**	**Microsomal glutathione S-transferase 1**	**17329.19**

61	**IPI:IPI00327781.1**	**Cytochrome P450 2C11**	**57144.53**
62	**IPI:IPI00364948.3**	**Fatty aldehyde dehydrogenase**	**54047.38**
63	**IPI:IPI00194925.1**	**Ribonuclease 4 precursor**	**16892.29**
64	**IPI:IPI00231473.4**	**Cytochrome P450 2D26**	**57392.14**
65	**IPI:IPI00198325.1**	**Cytochrome P450 2D4**	**56661.35**
66	**IPI:IPI00194404.5**	**Nucleoside diphosphate kinase A**	**17181.81**
67	**IPI:IPI00195585.1**	**Retinol dehydrogenase 3**	**35639.48**
68	**IPI:IPI00212110.1**	**UDP-glucuronosyltransferase 2B2 precursor**	**60945.65**
69	**IPI:IPI00231292.6**	**Ribonuclease UK114**	**14479.67**
70	**IPI:IPI00198324.1**	**Cytochrome P450 2B3**	**56348.04**
71	**IPI:IPI00191707.4**	**Pyruvate dehydrogenase E1 component alpha subunit, somatic form, mitochondrial precursor**	**43198.64**
72	**IPI:IPI00195160.1**	**Sulfated glycoprotein 1 precursor**	**61083.70**
73	**IPI:IPI00194324.2**	**Pyruvate dehydrogenase E1 component subunit beta, mitochondrial precursor**	**38957.08**
74	**IPI:IPI00361686.5**	**Complement component 1 Q subcomponent-binding protein, mitochondrial precursor**	**30977.52**
75	**IPI:IPI00231013.1**	**Isoform Short of Cytochrome b5**	**11268.60**
76	**IPI:IPI00560967.1**	**hypothetical protein**	**35126.32**
77	**IPI:IPI00195423.1**	**UDP-glucuronosyltransferase 2B5 precursor**	**60553.29**
78	**IPI:IPI00212015.1**	**Medium-chain specific acyl-CoA dehydrogenase, mitochondrial precursor**	**46525.83**
79	**IPI:IPI00211510.1**	**Isoform 1 of Acyl-coenzyme A oxidase 1, peroxisomal**	**74631.41**
80	**IPI:IPI00231356.8**	**C-1-tetrahydrofolate synthase, cytoplasmic**	**100801.20**
81	**IPI:IPI00205036.1**	**hemoglobin alpha 2 chain**	**15274.78**
82	**IPI:IPI00188989.1**	**Long-chain-fatty-acid--CoA ligase 1**	**78128.34**
83	**IPI:IPI00326140.3**	**Alpha-1-macroglobulin precursor**	**167018.90**
84	**IPI:IPI00197770.1**	**Aldehyde dehydrogenase, mitochondrial precursor**	**56452.72**
85	**IPI:IPI00191176.4**	**Cytochrome P450PB-1**	**42247.14**
86	**IPI:IPI00197696.2**	**Malate dehydrogenase, mitochondrial precursor**	**35660.82**
87	**IPI:IPI00204773.1**	**Isoform N-NOS-1 of Nitric-oxide synthase, brain**	**160457.60**
88	**IPI:IPI00369774.1**	**Methyltransferase-like protein 7B precursor**	**27885.51**
89	**IPI:IPI00201223.1**	**similar to NADH-cytochrome b5 reductase**	**34825.12**
90	**IPI:IPI00208209.1**	**PRx IV**	**30988.08**

91	**IPI:IPI00211730.2**	**Translation initiation factor eIF-2B subunit epsilon**	**80156.55**
92	**IPI:IPI00471911.6**	**Fructose-bisphosphate aldolase B**	**39462.19**
93	**IPI:IPI00193485.2**	**Isocitrate dehydrogenase [NADP], mitochondrial precursor**	**50934.94**
94	**IPI:IPI00202584.1**	**Cytochrome P450 2D10**	**57039.44**
95	**IPI:IPI00366293.2**	**Thiosulfate sulfurtransferase**	**33254.73**
96	**IPI:IPI00190499.5**	**Tripeptidyl-peptidase 1 precursor**	**61293.95**

Appendix 4: Proteins identified in mitochondria after PQ-treatment by LTQ-MS analyses, using ^{18}O-labeling.

	Accession	Reference	MW
	RSp	Scan(s)	Sp
1	IPI00210644.1	Cps1 Carbamoyl-phosphate synthase [ammonia], mitochondrial	164474.80
2	IPI00231742.5	Cat Catalase	59719.59
3	IPI00326948.2	Hsd17b4 Hsd17b4 protein	81037.99
4	IPI00188989.1	Acsl1 Long-chain-fatty-acid--CoA ligase 1	78128.34
5	IPI00232011.9	Ehhadh Peroxisomal bifunctional enzyme	78608.45
6	IPI00205561.1	Acox2 Peroxisomal acyl-coenzyme A oxidase 2	76750.05
7	IPI00325136.5	Scp2 Isoform SCPx of Non-specific lipid-transfer protein	58775.50
8	IPI00211510.1	Acox1 Isoform 1 of Peroxisomal acyl-coenzyme A oxidase 1	74631.41
9	IPI00207010.2	Baat Bile acid-CoA:amino acid N-acyltransferase	46435.08
10	IPI00193153.1	Hacl1 2-hydroxyacyl-CoA lyase 1	63575.34
11	IPI00191737.6	Alb Serum albumin	68686.20
12	IPI00209045.2	Acox3 76 kDa protein	75810.41
13	IPI00324633.2	Glud1 Glutamate dehydrogenase 1, mitochondrial	61377.36
14	IPI00231365.5	Uox Uricase	34911.90
15	IPI00201413.1	Acaa2 3-ketoacyl-CoA thiolase, mitochondrial	41844.49
16	IPI00551812.1	Atp5b ATP synthase subunit beta, mitochondrial	56318.59
17	IPI00197770.1	Aldh2 Aldehyde dehydrogenase, mitochondrial	56452.72
18	IPI00339148.2	Hspd1 60 kDa heat shock protein, mitochondrial	60917.48
19	IPI00210435.2	Pcx Pyruvate carboxylase, mitochondrial	129694.90
20	IPI00207941.1	Dmgdh Dimethylglycine dehydrogenase, mitochondrial	95987.51
21	IPI00206624.1	Hspa5 78 kDa glucose-regulated protein	72302.52
22	IPI00367281.2	LOC313220 Similar to bile acid Coenzyme A: amino acid N-acyltransferase	45980.94
23	IPI00231245.5	Hao2 Hydroxyacid oxidase 2	39176.43
24	IPI00192572.1	Phyh Phytanoyl-CoA dioxygenase, peroxisomal	38563.52
25	IPI00210920.1	Got2 Aspartate aminotransferase, mitochondrial	47284.15
26	IPI00205018.2	Aldh6a1 Methylmalonate-semialdehyde dehydrogenase [acylating], mitochondrial	57882.70
27	IPI00480639.3	C3 Complement C3 (Fragment)	186341.70
28	IPI00557975.1	Acad11 Acyl-Coenzyme A dehydrogenase family, member 11	87315.77
29	IPI00207601.1	Hao1 Hydroxyacid oxidase 1, liver	40942.25
30	IPI00326195.3	Pecr Peroxisomal trans-2-enoyl-CoA reductase	32830.77
31	IPI00231860.5	Abcd3 ATP-binding cassette sub-family D member 3	75267.27
32	IPI00201262.1	LOC297568;Mug1;Mug2 Alpha-1-inhibitor 3	163669.20
33	IPI00212622.2	Hadha Trifunctional enzyme subunit alpha, mitochondrial	82612.66
34	IPI00197696.2	Mdh2 Malate dehydrogenase, mitochondrial	35660.82
35	IPI00370596.2	RGD1562373 3-ketoacyl-CoA thiolase B, peroxisomal	43792.71
36	IPI00421374.1	Lonp2 LRRGT00016	89698.71
37	IPI00208917.4	Aldh7a1 similar to aldehyde dehydrogenase family 7, member A1	58711.46
38	IPI00396910.1	Atp5a1 ATP synthase subunit alpha, mitochondrial	59716.74
39	IPI00480620.1	Bdh1 3-hydroxybutyrate dehydrogenase, type 1	38308.38
40	IPI00188858.4	Amacr Alpha-methylacyl-CoA racemase	41801.50
41	IPI00198887.1	P4hb Protein disulfide-isomerase	56915.78
42	IPI00200659.1	Sdha Succinate dehydrogenase [ubiquinone] flavoprotein subunit, mitochondrial	71569.76
43	IPI00210029.1	Decr2 Peroxisomal 2,4-dienoyl-CoA reductase	31272.29
44	IPI00210444.5	Hmgcs2 Hydroxymethylglutaryl-CoA synthase, mitochondrial	56875.68
45	IPI00231148.8	Gpd1 Glycerol-3-phosphate dehydrogenase [NAD+], cytoplasmic	37428.25

46	IPI00193485.2	Idh2 Isocitrate dehydrogenase [NADP], mitochondrial	50934.94
47	IPI00231774.6	Maob Amine oxidase [flavin-containing] B	58421.43
48	IPI00209690.1	Ephx1 Epoxide hydrolase 1	52547.88
49	IPI00208203.2	Peci Peroxisomal delta3, delta2-enoyl-Coenzyme A isomerase	42994.03
50	IPI00475676.4	Tas1r2 Delta-1-pyrroline-5-carboxylate dehydrogenase, mitochondrial	61829.75
51	IPI00196656.2	Srprb Ba1-667	107383.30
52	IPI00326972.6	Ces3 Carboxylesterase 3	62107.82
53	IPI00327518.4	Arg1 Arginase-1	36480.91
54	IPI00369954.2	Pipox Pipecolic acid oxidase	43862.61
55	IPI00366293.3	Tst Thiosulfate sulfurtransferase	33385.77
56	IPI00205332.4	Etfa Electron transfer flavoprotein subunit alpha, mitochondrial	34929.47
57	IPI00231253.5	Hsd17b10 3-hydroxyacyl-CoA dehydrogenase type-2	27228.57
58	IPI00324741.2	Pdia3 Protein disulfide-isomerase A3	57043.07
59	IPI00198750.1	Acot12 Acyl-coenzyme A thioesterase 12	61978.86
60	IPI00210139.1	Otc Ornithine carbamoyltransferase, mitochondrial	39860.83
61	IPI00358163.3	Slc25a13 similar to Calcium-binding mitochondrial carrier protein Aralar2	74351.98
62	IPI00421874.4	Vdac1 Voltage-dependent anion-selective channel protein 1	30736.57
63	IPI00781636.1	Acsm2 Protein	64427.12
64	IPI00326140.3	Pzp Alpha-1-macroglobulin	167018.90
65	IPI00358033.1	Ndufs1 NADH-ubiquinone oxidoreductase 75 kDa subunit, mitochondrial	79361.70
66	IPI00332027.7	Bhmt Betaine--homocysteine S-methyltransferase 1	44947.86
67	IPI00327781.1	Cyp2c Cytochrome P450 2C11	57144.53
68	IPI00327079.5	Gstk1 Glutathione S-transferase kappa 1	25476.28
69	IPI00364925.3	Dhtkd1 Probable 2-oxoglutarate dehydrogenase E1 component DHKTD1, mitochondrial	102576.50
70	IPI00393599.3	LOC690745 similar to MOCO sulphurase C-terminal domain containing 1	37766.40
71	IPI00231292.6	Hrsp12 Ribonuclease UK114	14479.67
72	IPI00421539.3	Aco2 Aconitate hydratase, mitochondrial	85380.08
73	IPI00365985.4	Tra1 93 kDa protein	92474.11
74	IPI00193765.2	Ctsc Dipeptidyl-peptidase 1	52201.72
75	IPI00212811.1	Ctsb Cathepsin B	37445.62
76	IPI00209807.12	Sardh Sarcosine dehydrogenase, mitochondrial	101578.90
77	IPI00200466.3	Slc25a5 ADP/ATP translocase 2	32880.15
78	IPI00371236.3	Tufm Elongation factor Tu, mitochondrial	49491.04
79	IPI00558576.2	Lonp2 Peroxisomal Lon protease homolog 2	94334.38
80	IPI00364948.3	Aldh3a2 Fatty aldehyde dehydrogenase	54047.38
81	IPI00230788.6	Car3 Carbonic anhydrase 3	29412.72
82	IPI00364321.3	Etfb Electron transfer flavoprotein subunit beta	27670.06
83	IPI00213057.2	Acadvl Very long-chain specific acyl-CoA dehydrogenase, mitochondrial	71244.98
84	IPI00204118.1	Aifm1 Apoptosis-inducing factor 1, mitochondrial	66680.92
85	IPI00362963.1	RGD1310224 Similar to RIKEN cDNA 1810022C23	33665.14
86	IPI00363265.3	Hspa9 Stress-70 protein, mitochondrial	73811.90
87	IPI00870151.1	Bucs1 butyryl Coenzyme A synthetase 1	39651.20
88	IPI00189813.1	Acta1 Actin, alpha skeletal muscle	42023.86
89	IPI00191711.1	LOC259246 Major urinary protein	20723.51
90	IPI00190701.5	Apoe Apolipoprotein E	35731.37
91	IPI00212014.2	Vcp Transitional endoplasmic reticulum ATPase	89477.95
92	IPI00198324.1	Cyp2b3 Cytochrome P450 2B3	56348.04
93	IPI00211225.1	Acadl Long-chain specific acyl-CoA dehydrogenase, mitochondrial	47842.46
94	IPI00211779.1	Prdx1 Peroxiredoxin-1	22095.32
95	IPI00324302.3	Acat1 Acetyl-CoA acetyltransferase, mitochondrial	44666.50

96	IPI00358005.1	Chdh Choline dehydrogenase	66346.48
97	IPI00193279.1	Oat Ornithine aminotransferase, mitochondrial	48302.11
98	IPI00388265.2	Pgcp 48 kDa protein	48068.85
99	IPI00202658.1	Hibadh 3-hydroxyisobutyrate dehydrogenase, mitochondrial	35279.60
100	IPI00363176.1	Zadh2 zinc binding alcohol dehydrogenase, domain containing 2	40450.14
101	IPI00764690.2	Mtch2 mitochondrial carrier homolog 2	34447.39
102	IPI00204774.1	LOC501232 Liver carboxylesterase B-1	62454.86
103	IPI00212731.1	Ctsd Cathepsin D	44651.93
104	IPI00203690.5	Aldh9a1 4-trimethylaminobutyraldehyde dehydrogenase	56432.66
105	IPI00231106.5	Mpst 3-mercaptopyruvate sulfurtransferase	32919.45
106	IPI00194045.1	Idh1 Isocitrate dehydrogenase [NADP] cytoplasmic	46704.57
107	IPI00191728.1	Calr Calreticulin	47965.90
108	IPI00365929.1	Pdia6 protein disulfide isomerase associated 6	48729.69
109	IPI00411230.3	Gstm2 Glutathione S-transferase Mu 2	25685.97
110	IPI00765682.2	Pcca propionyl-coenzyme A carboxylase, alpha polypeptide	79943.18
111	IPI00215093.1	Ogdh 2-oxoglutarate dehydrogenase E1 component, mitochondrial	116221.50
112	IPI00202370.3	Maoa similar to Amine oxidase [flavin-containing] A	98012.69
113	IPI00188924.4	Uqcrc2 Cytochrome b-c1 complex subunit 2, mitochondrial	48366.24
114	IPI00213584.3	Agxt2 Alanine--glyoxylate aminotransferase 2, mitochondrial	57395.82
115	IPI00195109.3	Shmt2 Serine hydroxymethyltransferase	55729.75
116	IPI00327469.1	Ahsg Alpha-2-HS-glycoprotein	37958.24
117	IPI00231473.4	Cyp2d2 Cytochrome P450 2D26	57392.14
118	IPI00231359.3	Acads Acyl-Coenzyme A dehydrogenase, short chain	44939.09
119	IPI00213659.3	Decr1 2,4-dienoyl-CoA reductase, mitochondrial	36109.73
120	IPI00190790.1	Fabp1 Fatty acid-binding protein, liver	14263.30
121	IPI00230897.5	Hbb Hemoglobin subunit beta-1	15969.25
122	IPI00195372.1	Eef1a1 Elongation factor 1-alpha 1	50082.16
123	IPI00212220.2	Pdia4 Protein disulfide-isomerase A4	72674.80
124	IPI00554106.2	Acaa1 Isoform 2 of 3-ketoacyl-CoA thiolase A, peroxisomal	39085.98
125	IPI00230889.5	Mgst1 Microsomal glutathione S-transferase 1	17460.23
126	IPI00324380.3	Ttr Transthyretin	15709.92
127	IPI00207891.2	Vdac3 31 kDa protein	30892.42
128	IPI00231200.5	Por NADPH--cytochrome P450 reductase	76914.30
129	IPI00230857.7	Ak2 Adenylate kinase isoenzyme 2, mitochondrial	26362.55
130	IPI00211127.1	Ass1 Argininosuccinate synthase	46466.94
131	IPI00421888.3	Anxa6 Annexin A6	75706.58
132	IPI00205417.5	Slc27a2 Very long-chain acyl-CoA synthetase	70648.55
133	IPI00190759.2	Fgg Isoform Gamma-B of Fibrinogen gamma chain	50600.47
134	IPI00369217.1	Trap1 Heat shock protein 75 kDa, mitochondrial	80410.88
135	IPI00203054.2	Acsf2 Acyl-CoA synthetase family member 2, mitochondrial	67842.92
136	IPI00195585.1	Rdh7 Retinol dehydrogenase 3	35639.48
137	IPI00205745.3	Prdx5 Isoform Mitochondrial of Peroxiredoxin-5, mitochondrial	22164.57
138	IPI00209908.1	mt-Co2;mt-Co3 Cytochrome c oxidase subunit 2	25925.07
139	IPI00197711.1	Ldha L-lactate dehydrogenase A chain	36427.36
140	IPI00209893.4	RGD1308772 similar to F11C1.5a	226079.30
141	IPI00211096.1	Hsd11b1 Isoform 11-HSD1A of Corticosteroid 11-beta-dehydrogenase isozyme 1	31862.52
142	IPI00204365.2	Rpn1 Ribophorin I	68358.76
143	IPI00471539.4	Suclg2 Suclg2 protein	46958.84
144	IPI00555278.3	Gulo L-gulonolactone oxidase	50582.38
145	IPI00564133.1	Kat3 Kynurenine--oxoglutarate transaminase 3	51011.37

146	IPI00231782.7	Hsd3b5 3 beta-hydroxysteroid dehydrogenase type 5	42179.70
147	IPI00198327.2	Vdac2 Voltage-dependent anion-selective channel protein 2	31725.62
148	IPI00361686.5	C1qbp Complement component 1 Q subcomponent-binding protein, mitochondrial	30977.52
149	IPI00212015.1	Acadm Medium-chain specific acyl-CoA dehydrogenase, mitochondrial	46525.83
150	IPI00231864.5	Cycs Cytochrome c, somatic	11598.02
151	IPI00373331.2	Lactb lactamase, beta	60410.13
152	IPI00205374.1	Hmgcl Hydroxymethylglutaryl-CoA lyase, mitochondrial	34169.71
153	IPI00190499.5	Tpp1 Tripeptidyl-peptidase 1	61293.95
154	IPI00212110.1	Ugt2b UDP-glucuronosyltransferase 2B2	60945.65
155	IPI00361193.5	Aldh1l2 similar to aldehyde dehydrogenase 1 family, member L2	101674.90
156	IPI00471530.2	Lap3 Isoform 1 of Cytosol aminopeptidase	56114.77
157	IPI00200489.1	Mlycd Isoform Mitochondrial of Malonyl-CoA decarboxylase, mitochondrial	54727.34
158	IPI00190557.2	Phb2 Prohibitin-2	33291.91
159	IPI00209115.2	Slc25a3 Slc25a3 protein (Solute carrier family 25 (Mitochondrial carrier	39595.54
160	IPI00231643.5	Sod1 Superoxide dismutase [Cu-Zn]	15901.80
161	IPI00194324.2	Pdhb Pyruvate dehydrogenase E1 component subunit beta, mitochondrial	38957.08
162	IPI00211100.1	Akr1c14 3-alpha-hydroxysteroid dehydrogenase	37003.95
163	IPI00198467.1	Hadhb Trifunctional enzyme subunit beta, mitochondrial	51381.60
164	IPI00198966.3	Abat 50 kDa protein	50222.72
165	IPI00367889.1	Tysnd1 Trypsin domain containing 1	58949.51
166	IPI00214398.1	Mosc2 MOSC domain-containing protein 2, mitochondrial	38223.69
167	IPI00211959.1	Agxt Isoform Mitochondrial of Serine--pyruvate aminotransferase, mitochondrial	45805.08
168	IPI00195160.1	Psap Sulfated glycoprotein 1	61083.70
169	IPI00199636.1	Canx Calnexin	67212.71
170	IPI00454288.1	Atp5c1 ATP synthase gamma chain	67677.30
171	IPI00214373.1	Aadat Kynurenine/alpha-aminoadipate aminotransferase mitochondrial	47753.74
172	IPI00372804.2	Sccpdh Probable saccharopine dehydrogenase	47058.14
173	IPI00766371.1	LOC293589 hypothetical protein LOC293589	54983.86
174	IPI00471584.7	Hsp90ab1 Heat shock protein HSP 90-beta	83229.17
175	IPI00365545.1	Dld Dihydrolipoyl dehydrogenase, mitochondrial	54004.15
176	IPI00205389.6	Fgb Isoform 1 of Fibrinogen beta chain	54200.66
177	IPI00193716.1	Ivd Isovaleryl-CoA dehydrogenase, mitochondrial	46405.80
178	IPI00195423.1	Ugt2b37 UDP-glucuronosyltransferase 2B5	60553.29
179	IPI00471911.7	Aldob Fructose-bisphosphate aldolase B	39593.23
180	IPI00205157.1	Hadh Hydroxyacyl-coenzyme A dehydrogenase, mitochondrial	34425.90
181	IPI00373134.2	Fahd2a similar to fumarylacetoacetate hydrolase domain containing 2A	40314.03
182	IPI00205036.1	LOC360504 hemoglobin alpha 2 chain	15274.78
183	IPI00231013.2	Cyb5 Isoform Short of Cytochrome b5	11399.65
184	IPI00209363.1	Slc25a10 Mitochondrial dicarboxylate carrier (Solute carrier family 25 (Mitochondrial carrier	31434.09
185	IPI00231264.6	Pon1 Serum paraoxonase/arylesterase 1	39471.20
186	IPI00193919.5	Suox Sulfite oxidase, mitochondrial	60767.98
187	IPI00366416.2	Cyc1 similar to cytochrome c-1	35411.98
188	IPI00367152.1	Ndufv2 NADH dehydrogenase [ubiquinone] flavoprotein 2, mitochondrial	27360.89
189	IPI00192078.2	Bphl Biphenyl hydrolase-like	32802.13
190	IPI00198039.1	Ethe1 Ethylmalonic encephalopathy 1	27659.00
191	IPI00655249.1	LOC684538 Enoyl-CoA hydratase domain-containing protein 3, mitochondrial	32364.86
192	IPI00199482.2	Gstm4 Similar to glutathione transferase GSTM7-7	25536.95
193	IPI00211593.1	Sod2 Superoxide dismutase [Mn], mitochondrial	24658.58
194	IPI00480820.4	Pgrmc1 Membrane-associated progesterone receptor component 1	21584.70
195	IPI00471647.1	Ndufs2 NADH dehydrogenase [ubiquinone] iron-sulfur protein 2, mitochondrial	52527.64

196	IPI00203473.3	Ugt2b36 UDP-glucuronosyltransferase 2B4	61020.25
197	IPI00231204.5	Pxmp2 Peroxisomal membrane protein 2	22562.24
198	IPI00763831.1	LOC679565 similar to acyl-Coenzyme A binding domain containing 5	62087.35
199	IPI00324912.6	Cyp2e1 Cytochrome P450 2E1	56590.81
200	IPI00230838.5	Atp5h ATP synthase subunit d, mitochondrial	18751.60
201	IPI00191176.4	Cyp2c6 Cytochrome P450PB-1	42247.14
202	IPI00360618.3	RGD1564894 RGD1564894 protein	33964.06
203	IPI00464785.1	Ppgb Protective protein for beta-galactosidase	51183.02
204	IPI00194022.5	Crot Peroxisomal carnitine O-octanoyltransferase	70257.42
205	IPI00326433.11	Hspe1;Hspd1 10 kDa heat shock protein, mitochondrial	10894.86
206	IPI00389152.4	LOC688869;Cox6b1 similar to cytochrome c oxidase, subunit VIb polypeptide 1	10064.88
207	IPI00370752.3	Nit2 Nitrilase homolog 2	30681.66
208	IPI00364761.1	Lactb2 Beta-lactamase-like protein 2	32463.71
209	IPI00231714.3	Dlat Dihydrolipoyllysine-residue acetyltransferase component of pyruvate dehydrogenase complex, mitochondrial	67123.58
210	IPI00201276.5	Acp2 Lysosomal acid phosphatase	48288.52
211	IPI00202616.1	Ndufs3 NADH dehydrogenase (ubiquinone) Fe-S protein 3	30207.63
212	IPI00206948.1	Retsat All-trans-retinol 13,14-reductase	67487.41
213	IPI00213569.1	Ugt1a1 UDP-glucuronosyltransferase 1-1	59623.84
214	IPI00198325.1	Cyp2d4v1 Cytochrome P450 2D4	56661.35
215	IPI00555265.1	Nnt Nicotinamide nucleotide transhydrogenase	113796.40
216	IPI00190240.1	Rps27a Ribosomal protein S27a	17939.48
217	IPI00212316.1	Mttp microsomal triglyceride transfer protein	99124.76
218	IPI00200591.1	LOC299282 Serine protease inhibitor A3L	46248.14
219	IPI00565267.1	Fmo3 Dimethylaniline monooxygenase [N-oxide-forming] 3	59921.54
220	IPI00190020.3	Atp2a2 Isoform SERCA2B of Sarcoplasmic/endoplasmic reticulum calcium ATPase 2	115317.00
221	IPI00205076.1	Lonp1 Lon protease homolog, mitochondrial	105726.40
222	IPI00196696.6	Cyp2a1 Cytochrome P450 2A1	55959.18
223	IPI00231064.7	Aldh3a1 Aldehyde dehydrogenase, dimeric NADP-preferring	50306.73
224	IPI00558154.1	LOC100125372 60 kDa protein	59976.52
225	IPI00195673.1	Tubb6 Tubulin, beta 6	50027.16
226	IPI00339123.2	Acox3 Peroxisomal acyl-coenzyme A oxidase 3	78396.07
227	IPI00214787.1	Slc16a1 Monocarboxylate transporter 1	53203.47
228	IPI00763872.1	LOC681913 Similar to Maleylacetoacetate isomerase	23945.56
229	IPI00214454.2	Gcsh Glycine cleavage system H protein, mitochondrial	18473.39
230	IPI00215574.5	Dci 3,2-trans-enoyl-CoA isomerase, mitochondrial	32234.02
231	IPI00358757.5	Hint2 histidine triad nucleotide binding protein 2	17369.26
232	IPI00197555.6	Suclg1 Suclg1 protein	36125.00
233	IPI00325135.3	Ywhae 14-3-3 protein epsilon	29155.42
234	IPI00190402.1	Ugt2b1 UDP-glucuronosyltransferase 2B1	60445.31
235	IPI00365381.3	Pex26 Peroxisome biogenesis factor 26	33139.72
236	IPI00515762.1	Dmgdh Dimethylglycine dehydrogenase	95917.41
237	IPI00371385.3	RGD1309350 similar to Hypothetical transthyretin-like protein R09H10.3 in chromosome IV	15000.45
238	IPI00231639.7	Gstm1 Glutathione S-transferase Mu 1	25897.11
239	IPI00211507.3	Hpd 4-hydroxyphenylpyruvate dioxygenase	45083.91
240	IPI00231028.2	RGD1303003 ES1 protein homolog, mitochondrial	28154.87
241	IPI00364591.2	RGD1308734 Putative phospholipase B-like 1	62986.76
242	IPI00194222.1	Cox4i1 Cytochrome c oxidase subunit 4 isoform 1, mitochondrial	19502.08
243	IPI00364431.2	Sucla2 succinate-Coenzyme A ligase, ADP-forming, beta subunit	50274.26
244	IPI00764232.2	LOC687295 similar to translocase of inner mitochondrial membrane 50 homolog isoform 1	14257.50
245	IPI00207933.2	Dhrs4 dehydrogenase/reductase (SDR family) member 4	29802.84

246	IPI00454403.1	Isoc1 Isochorismatase domain-containing protein 1	31982.00
247	IPI00231662.6	Cyb5r3 Isoform 1 of NADH-cytochrome b5 reductase 3	34152.73
248	IPI00209290.3	Vapa Vesicle-associated membrane protein-associated protein A	27823.28
249	IPI00194550.5	Cth Cystathionine gamma-lyase	43577.32
250	IPI00454401.1	Dhrs7 Down-regulated in nephrectomized rat kidney #3	36378.20
251	IPI00196107.1	Atp5f1 ATP synthase subunit b, mitochondrial	28850.49
252	IPI00195593.1	Cpt2 Carnitine O-palmitoyltransferase 2, mitochondrial	74063.50
253	IPI00870114.1	Gcdh glutaryl-Coenzyme A dehydrogenase	49681.54
254	IPI00382270.1	Slc25a15 Ab1-114	36896.87
255	IPI00361819.2	Ociad1 OCIA domain-containing protein 1	27641.79
256	IPI00195516.6	Hpx Hemopexin	51318.33
257	IPI00213436.2	Ndufa4 Ndufa4 protein	9320.87
258	IPI00191416.1	Slc27a5 Bile acyl-CoA synthetase	76217.12
259	IPI00382228.1	Glyat 39 kDa protein	39427.87
260	IPI00231638.6	Gsta3;Gsta2;Gsta1 Glutathione S-transferase alpha-1	25590.55
261	IPI00192336.1	Anp32b Acidic leucine-rich nuclear phosphoprotein 32 family member B	31042.08
262	IPI00365813.3	RGD1565338 similar to Voltage-dependent anion-selective channel protein 1	35017.96
263	IPI00327694.3	Slc25a1 Tricarboxylate transport protein, mitochondrial	33813.84
264	IPI00373418.3	Dbt dihydrolipoamide branched chain transacylase E2	53240.08
265	IPI00564294.2	- 34 kDa protein	33718.22
266	IPI00327991.3	Cyp2c23 Cytochrome P450 2C23	56396.72
267	IPI00327335.3	Sult1b1 Sulfotransferase family cytosolic 1B member 1	34812.77
268	IPI00202498.1	REVPdgfra Alpha-type platelet-derived growth factor receptor	122564.60
269	IPI00764614.2	Nfx1 124 kDa protein	123847.30
270	IPI00560967.1	RGD1310475 hypothetical protein LOC293949	35126.32
271	IPI00204316.1	Atp5j ATP synthase-coupling factor 6, mitochondrial	12486.58
272	IPI00551702.2	Dlst Dihydrolipoyllysine-residue succinyltransferase component of 2-oxoglutarate dehydrogenase complex, mitochondrial	48894.45
273	IPI00231745.8	Fbp1 Fructose-1,6-bisphosphatase 1	39584.17
274	IPI00231478.5	Scarb2 Lysosome membrane protein 2	54056.44
275	IPI00188158.1	Hmgcs1 Hydroxymethylglutaryl-CoA synthase, cytoplasmic	57397.53
276	IPI00189759.1	Ndufa10 NADH dehydrogenase 1 alpha subcomplex 10-like protein	40518.61
277	IPI00210120.2	Vtn Aa1018	55924.79
278	IPI00231069.5	Dbi Acyl-CoA-binding protein	10021.15
279	IPI00207847.1	RGD1309228 Transmembrane protein C2orf18 homolog	41065.59
280	IPI00205255.1	Pigr Polymeric immunoglobulin receptor	84745.16
281	IPI00188967.1	LOC500183 Ig kappa chain C region, A allele	11724.61
282	IPI00193425.1	Bsg Isoform 2 of Basigin	29567.00
283	IPI00193171.1	Npc2 Epididymal secretory protein 1	16353.42
284	IPI00231260.5	Prdx6 Peroxiredoxin-6	24802.98
285	IPI00214031.1	Slco1a4 Solute carrier organic anion transporter family member 1A4	73203.16
286	IPI00367246.1	Nudt19 Nucleoside diphosphate-linked moiety X motif 19, mitochondrial	39913.27
287	IPI00203152.1	Ctbs Di-N-acetylchitobiase	41504.36
288	IPI00327626.1	Ugt2b5 UDP-glucuronosyltransferase 2B3	60485.04
289	IPI00870183.1	Cisd1 CDGSH iron sulfur domain 1	12089.14
290	IPI00193258.7	Pah Phenylalanine-4-hydroxylase	51789.41
291	IPI00198717.8	Mdh1 Malate dehydrogenase, cytoplasmic	36460.07
292	IPI00382223.1	RGD1308874 Ab2-305	43539.42
293	IPI00363571.3	LOC680409 similar to Proline oxidase, mitochondrial precursor (Proline dehydrogenase) isoform 2	68078.41
294	IPI00231963.5	Ddt D-dopachrome decarboxylase	13124.84

295	IPI00387771.6	Ppia Peptidyl-prolyl cis-trans isomerase A	17862.81
296	IPI00210423.4	Pex14 Peroxisomal biogenesis factor 14	40911.64
297	IPI00372845.2	Gstt1 28 kDa protein	27580.42
298	IPI00212708.2	Fetub Fetub protein	43141.72
299	IPI00213677.1	Arf2 ADP-ribosylation factor 2	20732.76
300	IPI00393921.2	Atad5 similar to chromosome fragility associated gene 1	205312.20
301	IPI00561751.1	Ndufs5 NADH dehydrogenase (ubiquinone) Fe-S protein 5b	12691.50
302	IPI00365962.1	Ndufs7 NADH dehydrogenase (Ubiquinone) Fe-S protein 7	23929.40
303	IPI00369093.1	Uqcrh Cytochrome b-c1 complex subunit 6, mitochondrial	10416.97
304	IPI00471645.1	Ddost Dolichyl-di-phosphooligosaccharide-protein glycotransferase	48865.02
305	IPI00204128.2	RGD1561381 similar to microsomal glutathione S-transferase 3	16752.52
306	IPI00205693.1	Atp1a2 Sodium/potassium-transporting ATPase subunit alpha-2	112145.60
307	IPI00231192.5	MGC72973;LOC689064;LOC100134871 Hemoglobin subunit beta-2	15972.29
308	IPI00204941.2	Dnaja3 Tid-1 long isoform	52366.46
309	IPI00214152.1	Hagh Hydroxyacylglutathione hydrolase	28877.78
310	IPI00360061.3	Fam82a Protein FAM82A	47187.46
311	IPI00191112.1	Ndufab1 NADH dehydrogenase (ubiquinone) 1, alpha/beta subcomplex, 1	17503.07
312	IPI00202580.2	Cyp2d3 Cytochrome P450 2D3	57105.55
313	IPI00382226.1	RGD1306939 Ab2-162	144618.50
314	IPI00464794.1	Cryz Quinone oxidoreductase	34953.15
315	IPI00202584.1	Cyp2d5 Cytochrome P450 2D10	57039.44
316	IPI00187967.1	Tmem205 transmembrane protein 205	21171.21
317	IPI00231368.5	Txn1 Thioredoxin	11665.66
318	IPI00768108.1	PRP-2 similar to CG7896-PA isoform 1	166723.00
319	IPI00207072.1	Ndufs6 NADH dehydrogenase [ubiquinone] iron-sulfur protein 6, mitochondrial	12774.62
320	IPI00213847.2	Grn Granulins	63492.03
321	IPI00326305.3	Atp1a1 Sodium/potassium-transporting ATPase subunit alpha-1	112982.00
322	IPI00209113.3	Myh9 Myosin-9	226196.40
323	IPI00231659.3	Tmed10 Transmembrane emp24 domain-containing protein 10	24841.85
324	IPI00209283.3	Vapb Vesicle-associated membrane protein-associated protein B	26898.99
325	IPI00210008.1	Tmed2 Transmembrane emp24 domain-containing protein 2	22718.35
326	IPI00362054.2	Rimbp3 similar to Peripheral-type benzodiazepine receptor-associated protein 1	178145.50
327	IPI00360993.3	Gldc glycine decarboxylase	113846.50
328	IPI00192310.2	Bcam Lutheran antigen	70854.26
329	IPI00194097.5	Gc Vitamin D-binding protein	53509.07
330	IPI00193151.1	Qdpr Dihydropteridine reductase	25535.87
331	IPI00192301.2	Gpx1 Glutathione peroxidase 1	22244.37
332	IPI00421939.1	Scgb3a2 Pneumo secretory protein 1	10035.68
333	IPI00194081.4	LOC686860 34 kDa protein	34160.89
334	IPI00388640.3	Nlrp1a similar to NACHT, leucine rich repeat and PYD containing 1	145790.30
335	IPI00362992.4	Aldh5a1 Isoform Long of Succinate-semialdehyde dehydrogenase, mitochondrial	56095.91

Appendix 5: Proteins identified in whole liver tissue homogenate after PQ-treatment by ^{18}O-labeling using LTQ-MS analyses.

	Accession	Reference	MW
	RSp	Scan(s), File	Sp
1	IPI00210644.1	Cps1 Carbamoyl-phosphate synthase [ammonia], mitochondrial	164474.80
2	IPI00197770.1	Aldh2 Aldehyde dehydrogenase, mitochondrial	56452.72
3	IPI00551812.1	Atp5b ATP synthase subunit beta, mitochondrial	56318.59
4	IPI00196725.5	Aldh1l1 10-formyltetrahydrofolate dehydrogenase	99063.85
5	IPI00231742.5	Cat Catalase	59719.59
6	IPI00201413.1	Acaa2 3-ketoacyl-CoA thiolase, mitochondrial	41844.49
7	IPI00201262.1	LOC297568;Mug1;Mug2 Alpha-1-inhibitor 3	163669.20
8	IPI00389611.3	Rgn Regucalcin	33368.38
9	IPI00206624.1	Hspa5 78 kDa glucose-regulated protein	72302.52
10	IPI00210435.2	Pcx Pyruvate carboxylase, mitochondrial	129694.90
11	IPI00197696.2	Mdh2 Malate dehydrogenase, mitochondrial	35660.82
12	IPI00205018.2	Aldh6a1 Methylmalonate-semialdehyde dehydrogenase [acylating], mitochondrial	57882.70
13	IPI00188989.1	Acsl1 Long-chain-fatty-acid--CoA ligase 1	78128.34
14	IPI00324633.2	Glud1 Glutamate dehydrogenase 1, mitochondrial	61377.36
15	IPI00189813.1	Acta1 Actin, alpha skeletal muscle	42023.86
16	IPI00396910.1	Atp5a1 ATP synthase subunit alpha, mitochondrial	59716.74
17	IPI00196656.2	Srprb Ba1-667	107383.30
18	IPI00210920.1	Got2 Aspartate aminotransferase, mitochondrial	47284.15
19	IPI00231745.8	Fbp1 Fructose-1,6-bisphosphatase 1	39584.17
20	IPI00205332.4	Etfa Electron transfer flavoprotein subunit alpha, mitochondrial	34929.47
21	IPI00358163.3	Slc25a13 similar to Calcium-binding mitochondrial carrier protein Aralar2	74351.98
22	IPI00327518.4	Arg1 Arginase-1	36480.91
23	IPI00332027.7	Bhmt Betaine--homocysteine S-methyltransferase 1	44947.86
24	IPI00205036.1	LOC360504 hemoglobin alpha 2 chain	15274.78
25	IPI00210444.5	Hmgcs2 Hydroxymethylglutaryl-CoA synthase, mitochondrial	56875.68
26	IPI00339148.2	Hspd1 60 kDa heat shock protein, mitochondrial	60917.48
27	IPI00230897.5	Hbb Hemoglobin subunit beta-1	15969.25
28	IPI00359623.3	LOC683474 similar to aldehyde dehydrogenase 8 family, member A1 isoform 2	53387.29
29	IPI00230788.6	Car3 Carbonic anhydrase 3	29412.72
30	IPI00326140.3	Pzp Alpha-1-macroglobulin	167018.90
31	IPI00207941.1	Dmgdh Dimethylglycine dehydrogenase, mitochondrial	95987.51
32	IPI00209807.12	Sardh Sarcosine dehydrogenase, mitochondrial	101578.90
33	IPI00476295.7	Ahcy Adenosylhomocysteinase	47507.29
34	IPI00471911.7	Aldob Fructose-bisphosphate aldolase B	39593.23
35	IPI00203690.5	Aldh9a1 4-trimethylaminobutyraldehyde dehydrogenase	56432.66
36	IPI00372498.1	Dak Dihydroxyacetone kinase	59406.42
37	IPI00190179.3	Pygl Glycogen phosphorylase, liver form	97421.10
38	IPI00325599.4	Asl Argininosuccinate lyase	51517.34

39	IPI00475676.4	Tas1r2 Delta-1-pyrroline-5-carboxylate dehydrogenase, mitochondrial	61829.75
40	IPI00480639.3	C3 Complement C3 (Fragment)	186341.70
41	IPI00480620.1	Bdh1 3-hydroxybutyrate dehydrogenase, type 1	38308.38
42	IPI00231253.5	Hsd17b10 3-hydroxyacyl-CoA dehydrogenase type-2	27228.57
43	IPI00211127.1	Ass1 Argininosuccinate synthase	46466.94
44	IPI00324741.2	Pdia3 Protein disulfide-isomerase A3	57043.07
45	IPI00190790.1	Fabp1 Fatty acid-binding protein, liver	14263.30
46	IPI00208917.4	Aldh7a1 similar to aldehyde dehydrogenase family 7, member A1	58711.46
47	IPI00195585.1	Rdh7 Retinol dehydrogenase 3	35639.48
48	IPI00411230.3	Gstm2 Glutathione S-transferase Mu 2	25685.97
49	IPI00231292.6	Hrsp12 Ribonuclease UK114	14479.67
50	IPI00194550.5	Cth Cystathionine gamma-lyase	43577.32
51	IPI00189795.1	Tuba1a Tubulin alpha-1A chain	50103.65
52	IPI00211392.1	Ftcd Formimidoyltransferase-cyclodeaminase	58876.71
53	IPI00207146.1	MGC72973 Zero beta-1 globin	16012.26
54	IPI00231639.7	Gstm1 Glutathione S-transferase Mu 1	25897.11
55	IPI00197711.1	Ldha L-lactate dehydrogenase A chain	36427.36
56	IPI00763872.1	LOC681913 Similar to Maleylacetoacetate isomerase	23945.56
57	IPI00189819.1	Actb Actin, cytoplasmic 1	41709.74
58	IPI00212622.2	Hadha Trifunctional enzyme subunit alpha, mitochondrial	82612.66
59	IPI00205561.1	Acox2 Peroxisomal acyl-coenzyme A oxidase 2	76750.05
60	IPI00200661.1	Fasn Fatty acid synthase	272475.30
61	IPI00208026.1	Selenbp1 Selenium-binding protein 1	52498.52
62	IPI00231260.5	Prdx6 Peroxiredoxin-6	24802.98
63	IPI00470304.1	Pon3 Serum paraoxonase/lactonase 3	39433.25
64	IPI00201436.1	Mat1a S-adenosylmethionine synthetase isoform type-1	43670.11
65	IPI00365985.4	Tra1 93 kDa protein	92474.11
66	IPI00230889.5	Mgst1 Microsomal glutathione S-transferase 1	17460.23
67	IPI00210566.3	Hsp90aa1 Heat shock protein HSP 90-alpha	84761.81
68	IPI00209113.3	Myh9 Myosin-9	226196.40
69	IPI00193258.7	Pah Phenylalanine-4-hydroxylase	51789.41
70	IPI00231767.5	Tpi1 Triosephosphate isomerase	26831.76
71	IPI00207003.1	Aco1 Cytoplasmic aconitate hydratase	98065.48
72	IPI00370752.3	Nit2 Nitrilase homolog 2	30681.66
73	IPI00421513.8	Got1 Aspartate aminotransferase, cytoplasmic	46399.55
74	IPI00195372.1	Eef1a1 Elongation factor 1-alpha 1	50082.16
75	IPI00207601.1	Hao1 Hydroxyacid oxidase 1, liver	40942.25
76	IPI00231426.6	Pgk1 Phosphoglycerate kinase 1	44510.01
77	IPI00211507.3	Hpd 4-hydroxyphenylpyruvate dioxygenase	45083.91
78	IPI00553996.3	Zxdc 79 kDa protein	78483.41
79	IPI00231638.6	Gsta3;Gsta2;Gsta1 Glutathione S-transferase alpha-1	25590.55
80	IPI00395267.1	Pck1 Phosphoenolpyruvate carboxykinase, cytosolic [GTP]	69371.10

81	IPI00421364.1	Shmt1 Serine hydroxymethyltransferase	75326.30
82	IPI00232011.9	Ehhadh Peroxisomal bifunctional enzyme	78608.45
83	IPI00192076.3	- 100 kDa protein	100174.60
84	IPI00197703.2	Apoa1 Apolipoprotein A-I	30043.23
85	IPI00331983.5	Adh1 Alcohol dehydrogenase 1	39619.57
86	IPI00203214.6	Eef2 Elongation factor 2	95223.02
87	IPI00366293.3	Tst Thiosulfate sulfurtransferase	33385.77
88	IPI00214480.1	Fah Fumarylacetoacetase	45946.07
89	IPI00205745.3	Prdx5 Isoform Mitochondrial of Peroxiredoxin-5, mitochondrial	22164.57
90	IPI00464815.11	Eno1 Alpha-enolase	47098.29
91	IPI00231139.6	Tkt transketolase	71113.45
92	IPI00190402.1	Ugt2b1 UDP-glucuronosyltransferase 2B1	60445.31
93	IPI00211100.1	Akr1c14 3-alpha-hydroxysteroid dehydrogenase	37003.95
94	IPI00421874.4	Vdac1 Voltage-dependent anion-selective channel protein 1	30736.57
95	IPI00231359.3	Acads Acyl-Coenzyme A dehydrogenase, short chain	44939.09
96	IPI00231641.5	Pgm1 Phosphoglucomutase-1	61364.68
97	IPI00339188.2	Haao 3-hydroxyanthranilate 3,4-dioxygenase	32561.25
98	IPI00194045.1	Idh1 Isocitrate dehydrogenase [NADP] cytoplasmic	46704.57
99	IPI00556987.2	Hgd Homogentisate 1, 2-dioxygenase	49867.58
100	IPI00471539.4	Suclg2 Suclg2 protein	46958.84
101	IPI00213057.2	Acadvl Very long-chain specific acyl-CoA dehydrogenase, mitochondrial	71244.98
102	IPI00198467.1	Hadhb Trifunctional enzyme subunit beta, mitochondrial	51381.60
103	IPI00208205.1	Hspa8 Heat shock cognate 71 kDa protein	70827.34
104	IPI00324302.3	Acat1 Acetyl-CoA acetyltransferase, mitochondrial	44666.50
105	IPI00395281.1	Etfdh Electron transfer flavoprotein-ubiquinone oxidoreductase, mitochondrial	68154.77
106	IPI00202651.1	Fga Isoform 1 of Fibrinogen alpha chain	86631.84
107	IPI00205374.1	Hmgcl Hydroxymethylglutaryl-CoA lyase, mitochondrial	34169.71
108	IPI00326972.6	Ces3 Carboxylesterase 3	62107.82
109	IPI00212220.2	Pdia4 Protein disulfide-isomerase A4	72674.80
110	IPI00197579.2	Tubb5 Isoform 1 of Tubulin beta-5 chain	49639.01
111	IPI00781636.1	Acsm2 Protein	64427.12
112	IPI00564133.1	Kat3 Kynurenine--oxoglutarate transaminase 3	51011.37
113	IPI00325136.5	Scp2 Isoform SCPx of Non-specific lipid-transfer protein	58775.50
114	IPI00392676.3	Blvrb biliverdin reductase B	22083.29
115	IPI00214665.2	Acly ATP citrate lyase isoform 1	120704.00
116	IPI00212015.1	Acadm Medium-chain specific acyl-CoA dehydrogenase, mitochondrial	46525.83
117	IPI00231611.7	Fh1 Isoform Mitochondrial of Fumarate hydratase, mitochondrial	54429.11
118	IPI00210139.1	Otc Ornithine carbamoyltransferase, mitochondrial	39860.83
119	IPI00190701.5	Apoe Apolipoprotein E	35731.37
120	IPI00200466.3	Slc25a5 ADP/ATP translocase 2	32880.15
121	IPI00202658.1	Hibadh 3-hydroxyisobutyrate dehydrogenase, mitochondrial	35279.60
122	IPI00565267.1	Fmo3 Dimethylaniline monooxygenase [N-oxide-forming] 3	59921.54

123	IPI00325765.2	Akr7a2 Aflatoxin B1 aldehyde reductase member 2	40649.32
124	IPI00421428.9	Pgam1 Phosphoglycerate mutase 1	28813.88
125	IPI00207010.2	Baat Bile acid-CoA:amino acid N-acyltransferase	46435.08
126	IPI00231013.2	Cyb5 Isoform Short of Cytochrome b5	11399.65
127	IPI00210823.1	Akr1d1 3-oxo-5-beta-steroid 4-dehydrogenase	37354.09
128	IPI00324019.1	Serpina1 Alpha-1-antiproteinase	46106.61
129	IPI00387771.6	Ppia Peptidyl-prolyl cis-trans isomerase A	17862.81
130	IPI00195803.1	Ugdh UDP-glucose 6-dehydrogenase	54857.36
131	IPI00192301.2	Gpx1 Glutathione peroxidase 1	22244.37
132	IPI00363265.3	Hspa9 Stress-70 protein, mitochondrial	73811.90
133	IPI00231659.3	Tmed10 Transmembrane emp24 domain-containing protein 10	24841.85
134	IPI00212316.1	Mttp microsomal triglyceride transfer protein	99124.76
135	IPI00362070.5	Ugp2 UDP-glucose pyrophosphorylase 2	56987.88
136	IPI00365929.1	Pdia6 protein disulfide isomerase associated 6	48729.69
137	IPI00195516.6	Hpx Hemopexin	51318.33
138	IPI00211989.2	Khk Isoform C of Ketohexokinase	32781.55
139	IPI00197371.4	Gstm6 Glutathione S-transferase, mu 6	25609.96
140	IPI00215107.3	Rpsa 40S ribosomal protein SA	32803.43
141	IPI00204774.1	LOC501232 Liver carboxylesterase B-1	62454.86
142	IPI00214299.6	Cbs Isoform I of Cystathionine beta-synthase	61415.39
143	IPI00193151.1	Qdpr Dihydropteridine reductase	25535.87
144	IPI00208970.1	Upb1 Beta-ureidopropionase	44014.00
145	IPI00231864.5	Cycs Cytochrome c, somatic	11598.02
146	IPI00231358.6	Pfn1 Profilin-1	14947.51
147	IPI00211225.1	Acadl Long-chain specific acyl-CoA dehydrogenase, mitochondrial	47842.46
148	IPI00230942.5	Gstm7 Glutathione S-transferase Yb-3	25664.02
149	IPI00231192.5	MGC72973;LOC689064;LOC100134871 Hemoglobin subunit beta-2	15972.29
150	IPI00196457.1	Sult1c1 Sulfotransferase 1C1	35740.71
151	IPI00205157.1	Hadh Hydroxyacyl-coenzyme A dehydrogenase, mitochondrial	34425.90
152	IPI00231963.5	Ddt D-dopachrome decarboxylase	13124.84
153	IPI00230937.5	Pebp1 Phosphatidylethanolamine-binding protein 1	20788.40
154	IPI00326195.3	Pecr Peroxisomal trans-2-enoyl-CoA reductase	32830.77
155	IPI00211779.1	Prdx1 Peroxiredoxin-1	22095.32
156	IPI00327781.1	Cyp2c Cytochrome P450 2C11	57144.53
157	IPI00362395.4	Esd S-formylglutathione hydrolase	31542.51
158	IPI00211096.1	Hsd11b1 Isoform 11-HSD1A of Corticosteroid 11-beta-dehydrogenase isozyme 1	31862.52
159	IPI00363828.3	Actr3 Actin-related protein 3	47481.05
160	IPI00231774.6	Maob Amine oxidase [flavin-containing] B	58421.43
161	IPI00364948.3	Aldh3a2 Fatty aldehyde dehydrogenase	54047.38
162	IPI00188359.3	Abhd14b Abhydrolase domain containing 14b	22603.70
163	IPI00198717.8	Mdh1 Malate dehydrogenase, cytoplasmic	36460.07
164	IPI00215574.5	Dci 3,2-trans-enoyl-CoA isomerase, mitochondrial	32234.02

165	IPI00551702.2	Dlst Dihydrolipoyllysine-residue succinyltransferase component of 2-oxoglutarate dehydrogenase complex, mitochondrial	48894.45
166	IPI00188858.4	Amacr Alpha-methylacyl-CoA racemase	41801.50
167	IPI00471540.1	Bhmt2 Betaine--homocysteine S-methyltransferase 2	39903.21
168	IPI00655249.1	LOC684538 Enoyl-CoA hydratase domain-containing protein 3, mitochondrial	32364.86
169	IPI00358033.1	Ndufs1 NADH-ubiquinone oxidoreductase 75 kDa subunit, mitochondrial	79361.70
170	IPI00191728.1	Calr Calreticulin	47965.90
171	IPI00231134.4	Gnb2l1 Guanine nucleotide-binding protein subunit beta-2-like 1	35396.76
172	IPI00231643.5	Sod1 Superoxide dismutase [Cu-Zn]	15901.80
173	IPI00337099.2	Acad9 Acad9 protein	68799.78
174	IPI00202584.1	Cyp2d5 Cytochrome P450 2D10	57039.44
175	IPI00191416.1	Slc27a5 Bile acyl-CoA synthetase	76217.12
176	IPI00205906.2	Dpys Dihydropyrimidinase	56778.73
177	IPI00212014.2	Vcp Transitional endoplasmic reticulum ATPase	89477.95
178	IPI00231202.6	Rps8 40S ribosomal protein S8	24190.17
179	IPI00358005.1	Chdh Choline dehydrogenase	66346.48
180	IPI00326948.2	Hsd17b4 Hsd17b4 protein	81037.99
181	IPI00193983.3	Cltc Clathrin heavy chain 1	191475.80
182	IPI00196696.6	Cyp2a1 Cytochrome P450 2A1	55959.18
183	IPI00382202.2	Hp Isoform 2 of Haptoglobin	42447.49
184	IPI00211756.1	Phb Prohibitin	29801.90
185	IPI00360148.3	- 92 kDa protein	92253.54
186	IPI00209045.2	Acox3 76 kDa protein	75810.41
187	IPI00204634.4	Sec14l4 SEC14-like 4	46987.95
188	IPI00364321.3	Etfb Electron transfer flavoprotein subunit beta	27670.06
189	IPI00369774.1	Mettl7b Methyltransferase-like protein 7B	27885.51
190	IPI00196751.2	Hspa1l;Hspa1b;Hspa1a Heat shock 70 kDa protein 1A/1B	70142.24
191	IPI00325135.3	Ywhae 14-3-3 protein epsilon	29155.42
192	IPI00382191.1	Pgd 6-phosphogluconate dehydrogenase, decarboxylating	120448.80
193	IPI00231648.5	Gnmt Glycine N-methyltransferase	32528.35
194	IPI00558154.1	LOC100125372 60 kDa protein	59976.52
195	IPI00231473.4	Cyp2d2 Cytochrome P450 2D26	57392.14
196	IPI00370348.3	- 28 kDa protein	27731.13
197	IPI00230859.5	Akr1a1 Alcohol dehydrogenase [NADP+]	36482.93
198	IPI00214373.1	Aadat Kynurenine/alpha-aminoadipate aminotransferase mitochondrial	47753.74
199	IPI00200659.1	Sdha Succinate dehydrogenase [ubiquinone] flavoprotein subunit, mitochondrial	71569.76
200	IPI00870151.1	Bucs1 butyryl Coenzyme A synthetase 1	39651.20
201	IPI00365545.1	Dld Dihydrolipoyl dehydrogenase, mitochondrial	54004.15
202	IPI00230901.7	Gpt Alanine aminotransferase 1	55073.95
203	IPI00195123.1	Atp5o ATP synthase subunit O, mitochondrial	23382.78
204	IPI00214394.1	Csad Cysteine sulfinic acid decarboxylase	55213.60
205	IPI00200447.2	Adh4 Ac1002	93787.09
206	IPI00193716.1	Ivd Isovaleryl-CoA dehydrogenase, mitochondrial	46405.80

207	IPI00212776.1	Rps3 40S ribosomal protein S3	26657.42
208	IPI00193425.1	Bsg Isoform 2 of Basigin	29567.00
209	IPI00365813.3	RGD1565338 similar to Voltage-dependent anion-selective channel protein 1	35017.96
210	IPI00212478.1	Hbe1 Epsilon 1 globin	16094.46
211	IPI00213422.1	Kmo Kynurenine 3-monooxygenase	54317.66
212	IPI00198324.1	Cyp2b3 Cytochrome P450 2B3	56348.04
213	IPI00324986.1	Gdi1 Rab GDP dissociation inhibitor alpha	50504.22
214	IPI00870114.1	Gcdh glutaryl-Coenzyme A dehydrogenase	49681.54
215	IPI00200593.1	Serpina3k Serine protease inhibitor A3K	46532.19
216	IPI00213569.1	Ugt1a1 UDP-glucuronosyltransferase 1-1	59623.84
217	IPI00231631.13	Eno3 Beta-enolase	46984.37
218	IPI00388209.2	Prkcsh Protein kinase C substrate 80K-H	59181.21
219	IPI00197900.5	Eef1d Translation elongation factor 1-delta subunit	28748.49
220	IPI00421328.1	Usp40 LRRGT00071	89548.09
221	IPI00560967.1	RGD1310475 hypothetical protein LOC293949	35126.32
222	IPI00324893.4	Ywhaz 14-3-3 protein zeta/delta	27753.74
223	IPI00231148.8	Gpd1 Glycerol-3-phosphate dehydrogenase [NAD+], cytoplasmic	37428.25
224	IPI00231264.6	Pon1 Serum paraoxonase/arylesterase 1	39471.20
225	IPI00197568.2	Gdi2 Rab GDP dissociation inhibitor beta	50504.75
226	IPI00198887.1	P4hb Protein disulfide-isomerase	56915.78
227	IPI00188304.3	Glo1 Lactoylglutathione lyase	20806.35
228	IPI00199636.1	Canx Calnexin	67212.71
229	IPI00327469.1	Ahsg Alpha-2-HS-glycoprotein	37958.24
230	IPI00193595.3	Eif4a2 Eukaryotic initiation factor 4A-II	46459.87
231	IPI00371705.4	Papss2 69 kDa protein	68897.28
232	IPI00193765.2	Ctsc Dipeptidyl-peptidase 1	52201.72
233	IPI00382226.1	RGD1306939 Ab2-162	144618.50
234	IPI00192572.1	Phyh Phytanoyl-CoA dioxygenase, peroxisomal	38563.52
235	IPI00393599.3	LOC690745 similar to MOCO sulphurase C-terminal domain containing 1	37766.40
236	IPI00555188.1	Stard10 START domain containing 10	32883.46
237	IPI00368708.2	Fahd1 Fumarylacetoacetate hydrolase domain-containing protein 1	24464.59
238	IPI00194404.5	Nme1 Nucleoside diphosphate kinase A	17181.81
239	IPI00187967.1	Tmem205 transmembrane protein 205	21171.21
240	IPI00188059.2	Rpn2 Dolichyl-diphosphooligosaccharide--protein glycosyltransferase subunit 2	69035.18
241	IPI00195673.1	Tubb6 Tubulin, beta 6	50027.16
242	IPI00199203.1	RGD1560826 similar to glyceraldehyde-3-phosphate dehydrogenase	35832.84
243	IPI00231782.7	Hsd3b5 3 beta-hydroxysteroid dehydrogenase type 5	42179.70
244	IPI00204365.2	Rpn1 Ribophorin I	68358.76
245	IPI00231106.5	Mpst 3-mercaptopyruvate sulfurtransferase	32919.45
246	IPI00193153.1	Hacl1 2-hydroxyacyl-CoA lyase 1	63575.34
247	IPI00870163.1	Agl amylo-1, 6-glucosidase, 4-alpha-glucanotransferase	174219.70
248	IPI00191521.2	Kynu Kynureninase	52436.29

249	IPI00370596.2	RGD1562373 3-ketoacyl-CoA thiolase B, peroxisomal	43792.71
250	IPI00212110.1	Ugt2b UDP-glucuronosyltransferase 2B2	60945.65
251	IPI00202580.2	Cyp2d3 Cytochrome P450 2D3	57105.55
252	IPI00231340.8	- 11 kDa protein	11474.42
253	IPI00197555.6	Suclg1 Suclg1 protein	36125.00
254	IPI00210090.3	Hnrnpu SP120	87693.66
255	IPI00360618.3	RGD1564894 RGD1564894 protein	33964.06
256	IPI00213033.2	Ppib 15 kDa protein	15243.07
257	IPI00199114.5	Anp32a Acidic leucine-rich nuclear phosphoprotein 32 family member A	28547.29
258	IPI00387868.2	Hspa4 Heat shock 70 kDa protein 4	93997.07
259	IPI00211897.4	Gsta3;Gsta2;Gsta1 Glutathione S-transferase alpha-5	25331.16
260	IPI00206780.1	Plg Plasminogen	90476.95
261	IPI00778252.1	Aldh2 Protein	53222.95
262	IPI00210280.1	Comt Isoform 1 of Catechol O-methyltransferase	29578.27
263	IPI00362243.7	Ak3 GTP:AMP phosphotransferase mitochondrial	25422.46
264	IPI00368347.2	Uba1 Ubiquitin-activating enzyme E1	117713.10
265	IPI00192078.2	Bphl Biphenyl hydrolase-like	32802.13
266	IPI00198966.3	Abat 50 kDa protein	50222.72
267	IPI00231650.7	Hist1h1d Histone H1.2	21974.04
268	IPI00195614.5	Rdh2 Retinol dehydrogenase 2	35574.29
269	IPI00327626.1	Ugt2b5 UDP-glucuronosyltransferase 2B3	60485.04
270	IPI00367666.3	- 34 kDa protein	34381.12
271	IPI00193919.5	Suox Sulfite oxidase, mitochondrial	60767.98
272	IPI00454401.1	Dhrs7 Down-regulated in nephrectomized rat kidney #3	36378.20
273	IPI00202549.1	Pklr Isoform R-type of Pyruvate kinase isozymes R/L	62161.68
274	IPI00198325.1	Cyp2d4v1 Cytochrome P450 2D4	56661.35
275	IPI00194974.2	Hnrnpk Hnrpk protein	50996.41
276	IPI00231825.5	Rbp1 Retinol-binding protein I, cellular	15823.80
277	IPI00205417.5	Slc27a2 Very long-chain acyl-CoA synthetase	70648.55
278	IPI00199273.1	St13 Hsc70-interacting protein	41253.41
279	IPI00214454.2	Gcsh Glycine cleavage system H protein, mitochondrial	18473.39
280	IPI00764690.2	Mtch2 mitochondrial carrier homolog 2	34447.39
281	IPI00366060.2	Nedd9 Neural cell expressed, developmentally down-regulated gene 9	92921.35
282	IPI00564294.2	- 34 kDa protein	33718.22
283	IPI00421539.3	Aco2 Aconitate hydratase, mitochondrial	85380.08
284	IPI00569616.2	- 36 kDa protein	36363.56
285	IPI00209363.1	Slc25a10 Mitochondrial dicarboxylate carrier (Solute carrier family 25 (Mitochondrial carrier	31434.09
286	IPI00231150.4	Gsta3;Gsta2;Gsta1 Glutathione S-transferase (Fragment)	25971.69
287	IPI00191711.1	LOC259246 Major urinary protein	20723.51
288	IPI00763564.1	LOC684270 similar to isochorismatase domain containing 2 isoform 1	24653.19
289	IPI00207217.1	Echs1 Enoyl-CoA hydratase, mitochondrial	31496.19
290	IPI00328013.4	Akr7a3 Aflatoxin B1 aldehyde reductase member 3	36723.36

291	IPI00201561.3	Prdx2 Peroxiredoxin-2	21770.07
292	IPI00326433.11	Hspe1;Hspd1 10 kDa heat shock protein, mitochondrial	10894.86
293	IPI00204316.1	Atp5j ATP synthase-coupling factor 6, mitochondrial	12486.58
294	IPI00555278.3	Gulo L-gulonolactone oxidase	50582.38
295	IPI00200145.1	Rplp1 60S acidic ribosomal protein P1	11490.69
296	IPI00194222.1	Cox4i1 Cytochrome c oxidase subunit 4 isoform 1, mitochondrial	19502.08
297	IPI00387720.3	- 50 kDa protein	49524.04
298	IPI00214456.2	Adk Adenosine kinase	40108.32
299	IPI00204128.2	RGD1561381 similar to microsomal glutathione S-transferase 3	16752.52
300	IPI00339167.4	Tuba1b Tubulin alpha-1B chain	50119.64
301	IPI00324443.1	Cyp2d1 Cytochrome P450 2D1	57138.68
302	IPI00382300.3	Rab1 Ac2-048	33642.78
303	IPI00210120.2	Vtn Aa1018	55924.79
304	IPI00213677.1	Arf2 ADP-ribosylation factor 2	20732.76
305	IPI00359103.4	Rpl11 60S ribosomal protein L11	20239.65
306	IPI00200591.1	LOC299282 Serine protease inhibitor A3L	46248.14
307	IPI00480820.4	Pgrmc1 Membrane-associated progesterone receptor component 1	21584.70
308	IPI00371266.1	Naca Naca protein	23369.71
309	IPI00201399.1	Alad Delta-aminolevulinic acid dehydratase	36008.41
310	IPI00192257.1	Rpl18a 60S ribosomal protein L18a	20718.89
311	IPI00192409.1	Gapdhs Glyceraldehyde 3-phosphate dehydrogenase	46677.82
312	IPI00230838.5	Atp5h ATP synthase subunit d, mitochondrial	18751.60
313	IPI00201932.2	Ssr4 Translocon-associated protein subunit delta	19094.61
314	IPI00470317.5	Eef1g Elongation factor 1-gamma	50029.21
315	IPI00208281.1	LOC286989 UDP-glucuronosyltransferase 2B8	60050.08
316	IPI00359732.2	RGD1564064 similar to Glyceraldehyde-3-phosphate dehydrogenase	16480.06
317	IPI00371173.2	RGD1307736 Uncharacterized protein KIAA0152 homolog	32397.75
318	IPI00476899.1	Eef1b2 eukaryotic translation elongation factor 1 beta 2	24660.29
319	IPI00389152.4	LOC688869;Cox6b1 similar to cytochrome c oxidase, subunit VIb polypeptide 1	10064.88
320	IPI00360056.1	Galm Aldose 1-epimerase	37869.16
321	IPI00215390.1	Slco1b2 Isoform 1 of Solute carrier organic anion transporter family member 1B2	72719.04
322	IPI00188924.4	Uqcrc2 Cytochrome b-c1 complex subunit 2, mitochondrial	48366.24
323	IPI00207980.1	Rpl23 60S ribosomal protein L23	14856.06
324	IPI00388265.2	Pgcp 48 kDa protein	48068.85
325	IPI00190759.2	Fgg Isoform Gamma-B of Fibrinogen gamma chain	50600.47
326	IPI00201032.1	Hnrpd Isoform 1 of Heterogeneous nuclear ribonucleoprotein D0	38168.18
327	IPI00230857.7	Ak2 Adenylate kinase isoenzyme 2, mitochondrial	26362.55
328	IPI00324020.6	Glul Glutamine synthetase	42240.34
329	IPI00231502.3	Ap2b1 Isoform 2 of AP-2 complex subunit beta-1	105624.80
330	IPI00359981.2	Ndufa13 similar to NADH dehydrogenase (ubiquinone) 1 alpha subcomplex, 13	16949.84
331	IPI00191738.1	Gclm Glutamate--cysteine ligase regulatory subunit	30528.57
332	IPI00190557.2	Phb2 Prohibitin-2	33291.91

333	IPI00188509.3	Dad1 Dolichyl-diphosphooligosaccharide--protein glycosyltransferase subunit DAD1	12488.55
334	IPI00190377.2	Taldo1 Transaldolase	37436.47
335	IPI00361869.3	REVYeats2 YEATS domain containing 2	148612.90
336	IPI00231978.5	Atp5i ATP synthase subunit e, mitochondrial	8249.47
337	IPI00200794.1	Dcxr L-xylulose reductase	25703.39
338	IPI00358481.3	Adhfe1 Hydroxyacid-oxoacid transhydrogenase, mitochondrial	50365.61
339	IPI00372179.1	Ndufb5 NADH dehydrogenase (ubiquinone) 1 beta subcomplex, 5	21650.49
340	IPI00369195.3	Ppa2 similar to inorganic pyrophosphatase 2	37818.08
341	IPI00214448.1	Crym Mu-crystallin homolog	33533.08
342	IPI00231662.6	Cyb5r3 Isoform 1 of NADH-cytochrome b5 reductase 3	34152.73
343	IPI00882532.1	LOC688283 similar to kynurenine formamidase	34347.33
344	IPI00191707.4	Pdha1 Pyruvate dehydrogenase E1 component subunit alpha, somatic form, mitochondrial	43198.64
345	IPI00209690.1	Ephx1 Epoxide hydrolase 1	52547.88
346	IPI00362353.3	Ctsg 30 kDa protein	29567.61
347	IPI00372845.2	Gstt1 28 kDa protein	27580.42
348	IPI00361192.3	RGD1561491 similar to ATP-binding cassette transporter sub-family A member 15	103027.20
349	IPI00230916.7	Rpl13 60S ribosomal protein L13	24294.46
350	IPI00561262.2	- 69 kDa protein	68945.21
351	IPI00369166.3	RGD1561178 similar to glyceraldehyde-3-phosphate dehydrogenase	20354.45
352	IPI00471584.7	Hsp90ab1 Heat shock protein HSP 90-beta	83229.17
353	IPI00373143.1	- 21 kDa protein	21019.25
354	IPI00212969.3	Hnrnpa2b1 Heterogeneous nuclear ribonucleoprotein B0b	33938.30
355	IPI00361193.5	Aldh1l2 similar to aldehyde dehydrogenase 1 family, member L2	101674.90
356	IPI00470325.1	RGD1303232 Probable oxidoreductase C10orf33 homolog	62839.52
357	IPI00365663.1	Bckdha branched chain ketoacid dehydrogenase E1, alpha polypeptide	50636.22
358	122056685.0	gi|122056685|ref|NP_037490.2| peptidylarginine deiminase type I [Homo sapiens]	74617.87
359	IPI00230915.5	Rpl10 60S ribosomal protein L10	24587.88
360	IPI00202370.3	Maoa similar to Amine oxidase [flavin-containing] A	98012.69
361	IPI00200757.1	Fn1 Isoform 1 of Fibronectin	272338.20
362	IPI00392830.3	- 77 kDa protein	76896.51
363	IPI00382228.1	Glyat 39 kDa protein	39427.87
364	IPI00763798.1	LOC691781 similar to Tubulin alpha-2 chain	9319.69
365	IPI00782231.1	Hmha1 histocompatibility (minor) HA-1	123000.50
366	IPI00206948.1	Retsat All-trans-retinol 13,14-reductase	67487.41
367	IPI00206222.3	- 29 kDa protein	29221.48
368	IPI00365944.5	Myl6l Myosin light polypeptide 6	16964.15
369	IPI00764950.1	- LOC685322 protein	7456.85
370	IPI00886474.1	Rps5 Rps5 protein	22892.07
371	IPI00372520.1	LOC361750 Ac2-067	27952.40
372	IPI00369635.3	Rdx Radixin	68501.38
373	IPI00197553.1	Npm1 Isoform B23.1 of Nucleophosmin	32539.84
374	IPI00198376.1	Sult1e1 Estrogen sulfotransferase, isoform 3	35392.54

375	IPI00209908.1	mt-Co2;mt-Co3 Cytochrome c oxidase subunit 2	25925.07
376	IPI00231368.5	Txn1 Thioredoxin	11665.66
377	IPI00230837.5	Ywhab Isoform Long of 14-3-3 protein beta/alpha	28036.83
378	IPI00358908.3	- 37 kDa protein	37449.47
379	IPI00210941.1	Tpm3 Isoform 2 of Tropomyosin alpha-3 chain	28702.68
380	IPI00207486.1	- 14 kDa protein	14253.70
381	IPI00231346.5	Rpl30 60S ribosomal protein L30	12775.74
382	IPI00191112.1	Ndufab1 NADH dehydrogenase (ubiquinone) 1, alpha/beta subcomplex, 1	17503.07
383	IPI00362927.1	Tuba4a Tubulin alpha-4A chain	49892.41
384	IPI00198620.1	Atp5d ATP synthase subunit delta, mitochondrial	17584.18
385	IPI00361404.2	- 17 kDa protein	17412.17
386	IPI00207115.3	Ube1y1 Ubiquitin-activating enzyme E1	117792.70
387	IPI00215208.3	Rpl8 60S ribosomal protein L8	28007.29
388	IPI00209037.3	Fkbp2 similar to FK506-binding protein 2 precursor	20722.09
389	IPI00192486.1	Rps6 40S ribosomal protein S6	28663.00
390	IPI00208657.1	RGD1565117 similar to 40S ribosomal protein S26	11884.34
391	IPI00203523.1	Rpl23a 60S ribosomal protein L23a	17684.13
392	IPI00371236.3	Tufm Elongation factor Tu, mitochondrial	49491.04
393	IPI00388726.2	Ldhd 51 kDa protein	51338.84
394	IPI00203730.1	- GTP-binding nuclear protein Ran, testis-specific isoform	24435.54
395	IPI00766037.2	LOC684314 Glycerate kinase	55153.06
396	IPI00188158.1	Hmgcs1 Hydroxymethylglutaryl-CoA synthase, cytoplasmic	57397.53
397	IPI00400739.1	Entpd5 Ectonucleoside triphosphate diphosphohydrolase 5	47342.86
398	IPI00373430.3	Dc2 DC2 protein	16803.82
399	IPI00190348.1	LOC680312;LOC682665 hypothetical protein LOC680312	13881.57
400	IPI00475639.4	Tubb2a Tubulin beta-2A chain	49874.99
401	IPI00388191.2	- 34 kDa protein	33937.52
402	IPI00201103.1	Hal Histidine ammonia-lyase	72238.66
403	IPI00203829.1	Atox1 Copper transport protein ATOX1	7287.69
404	IPI00365286.3	Vcl vinculin	116542.40
405	IPI00204831.1	Timm8a1 Mitochondrial import inner membrane translocase subunit Tim8 A	11035.32
406	IPI00361686.5	C1qbp Complement component 1 Q subcomponent-binding protein, mitochondrial	30977.52
407	IPI00230907.5	Mif Macrophage migration inhibitory factor	12469.17
408	IPI00557847.2	- 15 kDa protein	15423.82
409	IPI00421616.2	Acsm3 66 kDa protein	65984.41
410	IPI00454288.1	Atp5c1 ATP synthase gamma chain	67677.30
411	IPI00205076.1	Lonp1 Lon protease homolog, mitochondrial	105726.40
412	IPI00198316.1	Rab18 Ras-related protein Rab-18	22961.65
413	IPI00204311.1	Ak3l1 Adenylate kinase isoenzyme 4, mitochondrial	25187.26
414	IPI00371178.2	REVOasl1 2'-5' oligoadenylate synthetase-like 1 protein	58979.51
415	118595772.0	gi|118595772|sp|P68082.2|MYG_HORSE Myoglobin	17072.00
416	IPI00194097.5	Gc Vitamin D-binding protein	53509.07

417	IPI00188066.2	- 28 kDa protein	27757.58
418	IPI00555314.1	Ddx1 ATP-dependent RNA helicase DDX1	82444.89
419	IPI00210524.1	Lman2 Lman2 protein	40367.23
420	IPI00210975.1	Hyou1 Hypoxia up-regulated protein 1	111220.10
421	IPI00372388.1	Cct3 T-complex protein 1 subunit gamma	60608.46
422	IPI00191444.3	Capzb 31 kDa protein	31194.71
423	IPI00554039.1	RGD1565368 similar to glyceraldehyde-3-phosphate dehydrogenase	35760.09
424	IPI00364856.3	Ddx58 DEAD (Asp-Glu-Ala-Asp) box polypeptide 58	105903.10
425	IPI00394356.3	LOC691519;LOC687581 similar to ankyrin repeat domain 26	45281.70
426	IPI00370233.3	Trim31 38 kDa protein	37726.54
427	IPI00205036.1	LOC360504 hemoglobin alpha 2 chain	15274.78
428	IPI00213611.1	LOC287167 Alpha globin	15514.99
429	IPI00388302.2	- 22 kDa protein	21884.26
430	IPI00231745.8	Fbp1 Fructose-1,6-bisphosphatase 1	39584.17
431	IPI00364925.3	Dhtkd1 Probable 2-oxoglutarate dehydrogenase E1 component DHKTD1, mitochondrial	102576.50
432	IPI00201262.1	LOC297568;Mug1;Mug2 Alpha-1-inhibitor 3	163669.20
433	IPI00231742.5	Cat Catalase	59719.59
434	IPI00202549.1	Pklr Isoform R-type of Pyruvate kinase isozymes R/L	62161.68
435	IPI00331983.5	Adh1 Alcohol dehydrogenase 1	39619.57
436	IPI00231069.5	Dbi Acyl-CoA-binding protein	10021.15
437	IPI00551812.1	Atp5b ATP synthase subunit beta, mitochondrial	56318.59
438	IPI00421874.4	Vdac1 Voltage-dependent anion-selective channel protein 1	30736.57
439	IPI00326972.6	Ces3 Carboxylesterase 3	62107.82
440	IPI00558154.1	LOC100125372 60 kDa protein	59976.52
441	IPI00210644.1	Cps1 Carbamoyl-phosphate synthase [ammonia], mitochondrial	164474.80
442	IPI00211225.1	Acadl Long-chain specific acyl-CoA dehydrogenase, mitochondrial	47842.46
443	IPI00205332.4	Etfa Electron transfer flavoprotein subunit alpha, mitochondrial	34929.47
444	IPI00396910.1	Atp5a1 ATP synthase subunit alpha, mitochondrial	59716.74
445	IPI00190790.1	Fabp1 Fatty acid-binding protein, liver	14263.30
446	IPI00195673.1	Tubb6 Tubulin, beta 6	50027.16
447	IPI00231648.5	Gnmt Glycine N-methyltransferase	32528.35
448	IPI00211127.1	Ass1 Argininosuccinate synthase	46466.94
449	IPI00211507.3	Hpd 4-hydroxyphenylpyruvate dioxygenase	45083.91
450	IPI00471584.7	Hsp90ab1 Heat shock protein HSP 90-beta	83229.17
451	IPI00760137.1	Sord Sorbitol dehydrogenase	38209.82
452	IPI00208970.1	Upb1 Beta-ureidopropionase	44014.00
453	IPI00230897.5	Hbb Hemoglobin subunit beta-1	15969.25
454	IPI00231260.5	Prdx6 Peroxiredoxin-6	24802.98
455	IPI00358005.1	Chdh Choline dehydrogenase	66346.48
456	IPI00471911.7	Aldob Fructose-bisphosphate aldolase B	39593.23
457	IPI00231139.6	Tkt transketolase	71113.45
458	IPI00204365.2	Rpn1 Ribophorin I	68358.76

459	IPI00655249.1	LOC684538 Enoyl-CoA hydratase domain-containing protein 3, mitochondrial	32364.86
460	IPI00327518.4	Arg1 Arginase-1	36480.91
461	IPI00326948.2	Hsd17b4 Hsd17b4 protein	81037.99
462	IPI00358163.3	Slc25a13 similar to Calcium-binding mitochondrial carrier protein Aralar2	74351.98
463	118595772.0	MYG_HORSE Myoglobin	17072.00
464	IPI00210823.1	Akr1d1 3-oxo-5-beta-steroid 4-dehydrogenase	37354.09
465	IPI00208209.1	Prdx4 PRx IV	30988.08
466	IPI00191711.1	LOC259246 Major urinary protein	20723.51
467	IPI00205018.2	Aldh6a1 Methylmalonate-semialdehyde dehydrogenase [acylating], mitochondrial	57882.70
468	IPI00203481.1	LOC691716;LOC687680 similar to ribosomal protein S15a	14390.59
469	IPI00195585.1	Rdh7 Retinol dehydrogenase 3	35639.48
470	IPI00360618.3	RGD1564894 RGD1564894 protein	33964.06
471	IPI00199482.2	Gstm4 Similar to glutathione transferase GSTM7-7	25536.95
472	IPI00324741.2	Pdia3 Protein disulfide-isomerase A3	57043.07
473	IPI00189819.1	Actb Actin, cytoplasmic 1	41709.74
474	IPI00231292.6	Hrsp12 Ribonuclease UK114	14479.67
475	IPI00369550.3	- 28 kDa protein	28286.49
476	IPI00198325.1	Cyp2d4v1 Cytochrome P450 2D4	56661.35
477	IPI00204774.1	LOC501232 Liver carboxylesterase B-1	62454.86
478	IPI00324633.2	Glud1 Glutamate dehydrogenase 1, mitochondrial	61377.36
479	IPI00214582.1	Rps7;LOC497813 40S ribosomal protein S7	22113.26
480	IPI00411230.3	Gstm2 Glutathione S-transferase Mu 2	25685.97
481	IPI00767591.1	Grhpr Grhpr protein	35914.83
482	IPI00189795.1	Tuba1a Tubulin alpha-1A chain	50103.65
483	IPI00231631.13	Eno3 Beta-enolase	46984.37
484	IPI00568810.2	Gstt3 similar to glutathione S-transferase, theta 3	27968.68
485	IPI00364363.3	- 30 kDa protein	30276.29
486	IPI00231963.5	Ddt D-dopachrome decarboxylase	13124.84
487	IPI00332027.7	Bhmt Betaine--homocysteine S-methyltransferase 1	44947.86
488	IPI00339148.2	Hspd1 60 kDa heat shock protein, mitochondrial	60917.48
489	IPI00359623.3	LOC683474 similar to aldehyde dehydrogenase 8 family, member A1 isoform 2	53387.29
490	IPI00209690.1	Ephx1 Epoxide hydrolase 1	52547.88
491	IPI00211100.1	Akr1c14 3-alpha-hydroxysteroid dehydrogenase	37003.95
492	IPI00327991.3	Cyp2c23 Cytochrome P450 2C23	56396.72
493	IPI00475561.3	LOC685320;LOC499782;Rpl12 60S ribosomal protein L12	17834.55
494	IPI00210139.1	Otc Ornithine carbamoyltransferase, mitochondrial	39860.83
495	IPI00208026.1	Selenbp1 Selenium-binding protein 1	52498.52
496	IPI00197770.1	Aldh2 Aldehyde dehydrogenase, mitochondrial	56452.72
497	IPI00196656.2	Srprb Ba1-667	107383.30
498	IPI00231767.5	Tpi1 Triosephosphate isomerase	26831.76
499	IPI00210212.5	- 38 kDa protein	37955.79
500	IPI00475676.4	Tas1r2 Delta-1-pyrroline-5-carboxylate dehydrogenase, mitochondrial	61829.75

501	IPI00198966.3	Abat 50 kDa protein	50222.72
502	IPI00382270.1	Slc25a15 Ab1-114	36896.87
503	IPI00210435.2	Pcx Pyruvate carboxylase, mitochondrial	129694.90
504	IPI00364321.3	Etfb Electron transfer flavoprotein subunit beta	27670.06
505	IPI00196725.5	Aldh1l1 10-formyltetrahydrofolate dehydrogenase	99063.85
506	IPI00214456.2	Adk Adenosine kinase	40108.32
507	IPI00372498.1	Dak Dihydroxyacetone kinase	59406.42
508	IPI00360930.2	Car1 Carbonic anhydrase 1	28282.23
509	IPI00365545.1	Dld Dihydrolipoyl dehydrogenase, mitochondrial	54004.15
510	IPI00327469.1	Ahsg Alpha-2-HS-glycoprotein	37958.24
511	IPI00211593.1	Sod2 Superoxide dismutase [Mn], mitochondrial	24658.58
512	IPI00207010.2	Baat Bile acid-CoA:amino acid N-acyltransferase	46435.08
513	IPI00210280.1	Comt Isoform 1 of Catechol O-methyltransferase	29578.27
514	IPI00204634.4	Sec14l4 SEC14-like 4	46987.95
515	IPI00369166.3	RGD1561178 similar to glyceraldehyde-3-phosphate dehydrogenase	20354.45
516	IPI00208306.1	Tpt1 Translationally-controlled tumor protein	19449.55
517	IPI00204311.1	Ak3l1 Adenylate kinase isoenzyme 4, mitochondrial	25187.26
518	IPI00208917.4	Aldh7a1 similar to aldehyde dehydrogenase family 7, member A1	58711.46
519	IPI00365985.4	Tra1 93 kDa protein	92474.11
520	IPI00230787.5	Car2 Carbonic anhydrase 2	29095.60
521	IPI00231426.6	Pgk1 Phosphoglycerate kinase 1	44510.01
522	IPI00362070.5	Ugp2 UDP-glucose pyrophosphorylase 2	56987.88
523	IPI00882532.1	LOC688283 similar to kynurenine formamidase	34347.33
524	IPI00188924.4	Uqcrc2 Cytochrome b-c1 complex subunit 2, mitochondrial	48366.24
525	IPI00471530.2	Lap3 Isoform 1 of Cytosol aminopeptidase	56114.77
526	IPI00364474.1	Itpa inosine triphosphatase	21913.11
527	IPI00197696.2	Mdh2 Malate dehydrogenase, mitochondrial	35660.82
528	IPI00197711.1	Ldha L-lactate dehydrogenase A chain	36427.36
529	IPI00366293.3	Tst Thiosulfate sulfurtransferase	33385.77
530	IPI00231359.3	Acads Acyl-Coenzyme A dehydrogenase, short chain	44939.09
531	IPI00326433.11	Hspe1;Hspd1 10 kDa heat shock protein, mitochondrial	10894.86
532	IPI00363265.3	Hspa9 Stress-70 protein, mitochondrial	73811.90
533	IPI00367666.3	- 34 kDa protein	34381.12
534	IPI00202658.1	Hibadh 3-hydroxyisobutyrate dehydrogenase, mitochondrial	35279.60
535	IPI00198324.1	Cyp2b3 Cytochrome P450 2B3	56348.04
536	IPI00230889.5	Mgst1 Microsomal glutathione S-transferase 1	17460.23
537	IPI00231473.4	Cyp2d2 Cytochrome P450 2D26	57392.14
538	IPI00211989.2	Khk Isoform C of Ketohexokinase	32781.55
539	IPI00471608.1	Snd1 Staphylococcal nuclease domain-containing protein 1	101888.60
540	IPI00382320.3	RGD1311563 RGD1311563 protein	93375.64
541	IPI00192043.2	Mccc2 Methylcrotonoyl-CoA carboxylase beta chain, mitochondrial	61956.70
542	IPI00207941.1	Dmgdh Dimethylglycine dehydrogenase, mitochondrial	95987.51

543	IPI00189813.1	Acta1 Actin, alpha skeletal muscle	42023.86
544	IPI00197371.4	Gstm6 Glutathione S-transferase, mu 6	25609.96
545	IPI00195372.1	Eef1a1 Elongation factor 1-alpha 1	50082.16
546	IPI00210920.1	Got2 Aspartate aminotransferase, mitochondrial	47284.15
547	IPI00203690.5	Aldh9a1 4-trimethylaminobutyraldehyde dehydrogenase	56432.66
548	IPI00208348.1	Pdxk Pyridoxal kinase	34885.67
549	IPI00206624.1	Hspa5 78 kDa glucose-regulated protein	72302.52
550	IPI00188858.4	Amacr Alpha-methylacyl-CoA racemase	41801.50
551	IPI00214480.1	Fah Fumarylacetoacetase	45946.07
552	IPI00203558.1	Hdhd3 Haloacid dehalogenase-like hydrolase domain containing 3	27776.25
553	IPI00193258.7	Pah Phenylalanine-4-hydroxylase	51789.41
554	IPI00195060.4	- 29 kDa protein	28957.05
555	IPI00389611.3	Rgn Regucalcin	33368.38
556	IPI00209113.3	Myh9 Myosin-9	226196.40
557	IPI00421364.1	Shmt1 Serine hydroxymethyltransferase	75326.30
558	IPI00230859.5	Akr1a1 Alcohol dehydrogenase [NADP+]	36482.93
559	IPI00395251.1	- Glutathione transferase class alpha chain 10 (Fragment)	12441.80
560	IPI00373143.1	- 21 kDa protein	21019.25
561	IPI00198887.1	P4hb Protein disulfide-isomerase	56915.78
562	IPI00230788.6	Car3 Carbonic anhydrase 3	29412.72
563	IPI00363952.3	Phyhd1 Phytanoyl-CoA dioxygenase domain-containing protein 1	32532.29
564	IPI00190759.2	Fgg Isoform Gamma-B of Fibrinogen gamma chain	50600.47
565	IPI00190179.3	Pygl Glycogen phosphorylase, liver form	97421.10
566	IPI00194550.5	Cth Cystathionine gamma-lyase	43577.32
567	IPI00231782.7	Hsd3b5 3 beta-hydroxysteroid dehydrogenase type 5	42179.70
568	IPI00201333.4	Ganab 109 kDa protein	109363.00
569	IPI00325765.2	Akr7a2 Aflatoxin B1 aldehyde reductase member 2	40649.32
570	IPI00366416.2	Cyc1 similar to cytochrome c-1	35411.98
571	IPI00188359.3	Abhd14b Abhydrolase domain containing 14b	22603.70
572	IPI00202379.1	Farsb Phenylalanyl-tRNA synthetase, beta subunit	65609.59
573	IPI00194045.1	Idh1 Isocitrate dehydrogenase [NADP] cytoplasmic	46704.57
574	IPI00213584.3	Agxt2 Alanine--glyoxylate aminotransferase 2, mitochondrial	57395.82
575	IPI00232011.9	Ehhadh Peroxisomal bifunctional enzyme	78608.45
576	IPI00555188.1	Stard10 START domain containing 10	32883.46
577	IPI00870151.1	Bucs1 butyryl Coenzyme A synthetase 1	39651.20
578	IPI00421539.3	Aco2 Aconitate hydratase, mitochondrial	85380.08
579	IPI00556987.2	Hgd Homogentisate 1, 2-dioxygenase	49867.58
580	IPI00201564.4	Fmo1 Dimethylaniline monooxygenase [N-oxide-forming] 1	59786.84
581	IPI00231639.7	Gstm1 Glutathione S-transferase Mu 1	25897.11
582	IPI00554039.1	RGD1565368 similar to glyceraldehyde-3-phosphate dehydrogenase	35760.09
583	IPI00188158.1	Hmgcs1 Hydroxymethylglutaryl-CoA synthase, cytoplasmic	57397.53
584	IPI00763872.1	LOC681913 Similar to Maleylacetoacetate isomerase	23945.56

585	IPI00205389.6	Fgb Isoform 1 of Fibrinogen beta chain	54200.66
586	IPI00212015.1	Acadm Medium-chain specific acyl-CoA dehydrogenase, mitochondrial	46525.83
587	IPI00870183.1	Cisd1 CDGSH iron sulfur domain 1	12089.14
588	IPI00476295.7	Ahcy Adenosylhomocysteinase	47507.29
589	IPI00231643.5	Sod1 Superoxide dismutase [Cu-Zn]	15901.80
590	IPI00212110.1	Ugt2b UDP-glucuronosyltransferase 2B2	60945.65
591	IPI00327144.7	Cfl1 Cofilin-1	18520.67
592	IPI00870631.1	Np nucleoside phosphorylase	24320.93
593	IPI00359732.2	RGD1564064 similar to Glyceraldehyde-3-phosphate dehydrogenase	16480.06
594	IPI00192572.1	Phyh Phytanoyl-CoA dioxygenase, peroxisomal	38563.52
595	IPI00210566.3	Hsp90aa1 Heat shock protein HSP 90-alpha	84761.81
596	IPI00231192.5	MGC72973;LOC689064;LOC100134871 Hemoglobin subunit beta-2	15972.29
597	IPI00327830.3	Fabp5 Fatty acid-binding protein, epidermal	15049.54
598	IPI00201413.1	Acaa2 3-ketoacyl-CoA thiolase, mitochondrial	41844.49
599	IPI00193049.1	Sult1a1 Sulfotransferase 1A1	33884.02
600	IPI00193233.1	Cyb5b Cytochrome b5 type B	16254.83
601	IPI00205374.1	Hmgcl Hydroxymethylglutaryl-CoA lyase, mitochondrial	34169.71
602	IPI00231200.5	Por NADPH--cytochrome P450 reductase	76914.30
603	IPI00365929.1	Pdia6 protein disulfide isomerase associated 6	48729.69
604	IPI00361193.5	Aldh1l2 similar to aldehyde dehydrogenase 1 family, member L2	101674.90
605	IPI00201436.1	Mat1a S-adenosylmethionine synthetase isoform type-1	43670.11
606	IPI00212969.3	Hnrnpa2b1 Heterogeneous nuclear ribonucleoprotein B0b	33938.30
607	IPI00387720.3	- 50 kDa protein	49524.04
608	IPI00327781.1	Cyp2c Cytochrome P450 2C11	57144.53
609	IPI00368708.2	Fahd1 Fumarylacetoacetate hydrolase domain-containing protein 1	24464.59
610	IPI00210946.6	Rpl17 60S ribosomal protein L17	21383.38
611	IPI00327335.3	Sult1b1 Sulfotransferase family cytosolic 1B member 1	34812.77
612	IPI00193854.4	Pcbd1 Pterin-4-alpha-carbinolamine dehydratase	11992.01
613	IPI00205561.1	Acox2 Peroxisomal acyl-coenzyme A oxidase 2	76750.05
614	IPI00214889.1	Psmb3 Proteasome subunit beta type-3	22949.45
615	IPI00196118.5	Txnrd2 Isoform 1 of Thioredoxin reductase 2, mitochondrial	56492.04
616	IPI00464815.11	Eno1 Alpha-enolase	47098.29
617	IPI00560967.1	RGD1310475 hypothetical protein LOC293949	35126.32
618	IPI00202725.1	Rps21 40S ribosomal protein S21	9121.54
619	IPI00208645.6	Hsd17b12 Estradiol 17-beta-dehydrogenase 12	34818.68
620	IPI00326606.4	Ndrg2 Isoform 2 of Protein NDRG2	39245.31
621	IPI00214373.1	Aadat Kynurenine/alpha-aminoadipate aminotransferase mitochondrial	47753.74
622	IPI00564133.1	Kat3 Kynurenine--oxoglutarate transaminase 3	51011.37
623	IPI00205906.2	Dpys Dihydropyrimidinase	56778.73
624	IPI00210444.5	Hmgcs2 Hydroxymethylglutaryl-CoA synthase, mitochondrial	56875.68
625	IPI00209908.1	mt-Co2;mt-Co3 Cytochrome c oxidase subunit 2	25925.07
626	IPI00480639.3	C3 Complement C3 (Fragment)	186341.70

627	IPI00231953.10	Copb2 Coatomer subunit beta'	102486.30
628	IPI00200466.3	Slc25a5 ADP/ATP translocase 2	32880.15
629	IPI00231858.5	Gstt2 Glutathione S-transferase theta-2	27421.54
630	IPI00326140.3	Pzp Alpha-1-macroglobulin	167018.90
631	IPI00231694.7	Xdh Xanthine dehydrogenase/oxidase	146148.70
632	IPI00191728.1	Calr Calreticulin	47965.90
633	IPI00231955.6	Calm3;Calm1;Calm2 Calmodulin	16826.84
634	IPI00781636.1	Acsm2 Protein	64427.12
635	IPI00325189.4	Nme2 Nucleoside diphosphate kinase B	17271.89
636	IPI00212666.2	Mug1 Isoform 1 of Murinoglobulin-1	165220.90
637	IPI00191501.1	Psma6 Proteasome subunit alpha type-6	27381.81
638	IPI00196748.3	Cyp2c7 Cytochrome P450 2C7	56150.69
639	IPI00231774.6	Maob Amine oxidase [flavin-containing] B	58421.43
640	IPI00395285.3	Rpl3 60S ribosomal protein L3	46106.84
641	IPI00211096.1	Hsd11b1 Isoform 11-HSD1A of Corticosteroid 11-beta-dehydrogenase isozyme 1	31862.52
642	IPI00211510.1	Acox1 Isoform 1 of Peroxisomal acyl-coenzyme A oxidase 1	74631.41
643	IPI00364311.1	Gpi Glucose-6-phosphate isomerase	62787.21
644	IPI00553996.3	Zxdc 79 kDa protein	78483.41
645	IPI00214299.6	Cbs Isoform I of Cystathionine beta-synthase	61415.39
646	IPI00231638.6	Gsta3;Gsta2;Gsta1 Glutathione S-transferase alpha-1	25590.55
647	IPI00207146.1	MGC72973 Zero beta-1 globin	16012.26
648	IPI00366014.3	Rps13;LOC684988 40S ribosomal protein S13	17211.66
649	IPI00207933.2	Dhrs4 dehydrogenase/reductase (SDR family) member 4	29802.84
650	IPI00326195.3	Pecr Peroxisomal trans-2-enoyl-CoA reductase	32830.77
651	IPI00201548.1	Carhsp1 Calcium-regulated heat stable protein 1	15896.05
652	IPI00195516.6	Hpx Hemopexin	51318.33
653	IPI00471645.1	Ddost Dolichyl-di-phosphooligosaccharide-protein glycotransferase	48865.02
654	IPI00767531.2	LOC680217;LOC682465 similar to Ferritin light chain 2	15037.73
655	IPI00371141.3	Xylb Xylulose kinase	59541.69
656	IPI00382191.1	Pgd 6-phosphogluconate dehydrogenase, decarboxylating	120448.80
657	IPI00213659.3	Decr1 2,4-dienoyl-CoA reductase, mitochondrial	36109.73
658	IPI00363941.1	Stbd1 Starch-binding domain-containing protein 1	35472.71
659	IPI00203232.5	Macrod1 MACRO domain containing 1	35271.35
660	IPI00366218.3	Cct2 T-complex protein 1 subunit beta	57422.27
661	IPI00382228.1	Glyat 39 kDa protein	39427.87
662	IPI00198720.1	Idh3a Isocitrate dehydrogenase [NAD] subunit alpha, mitochondrial	39588.06
663	IPI00199641.5	Gcs1 Mannosyl-oligosaccharide glucosidase	91814.65
664	IPI00192078.2	Bphl Biphenyl hydrolase-like	32802.13
665	IPI00209038.1	Fbp2 Fructose-1,6-bisphosphatase isozyme 2	36863.94
666	IPI00421513.8	Got1 Aspartate aminotransferase, cytoplasmic	46399.55
667	IPI00231340.8	- 11 kDa protein	11474.42
668	IPI00200591.1	LOC299282 Serine protease inhibitor A3L	46248.14

669	IPI00193919.5	Suox Sulfite oxidase, mitochondrial	60767.98
670	IPI00197579.2	Tubb5 Isoform 1 of Tubulin beta-5 chain	49639.01
671	IPI00188989.1	Acsl1 Long-chain-fatty-acid--CoA ligase 1	78128.34
672	IPI00231245.5	Hao2 Hydroxyacid oxidase 2	39176.43
673	IPI00231356.9	Mthfd1 C-1-tetrahydrofolate synthase, cytoplasmic	100932.20
674	IPI00191142.1	Rps10 40S ribosomal protein S10	18903.83
675	IPI00358757.5	Hint2 histidine triad nucleotide binding protein 2	17369.26
676	IPI00231860.5	Abcd3 ATP-binding cassette sub-family D member 3	75267.27
677	IPI00193279.1	Oat Ornithine aminotransferase, mitochondrial	48302.11
678	IPI00363696.1	Hsd17b13 17-beta hydroxysteroid dehydrogenase 13	33473.15
679	IPI00191176.4	Cyp2c6 Cytochrome P450PB-1	42247.14
680	IPI00200659.1	Sdha Succinate dehydrogenase [ubiquinone] flavoprotein subunit, mitochondrial	71569.76
681	IPI00373331.2	Lactb lactamase, beta	60410.13
682	IPI00203106.6	Fmo5 Dimethylaniline monooxygenase [N-oxide-forming] 5	60017.27
683	IPI00198039.1	Ethe1 Ethylmalonic encephalopathy 1	27659.00
684	IPI00208205.1	Hspa8 Heat shock cognate 71 kDa protein	70827.34
685	IPI00475474.3	Rps4x 40S ribosomal protein S4, X isoform	29579.06
686	IPI00231253.5	Hsd17b10 3-hydroxyacyl-CoA dehydrogenase type-2	27228.57
687	IPI00207601.1	Hao1 Hydroxyacid oxidase 1, liver	40942.25
688	IPI00190348.1	LOC680312;LOC682665 hypothetical protein LOC680312	13881.57
689	IPI00200883.2	Gls2 Isoform 2 of Glutaminase liver isoform, mitochondrial	59165.78
690	IPI00358872.2	Amt Aminomethyltransferase	44035.90
691	IPI00372372.2	Serpinc1 Serine (Or cysteine) peptidase inhibitor, clade C (Antithrombin), member 1	52200.95
692	IPI00365737.3	Snrp70 Snrp70 protein	52101.96
693	IPI00195803.1	Ugdh UDP-glucose 6-dehydrogenase	54857.36
694	IPI00360794.4	- Protein	41520.49
695	IPI00387739.2	- 30 kDa protein	29483.80
696	IPI00205417.5	Slc27a2 Very long-chain acyl-CoA synthetase	70648.55
697	IPI00196457.1	Sult1c1 Sulfotransferase 1C1	35740.71
698	IPI00395281.1	Etfdh Electron transfer flavoprotein-ubiquinone oxidoreductase, mitochondrial	68154.77
699	IPI00395250.1	- Glutathione transferase 3 (Fragment)	13732.73
700	IPI00566322.2	- 35 kDa protein	34915.51
701	IPI00202580.2	Cyp2d3 Cytochrome P450 2D3	57105.55
702	IPI00202616.1	Ndufs3 NADH dehydrogenase (ubiquinone) Fe-S protein 3	30207.63
703	IPI00231148.8	Gpd1 Glycerol-3-phosphate dehydrogenase [NAD+], cytoplasmic	37428.25
704	IPI00197900.5	Eef1d Translation elongation factor 1-delta subunit	28748.49
705	IPI00371266.1	Naca Naca protein	23369.71
706	IPI00365960.2	Reep6 Receptor expression-enhancing protein 6	23298.26
707	IPI00358908.3	- 37 kDa protein	37449.47
708	IPI00189991.1	Mat2a S-adenosylmethionine synthetase isoform type-2	43688.39
709	IPI00214394.1	Csad Cysteine sulfinic acid decarboxylase	55213.60
710	IPI00202370.3	Maoa similar to Amine oxidase [flavin-containing] A	98012.69

711	IPI00201561.3	Prdx2 Peroxiredoxin-2	21770.07
712	IPI00196107.1	Atp5f1 ATP synthase subunit b, mitochondrial	28850.49
713	IPI00210234.4	Pls3 Plastin-3	70260.11
714	IPI00203443.3	Ltb4dh Prostaglandin reductase 1	35695.37
715	IPI00203214.6	Eef2 Elongation factor 2	95223.02
716	IPI00325136.5	Scp2 Isoform SCPx of Non-specific lipid-transfer protein	58775.50
717	IPI00364917.3	Akr1c12 similar to Aldo-keto reductase family 1 member C13	36876.82
718	IPI00389152.4	LOC688869;Cox6b1 similar to cytochrome c oxidase, subunit VIb polypeptide 1	10064.88
719	IPI00199426.8	Abat 4-aminobutyrate aminotransferase, mitochondrial	56419.52
720	IPI00766169.1	LOC687295 similar to translocase of inner mitochondrial membrane 50 homolog isoform 2	39829.70
721	IPI00421332.1	LOC306079 LRRGT00066	38341.46
722	IPI00207217.1	Echs1 Enoyl-CoA hydratase, mitochondrial	31496.19
723	IPI00361686.5	C1qbp Complement component 1 Q subcomponent-binding protein, mitochondrial	30977.52
724	IPI00196210.3	RGD1309586 hypothetical protein LOC364073	72949.20
725	IPI00470317.5	Eef1g Elongation factor 1-gamma	50029.21
726	IPI00190557.2	Phb2 Prohibitin-2	33291.91
727	IPI00195423.1	Ugt2b37 UDP-glucuronosyltransferase 2B5	60553.29
728	IPI00679256.1	Es22;LOC100125372 Liver carboxylesterase 4	62234.81
729	IPI00212014.2	Vcp Transitional endoplasmic reticulum ATPase	89477.95
730	IPI00360993.3	Gldc glycine decarboxylase	113846.50
731	IPI00209082.1	Actn1 Alpha-actinin-1	102895.60
732	IPI00366249.4	Dhx9 DEAH (Asp-Glu-Ala-His) box polypeptide 9	150137.00
733	IPI00192301.2	Gpx1 Glutathione peroxidase 1	22244.37
734	IPI00471872.1	Aldh1b1 Aldehyde dehydrogenase X, mitochondrial	57588.52
735	IPI00371705.4	Papss2 69 kDa protein	68897.28
736	IPI00480820.4	Pgrmc1 Membrane-associated progesterone receptor component 1	21584.70
737	IPI00203473.3	Ugt2b36 UDP-glucuronosyltransferase 2B4	61020.25
738	IPI00230937.5	Pebp1 Phosphatidylethanolamine-binding protein 1	20788.40
739	IPI00193234.1	Cyp2b2 Isoform 1 of Cytochrome P450 2B2	55897.07
740	IPI00213569.1	Ugt1a1 UDP-glucuronosyltransferase 1-1	59623.84
741	IPI00370752.3	Nit2 Nitrilase homolog 2	30681.66
742	IPI00566286.1	LOC499735 similar to heat shock protein 1, alpha	35079.59
743	IPI00214052.1	Cmbl Carboxymethylenebutenolidase homolog	27885.02
744	IPI00324020.6	Glul Glutamine synthetase	42240.34
745	IPI00231864.5	Cycs Cytochrome c, somatic	11598.02
746	IPI00198232.1	Tars 83 kDa protein	83335.95
747	IPI00391544.2	RGD1309534 Ester hydrolase C11orf54 homolog	34970.44
748	IPI00202651.1	Fga Isoform 1 of Fibrinogen alpha chain	86631.84
749	IPI00212622.2	Hadha Trifunctional enzyme subunit alpha, mitochondrial	82612.66
750	IPI00200447.2	Adh4 Ac1002	93787.09
751	IPI00208602.1	Rbbp9 Retinoblastoma-binding protein 9	20981.45
752	IPI00197555.6	Suclg1 Suclg1 protein	36125.00

753	IPI00364761.1	Lactb2 Beta-lactamase-like protein 2	32463.71
754	IPI00202512.7	Rpl4 60S ribosomal protein L4	47227.11
755	IPI00231857.5	Gamt Guanidinoacetate N-methyltransferase	26390.08
756	IPI00555310.1	Cabc1;Psen2 Chaperone activity of bc1 complex-like, mitochondrial	72179.88
757	IPI00372458.2	Copa Copa protein	138271.70
758	IPI00204128.2	RGD1561381 similar to microsomal glutathione S-transferase 3	16752.52
759	IPI00382223.1	RGD1308874 Ab2-305	43539.42
760	IPI00555278.3	Gulo L-gulonolactone oxidase	50582.38
761	IPI00231264.6	Pon1 Serum paraoxonase/arylesterase 1	39471.20
762	IPI00562527.1	Slc25a15 33 kDa protein	32775.67
763	IPI00421328.1	Usp40 LRRGT00071	89548.09
764	IPI00214665.2	Acly ATP citrate lyase isoform 1	120704.00
765	IPI00364884.1	Ssr1 Translocon-associated protein subunit alpha	35606.90
766	IPI00365170.1	Ndufb7 NADH dehydrogenase (ubiquinone) 1 beta subcomplex, 7	16557.20
767	IPI00211779.1	Prdx1 Peroxiredoxin-1	22095.32
768	IPI00371243.4	Qprt Nicotinate-nucleotide pyrophosphorylase [carboxylating]	31277.27
769	IPI00208281.1	LOC286989 UDP-glucuronosyltransferase 2B8	60050.08
770	IPI00231692.5	Rps15 40S ribosomal protein S15	17029.17
771	IPI00231379.2	Slc4a1 solute carrier family 4, member 1	103178.40
772	IPI00515762.1	Dmgdh Dimethylglycine dehydrogenase	95917.41
773	IPI00206020.1	Lrrc59 Leucine-rich repeat-containing protein 59	34847.76
774	IPI00382226.1	RGD1306939 Ab2-162	144618.50
775	IPI00393883.3	Cyp2c22 56 kDa protein	56419.17
776	IPI00364134.1	Nipsnap1 similar to Protein NipSnap1	33325.04
777	IPI00231346.5	Rpl30 60S ribosomal protein L30	12775.74
778	IPI00211216.4	Eif5a Eukaryotic translation initiation factor 5A-1	16821.41
779	IPI00364866.1	Txndc4 BWK4	46848.43
780	IPI00370348.3	- 28 kDa protein	27731.13
781	IPI00212220.2	Pdia4 Protein disulfide-isomerase A4	72674.80
782	IPI00189313.3	H2afv 9 kDa protein	9479.40
783	IPI00358127.2	Actr3b similar to ARP3 actin-related protein 3 homolog B	47604.26
784	IPI00364895.4	Immt 82 kDa protein	82197.93
785	IPI00421711.1	Atp5l ATP synthase, H+ transporting, mitochondrial F0 complex, subunit G	11453.09
786	IPI00215574.5	Dci 3,2-trans-enoyl-CoA isomerase, mitochondrial	32234.02
787	IPI00208135.1	LOC681730;Ocln;Tpmt Thiopurine S-methyltransferase	27674.15
788	IPI00190240.1	Rps27a Ribosomal protein S27a	17939.48
789	IPI00212655.4	Gnb1 Guanine nucleotide-binding protein G(I)/G(S)/G(T) subunit beta-1	37353.02
790	IPI00197703.2	Apoa1 Apolipoprotein A-I	30043.23
791	IPI00359647.2	H6pd hexose-6-phosphate dehydrogenase	89783.37
792	IPI00371236.3	Tufm Elongation factor Tu, mitochondrial	49491.04
793	IPI00231365.5	Uox Uricase	34911.90
794	IPI00421888.3	Anxa6 Annexin A6	75706.58

795	IPI00202584.1	Cyp2d5 Cytochrome P450 2D10	57039.44
796	IPI00471577.1	Uqcrc1 Cytochrome b-c1 complex subunit 1, mitochondrial	52815.46
797	IPI00200661.1	Fasn Fatty acid synthase	272475.30
798	IPI00207299.1	LOC246266 60 kDa lysophospholipase	60756.21
799	IPI00372388.1	Cct3 T-complex protein 1 subunit gamma	60608.46
800	IPI00203766.1	Msra Peptide methionine sulfoxide reductase	25834.70
801	IPI00325599.4	Asl Argininosuccinate lyase	51517.34
802	IPI00364286.3	Cct7 chaperonin subunit 7	59620.29
803	IPI00339188.2	Haao 3-hydroxyanthranilate 3,4-dioxygenase	32561.25
804	IPI00364948.3	Aldh3a2 Fatty aldehyde dehydrogenase	54047.38
805	IPI00206660.2	Dnajc3 DnaJ homolog subfamily C member 3	57525.32
806	IPI00327626.1	Ugt2b5 UDP-glucuronosyltransferase 2B3	60485.04
807	IPI00187628.4	Spnb1 262 kDa protein	262264.20
808	IPI00555265.1	Nnt Nicotinamide nucleotide transhydrogenase	113796.40
809	IPI00209807.12	Sardh Sarcosine dehydrogenase, mitochondrial	101578.90
810	IPI00370372.2	Ndufb8 NADH dehydrogenase	21944.41
811	IPI00367259.2	Nipsnap3a Nipsnap homolog 3A	28322.43
812	IPI00189416.2	RGD1565798 similar to tumor protein, translationally-controlled 1	19524.79
813	IPI00363180.4	Gbe1 similar to glucan (1,4-alpha-), branching enzyme 1	80367.51
814	IPI00192246.1	Cox5a Cytochrome c oxidase subunit 5A, mitochondrial	16119.31
815	IPI00390302.3	- 57 kDa protein	57286.97
816	IPI00209289.1	Dpyd Dihydropyrimidine dehydrogenase [NADP+]	111395.50
817	IPI00231013.2	Cyb5 Isoform Short of Cytochrome b5	11399.65
818	IPI00365663.1	Bckdha branched chain ketoacid dehydrogenase E1, alpha polypeptide	50636.22
819	IPI00370654.2	Inmt indolethylamine N-methyltransferase	29475.85
820	IPI00765682.2	Pcca propionyl-coenzyme A carboxylase, alpha polypeptide	79943.18
821	IPI00230942.5	Gstm7 Glutathione S-transferase Yb-3	25664.02
822	IPI00230838.5	Atp5h ATP synthase subunit d, mitochondrial	18751.60
823	IPI00198947.2	Cyp1a2 Cytochrome P450 1A2	58222.46
824	IPI00208598.1	Hdlbp Vigilin	141496.20
825	IPI00208659.1	Cfh Complement inhibitory factor H	140252.00
826	IPI00189415.1	Ttpa Alpha-tocopherol transfer protein	31825.55
827	IPI00231693.5	Rps3a 40S ribosomal protein S3a	29925.75
828	IPI00231663.7	Lgals5 Galectin-5	16186.03
829	IPI00231427.5	Gstt1 Glutathione S-transferase theta-1	27450.38
830	IPI00230857.7	Ak2 Adenylate kinase isoenzyme 2, mitochondrial	26362.55
831	IPI00326436.3	Oplah 5-oxoprolinase	137633.80
832	IPI00231662.6	Cyb5r3 Isoform 1 of NADH-cytochrome b5 reductase 3	34152.73
833	IPI00360056.1	Galm Aldose 1-epimerase	37869.16
834	IPI00195109.3	Shmt2 Serine hydroxymethyltransferase	55729.75
835	IPI00364701.4	RGD1311345 similar to Protein C9orf64	39034.84
836	IPI00231134.4	Gnb2l1 Guanine nucleotide-binding protein subunit beta-2-like 1	35396.76

837	IPI00205157.1	Hadh Hydroxyacyl-coenzyme A dehydrogenase, mitochondrial	34425.90
838	IPI00325135.3	Ywhae 14-3-3 protein epsilon	29155.42
839	IPI00369217.1	Trap1 Heat shock protein 75 kDa, mitochondrial	80410.88
840	IPI00358033.1	Ndufs1 NADH-ubiquinone oxidoreductase 75 kDa subunit, mitochondrial	79361.70
841	IPI00203829.1	Atox1 Copper transport protein ATOX1	7287.69
842	IPI00364318.2	RGD1310111 Putative L-aspartate dehydrogenase	31240.22
843	IPI00201932.2	Ssr4 Translocon-associated protein subunit delta	19094.61
844	IPI00212478.1	Hbe1 Epsilon 1 globin	16094.46
845	IPI00207328.3	As3mt Arsenite methyltransferase	41029.95
846	IPI00211075.1	Serpina3n Serine protease inhibitor A3N	46622.41
847	IPI00371518.1	Sdhc Succinate dehydrogenase complex, subunit C, integral membrane protein	18190.66
848	IPI00231150.4	Gsta3;Gsta2;Gsta1 Glutathione S-transferase (Fragment)	25971.69
849	IPI00870163.1	Agl amylo-1, 6-glucosidase, 4-alpha-glucanotransferase	174219.70
850	IPI00371957.2	Ppa1 similar to pyrophosphatase	45807.79
851	IPI00195999.1	RGD1560831 similar to 40S ribosomal protein S3	26613.30
852	IPI00464791.5	Acy1 Aminoacylase-1A	45775.17
853	IPI00190786.4	ENSEMBL:ENSRNOP00000001511 Tax_Cit;LOC288698 229 kDa protein	229099.40
854	IPI00395267.1	Pck1 Phosphoenolpyruvate carboxykinase, cytosolic [GTP]	69371.10
855	IPI00213463.2	Actn4 Alpha-actinin-4	104849.40
856	IPI00400573.1	Tubb2c Tubulin beta-2C chain	49769.03
857	IPI00205466.1	Cand1 Cullin-associated NEDD8-dissociated protein 1	136274.80
858	IPI00188142.1	Acy3 Aspartoacylase (Aminoacylase) 3	35396.66
859	IPI00215271.1	Nnmt nicotinamide N-methyltransferase	29496.80
860	IPI00366856.4	LOC680058;LOC686648 similar to destrin	18685.75
861	IPI00189189.2	Akr1c18 20alpha-hydroxysteroid dehydrogenase	34357.64
862	IPI00193151.1	Qdpr Dihydropteridine reductase	25535.87
863	IPI00569616.2	- 36 kDa protein	36363.56
864	IPI00763564.1	LOC684270 similar to isochorismatase domain containing 2 isoform 1	24653.19
865	IPI00212603.1	Pnpo Pyridoxine-5'-phosphate oxidase	30165.00
866	IPI00191748.3	Psma1 Proteasome subunit alpha type-1	29498.82
867	IPI00199636.1	Canx Calnexin	67212.71
868	IPI00464785.1	Ppgb Protective protein for beta-galactosidase	51183.02
869	IPI00231146.6	Hint1l Histidine triad nucleotide-binding protein 1	13770.11
870	IPI00365944.5	Myl6l Myosin light polypeptide 6	16964.15
871	IPI00781133.1	Aco1 99 kDa protein	98894.92
872	IPI00365935.3	Ptges3 Prostaglandin E synthase 3	18709.43
873	IPI00211970.5	Psme2 Proteasome activator complex subunit 2	26840.03
874	IPI00480620.1	Bdh1 3-hydroxybutyrate dehydrogenase, type 1	38308.38
875	IPI00231358.6	Pfn1 Profilin-1	14947.51
876	IPI00369143.2	Slc35a3 UDP-N-acetylglucosamine transporter	36055.21
877	IPI00212052.3	Ndufs4 NADH dehydrogenase [ubiquinone] iron-sulfur protein 4, mitochondrial	19728.23
878	IPI00470246.2	Ddc Aromatic L-amino acid decarboxylase	54393.63

879	IPI00565267.1	Fmo3 Dimethylaniline monooxygenase [N-oxide-forming] 3	59921.54
880	IPI00212316.1	Mttp microsomal triglyceride transfer protein	99124.76
881	IPI00202283.1	Psmd13 Proteasome (Prosome, macropain) 26S subunit, non-ATPase, 13	42790.21
882	IPI00189753.3	Cyp4f1 Cytochrome P450 4F1	59830.03
883	IPI00194097.5	Gc Vitamin D-binding protein	53509.07
884	IPI00388191.2	- 34 kDa protein	33937.52
885	IPI00197172.4	RGD1565829 similar to cation-dependent mannose-6-phosphate receptor	36985.50
886	IPI00213458.1	Surf4_predicted surfeit 4	30360.79
887	IPI00231611.7	Fh1 Isoform Mitochondrial of Fumarate hydratase, mitochondrial	54429.11
888	IPI00369231.3	Rpl3l similar to 60S ribosomal protein L3-like	46364.89
889	IPI00193716.1	Ivd Isovaleryl-CoA dehydrogenase, mitochondrial	46405.80
890	IPI00209045.2	Acox3 76 kDa protein	75810.41
891	IPI00188058.3	Rps18 40S ribosomal protein S18	17707.86
892	IPI00196783.2	- 19 kDa protein	18723.11
893	IPI00215093.1	Ogdh 2-oxoglutarate dehydrogenase E1 component, mitochondrial	116221.50
894	IPI00205745.3	Prdx5 Isoform Mitochondrial of Peroxiredoxin-5, mitochondrial	22164.57
895	IPI00198750.1	Acot12 Acyl-coenzyme A thioesterase 12	61978.86
896	IPI00197713.9	Rps11 40S ribosomal protein S11	18419.00
897	IPI00203310.1	Gstm3 Glutathione S-transferase Yb4	25626.93
898	IPI00382202.2	Hp Isoform 2 of Haptoglobin	42447.49
899	IPI00211392.1	Ftcd Formimidoyltransferase-cyclodeaminase	58876.71
900	IPI00214825.1	REFSEQ:NP_445855 Tax_Grb7 Growth factor receptor binding protein GRB7	59851.34
901	IPI00213644.3	Ppib Peptidyl-prolyl cis-trans isomerase B	23787.54
902	IPI00207355.4	Hspa2 Heat shock-related 70 kDa protein 2	69598.80
903	IPI00230914.5	Rpl5 60S ribosomal protein L5	34436.74
904	IPI00471545.5	Keg1 Glycine N-acyltransferase-like protein Keg1	33994.32
905	IPI00393599.3	LOC690745 similar to MOCO sulphurase C-terminal domain containing 1	37766.40
906	IPI00387771.6	Ppia Peptidyl-prolyl cis-trans isomerase A	17862.81
907	IPI00421357.2	Eprs 170 kDa protein	169979.80
908	IPI00362014.5	Tln1 Tln1 protein	270869.10
909	IPI00361121.4	Gsdmd similar to gasdermin domain containing 1	53164.29
910	IPI00555178.2	Gsta2 Glutathione S-transferase alpha-2	25542.53
911	IPI00339167.4	Tuba1b Tubulin alpha-1B chain	50119.64
912	IPI00213422.1	Kmo Kynurenine 3-monooxygenase	54317.66
913	IPI00555187.2	Cap1 Adenylyl cyclase-associated protein 1	51556.53
914	IPI00208707.2	LOC680988 similar to ribosomal protein S12	13602.08
915	IPI00195147.1	- 25 kDa protein	25234.34
916	IPI00392302.2	Tmem14a 16 kDa protein	15833.58
917	IPI00200360.1	G6pc Glucose-6-phosphatase	40529.23
918	IPI00365561.3	Maea Macrophage erythroblast attacher	45307.04
919	IPI00201103.1	Hal Histidine ammonia-lyase	72238.66
920	IPI00207668.1	Afm Afamin	69290.12

921	IPI00371511.4	Creg1 Cellular repressor of E1A-stimulated genes 1	24372.32
922	IPI00193983.3	Cltc Clathrin heavy chain 1	191475.80
923	IPI00779730.1	- 19 kDa protein	19323.46
924	IPI00193648.2	G3bp1 similar to Ras-GTPase-activating protein binding protein 1	58510.43
925	IPI00212314.5	Msn Moesin	67696.87
926	IPI00361478.2	Tymp Thymidine phosphorylase	49870.18
927	IPI00205163.3	Cnpy2 Canopy 2 homolog	20696.26
928	IPI00205749.1	Es22 Liver carboxylesterase 3	61675.54
929	IPI00198717.8	Mdh1 Malate dehydrogenase, cytoplasmic	36460.07
930	IPI00211445.2	Pcyt2 Isoform 1 of Ethanolamine-phosphate cytidylyltransferase	45191.57
931	IPI00189074.3	Pabpc1 Polyadenylate-binding protein 1	70656.05
932	IPI00411232.1	Ccbl1 Isoform 1 of Kynurenine--oxoglutarate transaminase 1, mitochondrial	51618.92
933	IPI00189981.1	F2 Prothrombin (Fragment)	70366.77
934	IPI00205135.6	Tgm2 Transglutaminase 2, C polypeptide	76887.20
935	IPI00193153.1	Hacl1 2-hydroxyacyl-CoA lyase 1	63575.34
936	IPI00324380.3	Ttr Transthyretin	15709.92
937	IPI00324172.2	Gys2 Glycogen synthase	80682.55
938	IPI00371462.3	Otub1 OTU domain, ubiquitin aldehyde binding 1	31250.40
939	IPI00563899.2	Gyk Glycerol kinase	60317.64
940	IPI00327879.1	Cyp27a1 Cytochrome P450 27, mitochondrial	60694.86
941	IPI00362105.2	Psmc6 similar to proteasome 26S ATPase subunit 6	45768.10
942	IPI00190377.2	Taldo1 Transaldolase	37436.47
943	IPI00326561.3	Ech1 Delta(3,5)-Delta(2,4)-dienoyl-CoA isomerase, mitochondrial	36148.43
944	IPI00767644.2	REFSEQ:NP_001101059 Tax_Ankrd2 ankyrin repeat domain 2	37050.23
945	IPI00213677.1	Arf2 ADP-ribosylation factor 2	20732.76
946	IPI00208495.3	- 33 kDa protein	32923.46
947	IPI00192257.1	Rpl18a 60S ribosomal protein L18a	20718.89
948	IPI00471540.1	Bhmt2 Betaine--homocysteine S-methyltransferase 2	39903.21
949	IPI00373140.2	LOC296197 similar to destrin	18507.48
950	IPI00198897.1	Ndufa6 similar to NADH dehydrogenase (ubiquinone) 1 alpha subcomplex, 6	15214.07
951	IPI00779131.1	ENSEMBL:ENSRNOP00000056148 Tax_- 31 kDa protein	30648.45
952	IPI00367281.2	LOC313220 Similar to bile acid Coenzyme A: amino acid N-acyltransferase	45980.94
953	IPI00557847.2	- 15 kDa protein	15423.82
954	IPI00210495.1	Rad23b UV excision repair protein RAD23 homolog B	43469.78
955	IPI00201528.3	Tsta3 tissue specific transplantation antigen P35B	35773.93
956	IPI00560990.2	Stt3a similar to Oligosaccharyl transferase STT3 subunit homolog	96072.74
957	IPI00190161.1	Ndufc2 Putative uncharacterized protein Ndufc2	14349.29
958	IPI00201307.1	Uqcrb;Uqcrbl Uqcrb_predicted protein	13549.92
959	IPI00324912.6	Cyp2e1 Cytochrome P450 2E1	56590.81
960	IPI00210900.1	Ambp AMBP protein	38825.96
961	IPI00369954.2	Pipox Pipecolic acid oxidase	43862.61
962	IPI00464564.1	Dync2li1 Isoform 2 of Cytoplasmic dynein 2 light intermediate chain 1	35302.16

963	IPI00764690.2	Mtch2 mitochondrial carrier homolog 2	34447.39
964	IPI00339123.2	Acox3 Peroxisomal acyl-coenzyme A oxidase 3	78396.07
965	IPI00359612.1	REFSEQ:NP_001000219 Tax_Olr252 olfactory receptor Olr252	35700.45
966	IPI00231445.5	Rpl15 60S ribosomal protein L15	24131.09
967	IPI00564294.2	- 34 kDa protein	33718.22
968	IPI00207191.1	Gjb1 Gap junction beta-1 protein	31982.60
969	IPI00191354.2	Tpm3 33 kDa protein	33128.81
970	IPI00558113.2	LOC680351 similar to growth and transformation-dependent protein	11112.02
971	IPI00369195.3	Ppa2 similar to inorganic pyrophosphatase 2	37818.08
972	IPI00558635.3	Hibch Isoform 1 of 3-hydroxyisobutyryl-CoA hydrolase, mitochondrial	42997.34
973	IPI00193765.2	Ctsc Dipeptidyl-peptidase 1	52201.72
974	IPI00371621.1	Mcee methylmalonyl CoA epimerase	18803.93
975	IPI00196764.1	Cyp3a2 Cytochrome P450 3A2	57694.40
976	IPI00196643.2	Slc2a2 Solute carrier family 2 (Facilitated glucose transporter), member 2	57190.93
977	IPI00212776.1	Rps3 40S ribosomal protein S3	26657.42
978	IPI00209980.6	Pmpcb Mitochondrial-processing peptidase subunit beta	54230.44
979	IPI00204099.5	Mcfd2 Multiple coagulation factor deficiency protein 2 homolog	16137.77
980	IPI00454288.1	Atp5c1 ATP synthase gamma chain	67677.30
981	IPI00765536.1	REFSEQ:XP_001076606 Tax_Spg21 similar to spastic paraplegia 21 homolog	35264.89
982	IPI00212708.2	Fetub Fetub protein	43141.72
983	IPI00231650.7	Hist1h1d Histone H1.2	21974.04
984	IPI00204467.1	Sult1c2 Sulfotransferase 1C2	34676.35
985	IPI00372845.2	Gstt1 28 kDa protein	27580.42
986	IPI00387641.2	LOC364773 17beta-hydroxysteroid dehydrogenase	37233.16
987	IPI00476178.3	Psma3l;Psma3 Proteasome subunit alpha type-3	28401.12
988	IPI00561751.1	Ndufs5 NADH dehydrogenase (ubiquinone) Fe-S protein 5b	12691.50
989	IPI00387868.2	Hspa4 Heat shock 70 kDa protein 4	93997.07
990	IPI00370596.2	RGD1562373 3-ketoacyl-CoA thiolase B, peroxisomal	43792.71
991	IPI00471647.1	Ndufs2 NADH dehydrogenase [ubiquinone] iron-sulfur protein 2, mitochondrial	52527.64
992	IPI00211756.1	Phb Prohibitin	29801.90
993	IPI00359981.2	Ndufa13 similar to NADH dehydrogenase (ubiquinone) 1 alpha subcomplex, 13	16949.84
994	IPI00367877.3	Pcdh1 similar to protocadherin 1 isoform 2 precursor	135607.20

Vita

Priya Venkatakrishnan, the daughter of K. Renganayaki and A. P. Venkatakrishnan, was born in Trichy, India on March 16, 1980. In 1997, Priya joined Birla Institute of Technology and Science, Pilani, India and received a Bachelor of Science in Pharmacy (Hons.) degree in 2001. Priya came to the United States in 2002 to the University of Kentucky, obtained a Master of Science degree in Toxicology and continued her doctoral studies under Dr. R.T. Miller. In august 2006, she transferred to the University of Texas at El Paso for the doctoral program in Biological Sciences and continued working in the laboratory of Dr. R.T Miller. Priya has exhibited her research ideas as posters and presentations in various societies including Society of Toxicology and the regional chapters: Ohio Valley Society of Toxicology and Gulf Coast Society of Toxicology, American Society for Biochemistry and Molecular Biology, Kentucky Science and Engineering Foundation, Society of Neuroscience-Blue grass Chapter and the Society for Advancement of Chicanos and Native Americans in Science- Paso Del Norte Student Chapter. The awards received during her masters and doctoral degree programs include: '2002 Research Challenge Trust Fund Graduate Student Fellowship' at the University of Kentucky, 'University of Texas at El Paso Graduate School Research Travel Award' in 2007 and 2008, *honorary mention* for 'Graduate Student Platform Presentation' and the 'Graduate Student Travel Award' in the 2007 Gulf Coast Society of Toxicology Meeting, first place for the 'Graduate Student Travel Award' for the '47th Society of Toxicology Annual Meeting and Tox Expo 2008' by the Gulf Coast Society of Toxicology, *honorary mention* in the 'Carl C. Smith Graduate Student Award Competition' in the Mechanisms Specialty Section, 47th Society of Toxicology Annual Meeting and Tox Expo 2008, Graduate Student Travel Fellowship Recipient from the American Society for Biochemistry and Molecular Biology (ASBMB) at the Experimental

Biology 2008 Meeting, 'Outstanding Poster Presentation' Award for Biology in the Research Expo 2008 from the Society for Advancement of Chicanos and Native Americans in Science - Paso Del Norte Student Chapter.

Email Address: priya603@gmail.com

This thesis/dissertation was typed by Priya Venkatakrishnan.